2022-01

The Application of the Reference Finite Helical Axis for Characterizing Knee Joint Kinematics

Bugajski, Tomasz

UNIVERSITY OF CALGARY

The Application of the Reference Finite Helical Axis for Characterizing Knee Joint Kinematics

by

Tomasz Bugajski

A THESIS

SUBMITTED TO THE FACULTY OF GRADUATE STUDIES

IN PARTIAL FULFILMENT OF THE REQUIREMENTS FOR THE

DEGREE OF DOCTOR OF PHILOSOPHY

GRADUATE PROGRAM IN BIOMEDICAL ENGINEERING

CALGARY, ALBERTA

JANUARY, 2022

Abstract

Altered knee kinematics are an important biomechanical marker for the development of tibiofemoral osteoarthritis (OA). They are associated with altered cartilage contact areas, resulting in forces acting on unadapted cartilage that may degrade over time. The conventional approach to quantify knee kinematics is with Cardan angles, but the uncommon helical axis (HA) approach may provide supplementary information. However, the HA is susceptible to stochastic errors when angular displacements are small. To alleviate this error, a reference position may be used that permits larger angular displacements. However, more assessments are required to determine the utility of this reference finite helical axis (rFHA) method to provide biomechanical markers of tibiofemoral OA.

The purpose of this thesis was to technically evaluate the rFHA and demonstrate its ability to distinguish knee kinematics of high tibiofemoral OA risk individuals. Technical evaluations consisted of 1) determining the effect of different smoothing techniques on rFHA accuracy, 2) assessing the sensitivity of the rFHA to reference position misalignments, and 3) comparing rFHA measures between an optical motion camera system (OMCS) and highspeed biplanar videoradiography system (HSBV). The utility of the rFHA was demonstrated by applying it to high tibiofemoral OA risk populations, specifically anterior cruciate ligament repaired (ACLR) knees and older knees.

A spline filter with outlier removal process was the top performing smoothing technique for rFHA accuracy, providing a 72.2-80.1% improvement in rotational speed differences. Substantial differences of the rFHA measures were determined with misaligned reference positions, ranging from 1.17-19.53 mm and 0.77-5.45 deg. rFHA measure differences were also found between the OMCS and HSBV, ranging from 10.19-58.03 mm and 3.39-13.63 deg. Finally, kinematic trends were found in ACLR knees during a vertical drop jump, showing greater magnitudes of rFHA

dispersion and helical internal rotation than healthy knees (dispersion: 0.46 deg; helical internal rotation: 2.18 deg). Additionally, significantly different rFHA path lengths were found between older and younger asymptomatic knees during walking (10.60 mm, $p = 0.01$).

These findings demonstrate the utility of the rFHA in biomechanics, providing a supplementary method of characterizing knee kinematics and distinguishing the movement patterns of healthy individuals from tibiofemoral OA prone individuals.

Keywords: Finite Helical Axis, Aging, Knee Injury, Kinematics, Knee, Osteoarthritis, Highspeed Biplanar Videoradiography

Preface

This study was approved by the Conjoint Health Research Ethics Board (ethics IDs: REB15-0554 and REB14-2212).

Segments of this thesis, or work related to this thesis, have been previously presented in the following proceedings:

1) Bugajski, T.*, Kuntze, G., Küpper, J., Ronsky, J. (2018). Quantifying Knee Joint Instability Using the Finite Helical Axis: Pilot Study. 20th Biennial Meeting of the Canadian Society for Biomechanics. Halifax, Nova Scotia, Canada (poster presentation).
2) Bugajski, T.*, Kuntze, G., Ronsky, J. (2019). Kinematic Changes Associated with Anterior Cruciate Ligament Deficiency Using the Finite Helical Axis. 27th Congress of the International Society of Biomechanics. Calgary, Alberta, Canada (podium presentation).
3) Bugajski, T.*, Küpper, J., Kuntze, G., Ronsky, J. (2021). The Use of the Reference Finite Helical Axis and High-Speed Biplanar Videoradiography to Characterize Knee Kinematics. 28th Congress of the International Society of Biomechanics. Stockholm, Sweden, 2021 (podium presentation).

Acknowledgements

I would like to thank the following individuals for their support for the last few years:

Dr. Janet Ronsky, for putting up with me for yet another graduate degree. How you did it is beyond me. However, your invaluable mentorship and knowledge have shaped me to who I am today. Thank you for everything.

Dr. Sarah Manske and Dr. Kelly Johnston, for your insight, guidance, and most importantly, patience throughout the hurdles of this thesis.

Dr. Gregor Kuntze, for your constant assistance despite your busy schedule. I will never forget our one hundred or more conversations about transformation matrices (math is fun!).

Dr. Carolyn Emery and her research team, for allowing me access to the pre-OA youth dataset.

Ronsky team members (Brodie, Jessica, and Greg), for allowing me to access the 'OMCS vs HSBV' and 'younger versus older' datasets.

Alonso Figueroa, for being an awesome lab mate and roommate. If it wasn't for our daily workouts and activities, I'd be a potato by now.

Dr. Jessica Küpper, for being the best 'lab mom' a doctoral student could ask for and dealing with my shenanigans. More importantly, your input and expertise were always appreciated.

Banafshe Felfeliyan, (aka Peps), for being an amazing and supportive lab mate. Working with you has been an absolute pleasure.

Marc & Nancy Schneider, I wouldn't be where I am now if you never took me into your clinic. Thank you for your support and believing in me through all these years.

The Boydians (Kara Sidhu, Tannis Kemp, Phil Spanswick, and Ryan Plett), for being the best next-door neighbours. Best of luck with future endeavours.

The Dual Fluo'Ronsky'py lab, for being a fun group of individuals to work with. Never a bad time with the gang.

Dedication

I dedicate this thesis to my family.

Table of Contents

List of Tables

List of Figures, Illustrations, and Other Graphics

List of Symbols, Abbreviations, and Nomenclature

Symbol	Definition
%Con	Percent contribution
3D	Three dimensional
Ab/Ad	Abduction/Adduction
ACL	Anterior cruciate ligament
ACLD	Anterior cruciate ligament deficient
ACLR	Anterior cruciate ligament repaired
ACS	Anatomical coordinate system
AP	Anteroposterior
ATM	Affine transformation matrix
BMI	Body mass index
CA	Cardan angles
CI	Confidence interval
CT	Computed tomography
EMG	Electromyography
F/E	Flexion/extension
FHA	Finite helical axis
GCV	Generalized cross validation
HA	Helical axis
HSBV	Highspeed biplanar videoradiography
I/E	Internal/External rotation
IHA	Instantaneous helical axis
IQR	Interquartile range
OA	Osteoarthritis
KOOS	Knee osteoarthritis outcome score
MDD	Minimum detectable difference
ML	Mediolateral
MOAKS	Magnetic resonance imaging osteoarthritis knee score
MRI	Magnetic resonance imaging
OA	Osteoarthritis
OMCS	Optical multi-camera system
PTOA	Post-traumatic osteoarthritis
Q-Q	Quantile-quantile
rFHA	Reference finite helical axis
RMSE	Root mean square error
RoM	Range of motion
RSA	Radiostereometric analysis
SLERP	Spherical linear interpolation
SA	Specific aim
SD	Standard deviation
sFHA	Stepwise finite helical axis
SI	Superoinferior
VDJ	Vertical drop jump

Chapter One: Introduction

1.1 Motivation

Altered knee kinematics are an important biomechanical marker for the onset/progression of knee osteoarthritis (tibiofemoral OA). They are associated with altered cartilage contact areas, resulting in forces acting on unadapted cartilage that may degrade over time [1]. The conventional method of quantifying joint kinematics in biomechanics has been with Cardan angles (CA). This method characterizes the relative movement of two bones as three rotations (flexion/extension [F/E], internal/external [I/E] rotation, and abduction/adduction [Ab/Ad]) and three translations (mediolateral [ML], superoinferior [SI], and anteroposterior [AP]) along their respective anatomical axes. However, the CA method has two known limitations: 1) CA assume that the rotations occur sequentially; simultaneous rotations about the anatomical axes cannot occur, and 2) the accuracy of the calculated rotations about each anatomical plane is limited to the accuracy of the anatomical axes (e.g., the CA for a single individual may differ if the directionality of the anatomical axes are not defined consistently). These limitations may result in crosstalk, resulting in erroneous kinematics. These factors may explain why CA have a small effect size when distinguishing knee kinematics of healthy and tibiofemoral OA individuals [2]. However, the quantification of knee kinematics is not limited to CA.

The helical axis (HA) approach may provide supplemental information to the CA. The HA characterizes knee movement as a rotation about a single axis and a translation along that axis. Therefore, the HA is not susceptible to crosstalk errors [3]. However, the HA has its own limitations, one being that HA outcome variables are difficult to understand and interpret clinically due to its limited its unfamiliarity. Another limitation is the appearance of stochastic error in its directionality and position when angular displacements are small [4]. This is a problem in biomechanics, where high sampling rates of the imaging systems (e.g., 60-240 Hz) result in small

angular displacements between image frames. Therefore, the HA is usually calculated after a specific interval of angular displacement (e.g., every 10 deg of knee flexion). However, this approach drastically decreases the temporal resolution of the data and has been a reason why the HA is not widely used in biomechanics. Fortunately, to alleviate this situation a reference position may be used that permits larger magnitudes of rotation and decreased error [5]. This method is termed the reference finite helical axis (rFHA).

The rFHA, in conjunction with an optical multi-camera system (OMCS), has been used once to successfully detect knee kinematic differences between healthy and anterior cruciate ligament deficient (ACLD) individuals during seated leg swings and single leg squats [6]. Although demonstrating to be a promising method, the rFHA still requires a thorough assessment to determine its potential as a biomechanical marker for detecting changes in knee kinematics. Specifically, the following limitations remain for the rFHA:

1. **Unknown effect of different smoothing techniques on the rFHA accuracy:** The rFHA has only been applied to kinematic data recorded with the OMCS, which is susceptible to movement artifacts due to the use of skin mounted markers [7]. Smoothing techniques, such as the Butterworth filter, are typically applied to the translations of the marker data to mitigate these artifacts [8]. Using a different imaging modality - highspeed biplanar videoradiography [HSBV] - avoids these artifacts completely by using X-rays to record bone movement directly. HSBV is a state-of-the-art technology that currently provides the most accurate motion data to assess the rFHA. To quantify kinematics with the HSBV, 2D-3D registration is performed by aligning 3D bone models to their respective HSBV biplanar (2D) images. However, misalignments of these bone models may still produce kinematic errors and require smoothing. The kinematic outputs of the 2D-3D registration are different

from the OMCS, being in the form of 4x4 affine transformation matrices (ATM). Each ATM contains a 3x3 rotation matrix and a 3x1 translation vector. Unlike the elements of the 3x1 translation vectors and the OMCS marker translations, the elements of the 3x3 rotation matrices exist in a non-linear space, thus requiring different procedures for the application of smoothing techniques. How these procedures and subsequent smoothing techniques influence the rFHA accuracy are not known.

2. **Unknown sensitivity of the rFHA to misaligned reference positions:** The rFHA requires a reference position to calculate knee kinematics. For example, a seated position with the knee in 90 deg of flexion may be used as a reference. When performing between-participant comparisons, it is important that the alignment of the reference position be consistent between all participants. However, slight misalignments may arise due to human imprecisions. It is unclear how sensitive the rFHA is to misaligned reference positions.
3. **Differences in the rFHA between the OMCS and HSBV have not been assessed:** The OMCS data is susceptible to movement artifacts, due to the placement and measurement of skin mounted markers that are used to represent rigid bony movement. These errors have been previously reported for translations and CA [7]. However, it is still unknown if similar errors are present when using the rFHA.
4. **Versatility of the rFHA not demonstrated:** The rFHA has only been applied to a single study and may be a powerful tool in other scenarios. For example, the rFHA has not been used to assess movement tasks of daily living, such as walking. Additionally, the rFHA may be a useful technique to characterize knee kinematics of other tibiofemoral OA prone groups, such as older and anterior cruciate ligament repaired (ACLR) individuals.

The purpose of this thesis was to obtain a better understanding of the rFHA and its outcome measures. The influence of different smoothing techniques on HSBV data were assessed, providing more accurate rFHA computations. The sensitivity of the rFHA to deviations of the reference position was also investigated. Additionally, knee rFHA measures from two imaging modalities (OMCS and HSBV) were compared. Finally, the rFHA was applied to datasets of different movement tasks and tibiofemoral OA prone populations to demonstrate its ability as a biomechanical marker that is sensitive to changes in knee kinematics. Understanding the application of the rFHA, and its use in biomechanics, may provide a supplementary method of characterizing the knee and distinguishing kinematics of healthy individuals from tibiofemoral OA prone individuals.

1.2 Background

This section will describe the common methods used to characterize kinematics of the knee, including their strength and limitations. Firstly, the optical methods used to record the knee movement will be explained (i.e., the OMCS and HSBV). Afterwards, the methods we use to quantify these recorded knee movements will be explained as well (i.e., CA and HA). The characterization of knee kinematics is important to understand what alterations occur with tibiofemoral OA; speculated to assist in the progression of the disease [9]. Therefore, a brief overview of tibiofemoral OA will also be provided in this section.

1.2.1 Optical Methods in Biomechanics

The calculation of the movements of human body segments first requires the ability to capture and record data representing the movements. This section includes of a brief overview of two methods used to record human motion: the standard, optical multi-camera system (OMCS) and the high speed biplanar videoradiography system (HSBV).

1.2.1.1 Optical Multi-Camera Systems

The conventional approach to capture human movements consists of multiple infrared cameras accompanied with skin mounted reflective markers (hereafter called the OMCS, Figure 1-1). However, the OMCS has methodological limitations, the most severe being the influence of skin movement artifacts. Reflective markers are mounted on the skin to represent three dimensional (3D) movements of body segments (e.g., thigh and shank). The analysis approach, based on rigid body dynamics, assumes that the segment is rigid and thus represents the underlying movement of the bones (e.g., femur and tibia). Unfortunately, vibrations of the skin and underlying muscles during various movement tasks can cause the markers to move relative to the underlying bone, inducing noise within the kinematic data. When calculated with Cardan angles (CA), a study by Benoit et al. (2006) found that this noise may produce kinematic errors at the knee ranging from 3.3 mm to 16.1 mm of translation, and 2.2 deg to 13.1 deg of rotation [7]. Skin movement artifacts have also been noted to produce outliers in the directionality of the HA. Outliers were defined as HA with directionalities that were 2 or more SD away from the mean HA directionality [10].

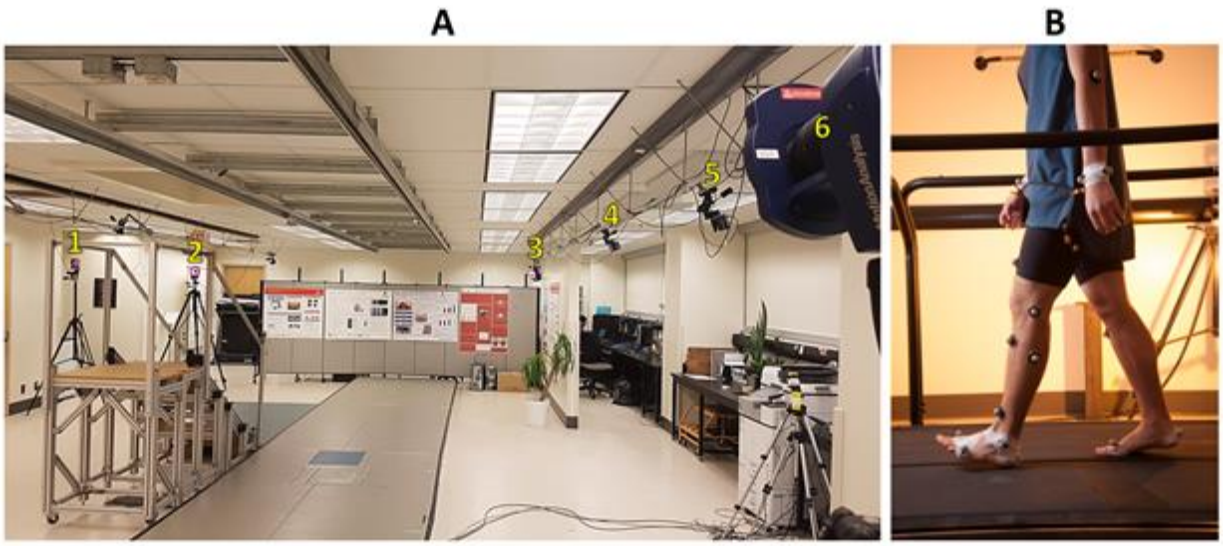

Figure 1-1 – A) The conventional OMCS with an eight-camera setup (six cameras [1-6] are shown, 2 additional cameras to left of image are not shown). B) Skin mounted reflective markers attached to the left limb of a participant.

The kinematic changes observed with both aging and OA using the OMCS have varied, with some studies finding differences where other have not [11], [12]. Whether or not these results are real or due to skin movement artifacts is unknown. It is speculated that the OMCS may be useful in measuring larger changes in movements, but aging and OA may demonstrate more subtle kinematic changes [12], [13]. For example, a study by Farrokhi et al. (2012) used the HSBV to determine significant knee kinematic differences between twelve healthy and seven medial tibiofemoral OA participants [14]. Knee excursion differences within F/E, I/E rotation, and Ab/Ad were 7.7 deg, 2.7 deg, and 1.2 deg between the two groups, respectively. These differences lie within the error range of skin movement artifacts. It is speculated that the OMCS may be useful in measuring larger changes in movements. However, aging and OA are likely to demonstrate subtle alignment/translation changes [12], [13] and may require a more accurate approach to record movements of the bone. Therefore, a system such as the HSBV may be required.

1.2.1.2 Highspeed Biplanar Videoradiography

The HSBV is a novel system that captures bone movement via dynamic X-rays. As opposed to the OMCS, the bone movement is measured directly with the HSBV, eliminating the problem of skin vibrations by avoiding the use of reflective markers. The HSBV (Figure 1-2) provides bi-planar X-ray images of the tibia and femur during movements. Within our laboratory, the HSBV consists of two X-ray generators (EMD Technologies, QC) paired with rotating anode X-ray tubes (Varian Medical Systems, USA) mounted to the ceiling with a tube crane (Del Medical, IL, USA). The X-rays travel through manual collimators (Eureka, IL, USA) before reaching two 406-mm-diameter image intensifiers (Toshiba, Japan). Afterwards, two high-speed digital video cameras (PCO AG, Germany; sample rate up to 1200 Hz) provide consecutive high resolution images (2016 x 2016 pixels^2) of the X-ray result during a movement [15], [16]. Accurate calibration of the system's components, combined with the independent generation of a 3D bone model (from Computed Tomography [CT] or Magnetic Resonance Imaging [MRI]) allow the ability to determine the bone locations in 3D space with very high accuracy (0.08 mm) [17].

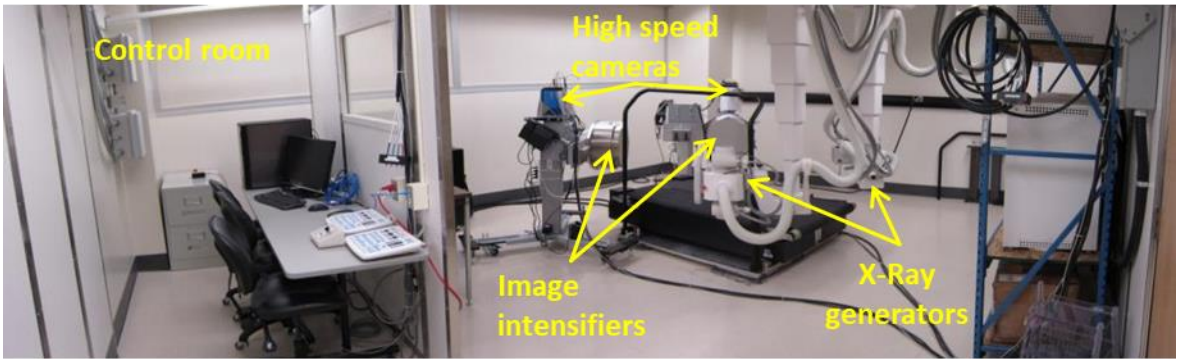

Figure 1-2 – The HSBV and its components: control room, high speed cameras, image intensifiers, and X-ray generators.

However, the HSBV does have its limitations. The first is that the HSBV uses X-rays to record bone movement, thus exposing the study participants to potentially harmful radiation. Therefore, data collection with the HSBV is limited to fewer trials with shorter time frames to reduce the effective dose that the participant is exposed to. Typical collections with the HSBV result in an effective dose of 1 mSv. Another limitation is that the image intensifiers provide an image with a field-of-view approximately the size of a basketball. This limited field-of-view does not allow the HSBV to simultaneously record multiple joints of the lower limb (e.g., ankle, knee, and hip). As a result, the use of the HSBV is dependent on the research questions investigated. Finally, the post-processing of HSBV data to calculate joint kinematics is an extensive process. The process consists of undistorting the HSBV images, obtaining calibration parameters, segmenting 3D bone models from MR or CT images, and 2D-3D registering the bone models to the captured trials. Therefore, HSBV studies tend to have smaller sample sizes.

The accuracy and reliability of the HSBV has been reported in several static validation studies. Brainerd et al. (2010) used an aluminum wand with two beads of known distance to determine the error between the actual distance and HSBV output. The average error was calculated to 0.037 mm [16]. In another study, Sharma et al. (2015) also calculated sub-millimeter accuracies with the HSBV using cadaveric bone models with and without metallic markers at different magnifications. For marker-based bones, the minimum detectable difference (MDD) ranged from 0.05 mm to 0.1 mm. For marker-less bones the MDD was 0.08 mm [17]. Thorhauer and Tashman (2015) performed a validation study in which laser scans and HSBV data of the knee were obtained from three cadaveric specimens [18]. The knees were moved in 5-degree flexion increments, with static laser and HSBV scans acquired at each increment. Bone models of the cadavers were obtained from MRI and aligned to the HSBV data. Obtaining the movements of the bone models from the

HSBV data, contact area and centroid of cartilage contact were evaluated based on these movements. The cartilage model determined from the laser scan was considered the gold standard cartilage geometry and provided the comparison for evaluation [18]. For contact area, the root mean square errors were determined to be 8.4% and 4.4% for the medial and lateral compartments, respectively. Intra-class correlations between the laser scan and HSBV data were 0.68 for the medial compartment and 0.88 for the lateral compartment. For the centroids of cartilage contact in the mediolateral direction, the intra-class correlations were 0.71 and 0.77 for the medial and lateral compartments, respectively. For the centroids of cartilage contact in the anteroposterior direction, the intra-class correlations were calculated to be 0.90 and 0.98 in the medial and lateral compartments, respectively [18].

Lastly, a study by Miranda et al. (2011) performed both static and dynamic validations of the HSBV using a single set of human cadaveric bones (distal femur, radius, and ulna) [19]. For static trials, each bone was mounted to a highly accurate apparatus with linear and rotary accuracies of 0.001 mm and 0.002 deg, respectively. Twenty trials were performed for each bone at fifteen different translational and rotational steps. For dynamic trials, each bone was mounted to a different apparatus, specifically an impact pendulum installed with an angular displacement transducer (precision: ±0.06 deg). Five trials were performed by dropping the bones into the field of view of the HSBV with the pendulum. For both static and dynamic trials, markerless tracking of the bones was compared to the apparatus measurements. Mean translational absolute errors for the static trials were 0.25 ± 0.16 mm, 0.33 ± 0.27 mm, and 0.30 ± 0.30 mm for the distal femur, distal radius, and distal ulna, respectively. Mean rotational absolute errors for the static trials were 0.30 ± 0.18 deg, 0.39 ± 0.18 deg, and 0.44 ± 0.26 deg for the distal femur, distal radius, and distal ulna, respectively. For the dynamic trials, mean rotational errors were 0.14 ± 0.09 deg, 0.10 ± 0.09

deg, and 0.14 ± 0.12 deg for the distal femur, distal radius, and distal ulna, respectively [19]. Overall, the HSBV has shown exceptional accuracy when evaluated to gold standards.

1.2.2 Quantification of Joint Kinematics

1.2.2.1 Affine Rotation Matrices and Quaternions

To quantify the orientation of a rigid body segment in 3D space, rotation matrices or quaternions may be used. To describe the derivation of a rotation matrix, it is helpful to illustrate the rotation of a XYZ coordinate system to a new coordinate system (X`Y`Z`) about a single axis. As seen in Figure 1-3, a XYZ coordinate system was rotated about the x-axis by a magnitude of $\theta_X$ to achieve a new X`Y`Z` coordinate system.

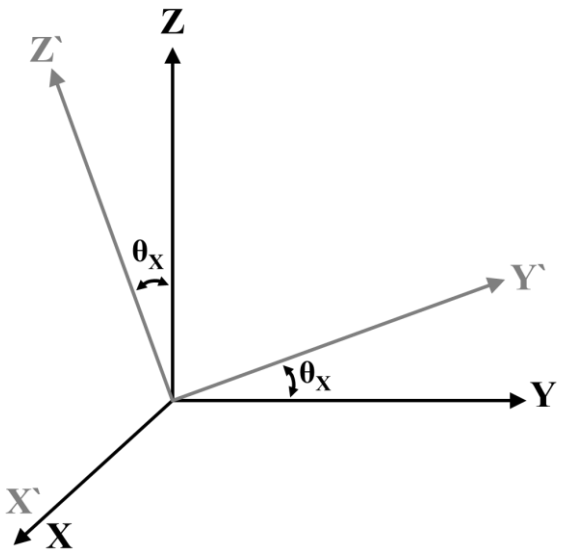

Figure 1-3 – An arbitrary XYZ coordinate system (black) being rotated about the x-axis by an angle θ_X to a new X`Y`Z` coordinate system (gray).

As a result, these two coordinate systems can be related as a system of three equations

$$X` = X \qquad \text{Eq. 1-1}$$

$$Y' = Y\cos(\theta_X) + Z\sin(\theta_X) \qquad \text{Eq. 1-2}$$

$$Z` = -Y\sin(\theta_X) + Z\cos(\theta_X) \quad \text{Eq. 1-3}$$

and in matrix form may be written as

$$\begin{bmatrix} X` \\ Y` \\ Z` \end{bmatrix} = \begin{bmatrix} 1 & 0 & 0 \\ 0 & cos(\theta_X) & sin(\theta_X) \\ 0 & -sin(\theta_X) & cos(\theta_X) \end{bmatrix} \begin{bmatrix} X \\ Y \\ Z \end{bmatrix} \quad \text{Eq. 1-4}$$

Equation 1-4 may be further simplified as $X'Y`Z` = R * XYZ$, where R represents the rotation matrix that rotates the XYZ coordinate system by a magnitude of θ_X about the x-axis to achieve a new X`Y`Z` coordinate system. Therefore, two other rotation matrices exist for rotating about the remaining two axes (i.e., y-axis [Equation 1-5] and z-axis [Equation 1-6]).

$$\begin{bmatrix} X` \\ Y` \\ Z` \end{bmatrix} = \begin{bmatrix} cos(\theta_Y) & 0 & -sin(\theta_Y) \\ 0 & 1 & 0 \\ sin(\theta_Y) & 0 & cos(\theta_Y) \end{bmatrix} \begin{bmatrix} X \\ Y \\ Z \end{bmatrix} \quad \text{Eq. 1-5}$$

$$\begin{bmatrix} X` \\ Y` \\ Z` \end{bmatrix} = \begin{bmatrix} cos(\theta_Z) & sin(\theta_Z) & 0 \\ -sin(\theta_Z) & cos(\theta_Z) & 0 \\ 0 & 0 & 1 \end{bmatrix} \begin{bmatrix} X \\ Y \\ Z \end{bmatrix} \quad \text{Eq. 1-6}$$

To combine multiple rotations the rotation matrices may be multiplied together. For example, a rotation about the x-axis, followed by the y-axis, and then finally the z-axis (XYZ rotation sequence) would be multiplied as follows:

$$[R_{XYZ}] = R_Z R_Y R_X =$$

$$\begin{bmatrix} cos(\theta_Z) & sin(\theta_Z) & 0 \\ -sin(\theta_Z) & cos(\theta_Z) & 0 \\ 0 & 0 & 1 \end{bmatrix} \begin{bmatrix} cos(\theta_Y) & 0 & -sin(\theta_Y) \\ 0 & 1 & 0 \\ sin(\theta_Y) & 0 & cos(\theta_Y) \end{bmatrix} \begin{bmatrix} 1 & 0 & 0 \\ 0 & cos(\theta_X) & sin(\theta_X) \\ 0 & -sin(\theta_X) & cos(\theta_X) \end{bmatrix} \quad \text{Eq. 1-7}$$

$$= \begin{bmatrix} \cos\theta_Z \cos\theta_Y & -\sin\theta_Z \cos\theta_X + \cos\theta_Z \sin\theta_Y \sin\theta_X & \sin\theta_Z \sin\theta_X + \cos\theta_Z \sin\theta_Y \cos\theta_X \\ \sin\theta_Z \cos\theta_Y & \cos\theta_Z \cos\theta_X + \sin\theta_Z \sin\theta_Y \sin\theta_X & -\cos\theta_Z \sin\theta_X + \sin\theta_Z \sin\theta_Y \cos\theta_X \\ -\sin\theta_Y & \cos\theta_Y \sin\theta_X & \cos\theta_Y \cos\theta_X \end{bmatrix}$$

As seen in Equation 1-7, when combining multiple rotations, the final rotation matrix is dependent on the sequence chosen (e.g., a XYZ rotation sequence would differ from ZYX). Further information on the derivation of rotation matrices can be found in work by Meirovitch (1970). Additionally, work by Challis (1995) describes the process of calculating rotation matrices from motion analysis data using a singular value decomposition approach. The rotations about the three axes may then be computed from these rotation matrices to obtain the Cardan angles θ_X, θ_Y, and θ_Z [21] or helical axis measures [22].

Quaternions are another approach to describing the orientation of a rigid body. The derivation of the quaternion is more complex than a rotation matrix and will not be provided. Further details of quaternions may be found in work by Vince (2021). For 3D rotations, quaternions take the general form of

$$q = cos(\frac{1}{2}\theta) + sin(\frac{1}{2}\theta)\vec{v} \quad \text{Eq. 1-8}$$

where $cos(\frac{1}{2}\theta)$ is a scalar term and $sin(\frac{1}{2}\theta)\vec{v}$ is a vector term of the quaternion. The vector $\vec{v}$ represents the directionality (i.e., unit vector) of the axis that a rigid body rotates about (by an angle of θ). Expanding Equation 1-8, the quaternion may also be written as four components,

$$q = s + xi + yj + zk \quad \text{Eq. 1-9}$$

where s is the scalar term and x, y, and z are the elements of the vector term. A rotation matrix $[R_{ij}]$, where i and j represent the element locations of R, may be converted into a quaternion using Equations 1-10 to 1-13 [23].

$$s = \frac{1}{2}\sqrt{1 + R_{11} + R_{22} + R_{33}} \quad \text{Eq. 1-10}$$

$$x = \frac{1}{4s}(R_{32} - R_{23}) \quad \text{Eq. 1-11}$$

$$y = \frac{1}{4s}(R_{13} - R_{31}) \quad \text{Eq. 1-12}$$

$$z = \frac{1}{4s}(R_{21} - R_{12}) \quad \text{Eq. 1-13}$$

Conversely, a quaternion may be converted to a rotation matrix $[R]$ using Equation 1-14 [23].

$$R = \begin{bmatrix} 2(s^2 + x^2) - 1 & 2(xy + sz) & 2(xz - sy) \\ 2(xy - sz) & 2(s^2 + y^2) - 1 & 2(yz + sx) \\ 2(xz + sy) & 2(yz - sx) & 2(s^2 + z^2) - 1 \end{bmatrix} \quad \text{Eq. 1-14}$$

1.2.2.2 Cardan Angles

In the biomechanics field, knee joint kinematics are typically quantified using CA. These angles are obtained by embedding orthogonal, anatomical coordinate systems (ACS) into the femur and tibia. The relative movement between the ACS subsequently describes the movement of the knee in six degrees of freedom, consisting of three rotations (flexion/extension [F/E], abduction/adduction [Ab/Ad], internal/external [I/E] rotation) and three translations (antero-posterior [AP], medio-lateral [ML], and supero-inferior [SI]) [24]. Although CA are easy to comprehend and interpret, there are three disadvantages with this method: 1) the CA rely on an accurate ACS to avoid crosstalk errors [25], 2) the angles are constrained to a specific rotational

sequence, and the selected sequence influences the output due to crosstalk errors [26], [27], and 3) the angles are susceptible to gimbal lock [28].

For the first disadvantage, because the CA rely on an ACS, any misdirection of the axes within a body segment may introduce crosstalk errors to the angles because the axes are not aligned with the true movement (e.g., Ab/Ad rotations may be registered as rotations about the I/E rotation axis). This may result in overestimated or underestimated joint angles [29]. As a result, ACS definitions have been standardized by the International Society of Biomechanics to minimize these errors [30], [31].

Elaborating on the second disadvantage of sequence dependency, envision rotating a 3D rectangle from point A to C as illustrated in Figure 1-4. Practically, an individual would likely describe its change in orientation from point A to C as a single rotation (e.g., they may physically move the rectangle within all axes simultaneously to achieve position C). However, the methodology of the CA quantifies the relative change in orientation from point A to C as rotations in a specific sequence [24]. In other words, the CA decompose the movement of the rectangle into successive rotations. In Figure 1-4, the movement of the rectangle is decomposed into two successive rotations. The first was performed by rotating about the x-axis (red) to achieve position B, and the second about the y-axis (green) to achieve the final position C. To apply this concept to human knee motion, two sets of axes would be mathematically embedded to the leg, one on the thigh/femur and the other on the shank/tibia. These axes would be aligned to the anatomical planes of their respective body segment/bone. The relative movement of the body segments/bones about the sagittal, frontal, and transverse planes would then correspond to the sequential F/E, Ab/Ad, and I/E rotation of the knee. Clearly, this sequential movement is not ideal to describe joints such

as the knee, which rotate and translate about all axes simultaneously and demonstrate out of plane movements.

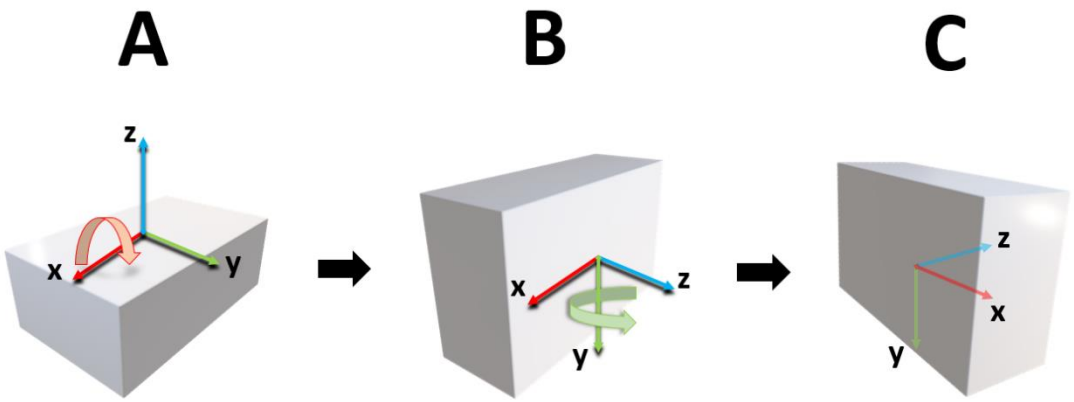

Figure 1-4 – A 3D rectangle rotating about two sequential axes (x-axis followed by y-axis) from the A position to C position, according to the Cardan angles.

Furthermore, the sequence of rotations selected can influence the final angle output [27]. This is because during each rotation within the sequence the directions of the axes are changed. This can be seen in Figure 1-4 after a rotation about the x-axis (A→B), where the directions of the y- and z-axis point differently at location 'B' when compared to location 'A'. As a result, the axis that represents the last rotation in the CA sequence is the most error prone, as the direction of the axis may not represent the corresponding anatomical movement [27]. This is yet another form in which crosstalk errors can arise, which have been reported in literature. Peak angles in the transverse and coronal planes for the ankle while running (4.0 m/s) were reported to be significantly different depending on the CA sequence used (e.g., the peak I/E angle measured -2.1 degrees with an 'XYZ' sequence, and -71.0 degrees with a 'YXZ' sequence) [29]. Lees et al. (2010) investigated the effect of different CA sequences on lower limb kinematics during a soccer kick [26]. Using root mean square errors (RMSE), the CA were compared to mathematically integrated angular velocities of

the limbs. Because angular velocities are independent of the selected rotation sequence, the resulting angles from integration would also be independent of the rotation sequence Therefore, they were chosen as the reference for comparison [32]. Maximum RMSE for the ankle, knee, hip, and pelvis were 7.9 degrees, 6.5 degrees, 15.7 degrees, and 4.7 degrees, respectively [26]. To accommodate these differences, standardizations several joints have been made to ensure the rotation sequence selected is consistent and accurate (i.e., for the knee the sequence is F/E, followed by Ab/Ad, followed by I/E rotation) [27].

The CA sequence dependency is also associated with the third and final disadvantage: gimbal lock. If the second rotation within the sequence is greater than 90 degrees, the corresponding axis will align with another axis, losing a degree of freedom in that moment [33]. This can be mathematically shown with a rotation matrix [R_{ij}]. For a 'XYZ' rotation sequence (refer to Equation 1-7), [R_{XYZ}] takes the form

$$\begin{bmatrix} \cos\theta_Z \cos\theta_Y & -\sin\theta_Z \cos\theta_X + \cos\theta_Z \sin\theta_Y \sin\theta_X & \sin\theta_Z \sin\theta_X + \cos\theta_Z \sin\theta_Y \cos\theta_X \\ \sin\theta_Z \cos\theta_Y & \cos\theta_Z \cos\theta_X + \sin\theta_Z \sin\theta_Y \sin\theta_X & -\cos\theta_Z \sin\theta_X + \sin\theta_Z \sin\theta_Y \cos\theta_X \\ -\sin\theta_Y & \cos\theta_Y \sin\theta_X & \cos\theta_Y \cos\theta_X \end{bmatrix}$$

To solve for the CA, the following equations may be used:

$$\theta_Y = \sin^{-1}(-R_{31}) \qquad \text{Eq. 1-15}$$

$$\theta_X = \sin^{-1}\left(\frac{R_{32}}{cos(\theta_Y)}\right) \qquad \text{Eq. 1-16}$$

$$\theta_Z = \sin^{-1}\left(\frac{R_{21}}{cos(\theta_Y)}\right) \qquad \text{Eq. 1-17}$$

where θ represents the rotation about the X, Y, or Z axis, and R_{ij} is the element of the rotation matrix in row i and column j. The second rotation, occurring along the y-axis, is used to calculate the remaining rotations along the x- and z-axis (equations 1-16 and 1-17, respectively). Notice that if the rotation about the y-axis reaches 90 degrees the denominator of the two equations becomes

zero, thus undefined. This can be troublesome with joints that have high mobility, such as the shoulder joint. Therefore, CA have been limited to joints that move primarily in a single plane such as the knee.

1.2.2.3 Helical Axis

The HA, also known as the equivalent screw axis, is a well-known concept in mechanics but infrequently used in human kinematics. However, the HA provides an alternative approach to calculating knee kinematics and can allow a more robust and supplementary characterization of knee kinematics to the CA approach.

With the HA, relative motion between segments can be described as a rotation and translation along a single axis (Figure 1-5). One advantage of the HA is that it is not constrained by gimbal lock. This is primarily because the HA describes relative movement as a simultaneous motion within the 3D planes, contrary to the sequential movement of the CA [3]. However, when characterizing the knee, the CA approach will never result in gimbal lock and is still an appropriate method to quantifying knee kinematics. A second advantage of the HA is that it is independent of the coordinate system it is defined in. In other words, the directionality and position of the HA is preserved regardless of the coordinate system used. However, it is important to note that some measures that are calculated using the HA are dependent on the coordinate system used (e.g., a measure between the HA and the femoral mediolateral axis would be dependent on how the ACS of the femur is defined, but the HA itself would not be affected by the ACS). Another limitation of the HA is that it can be difficult to conceptualize and interpret for both scientists and clinicians.

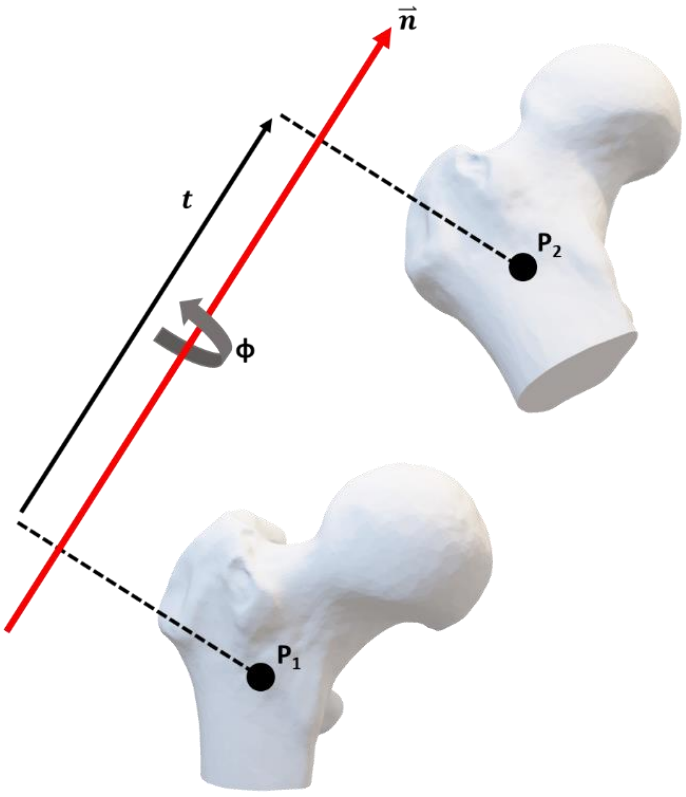

Figure 1-5 – An illustration of a femur rotating (ϕ) and translating (t) along the HA ($\vec{n}$).

There are two different forms of the HA: the instantaneous helical axis (IHA) and the finite helical axis (FHA). The FHA can be further categorized into the stepwise finite helical axis (sFHA) and reference finite helical axis (rFHA). In theory, the IHA and sFHA should provide equivalent HA [34]. However, due to error sources of the IHA and sFHA, this is typically not the case [4]. To elaborate, a more detailed description of both forms is required. The equations that are used to define the HA and its parameters are provided here. More in-depth descriptions and development of the related mathematical proofs are provided by Woltring et al. (1987) for the IHA [35] and Spoor et al. (1980) for the FHA [22].

1.2.2.3.1 Instantaneous Helical Axis

When one rigid body rotates relative to another rigid body, there will be a location of points with minimal velocity/movement. These points will lie along the IHA, which is fully defined by its directionality ($\vec{n}$), position ($\vec{s}$), translation (t), and rotation (ϕ). The directionality of the IHA is determined by the unit vector of the angular velocity vector ($\vec{w}$),

$$\vec{n} = \frac{\vec{w}}{|\vec{w}|} \qquad \text{Eq. 1-18}$$

The location of points with minimal movement defines the position of the IHA, determined as,

$$\vec{s} = \vec{p} + \vec{w} \times \frac{\dot{\vec{p}}}{|\vec{w}|^2} \qquad \text{Eq. 1-19}$$

where $\vec{p}$ is the translation vector of the rigid body's origin with respect to a global coordinate system, and '×' represents the cross product [35].

The magnitude of translational velocity (v) along the IHA is determined by projecting $\dot{\vec{p}}$ onto the IHA,

$$v = \vec{n} \bullet \dot{\vec{p}} \qquad \text{Eq. 1-20}$$

where '•' represents the dot product. The magnitude of rotation (ϕ) and translation (t) along the IHA can be calculated as the time (τ) integral of $|\vec{w}|$ and v, respectively (equations 1-21 and 1-22) [35],

$$\phi = \int_0^\tau |\vec{w}| \qquad \text{Eq. 1-21}$$

$$t = \int_0^\tau v \qquad \text{Eq. 1-22}$$

The IHA has the advantage of characterizing a joint's axis of rotation at any instance in time. However, as can be seen in equation 1-19, if the angular velocity approaches zero, the IHA

becomes undefined. Furthermore, determining the directionality of the IHA requires the process of differentiating angular rotations to obtain angular velocities. It is a well-known phenomenon that the differentiation process can amplify any noise (large or small) within the data [36], producing ill-defined IHA [35]. To overcome this differentiation problem, the FHA was introduced as a method to estimate the IHA.

1.2.2.3.2 Finite Helical Axis

The FHA characterizes the relative movement of two bodies between two discrete (finite) time points. The FHA approach can be subdivided into the stepwise FHA (sFHA) and reference FHA (rFHA). Both methods calculate the FHA similarly, with the only distinguishing factor being the location of the discrete time points. The sFHA is calculated from time points of neighbouring locations, while the rFHA is calculated from single time points relative to a reference position (Figure 1-6).

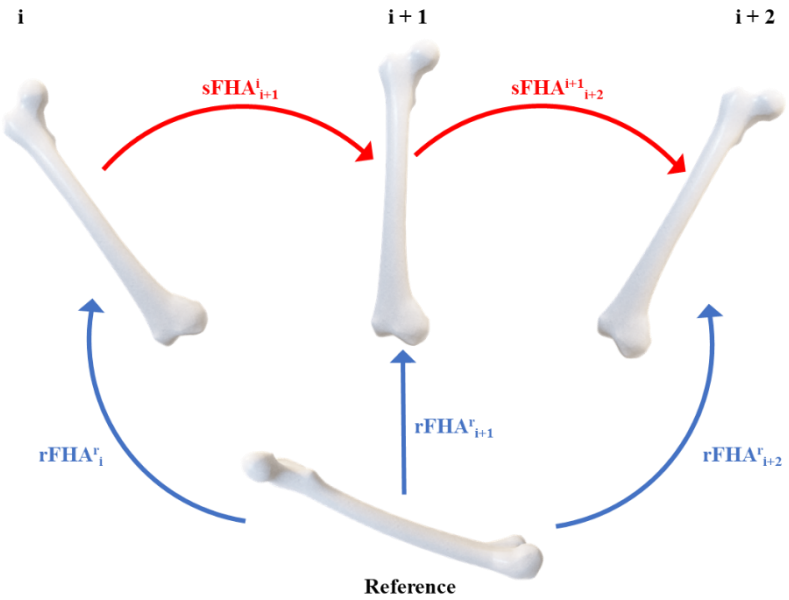

Figure 1-6 – Diagram of the discrete time points for the sFHA (red) and rFHA (blue). The sFHA is calculated between time points at neighbouring locations (e.g., i to i + 1, i + 1 to i + 2), while the rFHA is calculated from a single time point at the reference position 'r' (e.g., r to i, r to i + 1, r to i + 2).

The purpose of the reference position in the rFHA is to allow larger angular displacements between each frame, thus reducing FHA errors associated with small angular displacements (elaborated on later in this section). A method to reduce these errors with the sFHA is to calculate it at specific knee F/E intervals (e.g., 5 or 10 deg intervals). However, this reduces the temporal resolution of the sFHA, while the rFHA maintains temporal resolution. A study by Bishop et al. (2018) compared the errors associated with the sFHA and rFHA [5]. This was performed by calculating both the sFHA (at 5 deg increments) and the rFHA for a single female participant (age: 23 yrs, BMI: 22.1 kg/m^2) during two movement tasks: 1) seated leg swing and 2) single leg squat. The participant was also recorded in a seated position with their knee in 90 deg of flexion. This position was used as the reference position for the rFHA. Using error propagation formulas established by Woltring et al. [37], the rFHA showed a substantial decrease in error with its directionality and

position when compared to the sFHA. In addition to the error analysis, seven rFHA measures (explained later in section 2.3) were compared between the two methods. Visually, the rFHA provided a continuous representation of motion while the sFHA provided a more "fanned out" and discontinuous representation of knee movement. As a consequence, differences were noted between the sFHA and rFHA within the seven measures, such as increased magnitudes of dispersion with the sFHA [5]. It is clear that calculating the sFHA at specific intervals, thus reducing temporal resolution, still contains errors that may influence the final outcome measures. The FHA, like the IHA, is fully defined with its directionality, position, rotation, and translation. However, the equations used to quantify these variables are more complex. The relevant equations are provided here. Details regarding the origin and development of these equations can be found in Spoor et al. (1980) [22]. Assuming there is a rotation matrix [R_{ij}] that defines the rotation from time A to time B, with elements in row i and column j, the magnitude of rotation (ϕ) along the FHA can be calculated using,

$$\phi = \sin^{-1}\left(\frac{1}{2}\sqrt{(R_{32}-R_{23})^2+(R_{13}-R_{31})^2+(R_{21}-R_{12})^2}\right) \quad \text{Eq. 1-23}$$

or,

$$\phi = \cos^{-1}\left(\frac{1}{2}(trace(R)-1)\right) \quad \text{Eq. 1-24}$$

Either of these equations may be used to determine ϕ, but equation 1-23 is preferred if $sin(\phi) \leq \frac{\sqrt{2}}{2}$, and equation 1-24 if $sin(\phi) > \frac{\sqrt{2}}{2}$ [22]. Once ϕ is known, the directionality of the FHA may be determined by first computing the 3x3 matrix *N*,

$$N = \frac{1}{2}(R+R^T) - cos(\phi)I = [\{\vec{n}_1\},\{\vec{n}_2\},\{\vec{n}_3\}] \quad \text{Eq. 1-25}$$

where 'I' is a 3x3 identity matrix. *N* contains three vectors ($\vec{n}$) that run parallel with the FHA, the best vector to select is the one with the largest magnitude [22]. Therefore, the directionality of the FHA is calculated using,

$$\vec{n} = \frac{\vec{n}_{max}}{|\vec{n}_{max}|} \quad \text{Eq. 1-26}$$

The sign of $\vec{n}$ must be chosen such that the rotation in equation 1-24 remains positive [22]. In other words, if ϕ is negative, the directionality vector $\vec{n}$ is flipped. The translation (*t*) along the FHA and the position ($\vec{s}$) of the FHA are calculated with the following equations,

$$t = \vec{n} \bullet \vec{r} \quad \text{Eq. 1-27}$$

$$\vec{s} = -\frac{1}{2}\vec{n} \times (\vec{n} \times \vec{r}) + \frac{sin(\phi)}{2(1 - cos(\phi))}(\vec{n} \times \vec{r}) \quad \text{Eq. 1-28}$$

where $\vec{r}$ is the translation vector of the rigid body from time A to time B, and $\vec{s}$ is the shortest perpendicular vector from the rigid body origin to the FHA [22].

For the FHA to most accurately depict the IHA, small time ranges must be used. However, using small time ranges typically coincides with small angular displacements, and the FHA is susceptible to errors with small angular displacements [4], [38]. This is most obvious in equation 1-28, where smaller magnitudes of ϕ will produce a denominator closer to zero, resulting in a FHA with a position approaching infinity or that is undefined. Therefore, a compromise must be made when using the FHA; use sufficiently large displacements to avoid errors, but not too large to dissociate the FHA with the IHA [39]. This is the predicament between the sFHA and rFHA. The sFHA will provide smaller angular displacements, representing an axis more equivalent to the IHA. In contrast, the rFHA is purposely used to provide larger angular displacements, reducing the errors associated with small displacements, but does not represent the IHA. As a consequence, absolute measures of the sFHA provide more clinically meaningful values (e.g., location of the sFHA

relative to the joint centre) while the absolute measures of the rFHA do not. However, the rFHA may still show promise when characterizing relative patterns of knee kinematics, as it greatly reduces the errors associated with small angular displacements [5]. This is evident in prior work by Bishop (2015), which determined kinematic differences in ACLD knees during a single leg squat and seated leg extension [40]. However, further assessments of the rFHA are required, specifically for different movements and different tibiofemoral OA risk populations (e.g., ACLR or older knees).

1.2.3 Structure of Cartilage

The primary functions of cartilage are to provide joints a smooth, low friction surface to articulate on, as well as to distribute loads within the joint [9]. Cartilage is a unique tissue; being avascular, aneural, and alymphatic, cartilage has a slow turnover rate and lacks the ability to repair itself (unless under certain biological conditions) [9], [10]. Three categories of cartilage exist: hyaline, elastic, and fibrous [11]. Hyaline cartilage resides within the joints and is commonly referred to as articular cartilage [9]. Articular cartilage contains an extracellular matrix formed by chondrocytes (the only cells present within the cartilage). The main component of the extracellular matrix is water, making up 65% to 80% of cartilage's wet weight. Collagen (primarily type II) constitutes between 10% to 20% of cartilage wet weight. Proteoglycans, such as aggrecan and lubricin, comprise the third main component and may also contribute 10% to 20% of the wet weight of cartilage [11]. The primary function of aggrecan is to maintain water retention within the extracellular matrix, while the role of lubricin is to provide a lubricated surface [11], [12]. Four zones are identified to describe the structure of cartilage: the superficial zone, the middle zone, the deep zone, and the calcified zone (Figure 1-7). Each zone is speculated to perform a specific function [9].

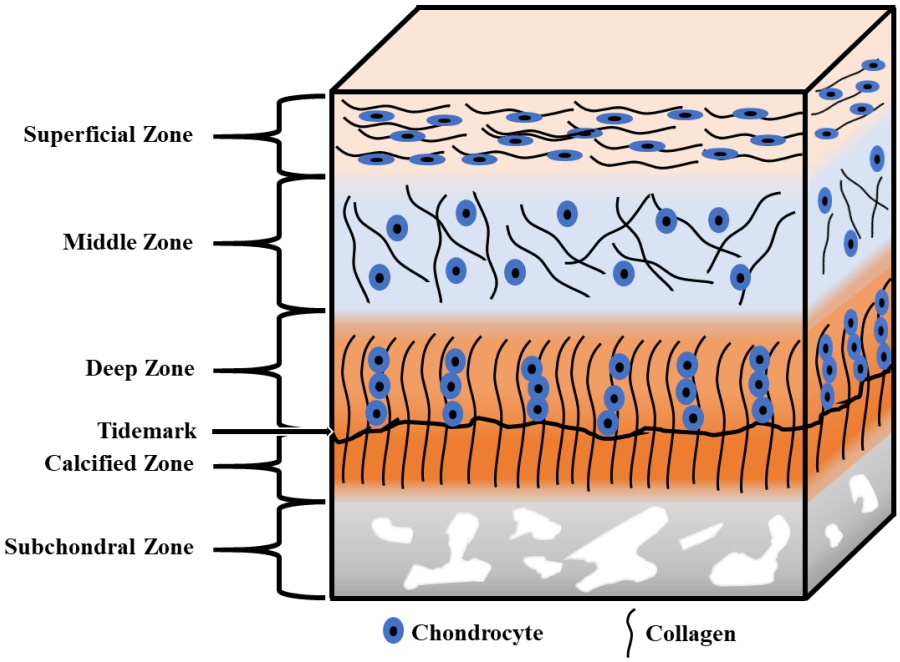

Figure 1-7 – An illustration of cartilage structure and zones.

The superficial zone contributes to approximately 10% to 20% of the cartilage thickness from the surface. Collagen fibers are aligned primarily parallel with the articular surface and provide most of the cartilage's tensile strength. The highest concentration of chondrocytes is in this zone, containing a "flattened" shape and lined by synovial fluid [41]. The synovial fluid provides lubrication at the cartilage surface, resisting shear forces [41], [42].

Underneath the superficial zone is the middle zone, representing 40% to 60% of the cartilage thickness. The collagen fibers are aligned primarily obliquely and contain a small, dispersed proportion of spherical chondrocytes. The middle zone assists in resisting compressive and shear forces applied to the cartilage [42].

The deep zone consists of 30% of the cartilage thickness. The collagen fibers are aligned primarily vertically (perpendicular to the articular surface) and have the largest diameter [41]. Additionally, the deep zone has the largest number of proteoglycans and lowest water content [42]. These characteristics allow the deep zone to provide primary resistance to compressive forces. The

chondrocytes are organized in columns, parallel to the collagen fibers. The final calcified zone acts as a transitional area for the cartilage to attach to the subchondral bone [42], [43]. This connection (or boundary) between the deep zone and calcified zone of the cartilage is visible through a microscope and is called the tidemark [44].

1.2.4 Aging & Osteoarthritis

Osteoarthritis (OA) is the most common joint disease in Canada, with approximately 10% of Canadians living with the disease, followed by rheumatoid arthritis at 1% [45]. Additionally, OA appears to develop more frequently in females [46] with a 3% greater prevalence than males [45]. Due to its high prevalence rate, costs associated with OA are significantly greater than other musculoskeletal diseases [47]. In 2010, costs in Canada were estimated to range between $1.2 to $4.2 billion dollars. Unfortunately, the prevalence of OA continues to increase, with a projected increase of 13.8% to 18.6%, producing increased costs of $2.9 to $7.6 billion dollars by 2031 in Canada [48]. The increase of OA within the population may be associated with a larger number of individuals above the age of 60 years [49]. A study performed in British Columbia (2015) reported that by age 80, 30% of men and 40% of women were living with osteoarthritis [49]. It is also known that OA and age share a strong positive relationship [49], [50]. Therefore, it is evident that aging has a significant role on the formation of OA, and is considered a strong risk factor [51].

OA is a complex disease that not only involves degradation of articular cartilage, but an interplay of the various joint components (i.e., cartilage, synovium, and bone) [51]. Therefore, there are several risk factors of aging that may contribute to the development of OA, including metabolism, genetics, cartilage and bone processes, joint kinematics, and muscle strength and activation patterns [46], [52]. Alterations or abnormalities of these factors may influence the onset or progression of OA [46]. Section 1.2.4.2 elaborates on joint kinematics and its role in OA. However, biological implication of OA will be first explained in the next section.

1.2.4.1 Biological Implications of OA

In the early stages of aging, cartilage demonstrates abnormalities within the superficial zone, resulting in higher susceptibility to injury from mechanical forces [53]. First, increased proteolytic activity within the extracellular matrix reduces the effectiveness of the collagen to resist tensile and shear forces acting on the cartilage [53], [54]. There is also a loss of aggrecan that results in a lessened ability for the cartilage to retain water, thus influencing its structural integrity when exposed to forces [53], [55]. Another common change is the formation of calcium crystals within the chondrocytes. The appearance of these crystals is generally accepted as a precursor to OA [56]. Furthermore, it is commonly seen that the greater the calcification of the cartilage, the greater the severity of the disease. This may be due to the chondrocytes releasing extracellular matrix degrading enzymes in response to the calcification, accelerating the progression of OA [53], [56]. Lastly, the concentration of chondrocytes within the cartilage lessens with age, potentially due to cellular apoptosis [57]. This results in a substantial loss of extracellular matrix maintenance and lubrication in the superficial layers. Additionally, aging chondrocytes develop a reduced capacity to respond to growth factors, resulting in a lower turnover rate [53].

Bone also reveals age and OA related changes within its structure, especially near the subchondral bone region [43]. Schaffler et al. (1995) tested several cortical bone samples and determined that age has a strong positive relationship with the number of microcracks found within the bone [58]. This may be due to the remodeling and modeling processes (via osteoclasts and osteoblasts) of the bone becoming unbalanced with aging [44]. Therefore, there is insufficient repair in the bone and subsequent microcracking. If these microcracks are within the subchondral region of the bone, it is evident that the biological response is to thicken the cortical bone of the subchondral region [59]. A thickening of the subchondral region has been associated with OA changes [60]. Consequently, there is a migration of the tidemark towards the deep zone of the cartilage [44]. As

the tidemark progresses towards the cartilage, the calcified cartilage region increases and the articular cartilage becomes thinner, thus becoming more susceptible to further microcracking and OA onset [59]. Lastly, osteophytes may be formed from the calcification of the distal cartilaginous matrix, and are a recognized feature of OA progression [44].

Ligaments, specifically the anterior cruciate ligament (ACL), may also undergo changes with aging. The earliest sign of ACL degeneration may appear as disorganized collagen fibrils, in conjunction with a decrease in fibril diameter [61]. Signs of inflammation, cystic areas, and calcium deposits may exist as well [62]. The amount of degeneration has been positively correlated with cartilage damage, suggesting that external factors may assist in the degeneration of ligaments [62]. A similar crosstalk phenomenon may be present in bone and cartilage as well. Uncalcified cartilage has been seen to bypass the tidemark to connect with the underlying calcified cartilage and subchondral bone, suggesting local cellular communication between the two tissues [63].

1.2.4.2 Joint Kinematics & OA

The healthy knee joint is a crucial component of human gait, maintaining a consistent kinematic cycle while tolerating forces 2-4 times our body weight [64], [65]. Any disruptions to this kinematic cycle may lead to alterations in the mechanical environment of the cartilage [64], prompting the development of OA [52]. To elaborate, the cartilage is adapted to the normal kinematic cycle of the individual. A study by Koo et al. (2011) reported that within the knee cartilage was thicker in areas of most frequent contact between the femur and tibia [66]. This thickness variation is speculated to allow cyclic forces to act at specific locations within the knee [67]. However, once the kinematic cycle is altered, forces within the knee may act at location within the cartilage that are thinner and unadapted to these greater loads. Consequently, this may lead to increased rates of cartilage thinning, or “wear and tear” damage [64]. This thinning may result from elevated levels of shear forces due to increased tibiofemoral sliding [68], increased

compressive loads [1], altered contact mechanics [64], and increased rotation of the tibia [69]. The thinning of articular cartilage via calcification (refer to section 1.2.4.1) may also impact the thickness adaptations that the cartilage has formed throughout time, contributing to the formation of tibiofemoral OA [1].

The kinematic alterations related to tibiofemoral OA are more frequently involved within the medial compartment of the knee [70]. This may be due to the fact that the medial compartment typically sustains 2.5 times more body weight than the lateral compartment [71]. These kinematic alterations may originate from muscle weakness, lack of proprioception, obesity, altered bone shape, joint space narrowing, increased joint laxity, and injury/pain. These are all factors associated with aging as well [9], [46], [72], [73]. Due to such a wide range of factors influencing tibiofemoral OA, it has been reported as the most common type of joint OA and is one of the largest contributors to a burden for lifestyle and healthcare costs [50].

1.3 Summary & Knowledge Gaps

CA have been the dominant method to characterize altered knee kinematics of tibiofemoral OA prone populations (e.g., aged and injured knees). However, there is inconclusive evidence to indicate what these changes are, as well as the magnitude of these potential changes. This discrepancy in study findings may be partially attributed to limitations of the OMCS and associated skin movement artifacts, providing kinematic errors that are larger than the subtle kinematic changes that exist with tibiofemoral OA. Additionally, CA are prone to crosstalk errors and gimbal lock, and are therefore dependent on the accuracy of the ACS and sequence of rotations chosen. Considering the CA limitations, the HA may provide a valuable alternative and supplementary method to quantify knee kinematics.

The HA is not commonly used in biomechanical applications and has been applied to the knee joint within few contexts. The overall applicability of the HA has its shortcomings, relating to the

derivations of angular displacement required to calculate the IHA (making it susceptible to error amplification) and the trade-off between accuracy and temporal resolution required with the sFHA. Alternatively, the rFHA maintains temporal resolution by using a reference position to provide large angular displacements. However, the rFHA does not accurately represent the IHA. The majority of the literature that has used the HA (either IHA, sFHA, or rFHA) to describe the kinematics of the knee has been qualitative with quantitative investigations lacking [3]. For example, the sFHA has been illustrated graphically at specific knee angles, providing an excellent visualization of the movement of the sFHA [74], [75]. Only few studies have quantified the magnitude and variability of sFHA measures within a specific population, such as older [76], ACLD [77], and ACLR [78] individuals. Additionally, the rFHA has only been used in a single study that demonstrated kinematic differences between the injured and contralateral healthy knees of ACLD participants [40]. The rFHA, with its ability to maintain temporal resolution, can provide kinematic information at time frames that would have otherwise been missed using the sFHA. Additionally, the rFHA has the advantage of characterizing knee rotations and translations about a single axis, avoiding the influence of crosstalk errors as seen with the use of CA. Therefore, the rFHA has the ability to measure the overall stability of the knee rather than categorizing the knee into planar movements. This could provide insight to how the rotations and translations of the knee interact with each other, which the CA approach is unable to do. However, because of its limited use the rFHA requires further technical assessments and practical applications to determine whether it is a suitable approach to assessing kinematic differences between healthy and tibiofemoral OA prone populations.

1.4 Objective & Specific Aims

The objectives of this thesis were as follows:

1. To advance the applicability of the rFHA in describing clinically relevant knee joint kinematics by evaluating its accuracy within the HSBV and its sensitivity to errors. This will provide technical considerations when using the rFHA to characterize knee kinematics most accurately.
2. To determine if the rFHA is capable of distinguishing knee kinematics of individuals at higher risk for tibiofemoral OA, such as older or injured knees.

The first objective was achieved through the following specific aims (SA):

SA 1. Determine the accuracy of the rFHA within the HSBV, and how different smoothing techniques applied to the ATM from the HSBV data may improve the accuracy (Chapter 3).

SA 2. Assess the mean differences and variabilities of the rFHA measures to reference position misalignments, thus establishing how sensitive the measures are to changes in the reference position (Chapter 4).

SA 3. Compare rFHA measure differences between the OMCS and HSBV to characterize potential skin movement artifact errors during movement tasks; and to identify rFHA measures that contain the least errors and therefore can be used with most confidence (Chapter 5).

The second objective will be achieved through the final SA:

SA 4. Apply the rFHA to two groups of individuals at higher risk of tibiofemoral OA (specifically youths with a history of ACL injury and older, asymptomatic individuals) to characterize the knee kinematics during various movement tasks and compare them to healthy controls. (Chapters 6 and 7).

1.5 Thesis Outline

The next chapter (Chapter Two) reviews the relevant tibiofemoral OA kinematic findings using both CA and rFHA methods, outlining the current knowledge gaps. The next five chapters of this thesis (Chapters Three to Seven) will focus on the evaluation and application of the rFHA, each relating to a SA of this thesis. Figure 1-8 provides the overall organization of these chapters, with each SA highlighted in orange.

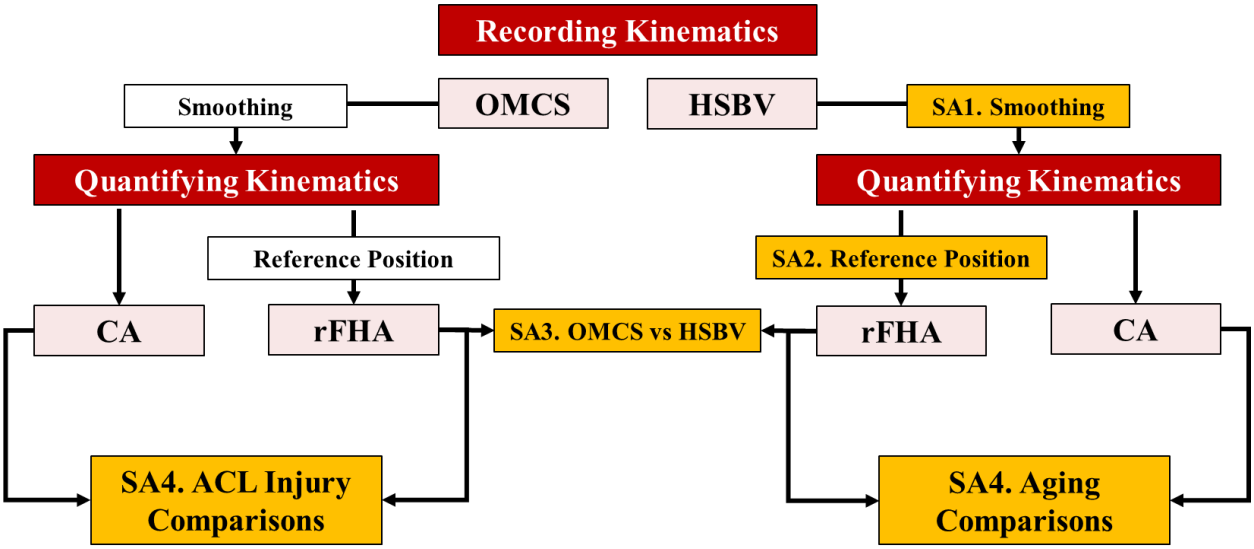

Figure 1-8 – A flow chart illustrating the organization of Chapters Three to Seven. Each chapter focuses on an individual specific aim (highlighted in orange).

To reiterate, characterizing kinematics of the knee first involves the process of recording movements of the thigh/femur and shank/tibia (Figure 1-8). This can be achieved using methods such as the OMCS and HSBV (section 1.2.1). Afterwards, the recorded data is commonly smoothed to minimize errors within the data (e.g., skin movement artifacts with the OMCS or 2D/3D registration misalignments with the HSBV). Chapter Three focuses on SA 1 of this thesis, investigating for the first time the rFHA accuracy when applying several smoothing techniques to ATM from 2D/3D registration (Figure 1-8, SA1. Smoothing). After smoothing the data, the

kinematics of the knee may be quantified, typically with the CA or HA (IHA, sFHA, or rFHA) approach (section 1.2.2). When using the rFHA, a reference position is required to provide large angular displacements. The influence of misaligned reference positions is still unknown (SA 2). Therefore, Chapter Four investigates the sensitivity of the rFHA when deviations of the reference position are present (Figure 1-8, SA2. Reference Position). When calculating the rFHA, it is still unknown how potential skin movement artifacts may influence the final rFHA measures of interest (SA 3). Consequently, Chapter Five investigates the differences in rFHA measures when using two imaging modalities: 1) the OMCS which is susceptible to skin movement artifacts and 2) the HSBV which does not require skin mounted reflective markers (Figure 1-8, SA3. OMCS vs HSBV). Finally, like the CA approach, the rFHA may be a useful method to characterize kinematic differences associated with tibiofemoral OA and better understand the disease. Chapters Six and Seven investigate the utility of the rFHA to evaluate two different tibiofemoral OA prone populations: 1) youth individuals with ACLD (Figure 1-8, SA4. ACL Injury Comparisons) and 2) older individuals with asymptomatic knees (Figure 1-8, SA4. ACL Aging Comparisons). The final chapter of this thesis (Chapter Eight) provides a summary of the thesis and future directions.

Chapter Two: Kinematics of Knee Osteoarthritis

2.1 Introduction

Knee kinematics are one of the crucial factors associated with tibiofemoral OA onset/progression. CA have been the conventional method used to quantify knee kinematics but have certain limitations, such as crosstalk. As a result, the HA was introduced as an alternative method, having its own advantages and disadvantages [35], [37]. The HA has not been widely used in biomechanics but shows promise in characterizing knee kinematics. This chapter provides a review of the current knee kinematic findings associated with tibiofemoral OA when using either CA or the HA.

2.2 Cardan Angle Kinematics

2.2.1 Walking

Walking is the primary method of locomotion for humans. It is not only important for transportation but is also associated with health benefits, such as lowered risk for cardiovascular disease [79]. Kinematic alterations of the gait cycle have been associated with OA progression, especially within the knee which tolerates forces two to four times our body weight [65], [80]. These alterations may originate from aging, due to muscle strength deficits [81] and changes in neuromuscular control [82]. Despite the risks associated with altered gait, most older individuals are still required to perform the task of walking to perform daily activities. As such, there is a need to understand the kinematic changes that occur with tibiofemoral OA to better inform rehabilitative programs and retain normal kinematics.

Differences in peak knee flexion angles have tended to be consistent, with older and tibiofemoral OA individuals having greater peak knee flexion angles throughout the gait cycle than healthy controls [83]–[86]. However, knee flexion angles from different studies have been contradictory at the loading response of gait (i.e., heel strike). Individuals with tibiofemoral OA have

demonstrated either greater knee flexion [14], [82], [86], lower knee flexion [14], [70], [87], or no differences [88] when compared to controls. Favre et al. (2014) suggested that these inconsistencies are associated with the experimental design of the studies; each using different data acquisition protocols and inclusion criteria (e.g., the location and severity of OA, age of the participants, and ground versus treadmill walking). Therefore, Favre et al. conducted a study that controlled for these confounding variables [89]. The study involved four cohorts (n = 110): younger asymptomatic (n = 29), older asymptomatic (n = 27), older moderate tibiofemoral OA (n = 28), and older severe tibiofemoral OA (n = 26). All tibiofemoral OA participants were diagnosed with medial tibiofemoral OA and could not have OA or an injury in any other lower extremity joint. All participants performed overground walking within an OMCS at their preferred speed and footwear. Two additional walking speeds were collected as well, one faster and one slower than the preferred speed of the participant (speeds were not specified). Knee kinematics were compared between all four groups during the full gait cycle of the knee of interest. Compared to the younger asymptomatic group, flexion at heel strike increased with age (4.1 deg increase) and severity of tibiofemoral OA (moderate: 4.3 deg increase, severe: 8.7 deg increase). The older severe tibiofemoral OA group also had greater knee flexion angles than the older asymptomatic group (4.6 deg increase) and older moderate tibiofemoral OA group (4.4 deg increase). Minimal differences between the moderate tibiofemoral OA and older asymptomatic group were found [89]. Significant findings were also determined at terminal stance, where the older severe tibiofemoral OA group demonstrated greater knee flexion than the younger asymptomatic group (7.1 deg increase) and older moderate tibiofemoral OA group (6.0 deg increase). These results highlighted an increase in knee flexion angle with aging, and further increases associated with the progression of medial tibiofemoral OA. This may relate to the onset/progression of tibiofemoral OA, as

increased magnitudes of knee flexion during heel-strike have been reported to promote thinning of the medial tibiofemoral cartilage due to altered contact locations. Furthermore, an increase in knee flexion during the loading phase was speculated to increase muscular co-contractions, increasing the load within the knee and promoting cartilage degradation [90].

The internal/external rotation of the knee has also shown inconsistent findings between different studies of tibiofemoral OA. Bytyqi et al. (2014) investigated the knee kinematics of thirty medial tibiofemoral OA participants and age-matched controls while walking on a treadmill at a self-selected speed [84]. During stance phase, specifically midstance, a decrease in tibial internal rotation (or a more 'neutral' tibia) was reported for participants with medial tibiofemoral OA when compared to the control group (OA group: -0.5 ± 0.4 deg, control group: -2.0 ± 0.7 deg). This was supported by another study from Weidow et al. (2016) that investigated knee kinematics of thirty symptomatic women (fifteen medial tibiofemoral OA and fifteen lateral tibiofemoral OA) and fifteen asymptomatic controls [91]. Knee kinematics were calculated during overground walking at a self-selected speed. The study determined that participants with medial tibiofemoral OA were significantly more externally rotated (median [range]: -17 [-27-3] deg), and those with lateral tibiofemoral OA were more internally rotated (-2 [-16-10] deg), when compared to the controls (-8 [-23-2] deg) at midstance. It was suggested that these differences may originate from abnormal hip kinematics, where the misaligned femur from the hip carries over to the femorotibial alignment [91]. Contrary to the previous studies, Nagano et al. (2012) found no differences in knee internal/external rotation at midstance [87]. This study investigated the kinematics of forty-five individuals with different tibiofemoral OA severities (early [n = 14], moderate [n = 17], and severe [n = 14]) and thirteen controls. Participants were asked to perform overground walking at a self-selected speed. At midstance, no significant differences in external tibial rotation were observed

(mean [SD] of controls: 1.6 [3.7] deg; early: 1.1 [3.5] deg; moderate: -0.7 [4.8] deg; severe: 0.6 [3.3] deg).

The knee angle within the frontal plane has been a consistently reported Cardan angle measure between different studies. Medial and lateral tibiofemoral OA have been associated with an increase in static knee adduction/varus and abduction/valgus angles, respectively, due to joint space narrowing [92]. Similar findings of increased knee Ab/Ad alignments have been reported during dynamic movements as well, such as walking. During the gait cycle, greater adduction angles have been associated with medial tibiofemoral OA [80], [83], [84], [87], [88], [91], and greater abduction angles with lateral tibiofemoral OA [14], [91]. These increased angles are speculated to provide greater magnitudes of load on the affected side of the knee, thus promoting the degradation of cartilage [1].

Despite some of these seemingly consistent findings, a meta-analysis of 41 publications performed by Mills et al. (2013) determined that knee kinematics calculated with CA still provide limited or conflicting evidence with respect to tibiofemoral OA severity [2]. Specifically, the effect sizes calculated for the knee kinematic variables did not exceed a value of 1.2 (i.e., mean differences did not exceed 1.2 SD). According to the criteria established by Hopkins et al. (2009), a large effect is considered if the effect size is greater than 1.2 [93]. The lack of larger effect sizes was attributed to the heterogeneity of the samples used in each study [2]. A similar finding was determined from a meta-analysis by Boyer et al. (2017) to assess knee kinematic differences in the sagittal plane between younger and older individuals using the OMCS and CA [94]. A small effect size was determined for knee kinematics (effect size = -0.40) and a moderate effect size for knee range of motion (RoM; effect size = -0.70). This was attributed to the inconsistent findings from several studies [94]. These inconsistencies may originate from skin movement artifacts originating

from reflective skin markers [95] and inaccuracies of axes alignment resulting in crosstalk [87], [96]. Further research is still required to determine the contribution of these methodological issues to the variability of reported knee kinematics.

2.2.2 Vertical Drop Jump

The vertical drop jump (VDJ) is a commonly used test to assess motor control and knee stability [97]. It is a useful test in the kinematic assessment of anterior cruciate ligament (ACL) injuries, as the VDJ landing requires a large contribution from the quadriceps and hamstrings to maintain knee stability [98]. However, studies comparing VDJ knee kinematics of healthy and ACL impaired individuals have provided inconclusive evidence to suggest any differences exist.

Decker et al. (2002) compared the landing strategies of eleven healthy and eleven ACL reconstructed (ACLR) participants during a VDJ from a 60 cm box [98]. Participants were matched by age, sex, experience in jumping and landing sports, footfall patterns, and landing stiffness. Footfall patterns and landing stiffness were assessed after data collection and used to match the participants for statistical analysis. Knee flexion angle was used to indicate whether an individual was a ‘soft’ lander or a ‘stiff’ lander. Participants were labelled as soft landers if they reached knee flexion magnitudes greater than 90 deg when landing. In contrast, those labelled as stiff landers did not reach knee flexions greater than 90 deg. On average, both groups performed a soft-landing strategy. Additionally, the ACLR group tended to have a more extended knee position at initial impact than the healthy group (ACLR: -26.35 [7.73] deg; Healthy: -29.91 [5.98] deg). However, this finding was not statistically significant [98].

In a more thorough knee kinematic analysis, Delahunt et al. (2012) investigated the differences in VDJ knee kinematics within all three planes (drop height was 35 cm) [99]. Fourteen ACLR females were recruited for this study and compared to matched (age, sex, and sport) controls. Knee F/E, Ab/Ad, and I/E rotation were calculated during the initial contact of the VDJ to 200 ms post-

contact. Knee angles were compared between the two groups throughout the timeframe. Compared to the controls, a significantly more extended knee (up to 10 degrees) was found in the ACLR group during the later stages of initial contact; between 106-182 ms post-impact. Additionally, knees in the ACLR group were less adducted angles (up to 8 degrees) when compared to the controls, from 78-104 ms and 146-200 ms post-impact. No differences were found in the I/E rotation of the knee. The kinematic differences in the ACLR group were suggested to be a mechanism of ACL-injury. Specifically, the decrease in knee flexion during the impact phase may increase anterior shear forces in the knee, producing greater amounts of strain on the ACL. Furthermore, a decrease in knee adduction, or an increase in knee abduction, during the first 40 ms of ground impact has been associated with ACL injury [99].

In contrast, Clarke et al. (2015) was unable to detect any kinematic differences between eighteen participants with ACLR and eighteen healthy matched (sex, height, age and sport) controls [100]. Limb comparisons within the ACLR group were also performed in this study. The knee peak angles and RoM were calculated during the total stance phase of the VDJ (impact to lift off) and the first 40 ms post-impact for a drop height of 30 cm. No kinematic differences were found within the knees of the ACLR group. Additionally, no differences were found in the peak knee angles between the ACLR and healthy groups. The magnitudes of these insignificant differences in kinematics were not provided. A significant increase in RoM for knee I/E rotation was reported in the ACLR group in comparison to the controls (total stance phase: 1.58 deg; 40 ms post-impact: 2.34 deg). The authors cited adaptations occurring within the ACLR limb over time as a potential explanation for the lack of significant differences [100]. However, this study and the Delahunt et al. (2012) study [99] both had participants with ACLR whose time since surgery was four to five years. Therefore, the inconsistencies between these studies despite similar inclusion criteria could

be explained by methodological limitations associated with the use of conventional CA and the OMCS (refer to sections 0 and 1.2.1.1).

2.3 Helical Axis Kinematics

The HA has been used to characterize knee kinematics within multiple contexts. Several studies have used the HA to describe the motion of the knee qualitatively, and others quantitatively. For the qualitative studies, descriptions of the knee will be provided but values associated with these descriptions may not have been reported. Values of the HA measures will be provided when possible. A description of the main HA outcome measures is provided for clarity. Seven HA measures are commonly used to quantify knee kinematics, and can be reported with respect to the femur or tibia (Figure 2-1):

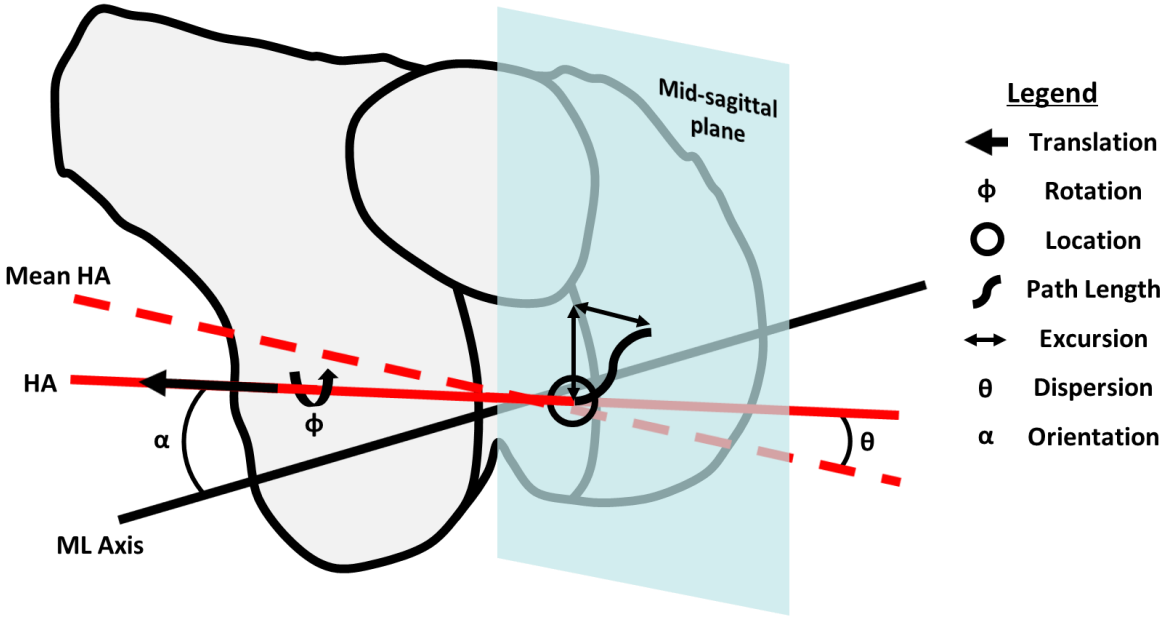

Figure 2-1 – Illustration of the six HA measures relative to the femur: translation (←), rotation (ϕ), location (O), path length (–), excursion (↔), dispersion (θ), and orientation (α). These measures can be calculated relative to the tibia as well.

1. **Translation (←)** – The summed magnitude of translation along the HA, thus representing the overall displacement the femur or tibia performed. The sign of the translation (positive or negative) dictates the direction of the displacement along the HA. A positive translation represents an overall displacement in the positive HA direction, while a negative translation represents an overall displacement in the negative HA direction.
2. **Rotation (ϕ)** – The magnitude of rotation along the HA throughout the movement. The rotation may be further multiplied by the directionality of the HA ($\vec{n}_i$) to obtain the helical angles (equation 2-1, where $\vec{n}_i$ represents the three components of the unit vector [$\vec{n}_1$, $\vec{n}_2$, $\vec{n}_3$]). The helical angles are similar to the CA, providing three individual rotations within the anatomical planes. However, due to the HA advantages (section 1.2.2.3), the helical angles are not susceptible to crosstalk errors [101].

$$Helical\ angles\ =\ \phi\ *\ \vec{n}_i \qquad \text{Eq. 2-1}$$

3. **Location (O)** – The mean antero-posterior (AP) and supero-inferior (SI) intersection of the HA with the mid-sagittal plane of the femur or tibia. This intersection is an approximation of the knee's center of rotation in the sagittal plane [102]. The AP and SI locations are viewed as a descriptor of rolling/sliding of the knee joint. If the locations have a magnitude of zero (on the origin of the bone), pure rolling has occurred with no translation. If AP location contains a more anterior location, the tibia or femur may have translated more anteriorly, as seen in ACLD individuals [77]. Additionally, if the SI location increases in magnitude (moving away from the origin), the magnitude of translation will also increase [102]. Therefore, if the HA is closer to the origin on the lateral side of the bone, and further away on medial side of the bone, one can speculate that there was more sliding on the medial side of the bone [102].

4. **Path Length (–)** – The path length is the summed 2D length/distance of the HA location trace along the mid-sagittal plane of the femur or tibia. If the HA shows larger shifts in its directionality or position, the path length will increase. Therefore, a larger path length may suggest a greater amount of femoral or tibial movement (i.e., rotations and/or translations) [40].
5. **Excursion (↔) –** The range of the path length in both the AP and SI directions along the femoral or tibial mid-sagittal plane. Larger excursions may suggest larger ranges of femoral or tibial movement [40].
6. **Dispersion (θ)** – The mean angular deviation of a single HA (i.e., at a single time point) with respect to the mean HA of the total movement. Greater magnitudes of dispersion may suggest unstable/erratic knee movements, due to motor control deficits and differences in the knee articular surface [76], [103]. In contrast, maintaining a knee motion within a constant plane will result in smaller magnitudes of dispersion because the directionality of the HA will have minimal change [76].
7. **Orientation (α)** – The mean angle of the HA with respect to the medio-lateral (ML) axis of the femur or tibia. The orientation of the HA can provide information on the coupled rotations of the knee. Specifically, if the knee is performing pure flexion, the orientation of the HA will be parallel to the ML axis of the bone. If coupled rotations exist, specifically I/E and Ab/Ad rotations, the orientation will be shifted within the coronal and transverse planes, respectively [75]. Therefore, the orientation angle may be represented as angles within those specific planes, providing information on how much coupled rotation is occurring along the I/E rotation and/or Ab/Ad axes.

2.3.1 Running

van den Bogert et al. (2008) used the sFHA to characterize running knee kinematics of three healthy males during stance phase [102]. Intracortical bone pins were used to avoid skin movement artifacts within an OMCS. The sFHA location and orientation were calculated relative to the tibia. However, the orientation was split into two separate angles (named deviation and inclination) by projecting the sFHA onto the transverse and frontal planes of the tibia. Specifically, the deviation was the angle between the sFHA and ML axis of the tibia in the transverse plane, providing an indication of Ab/Ad rotations. The inclination was the angle between the sFHA and ML axis of the tibia in the frontal plane, providing indications of I/E rotation [102].

The sFHA was located within the distal femur and possessed a primarily ML direction. During the flexion phase and initiation of the extension phase, the sFHA location shifted posteriorly approximately 30 mm. Throughout the remainder of extension phase, the sFHA location shifted anteriorly (magnitude not provided). Additionally, the sFHA was located 10 mm to 20 mm above the tibial plateau for the first half of the stance phase but followed a proximal shift (towards the femur) for the second half; the timing of this shift was slightly different for each participant. The sFHA deviation remained within 10 deg throughout the stance phase, but the sFHA inclination showed notable changes. Specifically, the sFHA showed an increase in inclination during the first half of the stance phase, then returned to the transverse plane briefly, before increasing once again during the second half of stance phase. Overall, the each of the two orientation parameters did not exceed a magnitude of 25 deg [102].

The posterior shift of the sFHA during flexion was speculated to arise from femoral rollback on the tibia, shifting the center of rotation backwards. Physiologically, this was speculated to represent an increase in the moment arm of the quadriceps muscle, reducing the force required to stabilize the knee during flexion. Furthermore, the intersection of the cruciate ligaments also

translates posteriorly during flexion of the knee and may play a role in the location of the sFHA during flexion. The angles determined for deviation and inclination were attributed to the coupled rotation of the knee during flexion. The inclination of the sFHA was angled medially (i.e., within the coronal plane, the sFHA pointed upward medially and downward laterally). It was suggested that because the lateral side of the sFHA was closer to the origin of the tibia (the tibial plateau), mainly rolling occurred on the lateral side of the knee. In contrast, with the medial side of the sFHA being further away from the origin, there was more sliding of the bones and less rollback. Therefore, the medial condyle was speculated to be the pivot of the knee joint during axial rotations [102].

2.3.2 Walking

In a recent study, kinematics of healthy/asymptomatic knees were characterized during walking using the sFHA and OMCS [76]. The sFHA was calculated in 10-degree increments of knee flexion. To assess knee stability, sFHA dispersion was compared between younger (23.3 ± 2.4 years) and older (69.3 ± 4.6 years) individuals with asymptomatic knees. Dominant knees between the groups were compared, as well as contralateral knees within each group. The dispersion of the sFHA was further divided into its sagittal, frontal, and transverse components [76]. The gait cycle was divided into four specific phases for dispersion comparisons: Phase 1) terminal swing to peak flexion in loading response, Phase 2) peak flexion in loading response to terminal stance, Phase 3) initial swing to peak knee flexion in swing phase, and Phase 4) peak flexion in swing phase to terminal swing. Significant between group differences were found in the sagittal plane dispersion of Phases 1 and 4, with older participants having greater dispersion (Phase 1 mean [SD]: younger = 12.5 [3.7] deg, older = 17.5 [5.3] deg; Phase 4: younger = 3.2 [1.2] deg, older = 4.8 [1.7] deg). Furthermore, non-dominant limbs were found to have greater dispersion than the dominant limbs. This finding was found within Phases 1 to 3 in the sagittal plane (younger difference range: 2.5-

4.0 deg; older difference range: 1.2-2.1 deg), Phase 4 in the frontal plane (younger difference: 4.4 deg; older difference: 4.2 deg), and Phases 1 and 4 in the transverse plane (younger difference range: 3.6-9.8 deg; older difference range: 2.1-2.9 deg) [76]. The increased dispersion within the elderly group was speculated to be associated with deficiencies in neuromuscular control (e.g., muscle activation patterns and co-contraction) and joint surface integrity. Additionally, the differences in dispersion between the non-dominant and dominant limbs were also cited to arise from differences in neuromuscular control [76].

Another study by Gale et al. (2020) investigated healthy knee kinematics during walking using the sFHA and HSBV [104]. Twenty healthy participants (10 male, 10 female, age range 22-42 years) walked on a treadmill at a self-selected speed. Two trials for each knee were recorded for contralateral limb comparisons. The sFHA excursion (relative to the femoral mid-sagittal plane) and orientation (additionally reported as angles within the coronal and transverse plane) were calculated. No differences were found between the contralateral knees within participants for both the sFHA location and orientation. Grouping the results of all participants, the excursion of the sFHA in the AP direction was 8.4 ± 3.9 mm, and 12.9 ± 6.1 mm in the SI direction. During knee flexion, the sFHA was oriented more posteriorly (2.9-4.2 deg) and superiorly (3.9-12.3 deg) in the transverse and coronal plane, respectively (relating to adduction and internal rotation, respectively). During knee extension, the sFHA was oriented more anteriorly (1.9-4.6 deg) and inferiorly (2.5-13.2 deg) in the transverse and coronal planes, respectively (relating to abduction and external rotation, respectively). These coupled motions exemplified the screw-home mechanism of the knee, where the tibia internally rotates during the first degrees of flexion and externally rotates during the last degrees of extension [104].

2.3.3 Jumping Tasks

Two studies, within the same research group, used the sFHA and OMCS to investigate the knee stability of anterior cruciate ligament deficient (ACLD) and/or repaired (ACLR) individuals during single leg hops [77], [78]. The first study by Grip et al. (2015) investigated the knee stability of both ACLR and ACLD participants, and compared their knee kinematics to age/sex matched controls [77]. ACLR and ACLD participants had a mean (SD) number of years since injury of 23.9 (3.3) years and 23.1 (1.3) years, respectively. The time between injury and surgery for the ACLR group was 3.8 (2.5) years. The sFHA was calculated relative to the femur at knee flexion intervals of 15 deg during a medial single leg side hop. The sFHA AP location and orientation were reported. However, the orientation angle was presented with respect to all three anatomical axes (these are referred to as ML orientation, AP orientation, and SI orientation). Both the ACLD group and ACLR group showed lesser knee stability than the control group, demonstrated by the greater ML orientation (ACL range: 21.7-25.2 deg; control range: 20.1-22.3 deg) and anterior location (ACL range: 24.8-38.8 mm; control range: 16.7-23.6 mm) during the landing phase of the hop. Within the ACL groups, the ACLD group showed the largest AP locations (take-off mean [SD]: ACLD = 23.7 [13.8] mm, ACLR = 19.7 [11.7] mm; landing: ACLD = 36.1 [16.7] mm, ACLR = 26.8 [12.0] mm). However, the ACLR group had greater AP/SI orientations at take off (AP orientation mean difference: 1.4 deg; SI orientation mean difference: 5.7 deg) and smaller AP/SI orientations at landing (AP orientation mean difference: -3.3 deg; SI orientation mean difference: -2.7 deg) compared to the ACLD group [77]. The differences in orientation and location between the ACL groups and the control groups were suggested to originate from knee instability. Specifically, the more anterior location of the sFHA in both the ACLD and ACLR groups was assumed to be from a lack of ACL function, causing the tibia to translate more anteriorly during the hop. Additionally,

greater orientations were associated with greater coupled rotations, suggesting rotational instability [77].

The second study, performed by Markström et al. (2020), compared knee kinematics of only ACLR individuals and healthy controls (matched by sex and age) [78]. Participants with ACLR had a median (interquartile range [IQR]) time of 16.0 (35.2) months post-surgery. Robustness of the knee (defined as its ability to resist perturbations and maintain a consistent configuration) was assessed for three different single leg hop movements using sFHA orientation. Because greater orientations are a consequence of increased coupled rotations, greater orientations may be associated with reduced knee robustness during a F/E movement, such as a single leg hop. The three movements performed were 1) a single leg hop for distance (jumping as far as possible), 2) a vertical single leg hop (jumping straight upwards), and 3) a standardized rebound side hop (hopping laterally on one leg, and rebounding back to the starting position [105]). No differences in sFHA orientations were found between ACLR and healthy controls for all single leg hop movements, ranging within 25-35 deg of sFHA inclination [78]. This may be due to the heterogeneity of the sample, as the ACLR group had a wide range of post-surgery times (IQR = 35.2 months). Individuals who have had a more recent surgery may demonstrate different knee kinematics than those 2-years post-surgery due to limb adaptations. A similar concept has been reported in participants with ACLR when comparing the injured and contralateral knee kinematics. Differences between the two knees decreased after 5 and 12 months post-surgery, suggesting the presence of limb adaptations [106].

2.3.4 Knee Flexion/Extension Movements

The sFHA has been used to provide a better understanding of the knee kinematics during passive or active flexion/extension movements. In an early qualitative study by Blankevoort et al. (1990), the general motion of the sFHA during passive knee flexion of four cadaveric specimens was

investigated [75]. The sFHA was calculated from full extension to approximately 95 degrees of flexion, with flexion increments ranging from 5-30 deg. Because a large range of flexion steps were used, a fifth cadaveric specimen was tested to confirm that sFHA patterns were retained when using varying flexion increments. All cadaveric specimens showed similar sFHA motion pathways. During the first degrees of flexion (ranges not provided), tibial rotation was present and the sFHA contained an 'oblique' orientation when observed in the frontal plane and no change in orientation within the other planes. With greater flexion angles (no ranges provided), the axial rotation of the tibia was reduced and the sFHA became more parallel with the F/E axis of the knee. These findings were suggested to portray the knee's well known 'screw home mechanism', as the initial stages of knee flexion consists of the tibia internally rotating about the femur. Furthermore, the sFHA location moved posteriorly (average 8 mm) when flexion reached magnitudes greater than 70 deg. Finally, overall medial translations along the sFHA during knee flexion to 95 deg were observed, ranging from 0.5 mm to 3.9 mm [75].

A more recent study quantified knee kinematics during active, unconstrained knee flexion/extension [3]. Twenty-five healthy participants (14 females and 11 males; mean [SD] age: 26.7 [8.8] years) were positioned in a 1.5T MRI. Using cine fast-phase contrast, images of the participant's knee were acquired during knee flexion from 45 deg to full extension (0 degrees). The IHA was calculated relative to the femur during the extension movement, and its orientation (relative to the frontal and transverse plane), location, and translation were compared between sexes. Evidence of the screw home mechanism was present; the IHA was primarily directed laterally at the beginning of knee extension at 45 deg, and angled more inferiorly towards full extension, suggesting an external rotation of the tibia. The changes in IHA orientation reached magnitudes of 38 deg in the frontal plane, and 8 deg in the transverse plane. Additionally, there

were significant sex differences in the frontal plane (~ 10 deg) and transverse plane (~ 5 deg) orientation at mid- and full extension, respectively. For all participants, the location of the IHA shifted posteriorly (~ 40 mm) and superiorly (~ 20 mm) during extension from 45-0 deg. This finding was speculated to arise from the femoral geometry. As knee extension increases towards full extension, the femoral condyle's geometry changes from a spherical surface to a flatter surface. Therefore, more tibial anterior sliding may occur during the end of extension, on the flatter section of the condyles, shifting the IHA superiorly. Translations were minimal and no differences were found between males and females in this healthy population [3].

Jonsson & Kärrholm (1994) performed a qualitative analysis on the sFHA for thirteen unilateral ACLD participants (10 males and 3 females; age range: 17-39 years) [107]. Tantalum beads inserted into both knees (healthy and injured/ACLD) of the participants provided fiducial markers for static, biplanar X-rays. The X-ray images were acquired during a knee extension movement to ascend onto a 40 cm platform. Because the X-rays were static, the biplanar images were acquired during knee extension angle increments. To elaborate, the knee of the limb being imaged was positioned at approximately 100 deg of flexion, with the foot raised on the 40 cm high platform. The participant then bore full weight on this limb at this angle, and X-rays were acquired. This protocol was repeated five to six times through different knee angles (~ 20 deg increments) until full knee extension was reached. The sFHA at each increment was calculated, and inter-limb comparisons of the orientation (relative to the frontal and transverse plane) and location were performed. The sFHA location was similar for both the ACLD and healthy limbs. During the initial stages of extension, the sFHA was located close to the ACL's femoral insertion. As extension increased, the sFHA translated anteriorly, towards the intersection point of the cruciate ligaments, suggesting ligament function may influence the location of the sFHA. The screw home mechanism

was not detected in this study for either limbs, with the orientation increasing (1.2 deg to 20-26.6 deg) throughout the whole extension movement, rather than the end of the movement towards full extension [107].

The sFHA has also been used to characterize knee kinematics during a lunge-like deep knee bend [74]. Using single plane fluoroscopy, the sFHA location and excursion (relative to the tibia) were compared between ten healthy (age range: 22-44 years) and five ACLD (age range: 25-47 years) participants. A notable, qualitative finding was that both healthy and ACLD participants showed similar patterns of sFHA location, translating posteriorly with progressive knee flexion. Additionally, a visual assessment of the sFHA excursion revealed greater excursions in the ACLD group than the healthy group. The greater excursion within the ACLD group was speculated to originate from a lack of ACL function, resulting in more variable knee movements [74].

One study has used the rFHA to distinguish differences in knee kinematics of healthy and ACLD participants [40]. Using an OMCS, ten unilateral ACLD (mean [SD] age: 28.8 [7.2] years) and twelve healthy (mean [SD] age: 24.0 [3.2] years) participants performed a single knee bend and seated leg extension. Six rFHA measures were compared between the two groups: translation, location, path length, excursion, orientation, and dispersion. A knee comparison was also performed within the ACLD group (healthy knee versus injured knee). No significant differences were found in any of the rFHA measures between the healthy and ACLD groups. This finding was partially attributed to the ACLD participants having a more recent injury (time since injury of six weeks), with kinematic changes potentially emerging later on in the recovery period. However, there was a significant difference between the healthy and injured knee of the ACLD participants. During the flexion phase of the single leg squat, the ACLD knee had greater rFHA orientation than

the contralateral knee. This finding was speculated to arise from an increased magnitude of tibial rotation within the injured knee, caused by a lack of ACL function.

2.3.5 Functional Flexion Axis

Besides its use to quantify knee kinematics, the HA has also been used to obtain functional axes of joints, improving the ACS definition of the limbs by avoiding the subjective selection of anatomical landmarks. Besier et al. (2003) compared the resultant lower limb kinematics of healthy individuals when using two different ACS [108]. The first ACS was determined by obtaining a F/E axis of the knee from the placement of reflective skin markers on the femoral epicondyles (the conventional method). A second ACS was obtained by having the participant perform a 'calibration movement' (i.e., single knee bend) to obtain a series of IHA. The mean IHA from the 'calibration movement' was selected to represent the F/E axis of the knee's ACS [108]. In general, both methods produced similar, repeatable lower limb kinematics. However, the IHA method produced more repeatable knee kinematics in the sagittal plane (IHA: $r^2 = 0.73$; Conventional: $r^2 = 0.57$) and transverse plane (IHA: $r^2 = 0.74$, Conventional: $r^2 = 0.67$). Furthermore, it was speculated that the IHA method may be more advantageous with novice investigators, overweight participants, or participants with bony deformities, as the anatomical landmarks may be more difficult to locate in these situations [108].

A similar study was performed to determine the influence of different femoral ACS definitions on the final output of knee kinematics [109]. Five methods were used to obtain a femoral ACS, including the IHA method reviewed in the Besier et al. (2003) study [108]. Comparison of these 5 methods revealed that the F/E angle was not dependent on the ACS method used. However, the orientation of the F/E axis was important for subsequent calculations of I/E rotation and Ab/Ad angles, as the variability due to the ACS was within the same magnitude as the kinematic

variability between participants [109]. The accuracy of each method was not investigated, but the use of the IHA to determine functional axes was shown to be feasible.

2.3.6 Summary of Helical Axis Trends

The majority of literature characterizing knee kinematics with the HA has been qualitative, providing a clear description of the HA behaviour during several movements [3]. Therefore, this section will briefly describe the patterns seen with the general use of the HA (i.e., using the IHA, sFHA, and rFHA).

The HA AP location tends to translate posteriorly during knee flexion, and anteriorly during knee extension, regardless of knee status (e.g., age or injury). This finding seems to be consistent with the movement of the intersection point of the cruciate ligaments. Therefore, the HA location may be related to ligament function and integrity. Furthermore, the HA SI location tends to be positioned away from the bone origin when the knee joint is sliding. This may occur during the beginning of flexion or the end of extension, when the femoral condyles lie flatter on the tibial plateau. The HA consistently supported the presence of the common ‘screw home mechanism’ in the knee. During early phases of knee flexion (or end phases of extension) the HA orientation angles increase. This finding exemplifies the existence of greater coupled rotations at the knee, especially the I/E rotation of the tibia.

There tends to be an increased variability of the HA measures with OA prone individuals. To elaborate, dispersion of the HA may increase with aging, suggesting more variable knee movements due to lack of motor control. In ACLD participants, the orientation, AP location, and excursion increases were speculated to increase due to a lack of ACL function, resulting in joint instability.

Chapter Three: The Influence of Smoothing Techniques on the Accuracy of the rFHA when applied to 2D/3D Registrations

3.1 Introduction

The High-speed Bi-planar Videoradiography system (HSBV) is an evolving X-ray technology that permits the determination of three-dimensional (3D) bone movements with sub-millimeter precision [17]. Using a pair of synchronized X-ray generators, image intensifiers, and high-speed digital cameras, the HSBV allows the user to record bi-planar X-ray videos of a human performing dynamic movements [15]. To quantify in-vivo bone movements, participant specific 3D bone models (segmented from Computed Tomography [CT] or Magnetic Resonance [MR] images) are registered to each pair of two-dimensional (2D) images from the HSBV video. This 2D-3D registration process can be performed manually or automatically. As the bone models are registered to each pair of image frames, a series of affine transformation matrices (ATM) for each bone are calculated, representing their 3D orientations and translations over time. The ATM may then be used to calculate different outcome variables, such as Euler/Cardan angles or the helical axis, to represent movements of the joints between bone segments of interest.

A complication with the 2D-3D registration process is the presence of bone alignment error during the manual or automatic processes. This error creates potentially non-negligible deviations from the true movements and decreases the accuracy of the outcome variables [110], [111]. During the manual registration process, the user will fit a bone model to the initial HSBV image frames. The accuracy of this initial position is subjective to the user. As the manual registration process continues in consecutive frames, miniscule and systematic errors may accumulate, eventually becoming detectable to the human eye. At this occurrence, the user will shift the bone model back to a more visually accurate position and the accumulation of errors resets to zero. This process may repeat itself throughout the remaining one hundred to two hundred image frames, depending

on the sample rate. Automatic segmentation techniques have been developed to overcome the limitation of the precision of the human eye involved with manual registration. Two primary techniques are used to automatically register bone models to the HSBV images: feature-based and intensity-based [111], [112]. Although automatic segmentation may be an improvement to manual segmentation by avoiding human subjectivity, the methods employed can still produce small errors in bone alignment. This can be due to algorithms detecting bone features incorrectly or having discrepancies between image and bone model intensities [113]. This can result in data points that have deviated from the true path. To minimize these deviations, data smoothing techniques may be applied to the ATM to increase the accuracy of the 2D-3D registration data.

Some of the common filters that have been used to smooth biomechanical data (e.g., Butterworth, wavelet, and moving averages [8], [114]) apply to data that lie within a linear vector space, such as the translations of skin mounted markers when using the OMCS. However, the orientation data obtained from HSBV do not exist in this space. Therefore, the direct application of these types of filters to the orientation component of the ATM is not possible. However, there are several different techniques that exist to smooth orientations and overcome this limitation. One method is to simply convert the non-linear orientation data into a linear vector space. For example, using unit quaternions (refer to section 1.2.2.1), angular positions or velocities have been transformed with a logarithmic map [115]–[117]. This transformation produces a series of linear vectors that are compatible with the common filters typically used in biomechanics (e.g., Butterworth, wavelet, and moving averages). Once the transformed angular positions or velocities are smoothed, they can be converted back to quaternion form. An advantage of this method is that it avoids the need to re-normalize the quaternions [117]. Another method to smooth orientations is using spherical linear interpolation (SLERP) [118] as a low pass filter; taking advantage of the similar properties

between SLERP and a single pole filter [119]. Finally, spline interpolation may also be applied to orientation data [35], [120]. Specifically, a piece-wise polynomial is fit to the noisy data of each quaternion component. The amount of smoothing performed by the spline fit is dictated by the smoothing factor. This factor can be manually adjusted by the user, and automated processes have also been developed [35]. An advantage of spline interpolation is the ability to simultaneously smooth and interpolate a dataset. However, the subjectivity of the smoothing factor may be a limitation.

With several options available to smooth orientation data, it is not clear which is most suitable for 2D/3D registration data. Therefore, the objective of this study was to investigate the effect of six smoothing techniques, when applied to ATM from manual 2D-3D registrations, on the accuracy of the finite helical axis (FHA). This was evaluated with ATM of a known, controlled rotation within the HSBV using 3D printed bones mounted on a turntable. It was speculated that applying the smoothing techniques to the ATM would increase the accuracy of the FHA directionality (i.e., more closely aligned with the turntable axis of rotation) and the rotational speed along the FHA.

3.2 Methods

3.2.1 Bone Prints

To acquire a set of femoral and tibial 3D printed bones, corresponding 3D stereolithography bone models were imported into a 3D printer (LulzBot® Taz 5, Aleph Objects Inc.©, CO, USA). The 3D bone models were acquired by segmenting CT images of a prior study participant (ethics ID: REB15-0554) using Amira software (Thermo Fisher Scientific, MA, USA). Following the creation of the 3D printed bones, a CT scan of them was performed to subsequently segment a new set of 3D stereolithography bone models. These newly acquired bone models, based on the 3D printed bones, accommodated any potential inaccuracies to the real bones, improving future 2D-3D registrations.

3.2.2 Turntable System & HSBV Image Acquisition

The 3D bone prints were mounted onto a foam support in a position that approximated standing in knee extension. A foam support was selected to remove potential occlusion and imaging artifacts of the 3D printed bones when recording with the HSBV (Figure 3-1). The bone prints were then placed onto a turntable (6034K31, McMaster-Carr, IL, USA) equipped with an optical encoder (EM2 Optical Encoder Module 2", US Digital®, WA, USA) and rotary encoder disk (DISK-2 2" Outside Diameter, 7200 counts/revolution, US Digital®, WA, USA) (Figure 3-2). The turntable rotated with a pre-defined speed of 2 RPM (or 12 deg/s). However, due to small amounts of friction and the weight of the bone prints, the turntable tended to produce small deviations from this pre-defined speed. Therefore, the encoder unit was installed to allow more accurate measurements of rotational speed. The optical encoder was mounted onto the turntable motor casing and remained stationary, while the encoder disk was mounted onto the motor shaft and rotated with the turntable. Light from the optical encoder passing through the series of 7200 slits on the encoder disk was detected by a photosensor on the opposite side of the encoder. The rate of rotation was calculated from the time interval between each detection of light passing through the encoder disk.

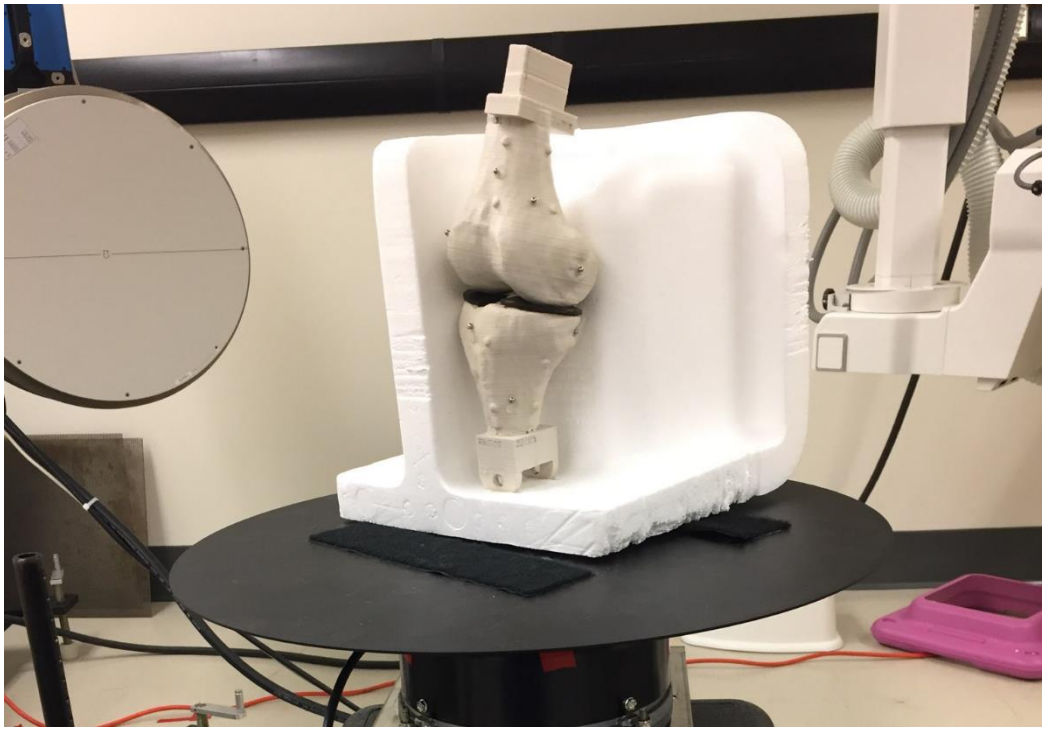

Figure 3-1 – The 3D printed bone models mounted onto the foam support in an approximate standing position.

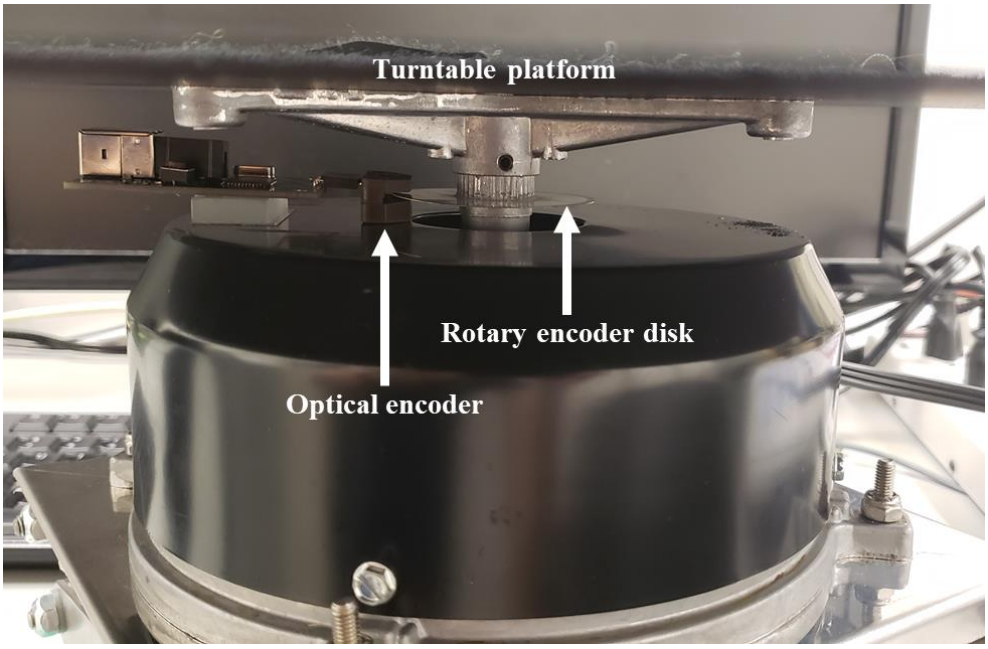

Figure 3-2 – The optical encoder and rotary encoder disk mounted on the turntable.

The turntable support and 3D printed bones were placed within the field of view of the calibrated HSBV system. A spirit level was used to visually inspect that the turntable's axis of rotation was as perpendicular as possible with the transverse plane of the HSBV coordinate system. A sub-analysis was performed to examine the spirit level's alignment accuracy using Radiostereometric Analysis (RSA). Two pairs of RSA beads were adhered to corners of the level, representing its orientation within the HSBV system (Figure 3-3). The level was placed on the turntable and aligned as parallel as possible with the HSBV transverse plane. An HSBV image was recorded for the level to complete a single trial. Afterwards, the level was removed completely from the HSBV, and the process was repeated for a second trial. Five trials were performed in total. The bead locations were determined using custom software (MATLAB, MathWorks, MA, USA), and the vertical axes of each bead pairs were calculated (Figure 3-3). If the alignment of the turntable was accurate, the vertical axes of the beads would lie parallel with the vertical axis of the HSBV (i.e., angle of 0 deg).

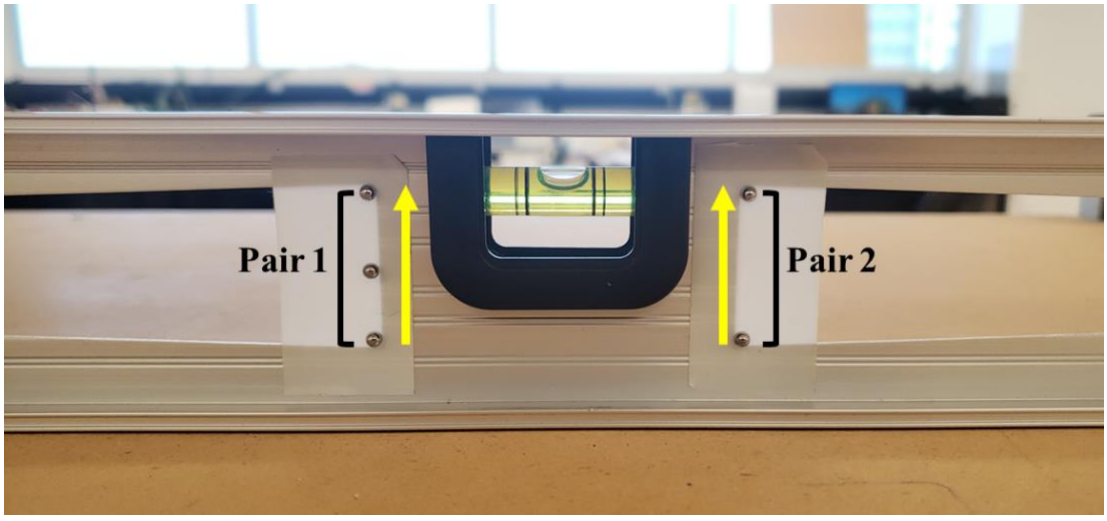

Figure 3-3 – The spirit level with two pairs of RSA beads adhered to four corners. The vertical axes of each pair of beads are illustrated as well (yellow arrows). Note: the purpose of the middle RSA bead on the left was to provide directionality within the HSBV images.

A custom MATLAB code (MathWorks, MA, USA) was used to synchronize the data from the encoder unit (240 Hz) and HSBV system (24 Hz). Specifically, the code detected the on/off signal of the HSBV, supplied by a digital to analog converter. This signal would initiate or terminate the collection of the encoder outputs. Five trials were recorded for 1/3rd of the turntable rotation (approximately 10 seconds). This time frame was chosen to accommodate the encoder hardware memory size. The turntable and 3D printed bones were not moved within the HSBV throughout all trials. Furthermore, start positions for the 3D printed bones on the turntable were random (i.e., each trial consisted of a random 1/3rd rotation of the turntable).

3.2.3 Data Processing

The rotation speed of the turntable was calculated by measuring the time between encoder detections. To satisfy the memory constraints of the encoder hardware, turntable speed was calculated at every eight detections (or 0.4 deg of rotation), resulting in less memory usage and longer HSBV recordings. The encoder data was down sampled to 24 Hz by averaging the rotational speed within each 0.04 s increment (Figure 3-4).

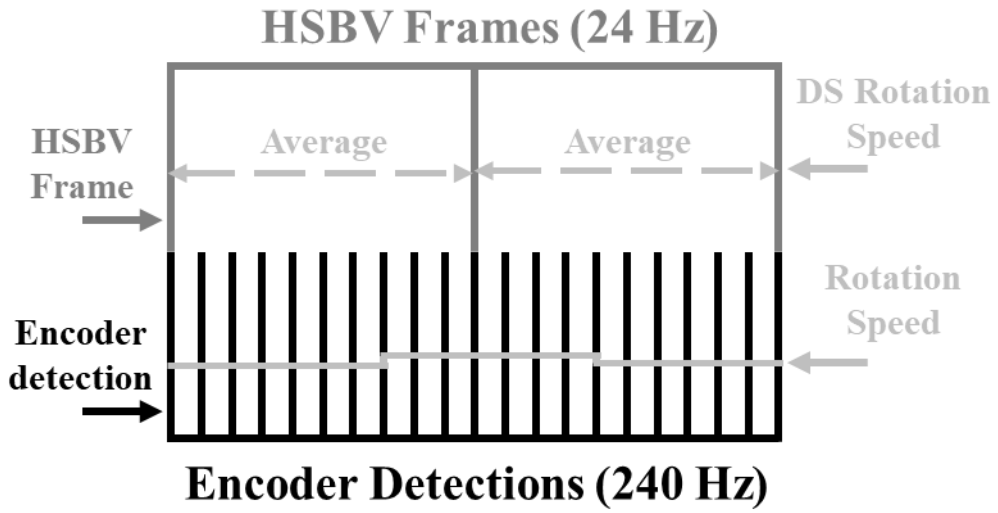

Figure 3-4 – Illustration of the down sampling process for the encoder data. Each vertical tick mark on the top half (dark grey) represents a recorded HSBV frame at 24 Hz. Each vertical tick mark on the bottom half (black) represents an encoder detection at 240 Hz. Note that the rotation speed (light grey solid line) calculated at every eighth encoder detection was assumed to be constant in the previous seven detections. The encoder data was down sampled (DS rotation speed) by averaging every 0.04 s time increment (dashed grey line).

HSBV images were undistorted and then imported into 2D-3D registration software (Autoscoper, Brown University, USA) with calibration parameters that relate the 2D locations of the biplanar images to a 3D space relative to the HSBV. The segmentation generated 3D bone models (femur and tibia) were then manually 2D-3D registered to the HSBV frames in Autoscoper. The femur and tibia were individually registered to all five trials by a single rater. ATM of a single trial were imported into custom MATLAB code that first converted the rotation component into quaternions. Afterwards, six different smoothing techniques were applied to the quaternions and translations (Table 3-1): Low pass Butterworth filter (BW), Daubechies Wavelet filter (DW), Gaussian filter

(G), Mean filter (M), Spherical Linear Interpolation (SLERP), and Spline interpolation with outlier removal (SPOUT).

Table 3-1 – List of the six smoothing techniques used, and the input parameters used.

Smoothing Technique	Parameters
Low pass Butterworth filter (BW)	Cut-off frequency: 1 Hz
Daubechies Wavelet filter (DW)	Wavelet transform: db4, Decomposition level: 2
Gaussian filter (G)	Window: $\left[\frac{1}{16}, \frac{4}{16}, \frac{6}{16}, \frac{4}{16}, \frac{1}{16}\right]$
Mean filter (M)	Window: $\left[\frac{1}{5}, \frac{1}{5}, \frac{1}{5}, \frac{1}{5}, \frac{1}{5}\right]$
Spherical Linear Interpolation (SLERP)[a]	hrange = 0.4, hbias = 0.5
Spline interpolation with outlier removal (SPOUT)[b]	Polynomial degree: 3, Q = 0.05

[a] refer to [119] for detailed descriptions
[b] refer to [121] for detailed descriptions

The BW, DW, G, and M filters required the quaternions to be converted into linear space using logarithmic mapping [117]. The BW was set with a cut-off frequency of 1 Hz. This was decided by first measuring the power spectral density of the converted quaternions using a fast Fourier transform, and then visually selecting a cut-off that retained the majority of the frequency content within the data [122]. A Daubechies 4 wavelet transform at the second decomposition level was used for the DW, as it has been reported to provide the best smoothing for kinematic data [123]. The M filter specified with a 208 ms window (i.e., five point moving average).

SLERP may be used as a low-pass filter on orientation data, such as quaternions, but not translation data. Therefore, to smooth the translations, the BW described above was used instead of SLERP as it is commonly used in biomechanics and also acts as a low-pass filter. SLERP can act similar to a single pole filter with the form,

$$y_k = y_{k-1} + \delta(x_k - y_{k-1}) \quad \text{Eq. 3-1}$$

where y_k and x_k are the filtered and original data point at time k, respectively, y_{k-1} is the previously filtered data point at time k-1, and δ is an adjustable proportion factor between 0 and 1. The formula states that the filtered point y_k is dependent on distance between the original point x_k and previously filtered point y_{k-1}, and the proportion factor. If the proportion factor is closer to 1 the filtered point y_k steers closer to the original data point x_k, while a proportion factor of 0 steers it closer to the previously filtered point y_{k-1}. In terms of quaternions, SLERP has the ability to steer a filtered quaternion (y_k) towards x_k or y_{k-1} depending on the distance between the two. If the distance is large then the filtered quaternion is steered towards y_{k-1}, and a small distance is steered towards x_k. However, the proportion factor can have poor performance with a range of 0 to 1. Therefore, the proportion factor of the SLERP filter was adjusted to range from 0.3 to 0.7 using a range of 0.4 (hrange = 0.4) and bias of 0.5 (hbias = 0.5) (Figure 3-5). A more detailed implementation of this filter can be found on the Mathworks® website [119].

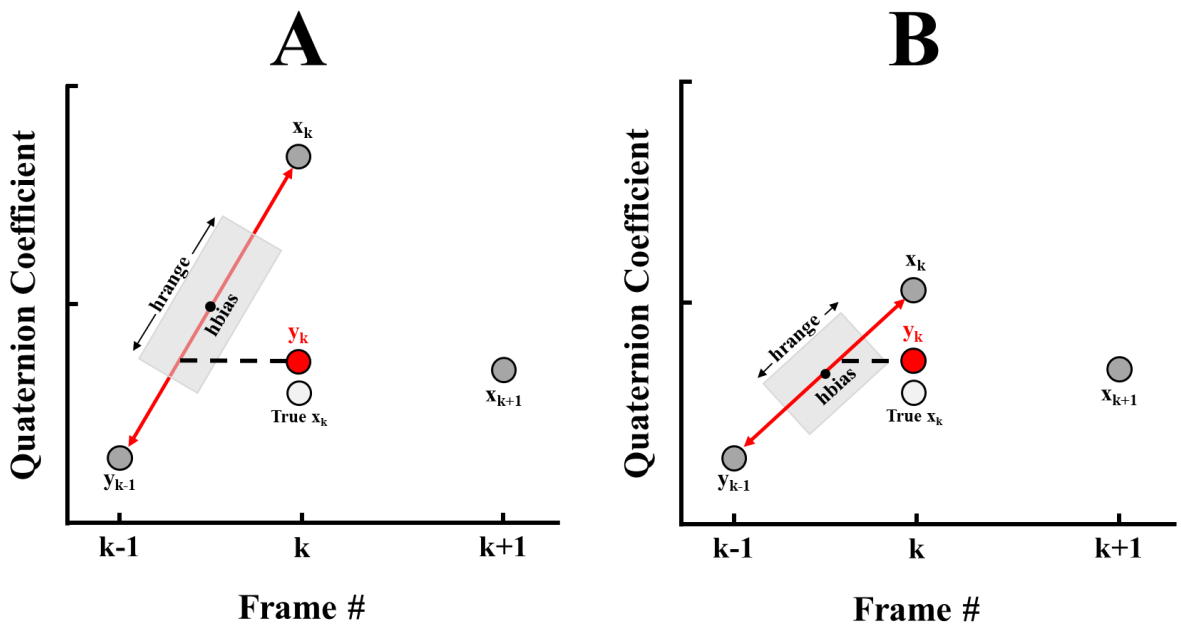

Figure 3-5 – A visualization of the SLERP filter. A) If the distance between x_k and y_{k-1} is large (solid red line), the filtered quaternion y_k (red circle) is steered towards y_{k-1} and is closer to the true value of x_k. B) In contrast, if the distance between x_k and y_{k-1} is smaller, the filtered quaternion y_k is steered more towards x_k. The hrange and hbias are illustrated as a light grey box and black dot, respectively.

Spline interpolation was performed twice using third degree B-splines [124]. The first interpolation was used to detect and remove any outliers that may exist within the quaternions and translations. Motulsky and Brown (2006) provide a detailed description of the outlier removal process using a false discovery rate approach. Briefly, a spline fit was performed, and a 'standard deviation of residuals' (SDR) was calculated using the formula,

$$SDR = P68 * \left(\frac{N}{N-K}\right) \quad \text{Eq. 3-2}$$

where P68 is the 68th percentile of the absolute value of residuals, N is the number of data points, and K is the number of parameters fit by the spline (e.g., splines of third-degree polynomials have K = 3). Afterwards, the absolute value residuals were ranked from lowest to highest, and two values were computed for the largest 70% of residuals: a critical value (α) and t-score (t),

$$\alpha_i = \frac{Q\,(N-(i-1))}{N} \quad \text{Eq. 3-3}$$

$$t = \frac{|Residual_i|}{SDR} \quad \text{Eq. 3-4}$$

where i dictates the rank of the residual and Q is the false discovery rate (e.g., a Q value of 0.05 represents a false discovery rate of 5%). A two-tailed p-value, with N-K degrees of freedom, was then obtained from the t-score of each residual. The smallest value residual that had a p-value less than the critical value was considered an outlier, along with any residual greater than this value

[121]. For this study, the outlier detection was set with a false discovery rate of 5%. Following the outlier removal, a second interpolation was performed on the outlier removed data to obtain the smoothed quaternions and translations. During both interpolations, smoothing factors for the splines were manually adjusted using a custom graphical user interface. The interface provided real-time visualization of the adjusted smoothing factors and the respective spline curve. The selected smoothing factors were subjective to the single rater. To ensure some consistency between trials and participants, spline curves were fit on the reference frame of following the original kinematic curve as close as possible but providing a smoother curve (Figure 3-6).

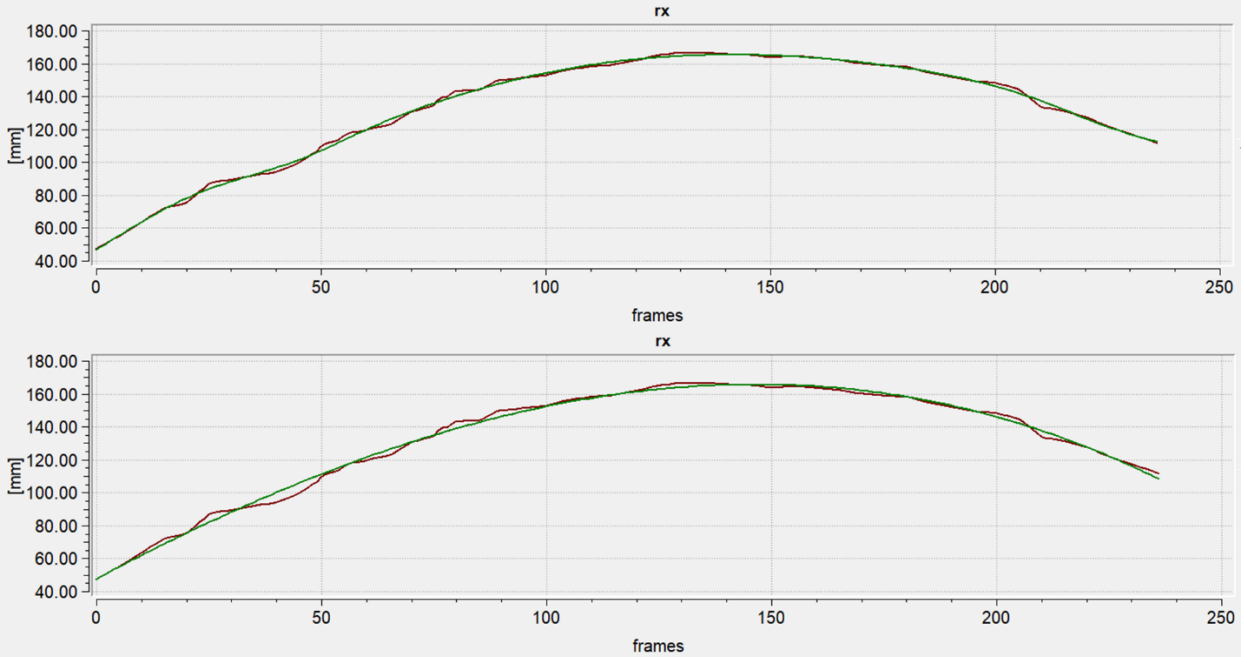

Figure 3-6 – Example of a good spline fit (top) and poor spline fit (bottom). The red line represents the original kinematic curve, while the green line represents the spline fit. The bottom spline curve has been over-smoothed, deviating too far from the original curve.

The smoothed quaternions and translations were converted back into ATM and used to obtain a series of FHAs. This process was performed for all trials for each 3D printed bone, resulting in ten series of FHAs for each smoothing technique (five for the femur and five for the tibia). For this

study a reference FHA (rFHA) was used instead of the traditional stepwise FHA (sFHA). The rFHA was selected to provide larger angular displacements, thus reducing or eliminating any errors associated with small angular deviations, as reported with the sFHA [5]. Therefore, the rFHA was calculated using a single reference position throughout the rotation rather than using neighbouring time points (as in the sFHA approach). The reference position was approximately 90 deg from the start position of the rotation, allowing adequate rotation to minimize helical axis step size errors [4], [5]. Three kinematic measures were calculated using the rFHA: orientation and dispersion (Figure 3-7), and rotation speed difference (RSD). Orientation was calculated as the average angle between the rFHA and vertical axis of the HSBV throughout a trial of 'n' frames (Equation 3-5). Dispersion was determined as the average angle between an individual rFHA and mean rFHA throughout the whole trial (Equation 3-6). The RSD was obtained by averaging the absolute difference between the rotation speed along the rFHA ($\dot{\theta}$) from the turntable speed recorded by the rotary encoder ($|\vec{\omega}|$) throughout the trial (Equation 3-7). The rotation speed along the rFHA was calculated by taking the first derivative of the rotation along the rFHA (Figure 3-7). The RSD was computed as an absolute value to highlight the magnitude of differences, disregarding the directionality of differences. For each 3D printed bone, means and standard deviations (SD) of the orientation, dispersion, and RSD from all five trials were calculated for each smoothing technique.

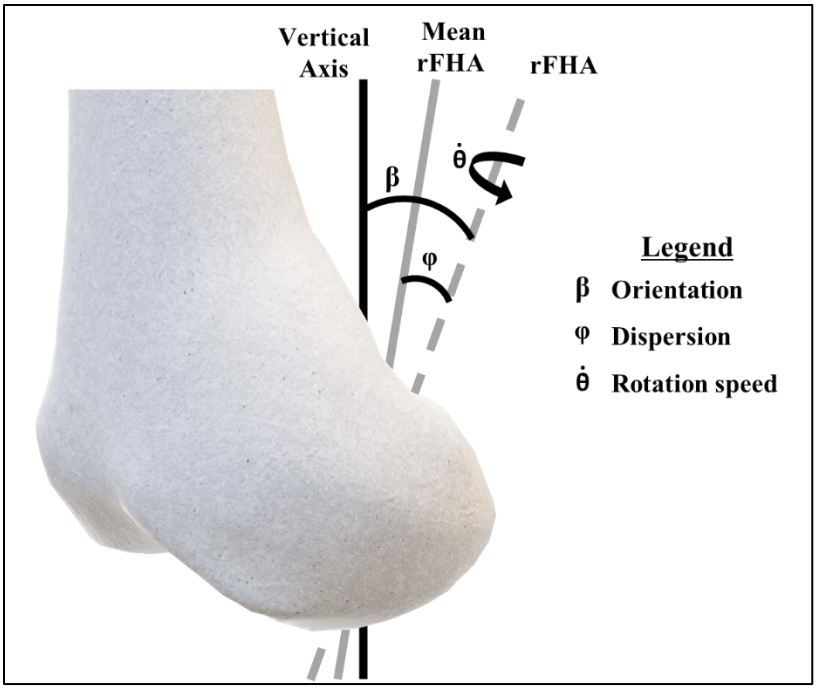

Figure 3-7 – Diagram of the three rFHA variables: orientation, dispersion, and rotation speed. Orientation was calculated as the average angle between the rFHA and vertical axis of the HSBV throughout a trial, dispersion as the average angle between an individual rFHA and mean rFHA throughout the movement, and rotation speed as the first derivative of the rotation along the rFHA.

$$Ori = \frac{1}{n}\sum_{1}^{n}\beta_n \qquad \text{Eq. 3-5}$$

$$Dis = \frac{1}{n}\sum_{1}^{n}\varphi_n \qquad \text{Eq. 3-6}$$

$$RSD = \frac{1}{n}\sum_{1}^{n}\left|\dot{\theta}_n - |\vec{\omega}_n|\right| \qquad \text{Eq. 3-7}$$

3.2.4 Data Analysis

Normality of the femoral and tibial RSDs (i.e., errors in the manual registrations) were evaluated using a Shapiro-Wilk test and visual assessment of the corresponding quantile-quantile (Q-Q) plots. To compare the smoothing techniques, each were ranked based on their mean (SD) rFHA orientation, dispersion, and RSD. The ranking process assumed that the turntable axis of rotation was parallel to the HSBV vertical axis. It was assumed that an rFHA orientation of 0 deg presented the most accurate axis alignment with the turntable, while larger values suggested deviations away from the turntable axis. Therefore, smoothing techniques with orientation values closer to zero were ranked higher. Furthermore, the turntable remained stationary throughout the data collection. Therefore, the axis of rotation would not have varied, pointing in a single direction. The dispersion would reflect this, as a magnitude of 0 deg would represent a stationary axis of rotation. Smoothing techniques with smaller dispersion values were ranked higher than those with larger dispersion values. Finally, an RSD of zero would represent perfect rotational speed relations between the 2D-3D registration and the rotary encoder outputs. Therefore, smoothing techniques were ranked higher when the RSD was smaller. This ranking process was performed for the femur and tibia individually. Means and associated SD were reported, along with relative percent changes of each smoothing technique to the original, unsmoothed data.

3.3 Results

It was determined that the mean (SD) angle between the vertical axis of the RSA beads on the level and the HSBV vertical axis was 1.20 (0.48) deg. Both the femoral and tibial RSDs were determined to be not normal, with significant ($p < 0.01$) results in the Shapiro-Wilk test and the Q-Q plots showing a non-linear trend (Figure 3-8).

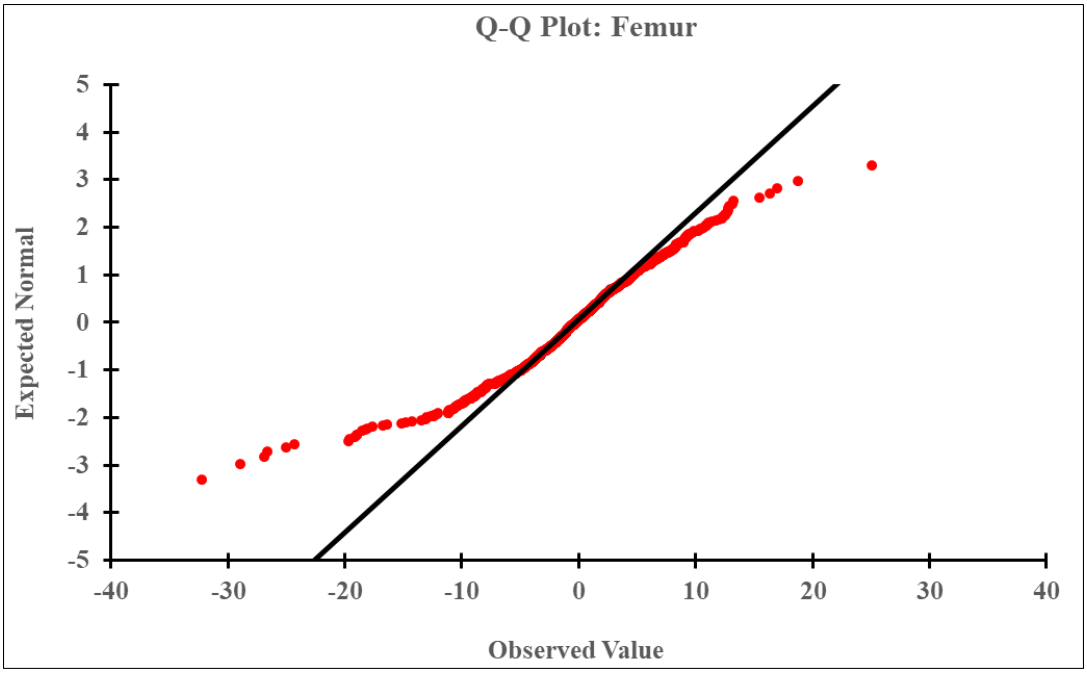

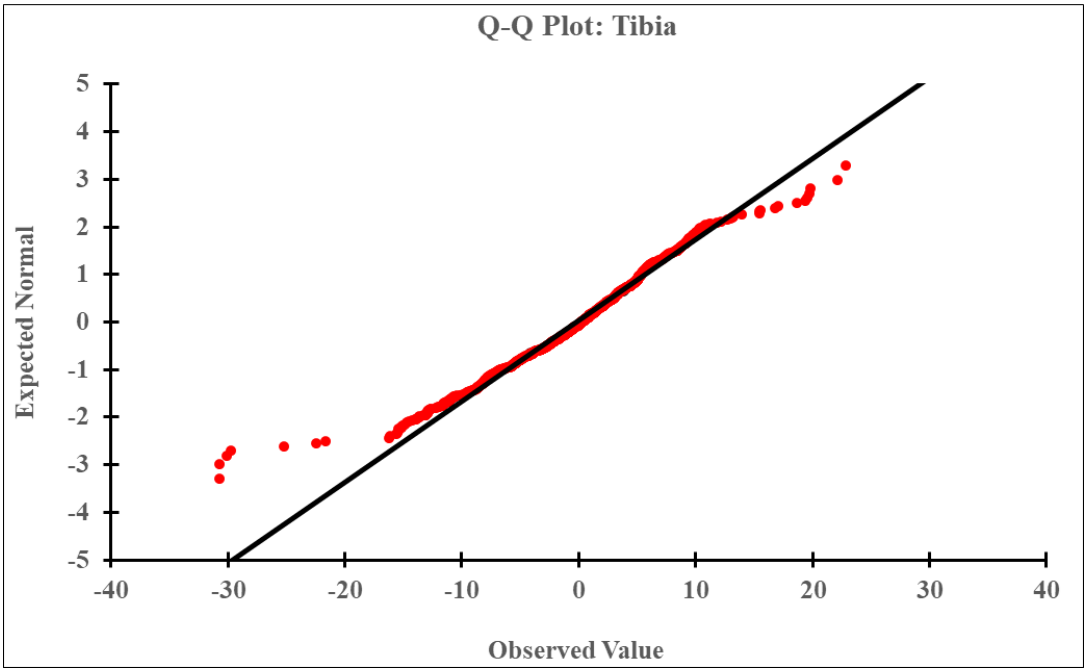

Figure 3-8 – Q-Q plots of the femoral and tibial RSDs, showing a non-linear trend. This suggests that the errors associated with manual registration are not normally distributed.

3.3.1 Femur

Without the use of a smoothing technique, the means (SD) of the rFHA orientation, dispersion, and RSD of the femur were 1.18 (0.30) deg, 0.36 (0.39) deg, and 4.22 (3.91) deg/s, respectively (Table 3-2). The smoothing techniques showed to have little or no effect on the orientation, with means ranging from 1.17 deg – 1.24 deg, translating to a -0.9% – 5.1% change relative to the unsmoothed data. Similar findings were observed for the measure of dispersion, with most smoothing techniques resulting in magnitudes -8.3% – 2.8% away from the original data. The exception was the SPOUT, showing a large improvement of 28% (0.26 [0.17] deg). Interestingly, the G filter appeared to slightly worsen the orientation and dispersion magnitudes, showing increases in orientation (1.24 [0.32] deg; 5.1%) and dispersion (0.37 [0.20] deg; 2.8%) compared to original data (Table 3-2).

Improvements in the RSD were observed with most of the smoothing techniques. SPOUT, SLERP, and the M filter were ranked as the top three performers, providing RSDs of 0.84 (2.20) deg/s, 2.26 (2.24) deg/s, and 2.34 (2.29) deg/s, respectively. This translated to an 80.1%, 46.4%, and 44.5% improvement for the SPOUT, SLERP, and M filter, respectively. However, the BW filter also provided substantial improvement to the RSD (2.74 (2.73) deg/s), showing an improvement of 35.1%, while the next best filter only provided a 4.7% improvement (W filter: 4.02 [3.94] deg/s). The G filter, consistent with rFHA orientation and dispersion, worsened the RSD by 1.9% (4.30 (4.23) deg/s) (Table 3-2).

Table 3-2 – Means (SD) of the femoral kinematic measures using each smoothing technique. Percentages for each smoothing technique represent the percent change relative to the original, unsmoothed data. Negative percentages dictate an improvement, while positive percentages dictate a diminishment.

Kinematic Measures	Femur						
	Smoothing Technique						
	None	BW	W	G	M	SLERP	SPOUT
Orientation (deg)	1.18 (0.30)	1.18 (0.29) 0.0%	1.18 (0.30) 0.0%	1.24 (0.32) 5.1%	1.18 (0.29) 0.0%	1.17 (0.29) -0.9%	1.17 (0.25) -0.9 %
Dispersion (deg)	0.36 (0.19)	0.34 (0.18) -5.6%	0.36 (0.19) 0.0%	0.37 (0.20) 2.8%	0.34 (0.18) -5.6%	0.33 (0.17) -8.3%	0.26 (0.17) -27.8%
RSD (deg/s)	4.22 (3.91)	2.74 (2.73) -35.1%	4.02 (3.94) -4.7%	4.30 (4.23) 1.9%	2.34 (2.29) -44.5%	2.26 (2.24) -46.4%	0.84 (2.20) -80.1

3.3.2 Tibia

The application of the smoothing techniques on the tibia demonstrated patterns similar to the femur. Without smoothing techniques, the rFHA orientation, dispersion, and RSD of the tibia were 1.26 (0.33) deg, 0.40 (0.23) deg, and 4.75 (4.11) deg/s, respectively (Table 3-3). Like the results of the femur, the smoothing techniques had little or no effect on the orientation, with means ranging from 1.24 deg – 1.34 deg, translating to a -1.6% – 6.3% change relative to the original data. The SPOUT filter also provided the largest improvement to the dispersion (0.37 [0.17] deg), relating to a 22.5% change relative to the original data. All other smoothing techniques had minimal influence on the dispersion, with changes relative to the original data ranging from -5.0% – 2.5%. Again, the G filter slightly worsened the orientation (1.34 [0.36] deg; 6.3%) and dispersion (0.41 [0.24] deg; 2.5%) (Table 3-3).

The RSD showed improvements with all smoothing techniques. SPOUT, SLERP, and the M filter were the top three performers, providing RSDs of 1.32 (2.36) deg/s, 2.93 (2.75) deg/s, and 3.07 (2.87) deg/s, respectively. This translated to an 72.2%, 38.3%, and 35.4% improvement for the

SPOUT, SLERP, and M filter, respectively. The BW filter also provided substantial improvements to the RSD (3.37 (2.98) deg/s; 29.1%). The G and W filters ranked in the bottom two, resulting in RSDs of 4.56 (4.01) deg/s, and 4.60 (3.97) deg/s, respectively. This related to 4.0% and 3.2% improvements for the G and W filters, respectively (Table 3-3). The smoothing techniques consistently showed smaller magnitudes of improvement to the tibial rFHA measures when compared to the femoral rFHA measures.

Table 3-3 – Means (SD) of the tibial kinematic measures using each smoothing technique. Percentages for each smoothing technique represent the percent change relative to the original, unsmoothed data. Negative percentages dictate an improvement, while positive percentages dictate a diminishment.

Kinematic Measures	Tibia						
	Smoothing Technique						
	None	BW	W	G	M	SLERP	SPOUT
Orientation (deg)	1.26 (0.33)	1.25 (0.32) -0.8%	1.26 (0.33) 0.0%	1.34 (0.36) 6.3%	1.25 (0.32) -0.8%	1.25 (0.32) -0.8%	1.24 (0.28) -1.6%
Dispersion (deg)	0.40 (0.23)	0.39 (0.21) -2.5%	0.40 (0.23) 0.0%	0.41 (0.24) 2.5%	0.39 (0.21) -2.5%	0.38 (0.20) -5.0%	0.31 (0.17) -22.5%
RSD (deg/s)	4.75 (4.11)	3.37 (2.98) -29.1%	4.60 (3.97) -3.2%	4.56 (4.01) -4.0%	3.07 (2.87) -35.4%	2.93 (2.75) -38.3%	1.32 (2.36) -72.2%

3.4 Discussion

The purpose of this study was to determine the effects of several smoothing techniques, when applied to ATM from 2D/3D registration, on the accuracy of the kinematic measures. It was speculated that the smoothing techniques would increase the accuracy of all kinematic measures. This was partially supported, as the orientation and dispersion were either not influenced by the smoothing techniques (e.g., the W filter, showing a 0% change to the original data) or worsened (e.g., the G filter, showing a 6.3% and 2.5% increase in tibial orientation and dispersion, respectively). However, the majority of smoothing techniques did substantially improve RSDs

between the rFHA and turntable. The lack of improvement in the orientation and dispersion suggests that a consistent alignment of the 3D bone models throughout the manual 2D/3D registration was already present. In contrast, the large improvements of the RSDs suggest that the magnitude of rotation between each registered frame was susceptible to alignment errors.

Application of the smoothing techniques resulted in minimal changes in the rFHA orientation and dispersion. The largest orientation value was observed for the tibia when using the G filter (1.34 [0.36] deg), representing a 6.3% (or 0.08 deg) increase relative to the original data. The smoothing technique with the greatest overall improvement to orientation was the SPOUT (femur: 0.9% or 0.01 deg; tibia: 1.6% or 0.02 deg). This minimal influence may be due to the rFHA orientation already being accurate within the original data (i.e., no smoothing techniques applied). The RSA sub-analysis revealed alignment errors of 1.20 ± 0.48 deg between the turntable axis and HSBV vertical axis. Therefore, the orientation of the rFHA within the original data may have already been accurate, which ranged from 1.18 – 1.26 deg. Similar to the orientation, the largest improvement of dispersion was seen in the SPOUT (femur: 27.8% or 0.1 deg improvement; tibia: 22.5% or 0.09 deg improvement). This is contrary to another study by De Lange et al. (1990), who reported 11.5 deg of improvement in the sFHA dispersion when using quintic splines [125]. This may have originated from the use of the sFHA instead of the rFHA. The sFHA is subjected to small angular displacements, a well known error source on HA accuracy [126]. Alternatively, the reference position of the rFHA serves the purpose of providing larger angular displacements to avoid this error source. Therefore, the directionality of the HA may have already been accurate, resulting in minimal influence of the smoothing techniques. Although sFHA orientation was not reported by De Lange, similar results would be expected as the dispersion and orientation are both dependent on the directionality of the HA.

The smoothing techniques provided substantial improvements for the RSD. The SPOUT technique provided the largest improvement for both the femur (80.1%) and tibia (72.2%), followed by SLERP (femur: 46.4%; tibia: 38.3%) and the M filter (femur: 44.5%; tibia: 35.4%). An extensive literature review revealed that no similar analysis has been performed, thus no direct comparisons can be made. Although SPOUT performed the best, it had the disadvantage of having manually selected smoothing factors, resulting in a subjective process to obtain an ideal spline fit. Consequently, the choice of smoothing factors may influence the final kinematic outcomes. The Generalized Cross-Validation (GCV) criterion can be further applied to SPOUT to automate the smoothing factor selection [127]. The effective performance of GCV spline filtering has been reported previously in a study that compared six smoothing techniques on simulated marker data during walking. When adding noise to the simulated data, GCV spline fitting was a top performer in noise removal, providing small RMSE to the original data [128]. Interestingly, the GCV automation process has been reported to select smoothing factors that result in a curve equivalent to a BW filter [35]. However, these equivalent curves were not previously assessed for outliers as done with SPOUT. By incorporating the GCV into SPOUT, the limitation of subjectivity may be eliminated. Further investigations are required to assess the performance of a GCV integrated SPOUT.

Although the SLERP smoothing technique resulted in smaller RSDs (femur: 2.26 [2.24] deg/s, 46.4%; tibia: 2.93 [2.75] deg/s, 38.3%) these results were close in magnitude to those obtained with the M filter (femur: 2.34 [2.29] deg/s, 44.5%; tibia: 3.07 [2.87] deg/s, 35.4%). Consequently, the M filter may be preferred as there is greater ease of application and lower computational costs compared to the intricacies of the SLERP technique implementation. The G filter resulted in worsened femoral RSDs and minimally improved tibial RSDs. The G filter assumes that the errors

form a Gaussian/normal distribution. Therefore, a poor performance with the G filter suggests that the errors may be systematic instead of randomly distributed; validated by the significant Shapiro-Wilk tests and a visual assessment of Q-Q plots for the femoral and tibial RSDs. This supports the notion that miniscule, systematic errors may accumulate to an instance that is eventually noticeable to the human eye. Furthermore, to the best of the author's knowledge, the error distributions seen with automatic registration algorithms have not been reported. Further investigations are required to understand what error distributions are associated with the different 2D/3D registration processes, allowing the implementation of appropriate smoothing techniques.

The ranking of the smoothing techniques was similar for both the femur and tibia. The top performer was SPOUT, followed by SLERP and the M filter, forming the top three. The BW filter was slightly worse, followed by the W filter and G filter as the bottom two techniques. Interestingly, the smoothing techniques tended to provide greater improvements to the femoral kinematics when compared to the tibia. This may have been a result of relative movements between the femur and tibia models on the turntable, resulting in different kinematic curves and noise levels between the two bones. However, a previous analysis of this data was performed and determined a mean (SD) relative translation of 0.09 (0.05) mm [129]. Therefore, it is unlikely that any relative movement occurred between the bones and instead rotated as a rigid body on the turntable, thus having equivalent kinematics. The differences in improvement may have originated from errors associated with the manual 2D/3D registration. The tibia, being more symmetrical than the femur, may yield visual difficulties when determining the correct alignment [130]. In other words, rotating the tibia a few degrees may still show an accurate alignment due to its symmetry. This may result in greater magnitudes of errors within the tibial kinematics. Although not formally reported, a similar finding was found by Postolka et al. (2020), who showed larger translational errors (up to

0.28 mm) and rotational errors (up to 0.72 deg) in manual registrations of the tibia compared to the femur [113]. However, this comparison was not a research objective of the study and a statistical analysis was not performed.

3.4.1 Limitations

It is acknowledged that there are limitations to this study. Firstly, the accuracy of the turntable rotation speed may have decreased when accommodating the memory limitations of the hardware. Specifically, the rotary encoder outputs were recorded at every eighth sensor detection, or 0.4 deg of turntable rotation. It was assumed that the previous seven detections were equal to the output of the eighth detection (Figure 3-4). As a result, averaging the encoder outputs during the down sampling process may not have contained the true encoder outputs. However, because every eight detections coincided with 0.4 degrees of turntable rotation, it was assumed that the turntable rotation speed would not fluctuate within such a small interval of rotation.

The 2D/3D registration was performed once, manually, by a single rater. Therefore, intra-rater and inter-rater reliability could not be assessed, and the reported errors may not extrapolate to the general process. However, a previous study using the same HSBV system and registration methods as in this study determined inter-rater intra-class correlations of 0.92, thus being reliable [131]. Furthermore, it would be expected that intra-rater reliability would be greater or equal to the inter-rater reliability. Therefore, these results may not differ if the registration process was performed by another rater or performed again by the same rater. Furthermore, only manual 2D/3D registration was performed in this study. One automated, intensity-based registration process provided greater errors in out-of-plane movements when compared to the manual registration counterpart [113]. Therefore, the smoothing techniques used here may have different performances when applied to kinematic curves obtained from automatic registration. Further investigations are

required to determine the influence of these smoothing techniques on ATM from automated registrations.

Lastly, the smoothing techniques were only applied to ATM of 3D printed bones during a turntable rotation. Therefore, this experimental design cannot be generalized to data obtained from human participants. For example, only the shape of the 3D printed bones was representative of *in-vivo* human bones. The biological composition of human bones and its surrounding soft tissue was not present, which may provide a different quality of HSBV images [132], [133], potentially giving rise to different magnitudes of errors within the corresponding 2D/3D registrations. How the smoothing techniques would manage these errors requires further investigation. Additionally, the smoothing techniques were only applied to a turntable rotation movement. The extension of these techniques to ATM of more complex, *in-vivo* movements (e.g., a squat or walking) may produce different results. However, obtaining a true measure of human kinematics for accuracy assessment is difficult to achieve. Therefore, the turntable with its 3D printed bones was used as an alternative approach.

3.5 Conclusions

It was unclear which of the several smoothing techniques available provide the best improvement on kinematic data, specifically ATM acquired from 2D/3D registrations. This study evaluated the influence of six smoothing techniques on ATM by assessing the accuracy of femoral and tibial rFHA measures. The smoothing techniques did not have a large impact on the rFHA orientation and dispersion, speculated to originate from the reference position providing more accurate HA directionalities. Nevertheless, the SPOUT was determined to be the best performer with an 80.1% and 72.2% RSD improvement for the femur and tibia, respectively. This was followed by the SLERP, M, BW, W, and G filter. The SPOUT contained a subjective adjustment of its smoothing factors. This limitation may be potentially avoided by automating the smoothing factor selection

with GCV integration. Further investigations are required to determine how these smoothing techniques would perform under *in-vivo* conditions/datasets.

Chapter Four: Sensitivity of the rFHA to Reference Position Deviations

4.1 Introduction

The stepwise FHA (sFHA) shows promising evidence to characterize kinematics of the knee. Its location and orientation has successfully described rotations of the knee during running and passive knee extension [3], [102]. A more anterior sFHA location and greater sFHA orientation have additionally described kinematics of ACLD knees [74], [77], [78]. Finally, greater magnitudes of sFHA dispersion have suggested a greater amount of knee instability in older participants [76]. However, the sFHA is susceptible to stochastic errors when angular displacements are small (refer to section 1.2.2.3.2) [4]. These errors can be alleviated in two ways: 1) by lowering the sampling rate, or 2) by calculating the sFHA at specific increments of angular displacement. The second approach is most commonly used in literature. Unfortunately, both methods result in the loss of temporal resolution. Therefore, to achieve larger angular displacements while preserving temporal resolution, the use of a reference position has been suggested to calculate the rFHA (Figure 1-6, refer to section 1.2.2.3.2) [5]. The rFHA characterizes knee movement with respect to this reference position, instead of neighbouring time points. Specifically, the reference position of the knee is aligned in a manner that exceeds the movement of interest's RoM. For example, during the heel strike to midstance phase of walking, the knee's peak flexion angle can reach approximately 20 degrees [134], [135]. A reference position of the knee in 90 deg of flexion would provide large angular displacements (at least 70 deg) throughout the movement, minimizing the stochastic errors associated with the sFHA while maintaining temporal resolution (Figure 4-1). The use of a reference position to assess rFHA knee kinematics

has been reported to successfully reduce the errors associated with the sFHA during a seated leg extension and single leg squat [5].

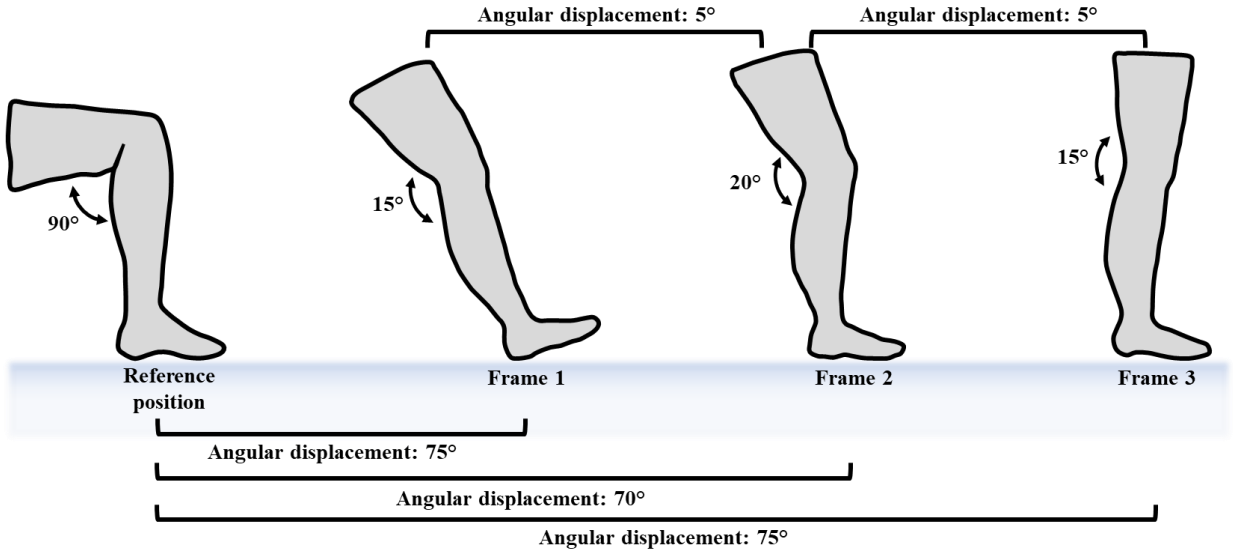

Figure 4-1 – An example of a reference position used to calculate the rFHA during a movement of interest. Maximum knee flexion during the movement of interest reaches 20 deg (Frame 2). Between each frame of data, the knee angular displacements reach a magnitude of 5 deg. The reference position (knee at 90 deg of flexion) is used to obtain larger angular displacements that are relative to the reference position itself. This provides angular displacements up to 75 deg for each frame of data. Note: Angular displacements of 5 deg between each frame are rare in biomechanics and are usually within sub-degree ranges due to high sample rates (typically 60-240 Hz). The values presented here are for illustration purposes.

The use of the rFHA may come with its own limitations. Similar to the placements of reflective skin markers [136], or the orientation of an anatomical coordinate system [137], the reference position may be susceptible to alignment errors that result in different rFHA measures. The

sensitivity of the rFHA and its outcome measures to misalignments of the reference position has not been assessed previously in the literature. A formal analysis of this sensitivity is important to provide an error range associated with misaligned reference positions. Understanding this error range would provide a foundation to the sensitivity of each rFHA measure when subjected to these inaccurate reference positions, an important factor when performing within- or between-participant comparisons. Therefore, the purpose of this study was to determine what magnitude of differences may be present in the rFHA measures over several reference position misalignments. A second study objective was to determine the contribution of an individual plane of rotation on the variability of the rFHA measure differences. Evaluating the sensitivity of the rFHA measures with altered reference positions will provide insight to the errors associated with misaligned reference positions.

4.2 Methods

4.2.1 Data Acquisition

A subset of previously collected data (REB15-0554) was used in this study. The original dataset consisted of six healthy, male participants performing a single leg squat and treadmill walking within the calibrated HSBV system. This study used a single trial from a treadmill walking task of one participant (age 24 years). High resolution MR images (magnet strength: 3T, sequence: fast imaging employing steady-state acquisition, resolution: 0.4 mm x 1.0 mm x 0.4 mm) of the participant's dominant knee were acquired. Afterwards, the participant performed treadmill walking (speed: 1.2 m/s) within a calibrated HSBV (sampling rate: 120 Hz). One full gait cycle (i.e., consecutive heel-strikes of the dominant leg) was recorded. A reference position was also recorded in which the participant stood upright with their feet hip width apart.

4.2.2 Data Processing

The images acquired from MRI were imported into Amira software (Thermo Fisher Scientific, MA, USA) for segmentation and generation of 3D femur and tibia models. Using modified methods of Miranda et al. (2010), the anatomical coordinate systems (ACS) of the femur and tibia bone models were defined [138]. Briefly, the femoral ML axis was defined as the line connecting the centres of spheres fit to each condyle. The center of this line was set as the femur origin. Afterwards, a temporary SI axis was obtained by calculating the smallest inertial axis of the femoral diaphysis. The AP axis was calculated by taking a cross product between the ML and temporary SI axis. The final SI axis was calculated as the cross product of the ML and AP axis, providing an orthogonal coordinate system. The tibia was first aligned to its inertial axes to isolate the tibial plateau, partitioned at the point of largest cross-sectional area along the transverse plane. The centroid of the tibial plateau was set as the origin. Afterwards, the inertial axes of the tibial plateau defined the ML, AP, and SI axes [138]. The ACS of both femur and tibia were aligned so that the ML axis was directed positive laterally, SI axis positive superiorly, and AP axis positive posteriorly. The formation of the ACS provided an affine transformation matrix (ATM) to relate the MRI coordinate system and the femoral or tibial ACS.

HSBV images were undistorted and then imported into 2D-3D registration software (Autoscoper, Brown University, USA) with calibration parameters that relate the 2D locations of the biplanar images to a 3D space relative to the HSBV. The 3D bone models (femur and tibia) were then manually 2D-3D registered to the HSBV frames in Autoscoper (Figure 4-2). Each registered frame in Autoscoper provided an affine transformation matrix, representing either the femur or tibia orientation and location with respect to the HSBV coordinate system. Therefore, two temporal series of ATM were acquired when registering a movement task, one for the femur and the other for the tibia. The reference position was also 2D-3D registered.

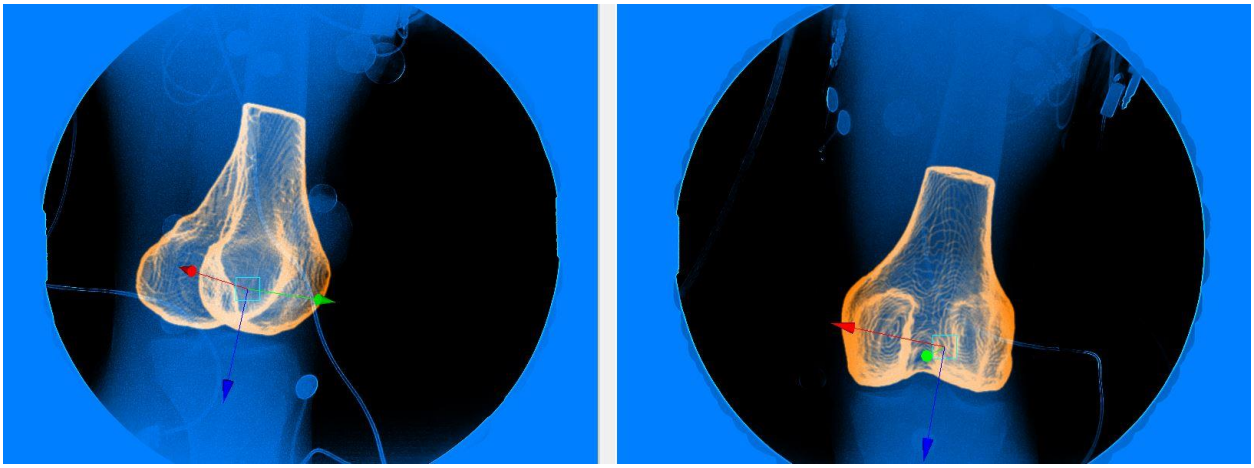

Figure 4-2 – A 3D model of the femur registered to the two 2D biplanar images of the HSBV. Registering all frames provides a temporal series of ATM for the femur.

The Autoscoper ATM for both the temporal series and reference position of the femur and tibia were imported into a custom MATLAB code (v2020b, MathWorks, MA, USA). The temporal ATM series were smoothed using a B-spline filter with an outlier removal process (SPOUT, refer to Chapter 3). The reference frames of the femoral and tibial ATM were converted from the HSBV coordinate system to the respective ACS, allowing subsequent rFHA calculations from the knee joint ATM relative to the reference position. Figure 4-3 provides a simplified illustration of this process.

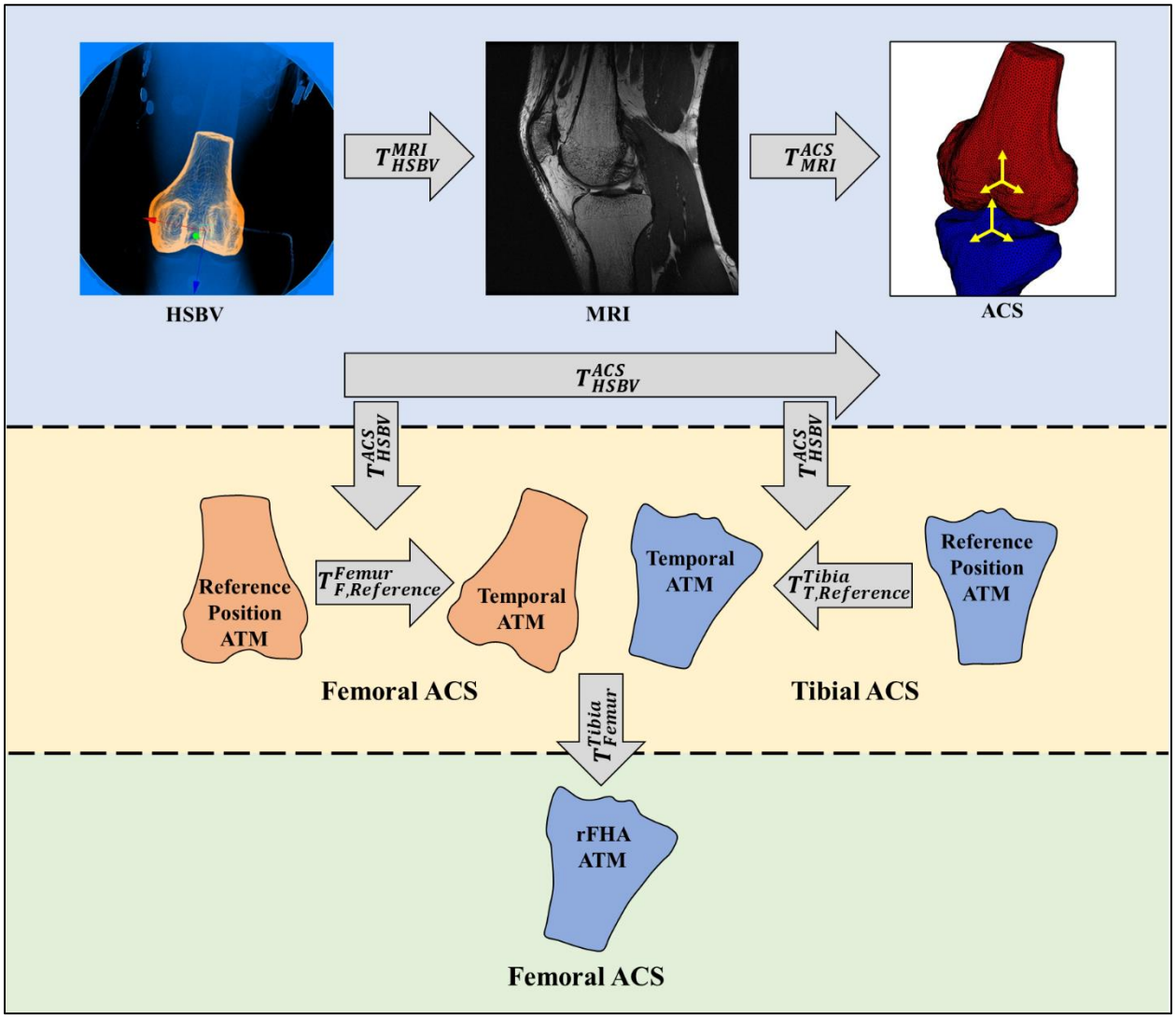

Figure 4-3 – A simplified illustration outlining the acquisition of the knee joint ATM for rFHA calculation in three steps/sections. Blue/top section: Summarizes the process of obtaining an ATM that relates the HSBV coordinate system to the femoral or tibial ACS ($[T^{ACS}_{HSBV}]$). Yellow/middle section: The application of $[T^{ACS}_{HSBV}]$ to the femoral and tibial ATM changes their reference frame to the respective ACS, allowing the calculation of the temporal ATM relative to the reference position ATM ($[T^{Femur}_{F,Reference}]$ and $[T^{Tibia}_{T,Reference}]$). Green/bottom section: The ATM of the tibia is calculated relative to the femoral ATM ($[T^{Tibia}_{Femur}]$), representing knee movement and the ATM required for rFHA calculations.

The conversion to the ACS was performed by calculating the ATM that relates the HSBV coordinate system and ACS (Equation 4-1; blue section in Figure 4-3),

$$[T_{HSBV}^{ACS}] = [T_{MRI}^{ACS}] * [T_{HSBV}^{MRI}] \quad \text{Eq. 4-1}$$

where $[T_{HSBV}^{MRI}]$ represents the ATM from the HSBV to MRI coordinate system, $[T_{MRI}^{ACS}]$ represents the ATM from the MRI to ACS, and $[T_{HSBV}^{ACS}]$ is the resulting ATM from the HSBV to ACS. Afterwards, the resulting transformation $[T_{HSBV}^{ACS}]$ was applied to the temporal series of ATM for both the femur and tibia, changing the reference frame from the HSBV coordinate system to the ACS (Equation 4-2; transition from the blue section to yellow section in Figure 4-3),

$$[T^{ACS}] = [T_{HSBV}^{ACS}] * [T^{HSBV}] * [T_{HSBV}^{ACS}]^{-1} \quad \text{Eq. 4-2}$$

where $[T^{HSBV}]$ is the temporal series of ATM from Autoscoper with respect to the HSBV coordinate system, and $[T^{ACS}]$ is the resulting temporal series of ATM within the ACS. The same procedure was performed for the reference position. ATM of the femoral and tibial temporal series were then calculated relative to the reference position (Equation 4-3; yellow section in Figure 4-3),

$$\left[T_{F,Reference}^{Femur}\right] = \left[T_{F.Reference}^{ACS}\right] * [T_{Femur}^{ACS}]^{-1} \quad \text{Eq. 4-3}$$

where $\left[T_{F,Reference}^{ACS}\right]$ and $[T_{Femur}^{ACS}]$ are ATM of the femoral reference position and temporal series in the ACS, respectively, and $\left[T_{F,Reference}^{Femur}\right]$ is the ATM of the femoral temporal series with respect to the reference position. Equation 4-3 was also applied to the tibia to obtain a temporal series of tibial ATM relative to the reference position. Finally, to obtain the temporal series of knee joint ATM to calculate the rFHA, the movement of the tibia was calculated relative to the femur (Equation 4-4; transition from the yellow section to green section in Figure 4-3),

$$\left[T_{Femur}^{Tibia}\right] = * \left[T_{F,Reference}^{Femur}\right] * \left[T_{T,Reference}^{Tibia}\right]^{-1} \quad \text{Eq. 4-4}$$

where $\left[T^{Femur}_{F,Reference}\right]$ and $\left[T^{Tibia}_{T,Reference}\right]$ represent the temporal series of the femur and tibia relative to their reference position, respectively, and $[T^{Femur}_{Tibia}]$ is the resulting temporal series of the tibia relative to the femur and used to calculate the rFHA (green section in Figure 4-3). The rFHA was calculated from heel-strike to mid-stance phases of the gait cycle. Six rFHA measures were determined: location, translation, orientation, dispersion, path length, and excursion (refer to section 2.3 for the measure descriptions).

4.2.3 Misalignment of the Reference Position

To simulate misalignments of the reference position, rotation matrices representing these misalignments were applied to the original position of the tibia, altering the knee angle. Specifically, deviations to the flexion/extension (F/E) and internal/external (I/E) rotation angles were applied. The abduction/adduction (Ab/Ad) angle was not altered due to the knee having a small RoM, both passively and dynamically, within this plane [126], [139]. The increments used to misalign the reference position were 4 deg in F/E and 1 deg in I/E rotation. These increments were selected from average differences relating to knee angle measurement modalities of three cadaveric knees at five different knee flexion angles (10°, 30°, 60°, 90°, and 120°) [140]. Specifically, the magnitude of 4 deg was chosen as traditional goniometers were reported to have 4 deg of F/E inaccuracy when compared to radiographic measurements. Furthermore, it was found that I/E rotation had differences of approximately 1 deg between different radiographic measurements [140]. As a result, the F/E angle was altered by four degrees in both directions, resulting in three F/E positions: original position (0 deg), more extended (+4 deg), and more flexed (-4 deg). The I/E rotation of the tibia was altered in one-degree increments, up to five degrees in both directions, resulting in eleven I/E positions: original position (0 degrees), internally rotated (+1, +2, +3, +4, and +5 degrees), and externally rotated (-1, -2, -3, -4, and -5 degrees). Overall, the

combinations of the three F/E and eleven I/E rotations provided a total of thirty-three different reference positions. For each reference position, six rFHA measures were calculated throughout the same trial and phase of walking: location, translation, orientation, dispersion, path length, and excursion (refer to section 1.2.2.3 for full definitions).

4.2.4 Data Analysis

For all six rFHA measures, the absolute differences between the original reference position (0 deg of F/E and I/E rotation) and misaligned reference positions (±4 deg of F/E and/or ±5 deg of I/E rotation) were calculated. This resulted in a total of thirty-two absolute differences. The mean difference, SD, and 95% CI of the thirty-two differences were calculated to determine the total influence of the misaligned reference positions. The percent change of the mean absolute difference with respect to the original reference position was also calculated.

The individual contribution of the F/E and I/E rotation angles to the total influence of the misaligned reference positions was assessed for each rFHA measure (Figure 4-4). To determine the influence of the I/E rotation angle, the mean differences and SD over the I/E rotation angles were calculated at each fixed F/E angle for each rFHA measure. Because three F/E angles were considered (-4 deg, 0 deg, +4 deg) a total of three means and SD were acquired. The three means and SD were further compiled into a single mean difference, SD, and 95% CI, representing the influence of the I/E rotation angle. A similar procedure was performed for the F/E angle, where the final mean difference, SD and 95% CI was compiled from eleven prior means and SD (i.e., I/E rotation angles from -5 deg to +5 deg in 1 deg increments).

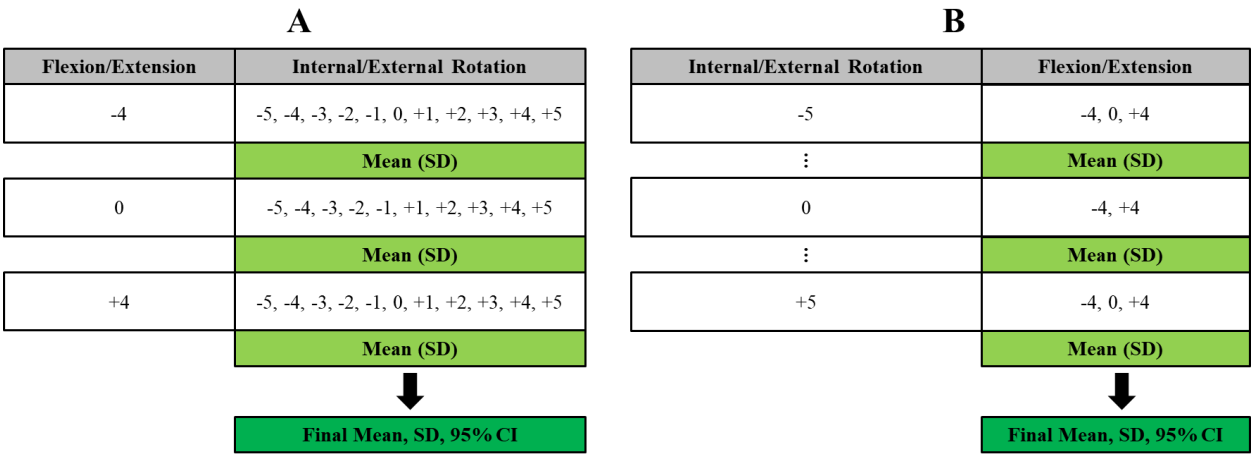

Figure 4-4 – A schematic diagram of the procedure used for isolating the individual influence of A) the I/E rotation misalignments and B) the F/E misalignments.

As a result, three different sets of mean differences and SD were acquired: one representing the total influence of the reference position misalignments, one representing the influence of the I/E rotation angle, and one representing the influence of the F/E angle. The SD for each set represented the variability of the total misalignments, I/E rotation angle, and F/E angle, respectively. To determine how much influence the I/E rotation and F/E angle had on the variability of the total misalignments for each rFHA measure, the percent contribution (%Con) of the I/E rotation (%Con IE) and F/E (%Con FE) were calculated using Equation 4-5 and Equation 4-6.

$$\%Con\ IE\ = \left(1\ -\ \frac{|IE\ SD\ -\ Total\ SD|}{Total\ SD}\right) * 100 \qquad \text{Eq. 4-5}$$

$$\%Con\ FE\ = \left(1\ -\ \frac{|FE\ SD\ -\ Total\ SD|}{Total\ SD}\right) * 100 \qquad \text{Eq. 4-6}$$

where $IE\ SD$, $FE\ SD$, and $Total\ SD$ represent the SD of the I/E rotation angle, F/E angle, and total misalignment, respectively. From the two equations, it can be seen that a %Con of one hundred would relate to the I/E rotation or F/E angle having a SD equal to the total misalignment.

Therefore, greater percentages were interpreted as greater contributions to the variability of the rFHA measures.

Finally, for each rFHA measure, the (not absolute) differences at every reference position misalignment were plotted. To determine if any patterns in the differences existed a line of best fit was incorporated to the plots and a coefficient of determination (R^2) calculated.

4.3 Results

An overall influence of the reference position misalignments was apparent (Table 4-1). Of the translational rFHA measures, the path length had the largest mean absolute difference (19.53 mm) and AP location the smallest (1.17 mm change). However, the AP location had the largest percent change (33.98%), while the remaining translational rFHA measures ranged from 13.72-20.57%. Of the angular rFHA measures, orientation demonstrated a larger mean absolute difference than the dispersion but similar percent changes (orientation: mean difference = 5.45 deg, percent change = 12.98%; dispersion: mean difference = 0.77 deg, percent change = 12.79%).

Table 4-1 – The total influence of the reference position misalignments from the original reference position. Mean absolute differences, SD, 95% CI, and percent change of each rFHA measure are provided.

rFHA Measure		Total				
		Original Reference Position	Mean Absolute Difference	SD	95% CI	% Change
Location (mm)	AP	3.44	1.17	0.81	(-0.42, 2.76)	33.98
	SI	-35.17	5.25	3.31	(-1.25, 11.74)	14.92
Translation (mm)		-9.19	1.26	0.84	(-0.38, 2.90)	13.72
Orientation (deg)		41.98	5.45	3.66	(-1.72, 12.61)	12.98
Dispersion (deg)		6.03	0.77	0.54	(-0.29, 1.83)	12.79
Path Length (mm)		112.29	19.53	13.39	(-6.72, 45.77)	17.39
Excursion (mm)	AP	71.43	10.73	7.63	(-4.22, 25.68)	15.03
	SI	33.93	6.98	4.20	(-1.26, 15.22)	20.57

The individual I/E rotation and F/E angles showed different influences on the variability of each rFHA measure (Table 4-2). The largest influences originated from the F/E angles, with %Con ranging from 72.28-98.26%. The I/E rotation tended to have smaller contributions, ranging from 3.64-98.57%. The F/E angles had greater influence than the I/E rotation angles in SI location (F/E: 89.18%; I/E: 33.78%), path length (F/E: 85.74%; I/E: 22.67%), AP excursion (F/E: 87.55%; I/E: 3.64%), and SI excursion (F/E: 88.74%; I/E: 50.80%). The I/E rotation angles had greater influence than the F/E angles in AP location (I/E: 89.43%; F/E: 72.28%). No difference in influence was found for translation (I/E: 98.57%; F/E: 97.95%), orientation (I/E: 96.84%; F/E: 95.38%), and dispersion (I/E: 97.40%; I/E: 98.26%).

Table 4-2 – The individual influence of the I/E rotation and F/E angles on the rFHA measures. The %Con of each angle to the variability of the total influence are also provided.

rFHA Measure		Internal/External Rotation				Flexion/Extension			
		Mean Absolute Difference	SD	95% CI	% Contribution	Mean Absolute Difference	SD	95% CI	% Contribution
Location (mm)	AP	1.17	0.73	(-0.25, 2.59)	89.43	1.15	0.59	(0.00, 2.30)	72.28
	SI	5.11	1.12	(2.91, 7.30)	33.78	5.31	3.67	(-1.88, 12.51)	89.18
Translation (mm)		1.26	0.83	(-0.36, 2.88)	98.57	1.25	0.82	(-0.36, 2.86)	97.95
Orientation (deg)		5.40	3.54	(-1.54, 12.34)	96.84	5.47	3.82	(-2.03, 12.97)	95.38
Dispersion (deg)		0.77	0.53	(-0.26, 1.80)	97.40	0.76	0.53	(-0.28, 1.80)	98.26
Path Length (mm)		18.99	3.04	(13.04, 24.94)	22.67	19.77	15.30	(-10.21, 49.76)	85.74
Excursion (mm)	AP	10.42	0.28	(9.87, 10.96)	3.64	10.88	8.58	(-5.93, 27.69)	87.55
	SI	6.84	2.13	(2.65, 11.02)	50.80	7.06	4.68	(-2.10, 16.22)	88.74

The graphs illustrated a distinct and consistent pattern of differences with each reference position misalignment (Figure 4-5). This was evident with second-degree polynomials, pertaining to the differences at each simulated reference position, having perfect coefficients of determination (R^2 = 1).

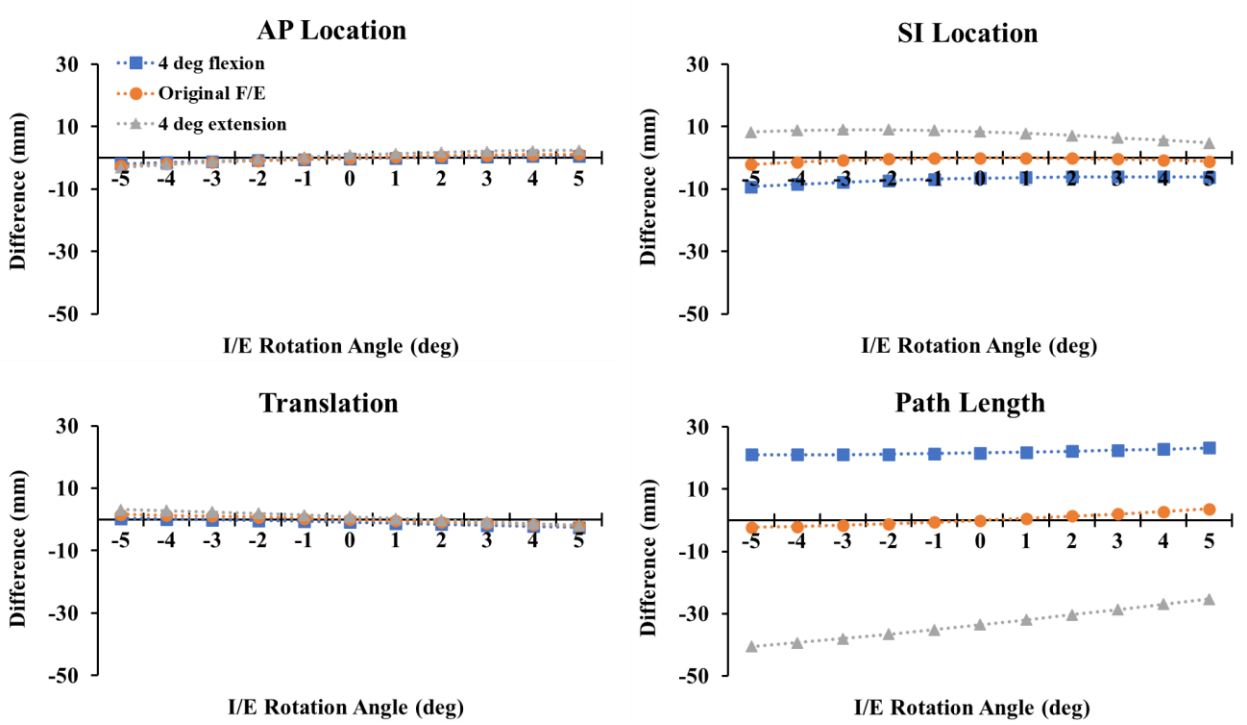

Figure 4-5 – Graphs for each rFHA measure illustrating the differences (original – misaligned) associated with the thirty-two reference position misalignments. Each line represents a specific F/E angle (blue = +4 deg flexion, orange = 0 deg flexion, grey = 4 deg extension) over the eleven difference I/E rotation angles (-5 – +5 deg). Second-degree polynomials at each F/E angle over the eleven I/E rotation angles had perfect coefficient of variations (R^2 = 1) and are thus not shown (figure continued on next page).

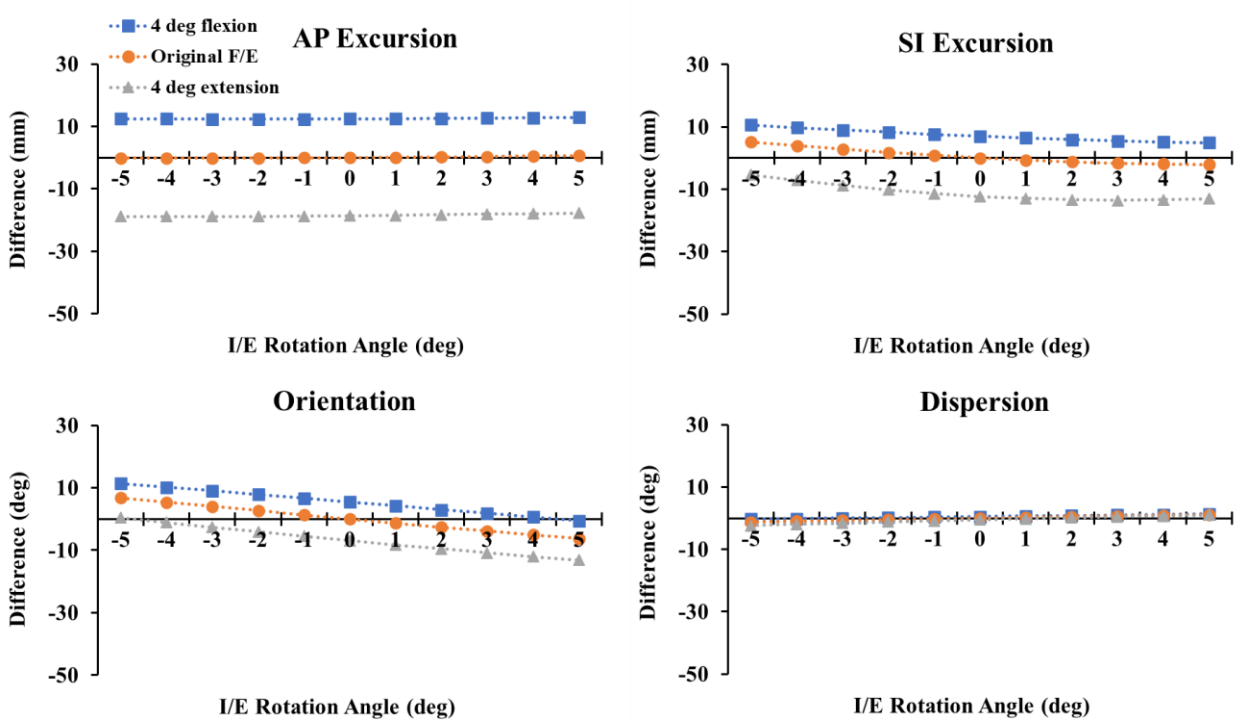

Figure 4-5 – Graphs for each rFHA measure illustrating the differences (original – misaligned) associated with the thirty-two reference position misalignments. Each line represents a specific F/E angle (blue = +4 deg flexion, orange = 0 deg flexion, grey = 4 deg extension) over the eleven difference I/E rotation angles (-5 – +5 deg). Second-degree polynomials at each F/E angle over the eleven I/E rotation angles had perfect coefficient of variations ($R^2 = 1$) and are thus not shown.

4.4 Discussion

This study investigated the influence of several misaligned reference positions on six rFHA measures. Two knee angles – F/E and I/E rotation – were computationally altered to produce thirty-two simulated misalignments from the original reference position. The differences associated with the total misalignments were assessed, as well as the individual influence of each angle.

The total misalignments of the reference position (i.e., combined F/E and I/E rotation angles) revealed the presence of differences for most of the rFHA measures (Table 4-1). Specifically, the

path length and AP excursion showed the largest mean absolute differences while the SI location, orientation, and SI excursion showed similar mean absolute differences. The AP location, translation, and dispersion showed the smallest mean absolute differences. The small differences in the rFHA translation and dispersion may be due to their independence of the reference position. The rFHA translation represents the summed translation that occurred throughout a movement task, while the dispersion is a measure of the rotational variability throughout a movement task. Therefore, a misalignment in the reference position (which acts as a baseline for the rFHA measures) would have a small effect on the amount of translation that occurred, and the variability of the movement performed. Regardless, the study findings indicate that the misalignment of the F/E and I/E rotation angles within the reference position can substantially influence the rFHA measures. Therefore, care must be taken when selecting and aligning the knee in its reference position to minimize these differences.

The study results suggest that misalignments of the F/E and I/E rotation angles may influence the rFHA measures differently. This was evident in their percent contribution (%Con) to the total misalignment variability (Table 4-2). The F/E angle of the reference position had the largest contributions, especially within the SI location, path length, and AP/SI excursion. This finding suggests that the knee F/E angle within the reference position may have a greater contribution to the rFHA measures than the I/E rotation angle. This may be a result of F/E being the most prominent rotation of the knee, while I/E rotation and Ab/Ad contain smaller magnitudes of movement and are considered secondary movements [139]. However, it is important to note that the I/E rotation misalignment had a higher contribution than the F/E misalignment for AP location. Although the %Con was not much greater (I/E rotation: 89.43%; F/E: 72.28%), it does suggest that the two anatomical planes of movement may uniquely influence specific rFHA measures. This

is best portrayed in the graphs of the AP location and AP excursion (Figure 4-5). In the AP location graph, it can be seen that at each I/E rotation increment, the three data points representing the F/E angles do not vary as much as the I/E angles at a fixed F/E angle (I/E rotation SD: 0.73 mm, F/E: 0.59 mm, Table 4-2). The opposite is seen within the AP excursion, where the variability at a single I/E increment resulted in large variability within the F/E angles, but minimal variability was observed throughout the I/E angles at a fixed F/E angle (I/E rotation SD: 0.28 mm, F/E: 8.58 mm, Table 4-2).

Lastly, second-degree polynomials fit to the rFHA measure differences resulted in perfect coefficients of variation ($R^2 = 1$). This is not surprising, as the reference position represents a baseline for the rFHA measures. Therefore, a change in the reference position would influence the rFHA measures in a specific and quantifiable manner. The polynomials determined at each F/E increment represent a function that relates the I/E rotation misalignment to the magnitude of error. As a result, there may exist the possibility to "correct" the rFHA measures to a specific reference position. This could be valuable for repeated measure studies, requiring multiple reference positions over time. For example, assume a reference position (and associated movement data) was collected at two time points for a single participant, with the purpose of performing an rFHA analysis of the knee. If the second reference position differed by 4 deg of flexion and 2 deg of internal rotation, a correction of the rFHA measures at the second time point may be feasible. This would be achieved by using the functions for each rFHA measure associated with 4 deg of knee flexion and inputting the corresponding I/E rotation parameters (i.e., +2 deg). This would produce the magnitude of errors that would be present for each rFHA measure and could be adjusted for within the data.

4.4.1 Strengths & Limitations

One strength of this study was the use of the HSBV, which supplied the ability to record bone movements directly, thus not relying on reflective skin markers. Therefore, skin movement artifacts were completely avoided, and more accurate knee kinematics were obtained. Another strength of this study was the use of simulated misalignments to the reference position. Firstly, simulating misalignments had the advantage of not exposing participants to unnecessary multiple trials within the HSBV, reducing the risk of unnecessary radiation. Secondly, this allowed known, controlled misalignments to be input to understand the effect of different reference positions on the rFHA measures. With human participants it would be challenging to accurately align the knee angle at the different increments used in this study. However, the misalignments used in this study may under- or over-estimate the true misalignments encountered with human positioning. Future studies may consider aligning human participants to a reference position for multiple trials. This would help to better understand what the actual range of knee angles may be when aligning the reference position. Additionally, the repeatability of the reference position could be assessed with multiple trials from human participants (this could not be addressed in this study). Investigating the expected variation in reference position alignment within and between participants is important to consider given the substantial impact of reference position misalignments on the rFHA measures. However, because the HSBV uses X-rays, the risk of radiation is present when performing multiple trials and may to lead to complications when establishing an experimental design.

Lastly, only a walking movement for one healthy participant was assessed in this study. A larger sample size would provide more confidence in the results of the study, ensuring the differences observed with one participant are observed in other participants. Other daily movement tasks, such as a step-up or knee bend, may provide different patterns and magnitudes of differences when

compared to walking and require further investigation. Because the reference position acts solely as a baseline for the rFHA measures, it would be expected that similar, relative patterns would exist with different movements and healthy participants. However, individuals with injured or OA knees may have altered differences with reference position misalignments when compared to healthy knees and the influence of this requires further investigation as well.

4.5 Conclusions

The purpose of this study was to determine the influence of reference position misalignments on the rFHA measures. This was achieved by simulating thirty-two misaligned reference positions and determining the mean absolute differences of the rFHA measures relative to the original position. It was found that the alignment of the reference position had a substantial impact on the rFHA measures, with mean absolute differences ranging from 1.17-19.53 mm and 0.77-5.45 deg. The percent change of the differences relative to the original reference position ranged from 12.79-33.98%. The variabilities of these differences were mostly associated with the F/E angle of the knee, with %Con ranging from 72.28-98.26%. These results provided an indication as to what rFHA measure differences may exist with misaligned reference positions. These differences could potentially be corrected for in repeated measure studies by using a ‘correction function’. However, future studies are recommended to consider the use of a device to position the femur and tibia into appropriate and repeatable alignments of knee F/E and I/E rotation.

Chapter Five: Differences in the rFHA Measures Between Two Imaging Modalities

5.1 Introduction

The rFHA is a promising method to quantify and distinguish the kinematics of individuals at high risk of tibiofemoral OA. With the use of the conventional OMCS, the rFHA provided measures that could detect kinematic differences between injured and contralateral knees of participants with ACLD [40]. However, due to the use of skin mounted reflective markers, the OMCS is susceptible to movement artifacts that potentially result in erroneous kinematics (refer to section 1.2.1.1). For the thigh and shank during a walking task, these artifacts have been reported to produce 4.4 deg and 13.0 mm of error within the CA and translations, respectively [7]. These ranges may be viewed as the minimal detectable difference (MDD), or the minimum difference required to confidently suggest that the difference observed is "true". Otherwise, any differences within the MDD may originate from skin movement artifacts. These artifacts have also been reported when using the sFHA, resulting in HA with impractical directionalities that exceed two SD away from the mean HA [10]. To avoid skin movement artifacts, alternative options exist that can capture joint motion without the use of skin mounted reflective markers (e.g., dynamic MRI [141], flock of birds [142], 4D CT [143]). One method in particular, HSBV, uses biplanar X-rays to capture bone movements within sub-millimeter accuracies (refer to section 1.2.1.2) [17].

The effect of skin movement artifacts on the rFHA remain unknown. However, the HSBV may provide a gold standard comparison to determine the influence of skin movement artifacts within the OMCS. Therefore, the purpose of this study was to compare six rFHA measures derived from both the OMCS and HSBV. This analysis will provide insight into the presence and influence of skin movement artifacts on the rFHA measures. It was hypothesized that the differences between

the two modalities would lie within the reported magnitudes of skin movement artifact errors (up to 4.4 deg and 13.0 mm).

5.2 Methods

The data and methods used in this study were partly described in the sub-analysis of Chapter 4 (section 4.2). Therefore, any additional information relevant to the study in this chapter will be provided in this section.

5.2.1 Study Participants

Six healthy male participants (ages 24-37) were recruited for this ethics approved study (REB15-0554) (Table 5-1). Healthy participants were considered as individuals with no knee pain or stiffness in the past year and no prior lower limb or knee surgery.

Table 5-1 – Participant measurements. Ages, heights, weights, and BMI are provided for all six participants.

Participant	Age (yrs)	Height (cm)	Weight (kg)	BMI
MADF 001	24	182	72	21.74
MADF 002	29	165	48	17.63
MADF 003	33	173	72	24.06
MADF 004	37	182	91	27.47
MADF 005	31	175	77	25.14
MADF 006	26	185	80	23.37
Mean (SD)	30 (4.73)	177 (7.46)	73.33 (14.25)	23.24 (3.34)

5.2.2 Data Acquisition

Data acquired for this study was also used for a validation study not related to this thesis. Additional measurement systems (e.g., electromyography [EMG]) and reflective skin markers were incorporated to achieve the objectives of the validation study. Only the measurement systems and reflective skin markers relevant to the objectives of the current study are presented here. Six

reflective markers were placed on the dominant leg of the participant – one triad on the thigh and the other on the shank – representing the underlying femur and tibia, respectively. Prior to kinematic data collection, images of the participant's dominant knee were acquired using a 1.5T MRI (sequence: fast imaging employing steady-state acquisition [0.40 x 1.00 x 0.40 mm]). Afterwards, the participant performed two movement tasks: treadmill walking (at 1.2 m/s) and single leg squats, within a synchronized OMCS (120 Hz) and HSBV (60 Hz) setup (Figure 5-1). Additionally, the participant was recorded in a standing position, which was to be used as the reference position for the rFHA. One trial of a full gait cycle (consecutive heel-strikes of the dominant leg) was collected for the walking task. Additionally, participants performed three trials of single leg squats. The depth of squat was not specified and subjective to the comfort of the participant.

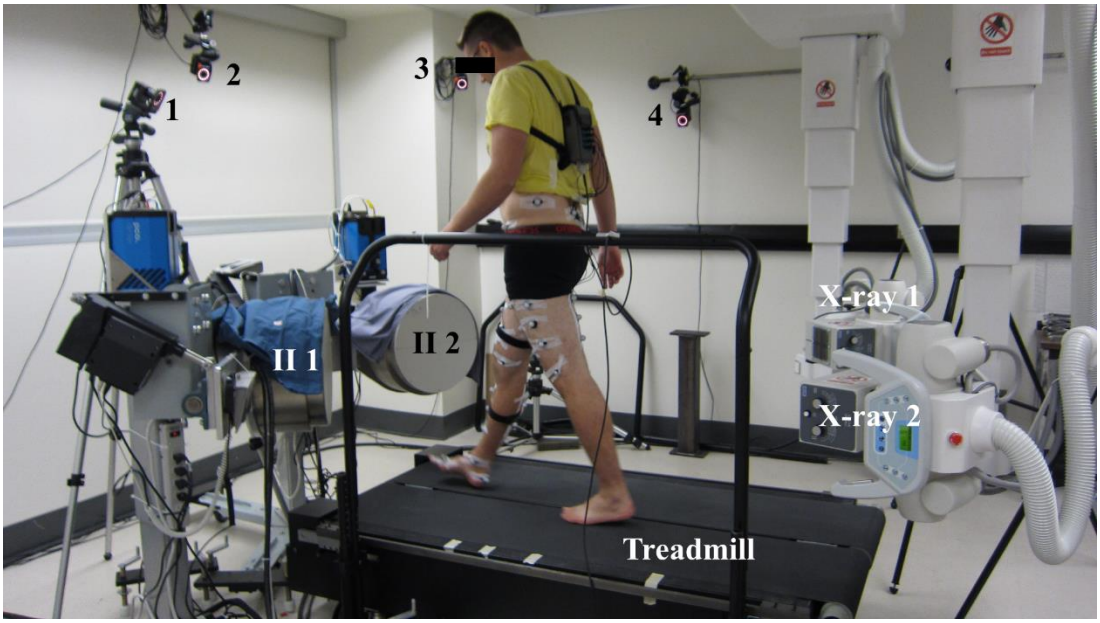

Figure 5-1 – The synchronized OMCS and HSBV setup. Four of eight cameras (1-4) for the OMCS are seen above the HSBV. Two image intensifiers (II 1 and II 2) and corresponding X-ray generators (X-ray 1 and X-ray 2) for the HSBV can be seen as well. Participants performed treadmill walking and a single leg squat within the two systems. Protective lead vests were worn during all HSBV trials.

To obtain a spatial relationship between the coordinate systems of the OMCS and HSBV, a custom calibration cube containing twelve reflective markers was imaged in both modalities (Figure 5-2). The locations of the markers on the calibration cube provided common reference markers within the OMCS coordinate system and the HSBV coordinate system. As a result, the magnitudes of rotation and translation to relate the two coordinate systems could be obtained.

Figure 5-2 – The custom calibration cube, containing twelve reflective markers, to relate the coordinate systems of the OMCS and HSBV.

5.2.3 Data Processing

A brief description of the data processing methods is supplied here. For a more detailed explanation, refer to Chapter 4 (section 4.2.2).

MR images were segmented using Amira software (Thermo Fisher Scientific Inc., MA, USA) to acquire 3D bone models of the femur and tibia. Afterwards, the bone models were 2D-3D registered to the biplanar images of the HSBV using Autoscoper (Brown University, RI, USA). Specifically, 3D bone models of the femur and tibia were individually aligned to each pair of frames provided by the HSBV. This process results in two separate series of affine transformation matrices (ATM), one for the femur and one for the tibia. The individual ATM series of the femur

and tibia were imported to a custom MATLAB code (v2020b, MathWorks, MA, USA). The ATM of the femur and tibia were filtered using a B-spline filter with outlier removal (SPOUT) and then used to calculate the rFHA of the knee relative to their respective femoral and tibial ACS [138].

For the OMCS data, reflective marker locations for the reference position and movement tasks were tracked using Cortex (Motion Analysis, CA, USA) and smoothed with a low pass Butterworth filter (cut-off frequency: 6 Hz). The selection of a 6 Hz cut-off frequency was based on a Fast Fourier Transform spectrum analysis, which determined that the majority of frequencies within both movement tasks fell under 3 Hz. To transform the marker locations of the thigh and shank to the same femoral and tibial ACS, respectively, an equation similar to Equation 4-1 (section 4.2.2) to transform the Autoscoper ATM to the ACS was used,

$$[T_{HSBV}^{ACS}] = [T_{MRI}^{ACS}] * [T_{HSBV}^{MRI}] \quad \text{Eq. 4-1}$$

where $[T_{HSBV}^{MRI}]$ represents the ATM from the HSBV to MRI coordinate system, $[T_{MRI}^{ACS}]$ represents the ATM from the MRI to ACS, and $[T_{HSBV}^{ACS}]$ is the resulting ATM from the HSBV to ACS. An additional ATM that relates the OMCS coordinate system to the HSBV coordinate system ($[T_{OMCS}^{HSBV}]$) was required, resulting in the equation

$$[T_{OMCS}^{ACS}] = [T_{MRI}^{ACS}] * [T_{HSBV}^{MRI}] * [T_{OMCS}^{HSBV}] \quad \text{Eq. 5-1}$$

$[T_{OMCS}^{HSBV}]$ was obtained from the images of the custom calibration cube (Figure 5-2) obtained in both the HSBV and OMCS systems. The marker locations of the neutral and movement trials, for both the thigh and shank, were then converted to the ACS,

$$[X_{ACS}] = [X_{OMCS}] * [T_{OMCS}^{ACS}] \quad \text{Eq. 5-2}$$

where $[X_{OMCS}]$ is a matrix that contains the marker locations (mm) of the thigh or shank marker triads within the OMCS coordinate system, and $[X_{ACS}]$ is a matrix that contains the marker

locations (mm) of the thigh or shank triads within the ACS. Afterwards, a singular value decomposition approach described by Challis (1995) was applied to the ACS marker locations of the thigh, obtaining a series of ATM that represent the kinematics of the thigh relative to its reference position. The same process was repeated for the shank. Afterwards, the ATM series of the tibio-femoral joint was calculated using Equation 4-4 (section 4.2.2).

$$\left[T_{Femur}^{Tibia}\right] = * \left[T_{F,Reference}^{Femur}\right] * \left[T_{T,Reference}^{Tibia}\right]^{-1} \quad \text{Eq. 4-4}$$

where $\left[T_{F,Reference}^{Femur}\right]$ and $\left[T_{T,Reference}^{Tibia}\right]$ represent the temporal series of the femur and tibia relative to their reference position, respectively, and $[T_{Tibia}^{Femur}]$ is the resulting temporal series of the tibia relative to the femur and is used to calculate the rFHA. In the case of the OMCS, the femur and tibia ATM are represented by the thigh and shank ATM, respectively.

Six rFHA measures were calculated: location, translation, orientation, dispersion, path length, and excursion (refer to section 2.3 for measure descriptions). For single leg squats, the rFHA measures were calculated during the extension phase of the squat – specifically from 40 deg to 20 deg of knee flexion. Trials were removed from analysis if they did not reach a squat depth to 40 deg, or had HSBV images unsuitable for tracking (e.g., the tibia was occluded, Figure 5-3). If more than two trials were removed for a participant, the participant was completely removed from the single leg squat analysis. For the single walking trial, the rFHA was calculated from heel-strike to mid-stance. Like the single leg squat, if the HSBV images were unsuitable for tracking due to bone occlusion the participant was removed from the walking analysis. Trials of both movements, from both the OMCS and HSBV, were normalized to 100 data points prior to calculating the rFHA measures. The remaining trials of the single leg squat for each imaging system were averaged for each participant.

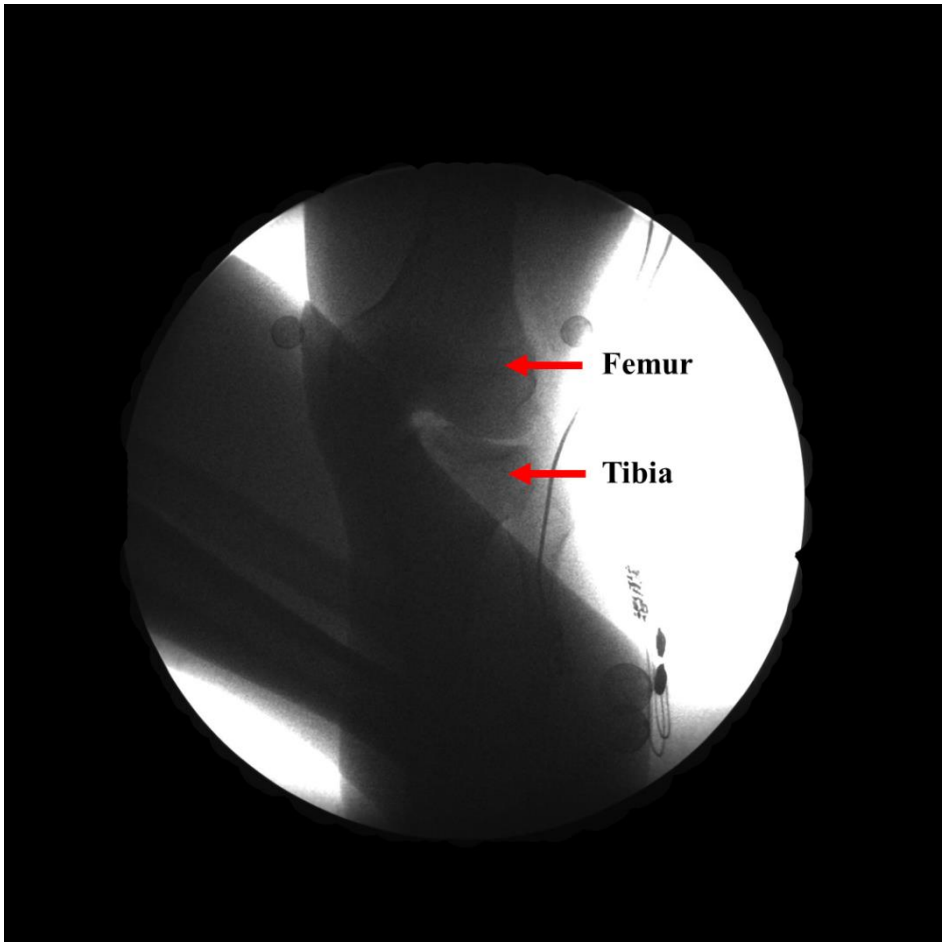

Figure 5-3 – Example of limb crossover during a single leg squat that resulted in an occluded tibia.

5.2.4 Data Analysis

For each participant, the rFHA measures derived from the HSBV data were subtracted from the matching OMCS data (HSBV – OMCS), thus acquiring paired differences of the two imaging modalities. Due to the small sample size of the study, a non-parametric Wilcoxon signed-rank test ($\alpha = 0.05$) was used to assess the paired differences of the rFHA measures. A Benjamini-Hochberg procedure with a false discovery rate of 5% was used to compensate for multiple testing and preserve the significance value to 0.05. Original p-values are reported, and those below 0.05 are explicitly stated if they remained significant after the application of the Benjamini-Hochberg

procedure. Additionally, for each rFHA measure, absolute values of the paired differences were compiled into a mean absolute paired difference and associated SD.

5.3 Results

Of the six participants recruited, four were included in both the single leg squat and walking analysis. Different participants were dropped between movement tasks. For the single leg squat, MADF 003 and MADF 004 were unable to reach knee flexions of 40 deg and/or had limb occlusion within two or more trials. For walking, MADF 004 and MADF 006 were removed due to their trials containing limb occlusion.

5.3.1 Single Leg Squat

Although not significant, paired differences (n = 4) in the AP location (p = 0.07), path length (p = 0.07), and AP excursion (p = 0.07) had consistent directionalities as all rank counts were positive or negative (Table 5-2). A tracing of the rFHA location along the femoral mid-sagittal plane for each participant illustrates these consistent differences (Figure 5-4). To elaborate, the AP location represents the mean AP intersection of the rFHA with the mid-sagittal plane of the femur, the path length represents the total distance the AP/SI location travelled along the mid-sagittal plane, and the AP excursion is the range of the AP intersection. The negative rank count in the AP location indicates a more anterior rFHA location in the OMCS. The positive rank counts in the path length and AP excursion indicate a shorter distance travelled and a smaller range of movement in the AP direction, respectively, for the OMCS. Therefore, the location tracings are more anterior and shorter for the OMCS (Figure 5-4). All other measures did not show a consistent directionality in their differences (Table 5-2).

Table 5-2 – Results of the Wilcoxon signed rank test (HSBV – OMCS) during the extension phase of the single leg squat for all rFHA measures. No significant findings were found, but the AP location, path length, and AP excursion had consistent directionalities in their differences, with all rank counts in positive or negative directions.

Single Leg Squat rFHA Measure		Rank Counts		Mean Rank		p-value
		Positive	Negative	Positive	Negative	
Location	AP	0	4	0.00	2.50	0.07
	SI	2	2	3.00	2.00	0.72
Translation		2	2	3.50	1.50	0.47
Orientation		2	2	2.50	2.50	1.00
Dispersion		3	1	2.33	3.00	0.47
Path Length		4	0	2.50	0.00	0.07
Excursion	AP	4	0	2.50	0.00	0.07
	SI	2	2	2.50	2.50	1.00

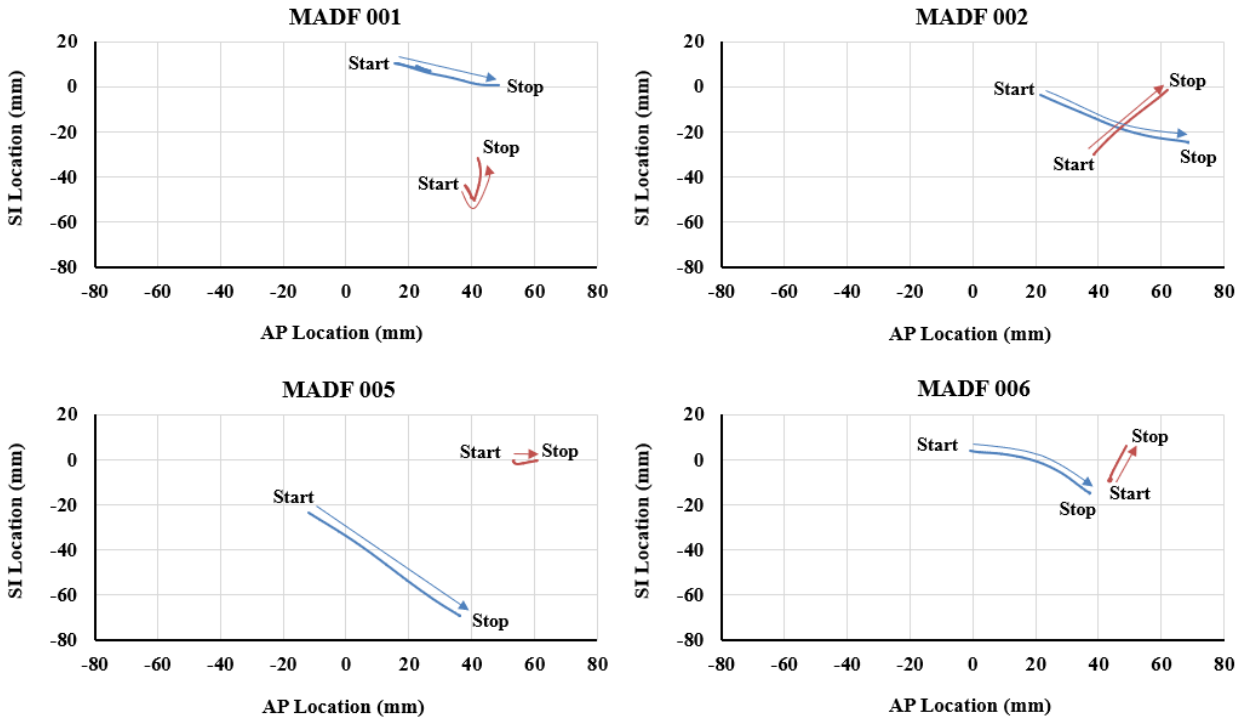

Figure 5-4 – Within-participant mean rFHA location tracings along the femoral mid-sagittal plane for both the HSBV (blue) and OMCS (red) during the single leg squat. OMCS tracings were more anterior and shorter in length. Start and stop indicate the beginning and end of the extension phase, respectively. Arrows dictate the direction of the trace.

The absolute paired differences of the rFHA measures ranged from 7.29-37.85 mm and 0.87-6.34 deg (Table 5-3). The largest absolute difference was seen in the path length (mean [SD] difference: 37.85 [18.42] mm). However, the AP/SI location and AP/SI excursion were also large. AP and SI locations showed mean (SD) absolute differences of 24.31 (17.15) mm and 24.41 (24.27) mm, respectively. AP and SI excursions showed absolute differences of 31.09 (7.21) mm and 15.59 (18.81) mm, respectively. Translation along the rFHA showed a smaller absolute difference of 7.29 (6.27) mm. The orientation and dispersion also demonstrated smaller absolute differences (orientation mean [SD] difference: 6.34 [2.10] deg; dispersion: 0.87 [0.34] deg).

Table 5-3 – The mean absolute paired differences (HSBV – OMCS) and associated SD of the rFHA measures during the extension phase of the single leg squat.

Single Leg Squat		HSBV		OMCS		Absolute Paired Difference	
rFHA Measure		Mean	SD	Mean	SD	Mean	SD
Location (mm)	AP	24.44	15.37	48.75	8.49	24.31	17.15
	SI	-13.67	20.68	-15.23	17.99	24.41	24.27
Translation (mm)		1.43	7.71	-3.08	3.73	7.29	6.27
Orientation (deg)		18.86	8.83	19.13	7.78	6.34	2.10
Dispersion (deg)		2.77	1.21	2.40	1.60	0.87	0.34
Path Length (mm)		58.87	22.02	21.03	15.68	37.85	18.42
Excursion (mm)	AP	42.16	10.33	11.07	8.06	31.09	7.21
	SI	24.30	14.98	16.73	11.89	15.59	18.81

5.3.2 Walking

No significant paired differences (n = 4) between the HSBV and OMCS were found for the rFHA measures from heel-strike to mid-stance of walking. However, the differences in path length contained the same directionality for all four participants, evident in its positive rank counts (positive rank count: 4; negative rank count: 0) (Table 5-4). This finding is further illustrated by the rFHA location tracing along the femoral mid-sagittal plane, where the length of the tracing tended to be longer within the HSBV (Figure 5-5).

Table 5-4 – Results of the Wilcoxon signed rank test (HSBV – OMCS) during the walking task from heel-strike to midstance for all rFHA measures. No significant differences were found, but the path length was seen to have all positive ranks.

Walking		Rank Counts		Mean Rank		p-value
rFHA Measure		Positive	Negative	Positive	Negative	
Location	AP	2	2	3.50	1.50	0.47
	SI	3	1	2.33	3.00	0.47
Translation		2	2	1.50	3.50	0.47
Orientation		2	2	1.50	3.50	0.47
Dispersion		3	1	3.00	1.00	0.14
Path Length		4	0	2.50	0.00	0.07
Excursion	AP	3	1	3.00	1.00	0.14
	SI	2	2	2.50	2.50	1.00

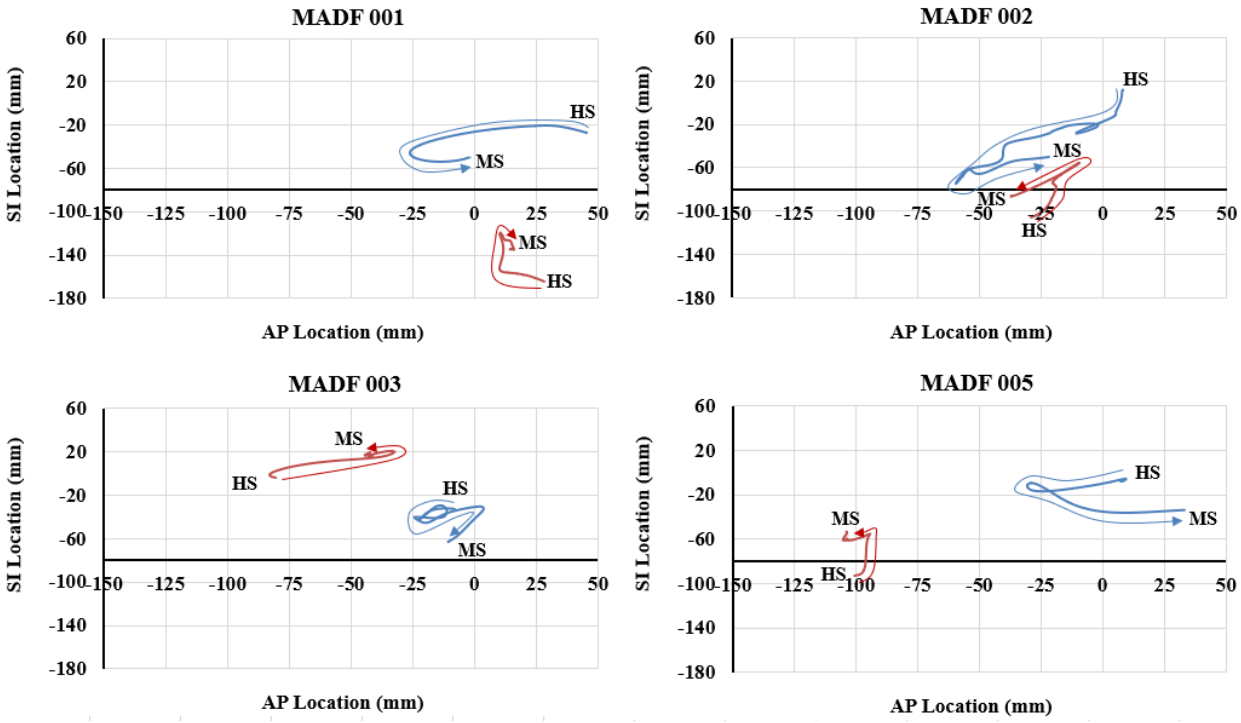

Figure 5-5 – The rFHA location tracings along the femoral mid-sagittal plane for both the HSBV (blue) and OMCS (red) during the walking task (heel-strike to midstance). Although not significant, all HSBV path lengths were greater than the OMCS. HS and MS indicate the time points of heel-strike and midstance, respectively. Arrows dictate the direction of the trace.

Similar patterns of the mean absolute differences to the single leg squat were observed. The path length had the largest absolute difference with mean (SD) difference of 101.84 (58.03) mm. AP/SI location and AP/SI excursion showed large magnitudes of absolute differences as well. AP and SI location had absolute differences of 35.55 (38.22) mm and 59.71 (27.84) mm, respectively. AP and SI excursion showed absolute differences of 47.32 (16.74) mm and 24.02 (29.42) mm, respectively. The translation had a smaller absolute difference of 11.87 (10.19) mm. Orientation and dispersion revealed absolute differences of 22.90 (13.63) deg and 4.13 (3.39) deg, respectively.

Overall, larger magnitudes (29-240%) of mean absolute differences were seen in the rFHA measures during walking when compared to the single leg squat (Table 5-5).

Table 5-5 – The mean absolute paired differences (HSBV – OMCS) and associated SD of the rFHA measures from heel-strike to mid-stance of walking.

Walking		HSBV		OMCS		Absolute Paired Difference	
rFHA Measure		Mean	SD	Mean	SD	Mean	SD
Location (mm)	AP	-12.11	13.21	-38.47	47.99	35.55	38.22
	SI	-32.10	10.92	-64.66	61.92	59.71	27.84
Translation (mm)		-9.53	6.58	-2.10	8.75	11.87	10.19
Orientation (deg)		29.42	13.32	39.94	15.51	22.90	13.63
Dispersion (deg)		6.49	3.18	2.94	1.44	4.13	3.39
Path Length (mm)		143.68	40.67	41.85	18.66	101.84	58.03
Excursion (mm)	AP	57.68	19.98	21.74	19.93	47.31	16.74
	SI	46.13	26.73	31.94	12.39	24.02	29.42

5.4 Discussion

The OMCS requires skin mounted markers to represent the underlying movement of the bones of interest. However, the presence of skin movement artifacts can introduce noise to the data, with CA errors reported to reach magnitudes of 4.4 deg for rotations and 13.0 mm for translations during a walking task [7], [144]. The HSBV has an advantage over the OMCS by eliminating skin movement artifacts and providing the ability to record bone movement directly. Therefore, this study investigated the influence of skin movement artifacts on rFHA measures by simultaneously collecting HSBV and OMCS data during a single leg squat (n = 4) and walking (n = 4). It was hypothesized that the differences in rFHA measures between the two imaging modalities would lie within the range of CA errors.

Paired differences of the path length, AP excursion, and AP location had consistent directionalities of differences during the single leg squat between the HSBV and OMCS (i.e., all four differences

were either negative or positive, Table 5-2). This was visible in the rFHA location trace, which depicted rFHA intersections along the femoral mid-sagittal plane that were more anterior and shorter in length in the OMCS compared to the HSBV (Figure 5-4). Furthermore, the direction of the trace for both systems appeared to visualize an accurate knee extension movement of the knee. During knee extension while running, it has been reported that the sFHA will shift anteriorly [102]. The rFHA trace of all participants, with the exception of the OMCS in MADF 001, demonstrated this anterior motion. However, this anterior shift appeared to be more pronounced with the HSBV. This finding also suggests that the rFHA can produce similar patterns to the sFHA but maintain temporal resolution.

The path length within the walking task showed a consistent directionality of differences, having all positive ranks (Table 5-4). This translated to the HSBV having greater path lengths than the OMCS. This was illustrated in the rFHA location trace, where the HSBV had greater trace lengths (Figure 5-4). Additionally, the HSBV tended to have a location trace that better represented the patterns of a walking task. In contrast to knee extension, where the sFHA shifts anteriorly, the sFHA will shift posteriorly during knee flexion [102]. Therefore, at heel-strike, where knee flexion begins, it makes sense that the rFHA location trace would shift posteriorly. Afterwards, when reaching the midstance of walking, the knee begins to extend again and the rFHA shifts anteriorly. This pattern was most clearly and consistently demonstrated by the HSBV, while the OMCS was considerably more variable.

It is also interesting to note that only the AP measures of the location and excursion contained a bias, while the SI measures did not. In a prior study by Cappozzo et al. (1996), it was discovered for seven participants that skin markers on the thigh or shank had a tendency to provide the same pattern of movement artifacts, but with different magnitudes depending on their placement [145].

Based on this finding, skin movement artifacts present in this study may have been similar for all participants as well, and specifically influenced the AP components of the rFHA measures. Further studies are required to investigate this speculation.

In general, the largest absolute differences were seen in the rFHA path length, excursion, and location, ranging from 18.67-101.84 mm (Table 5-3 and Table 5-5). In regards to the study hypothesis, these differences were greater than what was expected from skin movement artifacts, reaching values greater than 13.0 mm [7]. This finding may be partially attributed to the compounded errors to which three measures are susceptible. Specifically, the rFHA location is dependent on the physical position of the rFHA within the ACS. However, the physical position of the rFHA is influenced by both rotations and translations of the knee. Therefore, the rFHA location is susceptible to compounded errors of the translations and rotations due to skin movement artifacts. This could explain why the differences were larger than the expected errors. Because the rFHA path length and excursion are computed from the rFHA location measure, it was observed that these two measures also contained large differences. These compounded skin movement artifact errors within the OMCS may potentially mask the true movement of the underlying bones, producing erroneous bony movements that indicate smaller rFHA path lengths and/or excursions (as seen in the OMCS rFHA location tracings of Figure 5-5 when compared to the HSBV).

The differences associated with the rFHA translation, orientation, and dispersion agreed with the study hypothesis. Unlike the rFHA location, path length, and excursion, the translation, orientation, and dispersion of the rFHA are not susceptible to these compounded errors. The translation revealed absolute differences (8.21-11.87 mm) within the reported ranges of skin movement artifact using CA (up to 13.0 mm) [7]. Similarly, the angular rFHA measures - orientation and dispersion - revealed absolute differences (orientation: 6.74 deg; dispersion: 1.49-

4.13 deg) within or similar to the ranges provided by Benoit et al. (2006) (up to 4.4 deg deg) [7]. The one exception was the orientation differences during the walking task (22.90 deg, Table 5-5). Between the two movement tasks, larger differences were observed for walking compared to the single leg squat. This finding is speculated to be attributed to greater skin movement artifacts when walking. In a study by Miranda et al. (2013), OMCS and HSBV data were compared during a jump cut maneuver [146]. It was found that knee kinematic differences (using CA) between the two imaging modalities were similar until ground contact, where rotational differences reached up to 15 deg and translational differences up to 28 mm. This discrepancy was attributed to the impact from the jump cut producing skin oscillations, thus greater skin movement artifacts following ground contact. In this current study, the single leg squat is a slower movement and produces minimal impact oscillations on the leg. In contrast, walking is a faster movement and contains phases of impact (i.e., heel-strike) which can produce oscillations throughout the leg during early stance phase likely leading to greater magnitudes of skin movement artifacts.

5.4.1 Strengths & Limitations

This study used the highly accurate HSBV system as a gold standard comparison, providing the ability to record bone movement directly. The HSBV and OMCS were used simultaneously and synched together to perform direct comparisons between the two systems. Furthermore, the movement data acquired from these systems were transformed to the same ACS, defined directly from bone landmarks instead of skin mounted markers. However, this study still had its limitations. Firstly, this is the first time that direct comparisons of the rFHA between the HSBV and OMCS were performed for these movements. Therefore, it is challenging to compare these results to other studies. Secondly, only six total participants were assessed in this study, with four included in the analysis of each movement task due to trial quality control. For future studies, the quality of the trials may be improved by controlling for single leg squat angle and improving the alignment of

the HSBV system to reduce the time frame of limb crossover. Due to trial removal, this study resulted in four paired differences for the single leg squat and walking tasks. However, this sample size was selected according to a previous validation study, which acquired the data for different research questions and variables of interest. Because of this small sample size, the high risk of Type II errors (i.e., false negatives) exists. A larger sample size, especially for walking, may provide more statistical power and reduce the chances of Type II errors from occurring. The data obtained from this study may provide future rFHA studies a foundation to calculate a sample size with greater statistical power. Finally, the confined field of view of the HSBV limits the activities that can be measured. Activities with greater impacts that produce more substantial skin movement artifacts (e.g., running) are challenging to record but may provide different results. Further studies investigating movements with higher velocities and impacts are required to generalize the patterns of the rFHA differences found in this study with other movements.

5.5 Conclusions

The negative influence of skin movement artifacts on the computation of accurate knee kinematics has been reported when using CA and the sFHA. It was unknown how the rFHA is influenced by these skin movement artifacts and what magnitude of errors would be present. Therefore, this study investigated differences in six rFHA measures between the HSBV and OMCS; using HSBV as the gold standard system as it is not influenced by skin movement artifacts. The location, path length, and excursion of the rFHA showed the greatest magnitudes of differences (18.67-101.84 mm) and exceeded the expected error range. This was evident in the rFHA location tracing being consistently more anterior and shorter in length within the OMCS. This finding was speculated to originate from compounded rotational and translational errors of the knee due to skin movement artifacts, thus masking the true movement of the underlying bones. The interpretation of these measures within the OMCS should be approached with caution. On the other hand, the remaining

measures (with the exception of orientation during walking) were found to lie within the expected range of errors due to skin movement artifacts. The rFHA translation, orientation, and dispersion are better recommended for use within the OMCS as they are not susceptible to compounded errors.

Chapter Six: Characterization of rFHA Knee Kinematics in Young Adults with previous Youth Sport-Related Knee Injury

6.1 Introduction

The knee is one of the most commonly injured joints among adolescent sport [147], [148]. A knee injury may result in reduced ligament function, meniscal tears, and joint misalignment [149]. These three factors are known to contribute to altered knee kinematics, potentially resulting in the development of tibiofemoral OA (refer to section 1.2.4.2) [67], [150]. Therefore, altered knee kinematics due to knee injury may be related with the four- to six-fold increased risk of tibiofemoral OA development when sustaining a knee injury [151]–[153]. For adolescents who have received such an injury in sport, this is a substantial increase in risk with significant long-term health implications.

Several investigations have been performed that determined the existence of statistically significant altered kinematics for injured knees. However, there is a lack of consistent directionality within these changes, resulting in conflicting evidence towards what kinematic changes exist with a certain injury. For example, when compared to healthy controls, significant knee kinematic differences have been reported in ACLR females during a vertical drop jump (VDJ). ACLR females showed greater magnitudes of knee abduction at initial contact of the VDJ [99]. In a different study, males and females with ACLR were compared to sex matched controls during a VDJ of similar height [100]. However, no kinematic differences in the knees were reported during the initial contact of the VDJ [100]. The inconsistency of the findings between these two studies may be attributed to several potential sources, including source of the graft used for reconstruction [154], compounded effects of other knee deficiencies (e.g., meniscal tears) [155], and computational issues such as Cardan angle crosstalk errors [25]. Controlling for the first two sources is challenging, as it may limit the external validity of the study and impede the

fulfilment of a large sample size, respectively. However, using an alternative approach to quantify knee kinematics is a possible solution to eliminate the issue of crosstalk.

The finite helical axis (FHA) is an alternative and supplementary method to Cardan angles for quantifying knee kinematics. It is immune to CA crosstalk effects by assuming that the joint moves and translates along a single axis. Additionally, the helical angles, computed by projecting the rotation along the unit vector of the FHA, provide similar 3D angles to the CA but are not susceptible to crosstalk effects. The FHA (specifically the sFHA) has been applied previously to assess and compare ACLR knees with healthy controls during different single leg hop movements. No significant differences in the sFHA dispersion were found between the ACLR and healthy control knees [78]. While this finding may be true, it also may be potentially attributed to a limitation of the sFHA, where it is susceptible to stochastic errors when angular displacements are small [4]. The errors in this study were reduced by calculating the sFHA at 10-degree intervals throughout the movement, which also results in a reduction in temporal resolution. Consequently, the kinematic information becomes limited to specific time points and information between each 10-degree interval is lost. Therefore, differences associated with ACLR knee kinematics may have been lost as well within the omitted data. To avoid this issue, the rFHA may be used instead. However, it has not been used to assess ACLR knees during a jumping task such as the VDJ. Therefore, the purpose of this study was to use the rFHA to characterize VDJ knee kinematics of individuals with ACLR knees, and to compare the rFHA kinematic measures to those obtained for age, sex, and sport matched controls. CA, the conventional approach to quantifying knee kinematics, were also computed and compared between the ACLR group and their matched controls. It was hypothesized that the rFHA would successfully detect kinematic differences in ACLR knees when compared to the matched controls.

6.2 Methods

6.2.1 Study Participants

A total of forty-eight participants with ACLR (also referred to as the ACLR group) and their age, sex, and sport matched controls were analyzed in this matched-pairs design study (ACLR: n = 48, controls: n = 48, N = 96). All participants provided consent for this CHREB approved study (ethics ID: REB14-2212). These participants were acquired as a sub-sample from a larger dataset. The original dataset was previously collected for the Alberta Youth Prevention of Early Osteoarthritis historical cohort study conducted at the University of Calgary. This dataset consists of two groups: 1) one hundred individuals who sustained a youth (≤ 18 years old) sport-related injury 3 to 10 years earlier, and 2) one hundred age, sex, and sport matched controls. Of the one hundred injured participants, only those with a history of complete ACL tears, followed by surgical reconstruction, were included in this study. Consequently, fifty-four participants with ACLR were considered for this study. However, due to dropout or sustaining new injuries, six of these fifty-four were removed from the analysis.

More information on the recruitment, inclusion/exclusion criteria, and injury diagnosis has been previously reported for this dataset [156]. Additionally, this cohort study previously investigated the consequences of knee injury in youth sport and its association with OA development [157]. Briefly, the injured group participants were clinically diagnosed with a ligament, meniscus, or other intra-articular knee injury that required rehabilitation and disrupted sport participation. The matched control participants had no previous history of knee injuries that resulted in a time-loss of sport. Participants were excluded from the study if they were pregnant, received a musculoskeletal injury within three months prior to testing that resulted in a time-loss of work, school, or sport, received non-steroidal anti-inflammatory drugs or cortisone injections within

three months prior to testing, had a diagnosis of other arthritides, or had other medical conditions that prevented the completion of functional tests.

6.2.2 Data Collection

Lower limb kinematics and ground reaction forces during a VDJ were collected for each participant using an OMCS (Eagle Digital System, Motion Analysis, CA, USA, 240 Hz) and two force plates (Type 9287, Kistler Instruments AG, Switzerland, 2400 Hz), respectively. Prior to recording, participants were outfitted with thirty-eight reflective markers following International Society of Biomechanics recommendations (Figure 6-1). A table providing the specific marker locations can be found in Appendix A. A reference position trial was recorded with the participant standing barefoot with their feet shoulder width apart, hands on the hips, and head looking forward. Afterwards, ten trials of barefoot VDJ were performed. A successful VDJ trial consisted of the participant standing on a 31 cm box, with their feet shoulder width apart. Starting with both feet on the box, the participant would step off and drop onto the ground with both feet (one foot on each force plate) forming the first support phase. This was succeeded by a counter movement jump of maximal effort. The trial ended once the participant landed on both feet after the jump, forming the second support phase. A trial was unsuccessful if the participant jumped off the box (rather than stepped off), if both feet did not land on separate force plates during both first and second support phases, if the feet did not land simultaneously on the floor, or if they lost balance.

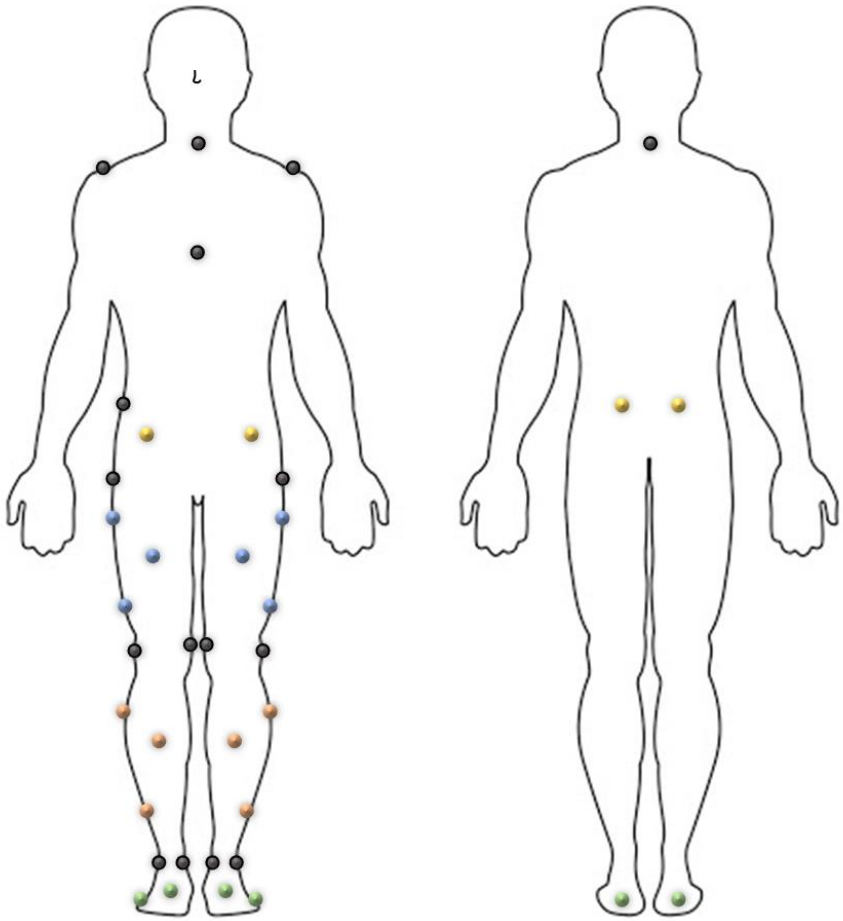

Figure 6-1 – Illustration of the thirty-eight reflective markers placed on the participants following the International Society of Biomechanics recommendations.

6.2.3 Data Processing

Reflective marker trajectories were tracked using Cortex Motion Capture Software (Version 3.6.1.1315, Motion Analysis Corporation, USA) for both the reference position trial and VDJ trials. The trajectories were imported into Visual3D (C-Motion Inc., USA) to define ACS of the thigh and shank, and subsequently compute 3D knee angles relative to the reference position. ACS definitions of the thigh and shank are outlined in Appendix B. The angles of both knees were specified in a 'X, Y, Z' CA sequence, relating to flexion/extension (F/E), abduction/adduction (Ab/Ad), and internal/external (I/E) rotation, respectively. Knee flexion, adduction, and internal

rotation indicated positive rotations. All angles were calculated relative to the femur. Vertical ground reaction forces from both feet were used to determine the time of foot contact during the first support phase. The start of the first support phase was designated by the first instance of ground contact by the left/right foot when stepping off the box and ended at the first instance of the left/right foot leaving the ground during the counter-movement jump.

To calculate the rFHA, CA of the knee for each participant were imported into custom Matlab (v2020b, MathWorks, MA, USA) and first converted into rotation matrices. The rotation matrices, already relative to the reference position and within the ACS, were then used to compute rFHA measures during the first support phase of the VDJ. The rFHA measures included the orientation, dispersion, and helical angles (Figure 6-2). Other rFHA measures (specifically rFHA location, path length, and excursion) were not included as their calculations require the magnitudes of joint translations. To elaborate, the VDJ consists of high impacts and velocities, producing large skin movement artifacts. Therefore, joint translations were deemed to be contain large errors during the VDJ and may be insufficiently accurate for rFHA calculations. This was evident in Chapter 5, where rFHA location, path length, and excursion differences between the OMCS and HSBV ranged from 18.67-101.84 mm, exceeding previously reported CA errors of up to 13.0 mm [7]. Orientation was defined as the mean angle between each individual rFHA and the mediolateral (ML) axis of the femur throughout the support phase. Dispersion was defined as the mean angle between each individual rFHA and the mean rFHA throughout the support phase. The helical angles were acquired through the scalar multiplication of the rotation along the rFHA (ϕ) by the directionality of the helical axis ($\vec{n}_i$) (Eq. 6-1, where $\vec{n}_i$ represents the three components of the unit vector [$\vec{n}_1$, $\vec{n}_2$, $\vec{n}_3$]).

$$Helical\ angles\ = \phi * \vec{n}_i \qquad \text{Eq. 6-1}$$

The multiplication in Equation 6-1 separates the rotation along the rFHA into three distinct rotations, like the CA. To elaborate, the directionality of the rFHA will change depending on the contribution of the knee planar rotations: pure F/E would result in a rFHA that is parallel with the ML axis of the femur, pure Ab/Ad would result in a rFHA that is parallel with the AP axis of the femur, and pure I/E rotation would result in a rFHA that is parallel with the SI axis of the femur. Therefore, by multiplying the rotation about the rFHA by the unit vector of the rFHA, the contribution of each planar movement can be separated into three distinct angles representing F/E, Ab/Ad, and I/E rotation. However, unlike the CA, the helical angles are not susceptible to crosstalk [101].

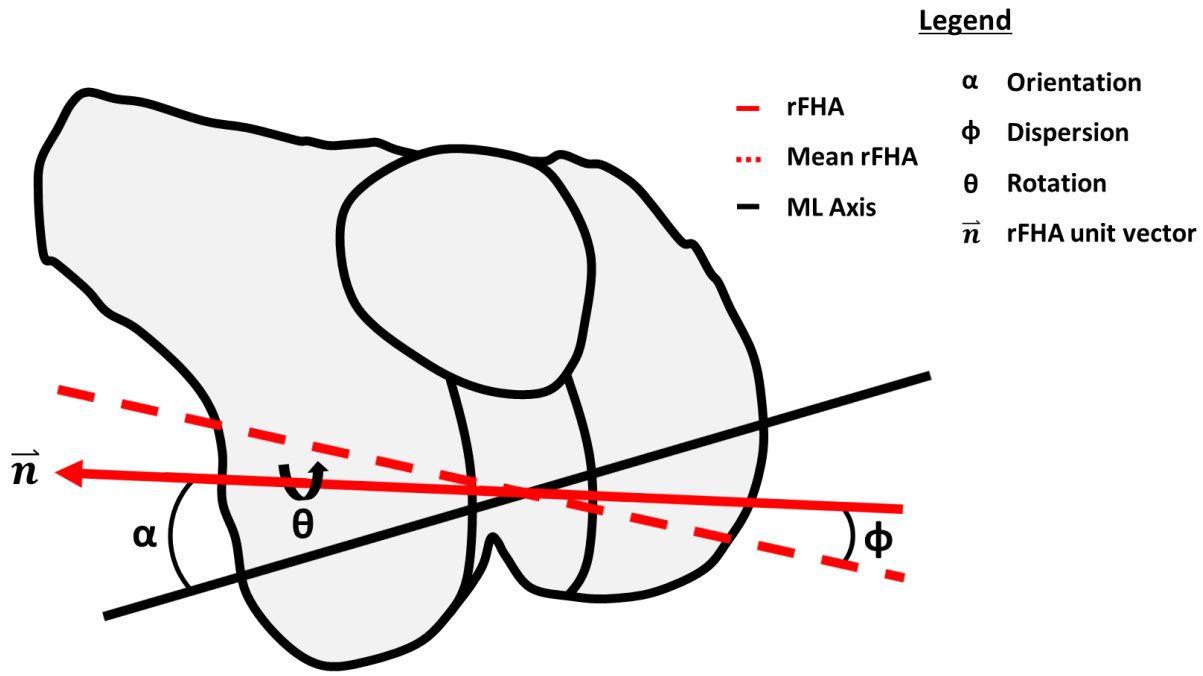

Figure 6-2 – The rFHA orientation (α), dispersion (ϕ), rotation (θ), and unit vector ($\vec{n}$). Orientation (α) was defined as the mean angle between each individual rFHA (solid red line) and mediolateral axis (solid black line) of the femur throughout the support phase. Dispersion (ϕ) was defined as the mean angle between each individual rFHA and the mean rFHA (dashed red line) throughout the support phase. The helical angles were acquired through the scalar multiplication of the rotation along the rFHA (θ) by the directionality of the helical axis ($\vec{n}$).

Data points for the orientation, dispersion, helical angles, and CA of each knee throughout the first support phase were obtained for each trial and normalized to one hundred data points. The orientation and dispersion measures were calculated for four sections of movement: full support phase, flexion segment of the support phase, extension segment of the support phase, and time from initial contact to maximum knee flexion (based on helical angles). For each section of

movement, the orientation and dispersion measures across all ten VDJ trials were averaged, resulting in a mean and SD for the orientation and dispersion for every participant.

To compare the helical angles and CA between the two groups, the time point at maximum knee flexion was also investigated. For each trial, the Ab/Ad and I/E rotation coinciding with maximum knee flexion (based on helical angles) were determined for both helical angles and CA approaches. The Ab/Ad and I/E rotation at maximum flexion were then averaged across all ten VDJ trials for each participant, yielding a mean and SD. Measures for the injured knees of the ACLR group and the same knee of the control group were used for further analysis (e.g., if the right knee was injured for an individual in the ACLR group, the right knee was assessed for their matched control).

6.2.4 Statistical Analysis

Participant demographics were reported using medians and ranges (min, max). Comparisons between the matched pairs/groups consisted of the frequency (i.e., count) of participant or knee characteristics. Additionally, comparisons of the age, height, and weight of the matched pairs were performed with mean paired differences (ACLR – control) and associated 95% CI.

All statistical tests to determine kinematic (rFHA and CA) differences were performed using SPSS Statistics 26 (IBM, NY, USA). The kinematic measures of the knee for comparisons between participants with ACLR and healthy controls were rFHA orientation, dispersion, and helical angles, and CA. All kinematic measures were checked for normality using a Shapiro-Wilk test and assessed visually using QQ plots. Two types of t-tests (or non-parametric equivalents if needed) were used to assess kinematic differences between the ACLR group and the matched controls for the different sections of movement within the first support phase of the VDJ. Group differences of the kinematic measures (orientation, dispersion, helical angles, and CA) between the ACLR and healthy participants were assessed using independent t-tests (or Mann-Whitney U tests if normality was violated). Additionally, because the matched pairs design of this study, the participants in the

ACLR group were compared to their specific matched control using paired t-tests (or Wilcoxon Signed Rank Test if normality was violated) [158]. All statistical tests were performed with a significance value of 0.05 ($\alpha = 0.05$). To account for multiple comparisons within the group and paired analyses (twelve comparisons performed in total for all kinematic measures at all movement sections) the Benjamini-Hochberg procedure was used with a 5% false discovery rate to preserve a significance value of 0.05 [159].

Group means, SD, and effect sizes (Cohen's D [160]) were reported for all tests. Additionally, the average within-participant SD of the rFHA orientation and dispersion was calculated for each group during the full support phase (table of results can be found in Appendix C). For parametric tests, mean group/paired differences with associated 95% confidence intervals (CI) were determined. For non-parametric tests, medians, interquartile ranges (IQRs), and percentage of matched pairs who changed in the direction of the main effect were determined. Magnitudes of the effect sizes were categorized as no effect (< 0.20), small (0.20-0.49), medium (0.50-0.79), and large (≥ 0.80) [160].

6.3 Results

The demographics of the ACLR and healthy groups were very similar. Ages of the participants with ACLR ranged from 18-26 yrs, with a median of 22 yrs (matched pair difference (SD) was -0.1 (0.7) yrs). The sample consisted primarily of females (67%). Median (max, min) height and weight of the participants with ACLR were 1.71 (1.56, 1.94) m and 69.0 (51.0, 100.7) kg, respectively (matched pair difference (SD) of height: -0.01 (0.09) m; weight: -5.8 (13.5) kg) (Table 6-1). The weight was significantly greater in the participants with ACLR, evident in the 95% CI of the mean paired difference not crossing zero (95% CI: 1.84-9.67, Table 6-1).

Table 6-1 – Descriptive statistics of the ACLR and healthy control groups. Ages, male/female ratio, height, weight, and injury counts are provided. All values are stated as median (max, min). Mean paired differences (ACLR – control) and 95% CI are reported as well. The weight of the participants with ACLR was significantly greater, evident in the 95% CI not crossing zero.

	ACLR	Healthy	Paired Difference (95% CI)
Number	n = 48	n = 48	-
Age (years)	22 (18, 26)	22 (18, 26)	0.06 (-0.14, 0.26)
Age at injury (years)	15 (9, 18)	N/A	-
Male/female ratio (%)	33/67	33/67	-
Height (m)	1.71 (1.56, 1.94)	1.71 (1.52, 1.88)	0.62 (-1.91, 3.16)
Weight (kg)	74.8 (52.2, 105.5)	69.0 (51.0, 100.7)	5.76 (1.84, 9.67)
ACL tear	48	0	-
Knee surgery	48	0	-
Associated meniscal injury	32	0	-
Contralateral knee injury	10	0	-
Contralateral knee surgery	9	0	-

The Shapiro-Wilk test for normality determined that the rFHA orientation and dispersion were not normally distributed ($p = 0.00$-0.05), with the exception of dispersion during the full support phase ($p = 0.38$), thus requiring the use of non-parametric tests. All other measures (CA and helical angles) were normally distributed and parametric tests were used ($p = 0.09$-0.80). Following the Benjamini-Hochberg procedure, no measures during any section of movement were significantly different. However, there are non-significant findings in this study that merit discussion. All p-values reported in this section are the original test values, prior to correcting for false discovery rates. Therefore, measures with p-values below the alpha value of 0.05 are not to be considered significant.

6.3.1 Dispersion & Orientation

Although no significant differences were found, the rFHA dispersion had a small effect size during the full support phase of the VDJ (Table 6-2). A group analysis revealed that the ACLR group may have had greater magnitudes of dispersion than the healthy group, with a mean difference of 0.46 deg (95% CI: -0.02 deg to 0.93 deg, effect size = 0.39, p = 0.06). A similar finding in the full support phase was observed when performing a paired analysis between the participants with ACLR and their matched controls, where participants with ACLR showed 0.46 deg of greater dispersion than their matched control (95% CI: 0.03 deg to 0.89 deg, effect size = 0.39, p = 0.04, Table 6-2). However, it is difficult to distinguish these differences when viewing a tracing of the rFHA unit vector within the sagittal plane throughout the full support phase (Figure 6-3). Interestingly though, an inferior offset can be seen within the rFHA tracing for the ACLR group (Figure 6-3). The dispersion IQR were also larger for the ACLR group for both the flexion phase (ACLR IQR: 1.68 deg; Healthy: 1.23 deg) and extension phase (ACLR IQR: 1.68 deg; Healthy: 1.30 deg) of the VDJ (Table 6-2). Similar findings were determined for the within-participant variabilities, with average within-participant SD being greater in the ACLR group for orientation (ACLR SD: 1.01 deg; Healthy: 0.92 deg; Appendix C) and dispersion (ACLR SD: 0.80 deg; Healthy: 0.58 deg; Appendix C).

During the flexion phase of the VDJ, the majority of participants with ACLR (% main effect = 64.58%) had greater magnitudes of dispersion than their matched controls with a medium effect size (ACLR median (IQR): 3.27 (1.68) deg; control median (IQR): 2.99 (1.23) deg; effect size = 0.52, p = 0.08). Similar findings were not observed for the rFHA orientation which had a small effect size (effect size = 0.25, p = 0.40; Table 6-2).

Table 6-2 – The group analysis (independent t-tests) and paired analysis (paired t-tests) of the rFHA orientation and dispersion at the full, flexion, and extension phase the VDJ. All values are in degrees except "% main effect", representing the percentage of matched pairs that followed the main effect. All p-values are from the original tests with corresponding effect sizes. No p-values were significant ($p \leq 0.05$) following the Benjamini-Hochberg procedure.

							Group Analysis			Paired Analysis			
Timeframe	**Measure**	**Group**	**Mean**	**SD**	**Median**	**IQR**	**Mean difference (ACLR - Healthy)**	**95% CI (lower, upper)**	**p-value (effect size)**	**Mean difference (ACLR - Healthy)**	**95% CI (lower, upper)**	**% main effect**	**p-value (effect size)**
Full support phase	Orientation	ACLR	9.19	4.46	8.18	4.31	-	-	0.41 (0.17)	-	-	50.00	0.69 (0.12)
		Healthy	9.60	3.95	8.50	4.81	-	-		-	-		
	Dispersion[a]	ACLR	4.13	1.25	-	-	0.46	(-0.02, 0.93)	0.06 (0.39)	0.46	(0.03, 0.89)	-	0.04 (0.39)
		Healthy	3.67	1.09	-	-							
Flexion phase	Orientation	ACLR	5.52	4.80	7.08	5.91	-	-	0.19 (0.27)	-	-	58.33	0.40 (0.25)
		Healthy	9.17	4.06	8.57	5.09	-	-		-	-		
	Dispersion	ACLR	3.46	1.20	3.27	1.68	-	-	0.20 (0.26)	-	-	64.58	0.08 (0.52)
		Healthy	3.16	1.15	2.99	1.23	-	-		-	-		
Extension phase	Orientation	ACLR	8.88	4.36	8.00	4.74	-	-	0.48 (0.15)	-	-	47.92	0.78 (0.08)
		Healthy	9.27	4.00	8.85	5.01	-	-		-	-		
	Dispersion	ACLR	3.53	1.26	3.27	1.68	-	-	0.36 (0.19)	-	-	60.42	0.11 (0.48)
		Healthy	3.21	1.00	3.20	1.30	-	-		-	-		

[a] designates the use of a parametric test (independent or paired t-test)

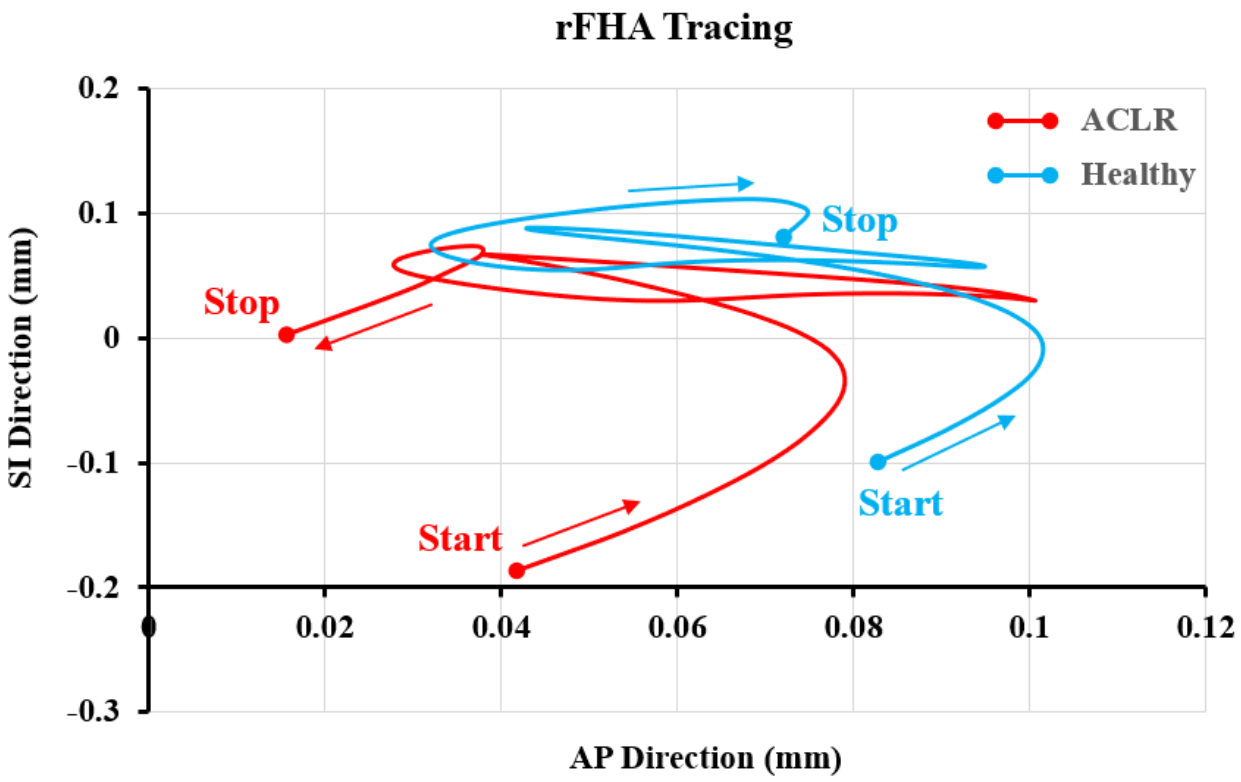

Figure 6-3 – A sagittal plane tracing of the rFHA unit vector during the full support phase of the VDJ. Greater magnitudes of dispersion (i.e., a more variable rFHA tracing) were not evident between the ACLR (red) and healthy (blue) groups. However, an inferior offset of the rFHA unit vector tracing was present within the ACLR group. Start and stop indicate the initial contact and take-off of the support phase, respectively. Arrows dictate the direction of the tracing.

6.3.2 Helical & Cardan Angles

Maximum knee helical flexion angles for the ACLR and healthy group were similar in magnitude (ACLR mean [SD]: 94.10 [10.27] deg; Healthy mean [SD]: 95.60 [10.12] deg) and equal in location (50% support phase). At the maximum point of flexion during the first support phase of the VDJ, only one notable (non-signficant) observation was seen with a small effect size. Specifically, a group analysis showed that the ACLR group positioned their knee in a less

internally rotated position during the squat (based on helical angles) than the control group, with a mean difference of -2.18 deg (95% CI: -4.55 deg to 0.18 deg, effect size = -0.37, p = 0.07; Table 6-3). This observation was more pronounced with the paired analysis between the participants with ACLR and their matched controls. The mean paired differences of the helical internal rotation reached magnitudes of -2.18 deg and contained a 95% CI that did not cross zero (95% CI: -4.11 deg to -0.25 deg, effect size = -0.37, p = 0.03; Table 6-3). A similar pattern was not observed based on the Cardan internal rotation, which had a negligible effect (effect size = -0.11; Table 6-3 & Figure 6-4).

Table 6-3 – The group analysis (independent t-tests) and paired analysis (paired t-tests) of the rFHA orientation, dispersion, helical angles, and CA at the maximum point of knee flexion during the VDJ. All values are in degrees except "% main effect", representing the percentage of matched pairs that followed the main effect. All p-values are from the original tests with corresponding effect sizes. No p-values were significant ($p \leq 0.05$) following the Benjamini-Hochberg procedure.

							Group Analysis			Paired Analysis			
Timeframe	**Measure**	**Group**	**Mean**	**SD**	**Median**	**IQR**	**Mean difference (ACLR - Healthy)**	**95% CI (lower, upper)**	**p-value (effect size)**	**Mean difference (ACLR - Healthy)**	**95% CI (lower, upper)**	**% main effect**	**p-value (effect size)**
Max Flexion	Orientation	ACLR	8.44	5.07	7.45	6.95	-	-	0.45 (0.15)	-	-	50.00	0.87 (0.05)
		Healthy	8.71	4.27	7.83	5.86	-	-		-	-		
	Dispersion	ACLR	3.02	1.38	2.70	1.81	-	-	0.49 (0.14)	-	-	56.25	0.32 (0.29)
		Healthy	2.77	1.21	2.56	1.40	-	-		-	-		
	Adduction (Cardan)[a]	ACLR	2.75	7.51	-	-	1.63	(-1.30, 4.55)	0.27 (0.22)	1.63	(-0.92, 4.18)	-	0.21 (0.23)
		Healthy	1.12	6.91	-	-							
	Adduction (Helical)[a]	ACLR	9.02	12.95	-	-	0.40	(-4.56, 5.35)	0.87 (0.03)	0.40	(-3.95, 4.75)	-	0.86 (0.03)
		Healthy	8.62	11.56	-	-							
	Internal Rotation (Cardan)[a]	ACLR	8.03	9.87	-	-	-1.04	(-4.86, 2.79)	0.59 (-0.11)	-1.04	(-4.31, 2.24)	-	0.53 (-0.11)
		Healthy	9.07	8.97	-	-							
	Internal Rotation (Helical)[a]	ACLR	3.32	5.65	-	-	-2.18	(-4.55, 0.18)	0.07 (-0.37)	-2.18	(-4.11, -0.25)	-	0.03 (-0.37)
		Healthy	5.51	6.03	-	-							

[a] designates the use of a parametric test (independent or paired t-test)

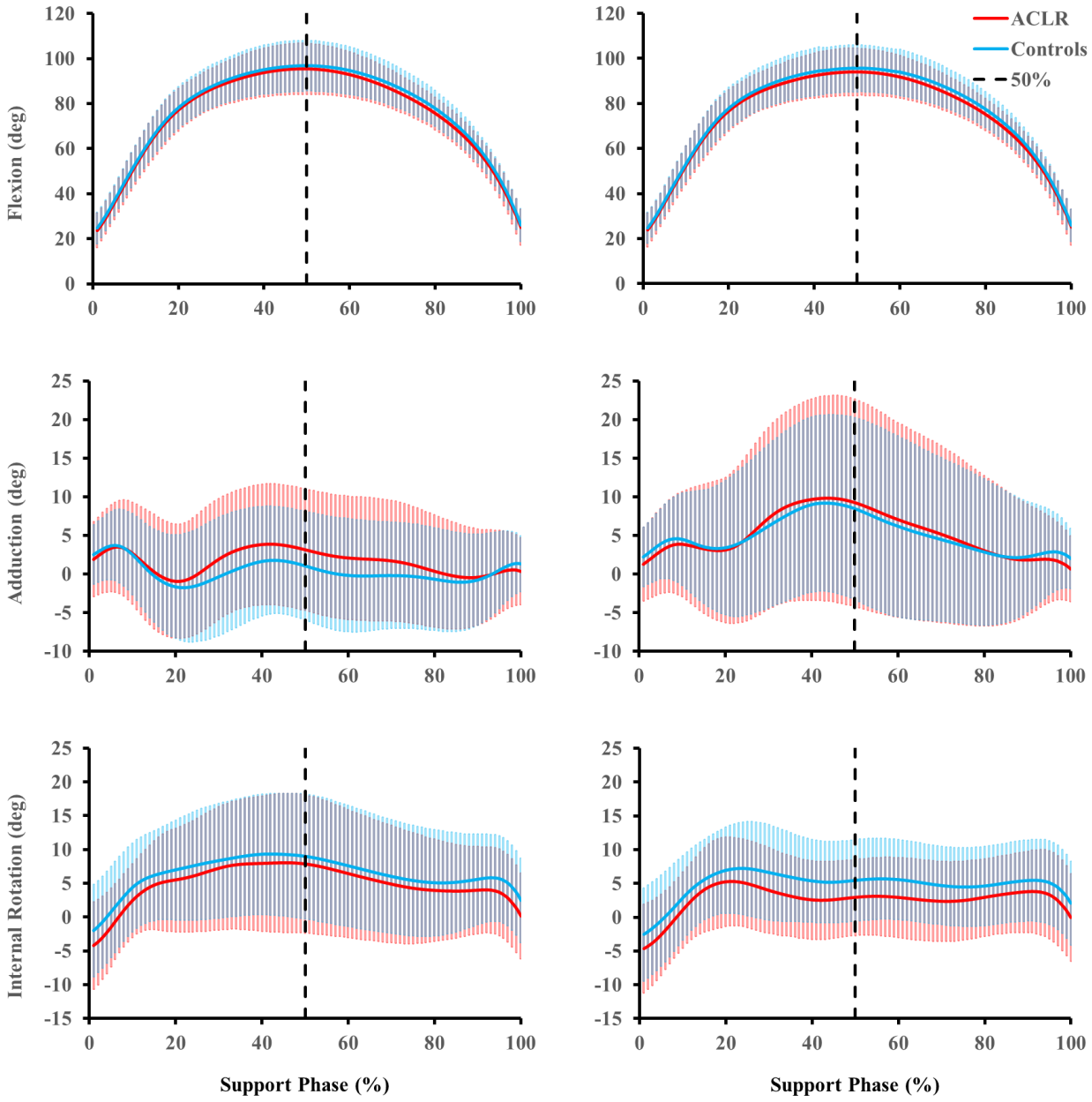

Figure 6-4 – The mean curves (with SD bars) of the Cardan angles (left) and helical angles (right) throughout the first support phase of the VDJ for the ACLR group (red) and control group (blue). A trend of lesser helical internal rotation in the ACLR group (bottom right graph) was seen at maximum knee flexion (50% support phase).

6.4 Discussion

The risk of developing tibiofemoral OA increases substantially after receiving a knee injury, such as an ACL tear. A contributing factor to this increased risk may be altered knee kinematics. However, there has been a lack of consistency in the directionality of these kinematic changes when using CA. The sFHA may be an alternative approach to quantify knee kinematics but lacks temporal resolution. Fortunately, the rFHA provides a promising alternative that preserves temporal resolution. Therefore, this study investigated knee kinematics of ACLR and matched (by age, sex, and sport) controls using the rFHA. Specifically, rFHA measures (orientation, dispersion, and helical angles) and CA were compared between the two groups during the first support phase of a VDJ.

6.4.1 Dispersion & Orientation

This was the first study to compare rFHA dispersion and orientation between ACLR and healthy participants during a VDJ. No statistical differences were found for the rFHA orientation and dispersion when performing a grouped and paired analysis between the ACLR group and their matched controls (Table 6-2 and Table 6-3). These findings did not support the hypothesis that kinematic differences would exist between these two groups. However, the rFHA dispersion may have had having greater magnitudes in the ACLR group throughout the full support phase of the VDJ, revealing a small effect size (effect size = 0.39, mean difference: 0.46 deg; Table 6-2). This finding was supported in both the group and paired analyses performed. Furthermore, the rFHA dispersion had a medium effect size (effect size = 0.52) during the flexion phase of the VDJ, with the majority of participants with ACLR having greater magnitudes than their matched controls (% main effect = 64.58%). This potential increase in rFHA dispersion suggests there may be a presence of knee instability in ACLR knees. To elaborate, the dispersion represents the average amount of angular deviation a single rFHA (from one data frame) had from the mean rFHA

throughout the full support phase. It is speculated that smaller dispersion values represent a knee with more stable movements. In contrast, greater dispersion values represent more variable movements of the knee. This greater variability was present within the dispersion IQR during the flexion and extension phases, with ACLR groups having greater IQR (0.38-0.45 deg) than the healthy controls. The greater ACLR dispersion may originate from altered neuromuscular control, stemming from ACL injuries and ACL reconstruction. EMG activation patterns of the lower limb muscles [161]–[163], as well as strength performance of the quadriceps muscles [164], have been reported to change following both ACL injury and reconstruction. These alterations may result in more variable knee movements, as the muscles surrounding the knee are unable to maintain greater levels of stability [163]. However, this study did not investigate muscle EMG patterns and this speculation requires further investigations. It is also important to note that a dispersion difference of 0.46 deg may be outside of the precision limits of the OMCS used in this study and could be due to errors within the system itself. Additionally, it is unknown if this magnitude of difference would contribute to tibiofemoral OA development. The clinical significance of this finding remains to be determined in future studies.

No differences in the rFHA orientation were observed. This finding is consistent with a study by Markström et al. (2020), which investigated sFHA orientation between ACLR and healthy participants during three different single-leg hop movements: one-leg hop for distance, one-leg vertical hop, and a standardized rebound side hop [78]. Although the VDJ was not performed, each movement had similarities to the VDJ, such as a vertical displacement in the vertical hop, and a countermovement jump in the rebound side hop. The authors speculated that sFHA orientation represented a general measure of knee robustness, or the ability for the knee to maintain a joint configuration that primarily results in F/E movements. It was suggested that if the knee performed

a pure F/E movement, the HA would be parallel to the ML axis of the knee and the orientation would be zero. Any other rotations (i.e., Ab/Ad and I/E rotation) would deviate the HA away from the ML axis of the knee, thus increasing the degree of orientation, indicating a decrease in knee robustness. However, Markström et al. (2020) did not find any differences in knee robustness between ACLR and healthy participants during the three single-leg hop movements [78]. This was speculated to originate from altered landing strategies within the ACLR group. Specifically, the injured legs of the ACLR group were found to contain 5% longer contact times and 4% lower peak vertical ground reaction forces than their contralateral limb. This finding was suggested to provide lower magnitudes of loading on the injured knee, thus an easier ability to maintain knee robustness throughout the single leg hop movements [78]. A similar outcome may be present within this VDJ study. participants with ACLR may have altered their landing strategy to reduce the magnitude of load on the injured knee, thus maintaining knee robustness levels similar to healthy control. However, this study did not investigate loading differences between limbs and future studies are required to confirm if similar approaches are used by participants with ACLR during a VDJ. Furthermore, the purpose of reconstructing the ACL is to retain knee function. Therefore, the lack of differences in the rFHA dispersion and orientation may be a result of the reconstructive surgery maintaining normal kinematics of the knee. Further studies are required to investigate ACLD knee kinematics during a VDJ.

6.4.2 Helical & Cardan Angles

The helical angle approach has never been used previously to quantify kinematics of the ACLR knees. Following the Benjamini-Hochberg procedure, no significant differences were found in helical and Cardan angles at maximum knee flexion angle of the VDJ, thus refuting the study hypothesis. However, when using the helical angle approach, the I/E rotation of the knee had a small effect size. This suggests that the ACLR group may have had a less internally rotated tibia

(2.18 deg) at maximum knee flexion of the VDJ. This was seen in the group analysis (effect size = -0.37, p = 0.07) and paired analysis (effect size = -0.37, p = 0.03). The rFHA unit vector trace helps visualize this notion (Figure 6-3). It can be seen that the ACLR rFHA trace had an inferior offset to the healthy trace. This indicates that the ACLR group had a smaller (or more negative) rFHA unit vector in the SI direction. To elaborate, if the rFHA were purely vertical it would have a magnitude of one on the SI axis. Therefore, a greater magnitude on the SI axis corresponds to greater magnitudes of I/E rotation. Furthermore, the sign of the unit vector in the SI direction dictates the direction of the rotation. A positive unit vector in the SI axis indicates a positive (i.e., internal) rotation, while a negative unit vector in the SI axis indicates a negative (i.e., external) rotation. Therefore, the inferior offset of the ACLR group resulted in smaller or more negative SI unit vectors, indicating that they had lesser magnitudes of internal rotation throughout the support phase of the VDJ. No such pattern in internal rotation was found using the CA approach. This finding for the CA approach may be due to the susceptibility to crosstalk, originating from two sources (refer to Section 1.2.2.2). First, crosstalk may originate from misaligned Ab/Ad and I/E rotation axes, resulting from inaccurate landmark locations when defining an ACS. This may result in the two rotations about these axes coinciding with each other. In other words, I/E rotations of the knee may be partially registered as Ab/Ad movements, and vice versa [25]. The second source is the selection of the order of rotations when computing the CA. This study used a CA rotation sequence of F/E, followed by Ab/Ad, and finally I/E rotation. Because I/E rotation was the last rotation of the CA sequence, it would be the most susceptible to crosstalk errors. The helical angle is not susceptible to crosstalk errors and provides an alternate approach to characterizing 3D knee kinematics.

The impression of a less internally rotated tibia of the ACLR knee at maximum knee flexion may be a compensatory mechanism to limit strains on the reconstructed ligament, as excessive internal rotations of the tibia have been suggested as a risk factor for ACL injury [165], [166]. However, these lesser internal rotations (or greater external rotations) may come with another risk. A study by Tashman et al. (2004) had reported that ACLR knees during downhill running had 4 deg greater external tibial rotation when compared to their contralateral, un-injured knees [167]. Using a geometric analysis, it was observed that applying these altered I/E rotations to 3D bone models resulted in a 3.5 mm anterior shift in the lateral tibial plateau contact location. These shifts may result in abnormal contact forces on the cartilage - another risk factor of OA [167]. Furthermore, a study by Kroker et al. (2018) used the same study cohort to compare the subchondral bone microarchitecture of fifteen female participants with ACLR and fourteen age-matched controls [168]. It was found that the participants with ACLR had subchondral bone plates on the lateral femur that were 47.9-53.7% thicker than the controls. This may be related to the lessened tibial internal rotation of the ACLR group. Using a computer simulation, Andriacchi et al. (2006) found that increased internal tibial rotation of the tibia may increase cartilage thinning on the medial compartment of the knee [69]. Therefore, it could be speculated that a decrease in tibial internal rotation may increase cartilage thinning on the lateral compartment of the knee, resulting in greater magnitudes of forces acting on the underlying subchondral bone. Therefore, the subchondral bone may thicken to compensate for these increased loads. However, the bone microarchitecture of the participants in this study were not assessed and requires further investigation.

It is also important to note that the smaller helical internal rotations at the point of maximum knee flexion within ACLR knees conflicts with the rFHA orientation angles averaged throughout the full support phase. The finding of no difference in rFHA orientation angles between ACLR and

healthy participants suggests similar levels of knee robustness (i.e., similar magnitudes of out-of-F/E-plane rotations). This finding implies that the ACLR group had similar rotations along the Ab/Ad and I/E rotation axes when compared to the healthy controls. However, according to the helical angles these variables were not similar at the point of maximum knee flexion. These contradictory findings may be a result of the different timeframes over which the rFHA orientation and helical angles were calculated. The rFHA orientation was calculated as an average measure throughout the total time frame of the support phase, while the helical angles were calculated at a single time point (i.e., maximum knee flexion). Therefore, it may be valuable to investigate the rFHA orientations at a single time point or throughout shorter time frames to avoid masking potential differences that may occur within the overall movement.

Using the same sub-sample as this current study, Kuntze et al. (2021) determined a significantly greater rate of change for Cardan knee abduction angle in the injured participants when compared to the controls [169]. Specifically, injured participants had a mean difference (95% CI) of -0.04 (-0.07, 0.00) deg/s in Ab/Ad slope during 35-90% of the support phase (i.e., the transition from landing to push-off, Figure 6-4). This finding indicates that the injured participants shifted their knee alignment into abduction more quickly. This increased rate of change was speculated to originate from a lack of knee control within the coronal plane, likely due to deficits in hip muscle strength and neuromuscular control [169]. The small effect size of increased rFHA dispersion found in the current study also suggests increased knee instability and supports these CA findings on altered in Ab/Ad slope.

It is clear that the rFHA has strong potential to detect kinematic differences between ACLR and healthy knees. The helical angles, with their insensitivity to crosstalk errors, provided the notion that ACLR knees had lesser knee internal rotation at the maximum depth of the VDJ. Further

applications of the rFHA are required to determine its utility within biomechanics (e.g., different movements and knee injuries/status).

6.4.3 Strengths & Limitations

A strength of this study was the use of the helical angles as an alternative approach to characterizing 3D rotations of the knee. Unlike the CA, the helical angles are not susceptible to crosstalk errors and yielded similar overall results. Furthermore, the helical angles were able to detect a trend of lesser internal rotations within the ACLR group, a finding the CA approach was unable to achieve. The helical angles may be a useful alternative within the OMCS to characterize knee kinematics.

This study had a large sample size of 48 matched pairs, which is uncommon in biomechanical analysis and a strength of this study. However, significant findings were still lacking following the Benjamini-Hochberg procedure. The absence of significant findings may be a result of type II errors (i.e., false negatives). Larger sample sizes would minimize this error and provide greater statistical power. Despite the participants with ACLR being matched to healthy controls for age, sex, and sport, confounding variables may have remained. For example, the participants may have competed in more than one sport, thus exposing them to other injury risk factors associated with that sport and potentially influencing their kinematics. Additionally, matched controls were recruited based on self-report histories of no injury, while participants with ACLR were recruited from clinics with consistent clinical assessment protocols. As a result, there is a potential for recall bias within the matched controls when remembering their knee injury history.

The orientation was measured as the overall angle between the rFHA and ML axis of the knee. This is ideal for measuring knee robustness, which is the ability of the knee to maintain a F/E movement and minimize the simultaneous rotations about the Ab/Ad and I/E rotation axes. However, a consequence of this method is that it masks the individual influence of knee Ab/Ad

and I/E rotation on the rFHA directionality. For example, two participants may achieve equal magnitudes of rFHA orientation, but how this was achieved may be dominated or equally affected by Ab/Ad or I/E rotation. The current method of calculating rFHA orientation does not allow this concept to be examined. Therefore, future studies may consider dividing the orientation angle into two separate angles. This would be achieved by projecting the orientation onto the frontal and transverse planes, representing individual angles that represent the contributions of the Ab/Ad and I/E rotations, respectively [102].

6.5 Conclusions

For the first time, kinematic differences during a VDJ between adolescents with a sustained ACL injury and matched (age, sex, and sport) controls were assessed using the rFHA. No differences in rFHA orientation between the ACLR and healthy controls were found, suggesting that both groups were able to maintain similar levels of knee robustness throughout the VDJ. However, trends of greater rFHA dispersion (0.46 deg) in the ACLR knees indicates that there may be a lack of neuromuscular coordination, resulting in more erratic knee movements. Additionally, helical angles were used for the first time to quantify and compare the kinematics of ACLR knees to healthy controls. ACLR knees tended to have lesser magnitudes (2.18 deg) of helical internal rotation at maximum knee flexion, a finding that was lacking within the Cardan internal rotation. Lesser magnitudes of helical internal rotation may potentially act as a safety mechanism to reduce strains on the ACL. However, these altered rotations may result in abnormal cartilage contact locations, potentially contributing to the formation of tibiofemoral OA. This information may provide mechanistic insights to the onset of tibiofemoral OA in adolescents with ACL injury.

Chapter Seven: Kinematic Differences Associated with Aging Using the rFHA

7.1 Introduction

Aging has a strong association with OA, with approximately 30-40% of individuals at the age of 80 years developing the joint disease [49]. This prevalence has been linked to altered musculoskeletal function/structure originating from the aging process, including changes in bone morphology [170], cartilage biochemistry [171], neuromuscular activity [172], [173], and decreased levels of muscle strength and size [174]–[176]. In the lower limbs, these elements have been associated with abnormal knee kinematics. Therefore, abnormal knee kinematics are considered risk factors for the onset or progression of tibiofemoral OA (refer to section 1.2.4) [67]. Changes in knee kinematics due to aging have been extensively investigated but with conflicting results reported. In a recent meta-analysis of twenty-nine studies, the effect size of aging as a factor towards altered knee kinematics in the sagittal plane was small when using CA (standardized effect = -0.40 [p = 0.00]) [94]. Although there was abundant evidence to suggest that kinematic changes in the sagittal plane of the knee exist with aging, there was a lack of consistency in the directionality of the kinematic changes. Additionally, a moderate effect was found in the knee RoM within the sagittal plane (standardized effect = -0.70 [p = 0.00]), suggesting that older individuals had a larger RoM in knee F/E. However, several other studies contradict this finding, determining that older individuals have a smaller RoM [177], [178]. These inconsistent findings in knee kinematics with aging were suggested to arise from methodological heterogeneity (e.g., different walking speeds). However, there are two other factors that may contribute to these inconsistencies: 1) skin movement artifacts associated with skin mounted reflective markers, especially located on the thigh and shank [7], and 2) crosstalk errors associated with the use of CA, resulting from inaccurate ACS definitions [96].

To address the first factor - the potential error source of skin movement artifacts - HSBV may be used instead for kinematic assessments. Specifically, HSBV uses biplanar X-rays to record bone movements directly instead of relying on skin mounted markers to represent the underlying bone movements. HSBV has been used in previous studies to characterize CA kinematic envelopes of asymptomatic knees for younger [139] and older [179] individuals during the gait cycle. For fifteen younger participants (9 males and 6 females, ages 30.5 ± 6.2 yrs), Gray et al. (2019) found peak-to-peak displacements (i.e., RoM) in F/E, I/E rotation, and Ab/Ad to be 70.7 deg, 9.2 deg, and 1.9 deg, respectively, during the full gait cycle of level walking [139]. For eight older, asymptomatic participants (4 male, 4 female, ages 61.7 ± 5.4), Kefala et al. (2017) found average RoM in I/E rotation and Ab/Ad angles to be 3.6 ± 1.1 deg and 2.3 ± 0.6 deg, respectively, during the stance phase of level walking [179]. However, the kinematic results of these two studies are difficult to compare due to different time frames analyzed (i.e., full gait cycle versus stance phase only). To date, no direct comparisons of asymptomatic knee kinematics between younger and older individuals have been reported. The second factor - presence of crosstalk - may be avoided by using the HA instead of the conventional CA approach (refer to section 1.2.2). Only one study, performed by Temporiti et al. (2020), has used the HA (specifically the sFHA) to compare healthy knee kinematics of twenty younger and twenty older individuals [76]. During treadmill walking, the study revealed significant differences in the sFHA dispersion, with 2.8-5.0 deg of greater magnitudes in the older participants. However, the OMCS was used in this study and the authors specified that skin movement artifacts within the data may have remained despite using filters to minimize these errors [76]. Additionally, the sFHA is susceptible to stochastic errors if the angular displacements are small [4]. Temporiti managed this issue by calculating the knee kinematics at every ten degrees of rotation along the sagittal plane. However, this method reduces the temporal

resolution of the data and omits large time frames of data that may have contained significant kinematic differences. The rFHA has the ability to preserve temporal resolution by using a reference position instead to achieve larger angular displacements [5]. Consequently, the limitations surrounding the Temporiti study may be alleviated by using the rFHA in conjunction with the HSBV.

Furthermore, several other HA measures exist to characterize knee kinematics but have not been investigated with an aging population. For example, during a squat it was found that ACLD knees had a more anterior sFHA location (2.6-15.9 mm; the intersection of the sFHA with the femoral mid-sagittal plane) and greater sFHA orientation (1.0-3.2 deg; angle between the sFHA and femoral ML axis) when compared to healthy controls. This result was speculated to arise from translational and rotational instabilities of the knee, respectively, which correlated with tibiofemoral OA severity [77]. Similar measures with the rFHA may provide a more thorough assessment of knee kinematics in older individuals, who may show equivalent patterns of movement to the ACLD group as they are at higher risk of tibiofemoral OA. Additionally, the trace of the rFHA location along the femoral mid-sagittal plane may provide information regarding the amount of movement and RoM of the knee (i.e., path length and rFHA AP/SI excursion, section 2.3).

The purpose of this study was to compare rFHA measures and CA between younger and older individuals with asymptomatic knees during level walking using the HSBV. It was hypothesized that the younger group would demonstrate different knee kinematics than the older group. Specifically, the older group would have greater magnitudes of rFHA path length and AP/SI excursion (relating to a greater knee movement and RoM), and greater magnitudes of rFHA

orientation (relating to decreased rotational knee stability). CA were also compared to the rFHA helical angles as an exploratory analysis (as in Chapter 6).

7.2 Methods

The data used in this study was previously collected as part of a larger study, approved by the Conjoint Health Research Ethics Board (REB15-0554). The data was previously analyzed by Ritchie (2017) and Kupper (2020, thesis publication pending), who investigated different research questions and variables to this current thesis research. Only methods related to this thesis will be described in this section.

7.2.1 Study Participants

Ten male participants were recruited for this study and assigned in equal numbers to one of two groups: 20-to-30-year age group (ages 25.8 ± 1.9 years, body mass index (BMI) 22.5 ± 1.1 kg/m^2) and 50-to-60-year age group (ages 55 ± 2.4 years, BMI 26.8 ± 4.0 kg/m^2). Inclusion criteria required participants to be under 190 cm tall to accommodate HSBV height restrictions, have no history of lower limb injury or surgery, have no form of musculoskeletal injury within 6 months prior to testing, and be self-reported as asymptomatic for tibiofemoral OA. All participants provided informed consent prior to participation (ethics ID: REB15-0554).

7.2.2 Data Collection

Each participant first completed the Knee Osteoarthritis Outcome Score (KOOS) to obtain a better description of participant knee symptoms and function [181]. Prior to HSBV collection, MR images of the right limb for each participant were acquired (General Electric Medical Systems 3T Discovery 750; Steady State Free Precision, slice thickness 1 mm; slice spacing 0.5 mm; field of view 24 × 24 cm; matrix 512 × 512 pixels; echo time: 2.32 ms; repetition time: 7.513 ms; flip angle 35°; acquisition time 7’01”). Participants were asked to avoid strenuous activity (e.g., lifting, running, strenuous or extensive walking or cycling) twelve hours before imaging, and remained

non-weight bearing an hour before imaging. Following MR imaging, participants were taken to the HSBV lab (refer to section 1.2.1.2). All participants were fit with protective lead garments to shield against stray x-rays. Participants were positioned within the calibrated HSBV and walked on a split-belt Bertec (USA) treadmill (1.2 m/s) instrumented with force plates (1000 Hz). A warmup was first performed on the treadmill for two minutes to acclimatize the participant to the walking speed [182]. Three trials (i.e., successive gait cycles) of the right leg were then recorded with the HSBV (120 Hz, 64-72 kV, 100 mA, 1 ms pulse, effective dose 1.0 mSv, inter-beam angle 60 deg) along with ground reaction forces from the force plates. A sync pulse was used to synchronize the HSBV and force plate data.

7.2.3 Data Processing

It has been found that asymptomatic knees may still show signs of OA within MR images [183]. Therefore, Magnetic Resonance Imaging Osteoarthritis Knee Scores (MOAKS) were acquired to determine the OA status of each participant, where higher scores relate to greater severities of OA [184]. Using the high-resolution knee MR images, a trained musculoskeletal radiologist reported MOAKS for all ten healthy, self-reported asymptomatic participants. MOAKS scores were categorized as very low (0-4), low (5-19), moderate (20-39), and high (>40). MR images of the right knee were also imported into Amira (Thermo Fisher Scientific, MA, USA) for manual segmentation of the femur and tibia, providing 3D models of the respective bones. These bones were then transformed into an ACS using methods described previously [185]. For the femur, the ML axis of the knee was defined by fitting and connecting the centres of spheres to each femoral condyle. The centre of this ML line was designated as the origin of the femur. A temporary SI axis was created by connecting a line between the hip centre (defined as the centroid of a sphere fit onto the femoral head) and femur origin. Afterwards, the AP axis was obtained by determining a vector cross product between the ML and temporary SI axis. The final SI axis was then calculated

by computing a vector cross product between the ML and AP axis to obtain an orthogonal system. For the tibia, the origin was defined as the centre of the intercondylar eminence. Similar to the femur, the ML axis was obtained by connecting a line between the centres of the medial and lateral plateaus. A temporary SI axis was obtained by connecting the tibial origin and ankle centre (mid-point of a line connecting the medial and lateral malleolus). The AP axis was obtained by computing a vector cross product between the ML axis and temporary SI axis. The final SI axis was calculated by computing a vector cross product of the ML and AP axes. The ACS of the femur and tibia were both oriented such that lateral, superior, and anterior directions were positive [185]. Knee extension, adduction, and internal rotation were designated as positive rotations.

HSBV images were undistorted and then imported into 2D-3D registration software (Joint Track Biplane, University of Florida, USA) with calibration parameters that relate the 2D locations of the biplanar images to a 3D space relative to the HSBV. The 3D bone models, within their respective ACS, were then 2D-3D registered to the HSBV images. Joint Track Biplane outputs a series of Cardan angles ('F/E, Ab/Ad', I/E sequence [27]) and translations relating to the movement of the bone being registered. Therefore, two kinematic series were acquired for each trial, one for the femur and another for the tibia. Due to lower limb crossover during the gait cycle, resulting in bone occlusion during a segment of the walking movement, registration of the femur and tibia was only possible for partial sections of the stance and swing phase (stance: ~0-25%; swing: ~70-100%). Additionally, if the femur and/or tibia of the participant during a trial did not align properly with the HSBV (resulting in the femur and/or tibia not appearing within the images), the trial was eliminated. Within each trial for each participant, the kinematic series of both bones were normalized to a percent gait cycle, where 0% represents heel-strike and 100% represents toe-

off (Figure 7-1). The cut-offs for these events were determined using the vertical ground reaction force signals.

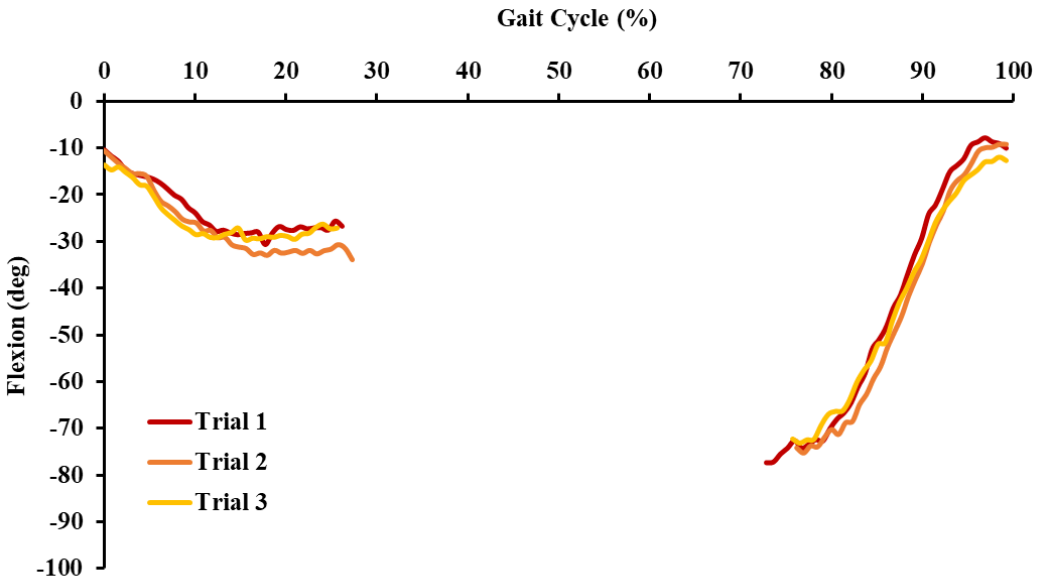

Figure 7-1 – Example of kinematic curves normalized to 100% gait cycle. Three trials of knee F/E for a single participant are illustrated. 0% represented heel-strike and 100% represented toe-off. The gap within the data (~25-70%) is due to the inability to register the bones because of lower limb crossover.

Knee rFHA parameters were obtained using a custom Matlab program (v2020b, MathWorks, MA, USA) during two movement segments: 1) from 0-25% of the gait cycle (i.e., heel-strike to mid-stance) and 2) from heel-strike to the occurrence of peak vertical ground reaction force during 0-25% gait cycle (referred to as peak force [PF] henceforth). The swing phase was not assessed for kinematics as the largest magnitudes of joint reaction forces occur during the stance phase. This process requires converting the Cardan angles of both bones into a rotation matrix using a 'ZXY' sequence,

$$\begin{bmatrix} c\,\theta_Y\,c\,\theta_Z + s\,\theta_Y\,s\,\theta_X\,s\,\theta_Z & c\,\theta_X\,s\,\theta_Z & -s\,\theta_Y\,c\,\theta_Z + c\,\theta_Y\,s\,\theta_X\,s\,\theta_Z \\ -c\,\theta_Y\,s\,\theta_Z + s\,\theta_Y\,s\,\theta_X\,c\,\theta_Z & c\,\theta_X\,c\,\theta_Z & s\,\theta_Y\,s\,\theta_Z + c\,\theta_Y\,s\,\theta_X\,c\,\theta_Z \\ s\,\theta_Y\,c\,\theta_X & -s\,\theta_X & c\,\theta_Y\,c\,\theta_X \end{bmatrix} \quad \text{Eq. 7-1}$$

where ‘c’ and ‘s’ represent cosine and sine functions, respectively, and θ represents the Cardan angle about a specific axis (X, Y, or Z). This provides a 3x3 rotation matrix representing the orientation of the femur or tibia within the ACS. The ‘ZXY’ sequence was chosen because the same sequence was used by the Joint Track Biplane software to calculate the CA. These rotation matrices were subsequently smoothed using a B-spline filter with outlier removal process (SPOUT, refer to Chapter 3).

To obtain a reference position for the rFHA, knee angles (tibia relative to the femur) were calculated during the first of the three swing phases recorded. The swing phase was selected as greater magnitudes of knee flexion occur within this phase, providing a reference position that supplies large angular displacements relative to the stance phase. The magnitude of helical flexion during swing phase was first calculated. The time point corresponding to 60 deg of knee flexion was selected as the reference position. It is important to note that the rotation about the HA is not affected by errors due to small angular displacements, only the directionality and position of the HA are affected [37]. Therefore, the helical flexion angle used to define the reference position was considered accurate. Because the alignment of the reference position may influence the rFHA measures in this study (refer to Chapter 4), the helical angles within the other planes of motion (Ab/Ad and I/E rotation) were averaged across all participants, providing a mean (SD) and 95% CI of the reference position alignments in those two planes.

For all gait cycle trials successfully recorded, the femur and tibia rotation matrices during 0-25% gait cycle were calculated relative to the reference position. Next, the relative bone movements (tibia relative to femur) were calculated to obtain knee joint rotation matrices. Using these

matrices, the rFHA measures were quantified: AP and SI location, translation, orientation, dispersion, path length, AP and SI excursion, and helical angles (refer to section 1.2.2.3 for definitions). For each participant, the rFHA measures from 0-25% gait cycle and 0-PF were averaged across all trials to obtain a mean (SD) rFHA measure at each movement segment.

7.2.4 Statistical Analysis

Due to the small sample size (n = 5 per group), a non-parametric Mann-Whitney U test was performed to determine group differences in rFHA measures from 0-25% gait cycle and 0-PF. Mean differences (younger – older) and accompanying SD were reported to supplement the Mann-Whitney U test. Cardan and helical angles at the single instance of PF were only included in the PF Mann-Whitney U test analysis. Tests were performed with a significance value of ($\alpha = 0.05$) and effect sizes reported (Cohen's D). Magnitudes of the effect sizes were categorized as no effect (< 0.20), small (0.20-0.49), medium (0.50-0.79), and large (≥ 0.80) [160]. To accommodate for multiple tests (eight rFHA measures at 0-25% gait cycle and fifteen measures [rFHA and CA] from 0-PF or at PF) the Benjamini-Hochberg procedure was used with a false discovery rate of 5% to preserve the significance value to 0.05 [159]. Original p-values are reported in this study, prior to the Benjamini-Hochberg procedure. Therefore, p-values smaller than 0.05 may not be significant and will be explicitly stated when significance was maintained. To assess differences in kinematic variability, inter-quartile ranges (IQR) of each measure were compared between the younger and older groups. These IQR were further illustrated with box plots for qualitative assessments. Tracings of the rFHA AP/SI location were also shown to provide a visual assessment of the rFHA path length and AP/SI excursions.

7.3 Results

7.3.1 KOOS and MOAKS

The high KOOS scores of all ten participants indicated that all had low levels of knee pain and high knee function (Table 7-1). The lowest symptoms score was 79/100 in the older group and 93/100 in the younger group, where a score of 100 indicates no symptoms. Younger participants scored 100/100 in all other KOOS categories (pain, activities of daily living, sports and recreation, and quality of life). The lowest pain score in the older participants was 83/100, where a score of 100 indicates no pain. The remaining KOOS measures ranged from 85-100 out of 100.

The MOAKS of all ten participants are also provided in Table 7-1. Overall, the participants had healthy joint scores All younger participants had a MOAKS of 0, indicating very minimal to no signs of OA. Older participants generally had greater MOAKS, ranging from 0-26. Four of the five older participants were considered to have very low or low signs of tibiofemoral OA. Only one older participant was categorized within moderate OA, having a MOAKS of 26.

Table 7-1 – KOOS scores and MOAKS for younger (Y1-Y5) and older (O1-O5) participants. High KOOS scores (maximum 100) indicate no problems in that category.

Participant	KOOS (out of 100)					MOAKS	
	Symptoms	Pain	Activities of Daily Living	Sports and Recreation	Quality of Life	Score	Definition
Y1	93	100	100	100	100	0	Very Low
Y2	96	100	100	100	100	0	Very Low
Y3	100	100	100	100	100	0	Very Low
Y4	100	100	100	100	100	0	Very Low
Y5	100	100	100	100	100	0	Very Low
O1	100	100	100	100	100	0	Very Low
O2	79	83	100	85	88	8	Low
O3	89	100	100	100	100	11	Low
O4	93	92	100	100	94	3	Very Low
O5	100	97	99	95	100	26	Moderate

7.3.2 Reference Position & Trial Elimination

Variability of the reference positions was present. Mean (SD) helical Ab/Ad within the reference position was -2.61 (4.51), corresponding to a 95% CI of -5.40–0.19 deg. Mean (SD) helical I/E rotation within the reference position was 4.33 (4.88), corresponding to a 95% CI of 1.30-7.35 deg. A single trial for Y1, O1, O3, and O5 were removed from the analysis due to the lower limb not being sufficiently visible for 2D/3D registration.

7.3.3 Path Length, Location, Excursion, and Translation

The rFHA path length was significantly different between younger and older asymptomatic participants from 0-25% of the gait cycle. Younger participants demonstrated 37% greater path length magnitudes than the older participants (mean difference [SD]: 10.60 [9.23] mm, effect size: 2.93, p = 0.01; Table 7-2). This is evident in a visual inspection of the rFHA location tracing, where on average the younger group had a longer tracing length than the older group (Figure 7-2). This was also evident in the individual rFHA tracings for each participant (refer to Appendix D). This significant difference in path length was not found from 0-PF, but a large effect size remained (mean difference [SD]: 8.05 [3.21] mm, effect size: 2.34, p = 0.02; Table 7-3). Additionally, the path length variability was smaller within the older group for both the 0-25% gait cycle segment (younger IQR: 13.36 mm, older IQR: 4.19 mm; Table 7-2 & Figure 7-3) and in the 0-PF segment (younger IQR: 10.38 mm, older IQR: 2.98 mm; Table 7-3 & Figure 7-4).

The rFHA location, excursion, and translation did not reveal any statistically significant differences between the two groups for both movement segments of interest (Table 7-2 & Table 7-3). AP and SI location had a mean difference (SD) of -22.34 (55.30) mm and 3.53 (37.64) mm from 0-25% gait cycle, and -24.46 (55.50) mm and 3.43 (37.15) mm from 0-PF, respectively. AP and SI excursion had a mean difference (SD) of 4.05 (4.85) mm and 3.48 (6.58) from 0-25% gait cycle (Figure 7-2), and 4.31 (5.23) mm and 5.62 (6.40) mm from 0-PF, respectively. The

translation along the rFHA showed mean differences (SD) of 1.51 (2.82) mm from 0-25% gait cycle and 0.76 (1.35) mm from 0-PF. Similar to the path length, the rFHA location, excursion, and translation were more variable (i.e., larger IQRs) within the younger group, with the exception of translation at 0-25% gait cycle (Table 7-2 & Table 7-3).

Table 7-2 – Statistics for each rFHA measure for the younger and older groups from 0-25% gait cycle. Group means and mean differences (younger - older) with associated SD and 95% CIs are provided, as well as U scores and p-values (with corresponding effect sizes) from the Mann-Whitney U tests.

0-25% Gait Cycle	Younger				Older				Mean Difference	SD	U Score	p-value (effect size)
rFHA Measure	Mean	SD	Median	IQR	Mean	SD	Median	IQR				
Location (AP) (mm)	-2.05	40.68	2.29	77.67	20.30	37.47	33.15	72.52	-22.34	55.30	7.00	0.31 (0.78)
Location (SI) (mm)	-4.35	31.36	5.23	58.13	-7.88	20.81	-2.38	36.79	3.53	37.64	11.00	0.84 (0.20)
Translation (mm)	-5.42	1.92	-6.30	3.05	-6.93	2.07	-6.36	3.09	1.51	2.82	8.00	0.42 (0.62)
Orientation (deg)	8.55	2.31	8.13	4.58	8.03	4.72	5.62	8.31	0.52	5.26	8.00	0.42 (0.62)
Dispersion (deg)	2.78	0.32	2.70	0.62	3.40	1.06	2.85	1.41	-0.61	1.11	6.50	0.22 (0.87)
Path Length (mm)	29.01	8.91	25.81	13.36	18.41	2.41	18.73	4.19	10.60	9.23	0.00	0.00* (2.93)
Excursion (AP) (mm)	9.76	4.74	8.48	8.42	5.71	1.03	5.49	1.90	4.05	4.85	5.00	0.15 (1.14)
Excursion (SI) (mm)	13.86	5.56	11.73	7.76	10.38	3.52	9.92	4.94	3.48	6.58	7.00	0.31 (0.78)

* dictates a significant difference after the Benjamini-Hochberg procedure

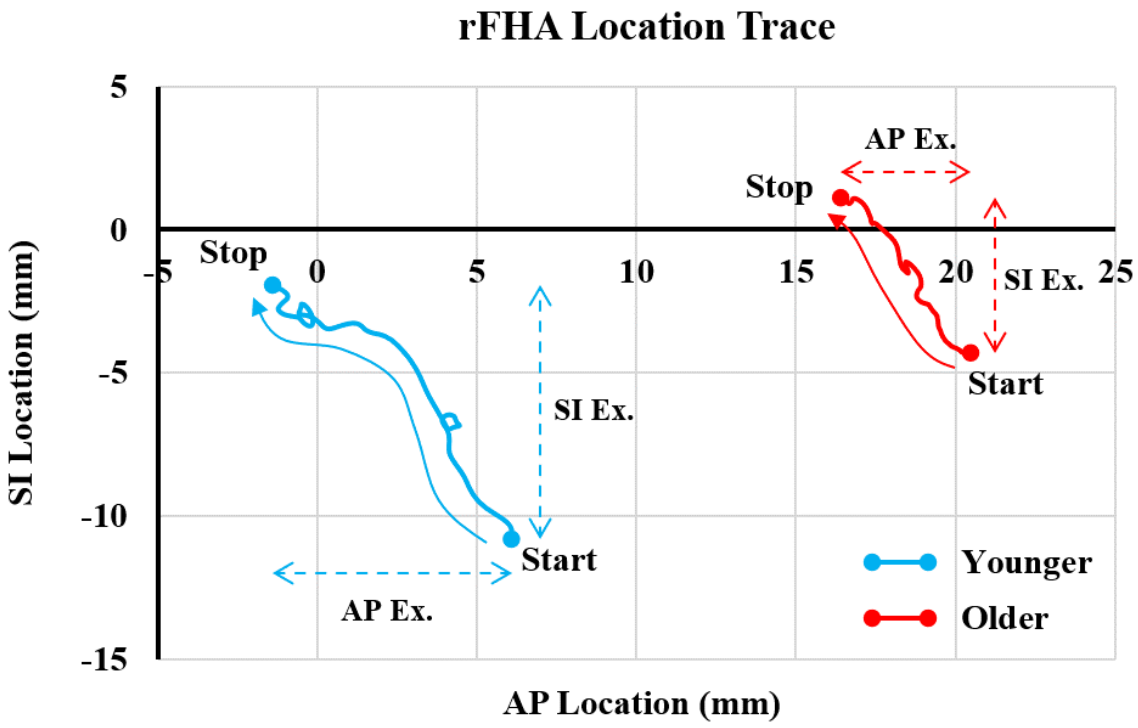

Figure 7-2 – The rFHA location trace along the femoral mid-sagittal plane from 0-25% gait cycle. A significant difference in path length was found, with younger (blue) participants having greater path lengths than older (red) participants. This is evident in the longer trace length of the younger participants. AP/SI excursions (dashed arrows) were not significantly different. Start indicates 0% gait cycle and stop indicates 25% gait cycle. The solid arrows dictate the direction of the trace.

Table 7-3 – Statistics for each rFHA measure for the younger and older groups from 0-PF. Group means and mean differences (younger - older) with associated SD and 95% CIs are provided, as well as U scores and p-values (with corresponding effect sizes) from the Mann-Whitney U tests.

Peak Force	Younger				Older				Mean Difference	SD	U Score	p-value (effect size)
rFHA Measure	Mean	SD	Median	IQR	Mean	SD	Median	IQR				
Location (AP) (mm)	-4.46	40.59	-0.25	77.57	19.81	37.84	33.27	73.19	-24.26	55.50	7.00	0.31 (0.78)
Location (SI) (mm)	-2.62	30.80	0.41	56.21	-6.05	20.78	-1.13	37.05	3.43	37.15	11.00	0.84 (0.20)
Translation (mm)	-3.53	2.16	-4.42	3.96	-4.30	2.10	-3.56	2.80	0.76	1.35	12.00	1.00 (0.07)
Orientation (deg)	10.53	3.37	11.84	6.45	9.35	5.74	6.40	8.84	1.18	6.66	8.00	0.42 (0.62)
Dispersion (deg)	3.60	0.43	3.48	0.85	3.42	1.15	2.90	2.06	0.18	1.23	8.00	0.42 (0.62)
Path Length (mm)	21.10	7.01	19.43	10.48	15.05	1.57	12.22	2.98	8.05	3.21	1.00	0.02 (2.34)
Excursion (AP) (mm)	8.26	5.09	7.39	8.62	3.95	1.21	4.09	2.35	4.31	5.23	5.00	0.15 (1.14)
Excursion (SI) (mm)	12.82	6.21	11.66	9.43	7.19	1.54	6.53	2.77	5.62	6.40	5.00	0.15 (1.14)
Helical Adduction (deg)	-1.72	4.80	-1.32	8.54	-3.01	2.22	-2.13	3.52	1.30	5.29	9.00	0.55 (0.48)
Cardan Adduction (deg)	-1.43	4.30	-0.42	6.05	-1.52	3.02	-0.91	5.14	0.09	5.25	10.00	0.69 (0.34)
Helical Internal Rotation (deg)	0.48	6.85	-1.51	11.81	4.06	4.45	3.09	6.68	-3.58	8.17	7.00	0.31 (0.78)
Cardan Internal Rotation (deg)	1.03	6.97	1.82	12.40	4.81	3.73	3.56	5.00	-3.78	7.90	8.00	0.42 (0.62)
Helical Extension (deg)	38.60	5.79	40.44	8.00	39.22	3.35	40.34	4.30	-0.62	6.69	12.00	1.00 (0.07)
Cardan Extension (deg)	38.68	5.82	40.48	8.10	39.26	3.40	40.40	4.39	-0.58	6.74	12.00	1.00 (0.07)

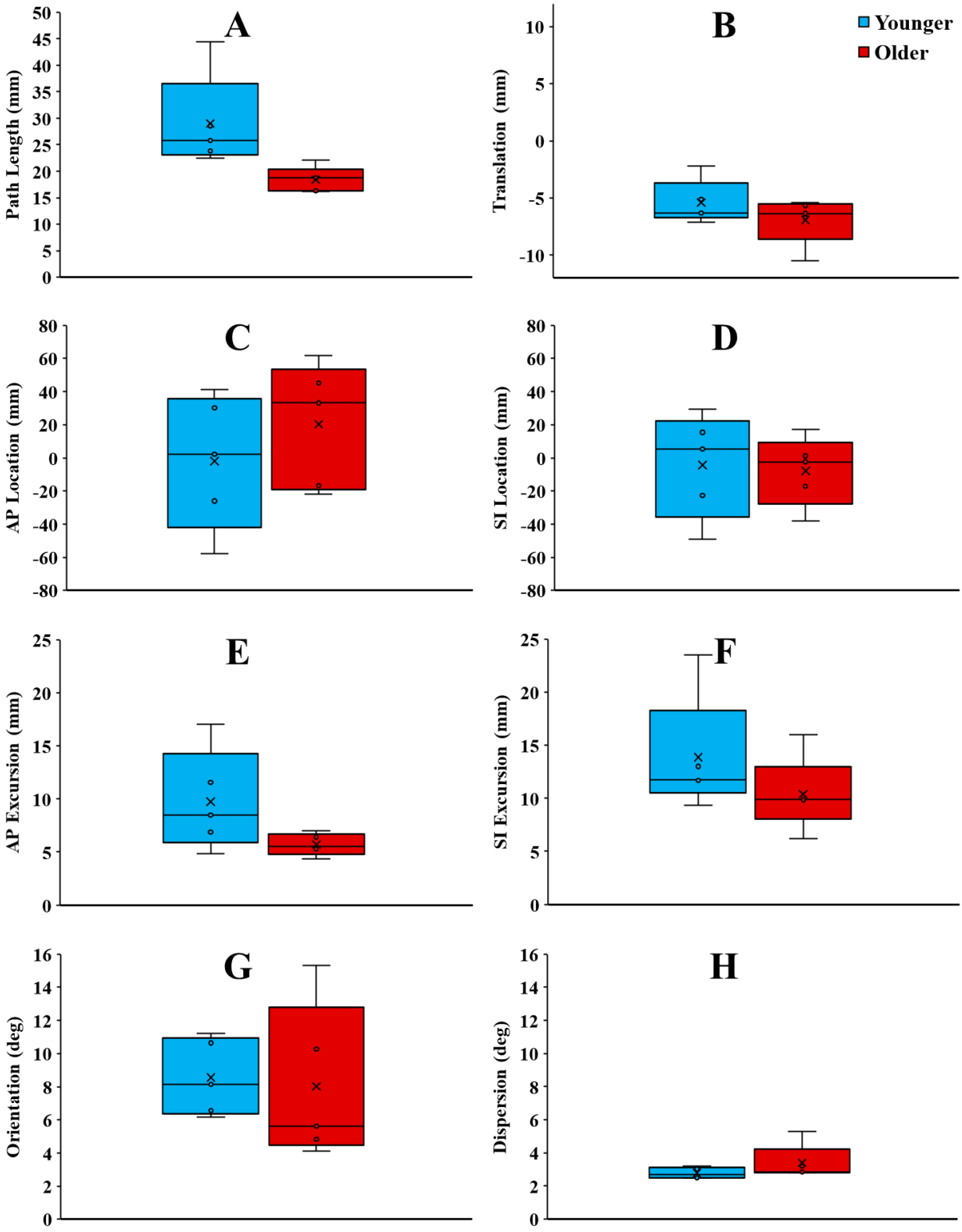

Figure 7-3 – Box plots of the rFHA measures (A-H) from 0-25% gait cycle for the younger (blue) and older (red) groups. The '×' symbol represents the group mean.

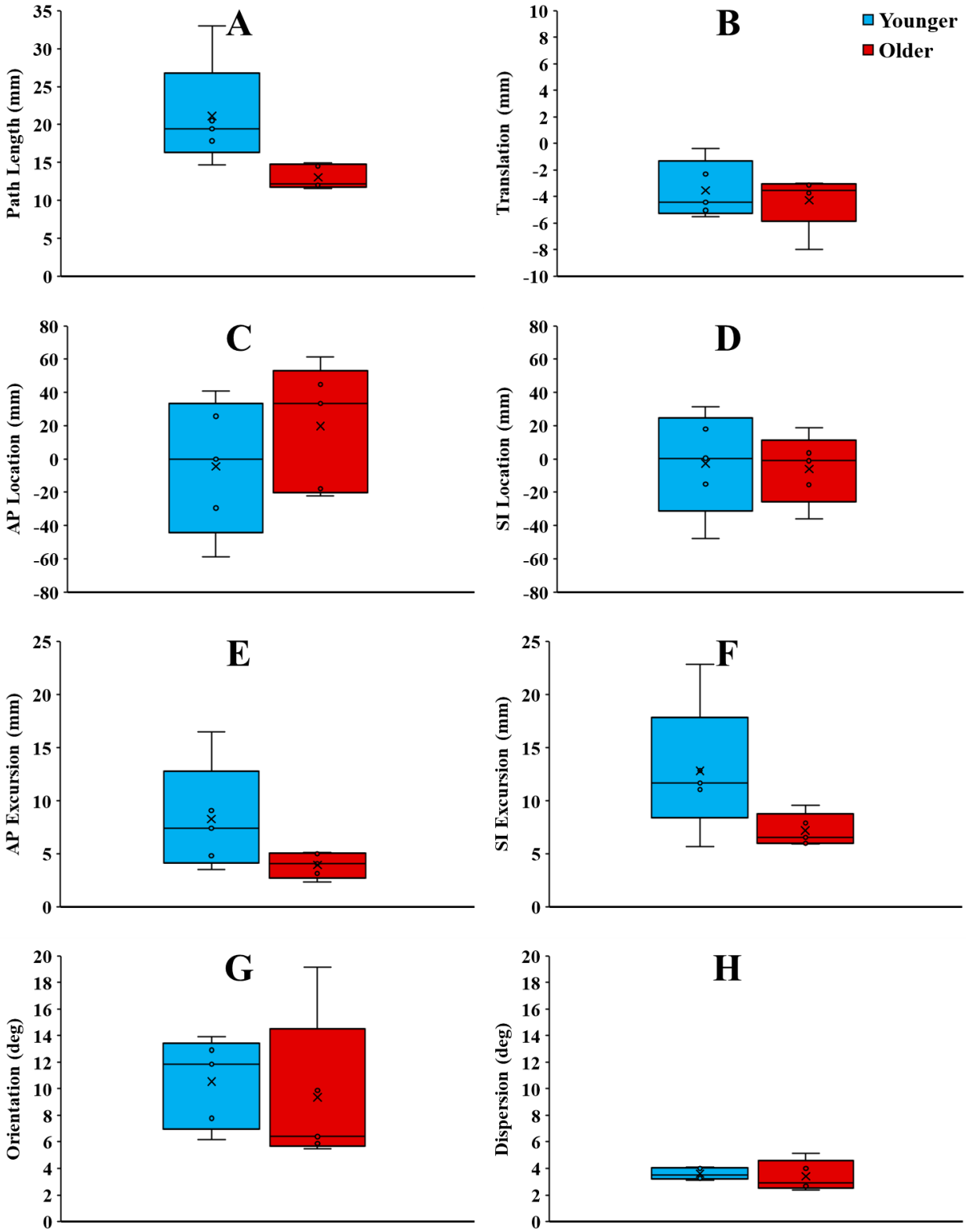

Figure 7-4 – Box plots of the rFHA measures (A-H) from 0-PF for the younger (blue) and older (red) groups. The '×' symbol represents the group mean.

7.3.4 Orientation & Dispersion

Orientation and dispersion of the rFHA did not show any significant differences between the younger and older participants (Table 7-2 & Table 7-3). The mean difference (SD) of the orientation was 0.52 (5.26) deg from 0-25% stance phase and 1.18 (6.66) deg from 0-PF. The IQR of the orientation was larger in the older group from 0-25% gait cycle (younger IQR: 4.58 deg, older IQR: 8.31 deg; Table 7-2 & Figure 7-3) and from 0-PF (younger IQR: 6.45 deg, older IQR: 8.84 deg; Table 7-3 & Figure 7-4). The dispersion showed mean differences (SD) of -0.61 (1.11) deg from 0-25% gait cycle and 0.18 (1.23) deg from 0-PF. Similar to orientation, the older group showed greater IQR for dispersion for both 0-25% gait cycle (younger IQR: 0.62 deg, older IQR: 1.41 deg; Table 7-2 & Figure 7-3) and 0-PF (younger IQR: 0.85 deg, older IQR: 2.06 deg; Table 7-3 & Figure 7-4).

7.3.5 Helical & Cardan Angles

There were no group differences (younger - older) discovered for either the helical or Cardan angles at the single instance of PF (Table 7-3). Helical and Cardan adduction angles showed mean differences (SD) of 1.30 (5.39) deg and 0.09 (5.25) deg, respectively. Helical and Cardan internal rotation had mean differences (SD) of -3.58 (8.17) deg and -3.78 (7.90) deg, respectively. Finally, helical and Cardan extension showed mean differences (SD) of -0.62 (6.69) deg and -0.58 (6.74) deg, respectively. The older participants tended to have less variable helical and Cardan angles at PF, demonstrating 14.90-59.68% smaller IQR (Table 7-3 & Figure 7-5). Temporal graphs of the helical and Cardan angles from 0-25% gait cycle can be found in Appendix E.

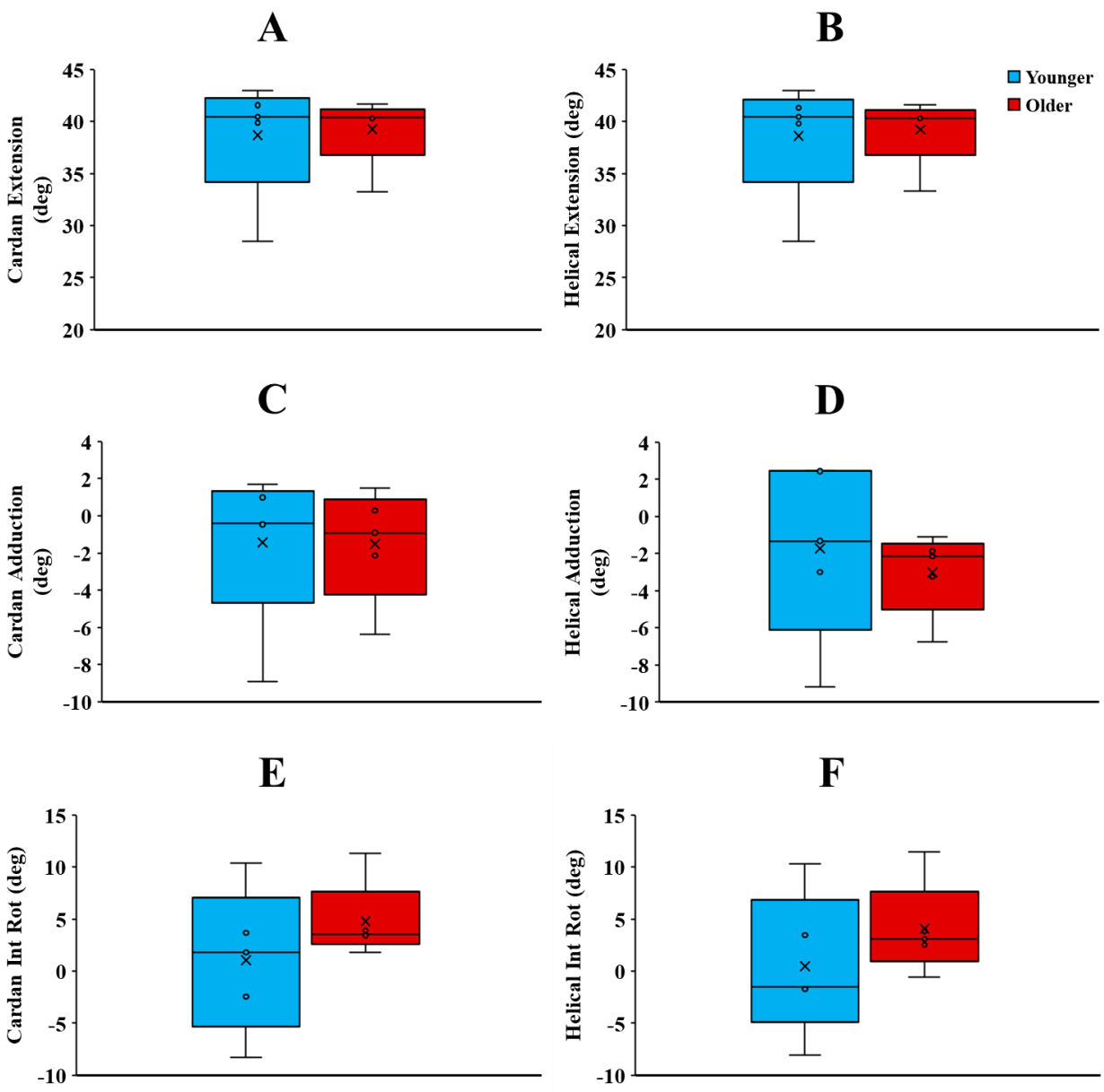

Figure 7-5 – Box plots of the CA (graphs A, C, and E; rotation sequence of F/E, Ab/Ad, I/E) and helical angles (B, D, and F) at PF for the younger (blue) and older (red) groups. The '×' represents the group mean.

7.4 Discussion

Aging is a major risk factor for the onset and progression of tibiofemoral OA. This is because aging has been partly linked to altered knee kinematics that result in changes of knee stability and RoM. These changes ultimately lead to altered contact locations on the femur and tibia. However, there is a lack of strong evidence to suggest that these kinematic differences exist when using CA, as the directionality of the changes have been inconsistent (e.g., studies have reported both larger and smaller RoM for older groups when compared to younger groups). This may be due to certain methodological limitations, such as skin movement artifacts with the OMCS and crosstalk when using CA. Therefore, the rFHA, in conjunction with HSBV, was used in this study to investigate the knee kinematic differences of five younger and five older participants from 0-25% gait cycle and from 0-PF (or at PF). It was hypothesized that the older group would have greater magnitudes of rFHA path length, AP/SI excursion, and orientation, and a more anterior rFHA location.

7.4.1 Path Length & Excursion

It was hypothesized that the older group would have greater magnitudes of rFHA path length. This hypothesis was not supported in the study, as the older group had significantly smaller magnitudes of rFHA path length when compared to the younger group. This was visible in the rFHA location trace, where it is clearly shown that the older group had a smaller trace length than the younger group (Figure 7-2). The younger group revealed a larger path length than the older group from 0-25% gait cycle (mean difference [SD]: 10.60 [9.23] mm, effect size: 2.93, $p = 0.00$). Although not significant following the Benjamini-Hochberg procedure, a large effect size was seen from 0-PF (mean difference [SD]: 8.05 [3.21] mm, effect size: 2.34, $p = 0.02$). The rFHA path length represents the rFHA location's total distance travelled (represented by the length rFHA location trace; Figure 7-2). If the rFHA contains smaller movements in its directionality and/or position across the movement of interest, the path length will be smaller. A smaller path length may be

associated with ‘stiffer’ knee kinematics that result in reduced bone movements [40]. Therefore, the older group walked with a stiffer knee that did not rotate and/or translate as much as the younger group. This finding was further supported by the smaller path length variability of the older participants, suggesting that this stiffer knee strategy was performed consistently throughout 0-25% gait cycle and 0-PF. It is speculated that a reduced RoM in the knees of the older participants may result in loads that act within a smaller surface area of knee cartilage when compared to the younger participants. Consequently, the cartilage within that area may be more frequently exposed to habitual loading, thus increasing the risk of cartilage degradation in that region. However, a previous study by Kupper (2020), using the same data as in this study, does not confirm this speculation [186]. To elaborate, the study by Kupper compared the path travelled of the femoral and tibial cartilage contact regions (i.e., weighted centroids) between the younger and older participants. No statistically significant group differences were found in the path travelled of the weighted centroid. This was suggested to be a result of the small sample size, thus not having sufficient power in the study. However, the study did note that some older participants had large oscillations in the weighted centroid location [186]. This may result in a larger surface area in which the loads within the knee act, thus contradicting the finding in this study where older participants had a smaller rFHA path length. Future studies are required with a larger sample size to increase the power of the study, and to better determine the relationships between the rFHA path length and cartilage contact regions.

The smaller magnitudes of path length in the older group may also be an accommodation at older ages to minimize the risk of injury/falling. Older individuals have been reported to have decreased levels of knee proprioception, or a lessened capacity to detect the position/orientation of their knee joint [187], [188]. As a result, they may ‘stiffen’ their gait (i.e., reduce their knee RoM) to provide

minimal joint displacements, thus maintaining a safer knee position to avoid a loss of balance. This study did not find statistically significant differences in rFHA excursion to further support the notion of decreased knee RoM. However, older individuals have been previously reported to have smaller RoM within the knee during waking [177]–[179]. This decrease in RoM has been speculated to increase stability of the knee and promote greater balance [189]. These speculations have been substantiated with EMG studies, where increased levels of muscular co-contractions were present with aging, providing more stability to the knee [189], [190]. However, increases in muscular co-contraction may lead to greater forces within the joint, promoting the progression of tibiofemoral OA [191]. Similar, but more drastic decreases in proprioception and increases in muscular co-contractions have been observed in participants with tibiofemoral OA to increase knee stability [73], [191]–[193]. A similar pathogenesis may exist within older, asymptomatic individuals and requires further investigation.

7.4.2 Orientation & Dispersion

The orientation of the rFHA did not differ between the two groups, thus refuting the study hypothesis that orientations would be greater in the older group. The same observation was seen with the translation along the rFHA. This is an interesting finding because the path length, which was significantly different, is dependent on these measures. Specifically, the directionality of the rFHA (measured with orientation) and the physical position of the rFHA in 3D space (influenced by knee translations) will affect the point of intersection between the rFHA and femoral sagittal plane (i.e., the rFHA location). Therefore, it would be expected that at least one of these measures would be a differentiating factor between the two groups. It may be that a larger sample size is required to determine these differences, as this study had a small sample size (n = 5 for each group). However, these findings may also suggest that the knee kinematics of older, asymptomatic individuals are not simply distinguished by rotations and translations individually. Instead,

differences in knee kinematics could reside within the combined alterations of the two movement types. The rFHA, because of its ability to combine rotations and translations as a single, quantifiable measure, may prove to be a powerful supplementary tool to kinematic analyses.

The dispersion of the rFHA was not significantly different between the two groups for either movement segment assessed. This finding is contrary to a recent OMCS study performed by Temporiti et al. (2020), who determined significantly greater magnitudes of sFHA dispersion (1.8-5.0 deg) during 95-10% and 75-95% of the gait cycle in twenty older, asymptomatic participants when compared to twenty younger, healthy controls [76]. These conflicting results may originate from three methodological differences. Firstly, the phases of gait that were assessed were not the same, as our study investigated 0-25% of the gait cycle. 0-25% (heel-strike to midstance phase of walking) was selected for this study as the largest joint reaction forces occur during the stance phase of gait. However, measuring dispersion from 95-10% (terminal swing to foot flat) and 75-95% (initial swing to terminal swing) of the gait cycle may provide different results. These movement segments involve different kinetic chains (swing = open chain; stance = closed chain) which may require different kinematic strategies. Further investigations are required for these speculations. Secondly, Temporiti asked the participants to walk on a treadmill at a self-selected speed, whereas this study had a fixed treadmill speed of 1.2 m/s. It has been shown that magnitudes of knee F/E are influenced by walking speed [194], [195]. However, during passive knee flexions it was demonstrated that Ab/Ad and I/E rotation of the knee were closely coupled with F/E angle [126], [196]. Although not a passive movement, any knee F/E changes due to different walking speeds may potentially extend into the Ab/Ad and I/E rotations of the knee. Therefore, caution should be used when comparing kinematics of individuals walking at different speeds. Finally, Temporiti used the sFHA instead of the rFHA. The sFHA is susceptible to small angular

displacements, resulting in potentially erroneous positions and directionalities of the sFHA [4]. To mitigate this complication, Temporiti calculated the sFHA at every 10 deg increment of sagittal knee motion. However, this results in the temporal resolution being reduced, resulting in the computation of the sFHA at limited and specific time points. In the case of the rFHA, temporal resolution is maintained due to the use of a reference position. Therefore, the calculation of dispersion differs between the rFHA and sFHA. The rFHA dispersion is calculated using a greater amount of data that may be more variable, whereas the sFHA dispersion is calculated using limited data at specific intervals.

7.4.3 Helical & Cardan Angles

No group differences were found for knee angles at the single instance of PF when using both the helical and Cardan angle approach. However, both approaches revealed smaller angle variabilities within the older group (14.90-59.68% smaller IQR, Figure 7-5) when compared to the younger group). This is an interesting finding, because the variability (IQR) of the rFHA orientation in older participants was found to be 81.44% and 37.05% greater from 0-25% gait cycle (Table 7-2) and 0-PF (Table 7-3), respectively. These conflicting variabilities are speculated to result from the time frames each measure is calculated from (similar to the helical angle and orientation results from Chapter 6, refer to section 6.4.2). The helical and Cardan angles were analyzed at a specific instance of time (PF) while the rFHA orientation was averaged throughout the whole segment of movement (0-25% gait cycle and 0-PF). Therefore, direct comparisons of these two measures are challenging. Assessing the rFHA orientation temporally or at a specific instance of time may be beneficial to determine its relationships with the helical and Cardan angles; future investigations are required.

The decrease in helical and Cardan angle variability may have been a safety mechanism for the older participants to maintain a stable knee and avoid falling during the stance phase of walking

[197], [198]. To elaborate, older individuals experience a decline in proprioceptive function, which has been related to an increased risk of falling [187]. Therefore, older individuals may not be able to control their knee movements to the extent that younger individuals can. During stance phase, where peak reaction forces occur within the knee, older individuals may seek to minimize their risk of falling by reducing the RoM of the knee and maintaining a more stable configuration. Similar decreases in proprioception and joint angle variability have been determined in individuals with tibiofemoral OA [199], [200]. However, due to the cross-sectional design of this study, it is not possible to determine if these stiffer gait patterns in the older, asymptomatic individuals are associated with tibiofemoral OA development. Future studies are recommended to use a longitudinal study design to establish a cause-effect relationship between these stiffer gait patterns and tibiofemoral OA development.

The supplementary findings provided by the rFHA and CA provide additional insights that inform the utility of the rFHA within biomechanics. It is evident that the rFHA is a feasible and promising approach to characterize knee joint stability in a relatively novel perspective.

7.4.4 Strengths & Limitations

One strength of this study includes the use of the HSBV to record bone movements of the participants directly, providing accurate kinematics that are not influenced by skin movement artifacts. Additionally, this study was able to assess the rFHA kinematics from heel-strike to the moment of peak vertical ground reaction force (i.e., 0-PF), as well as helical and CA at the single instance of PF. This is a valuable time frame/point as this is when the knee is subjected to large magnitudes of reaction forces, which are speculated to be a key factor to the development of tibiofemoral OA. Furthermore, the assessment of the helical angles at PF is more efficient using the rFHA, due to its ability to preserve temporal resolution. The alternative sFHA is typically calculated at large angular intervals (e.g., every 10-degrees of knee F/E) to reduce stochastic errors.

Consequently, there is a loss of temporal resolution and it may be difficult to achieve the sFHA measures at the exact time of PF. This is not an issue with the rFHA. A final strength of this study was the use of KOOS and MOAKS to assess knee symptoms/function and health, respectively. All participants in this study provided self-reports of asymptomatic knees. Therefore, older participants considered themselves to be functionally indifferent to the younger participants, being able to perform similar movements without impairment or pain. However, asymptomatic knees of older participants revealed some signs of OA [183]. The use of KOOS and MOAKS informed the study of what levels of knee pain/function and OA each participant had and to ensure both groups were similar.

Limitations in this study are acknowledged as well. First, based on MOAKS, a participant within the older group had moderate signs of OA while the remaining participants of had very low or low signs of OA. Because this one participant's OA status was more severe, their knee kinematics may have increased the variability of the data within the older group. Secondly, the small sample size is a crucial factor that lessens the statistical power of the study. However, the post-processing of HSBV data for a single participant is time consuming and larger sample sizes are difficult to obtain in HSBV studies (refer to section 1.2.1.2). Furthermore, the rFHA and CA presented in this study were exploratory variables from the primary study design. Consequently, the sample size was calculated based on different variables that were not related to the research questions presented here (e.g., cartilage contact path locations). Furthermore, a small sample size may increase the risk of Type II errors (i.e., false negatives). A larger sample size would reduce the risk of Type II errors and potentially reveal more significant findings to substantiate the current rFHA findings. However, the rFHA is a relatively new approach to characterize knee kinematics. Due to limited rFHA studies, it was challenging to perform a sample size calculation. However, the exploratory

findings of this thesis provide a basis for sample size calculations in future studies. Finally, a reference position for each study participant was acquired during their respective swing phase, specifically at 60 deg of knee flexion along the HA. However, according to the helical angles, it was determined that Ab/Ad and I/E rotation angles between the reference positions ranged from -5.40–0.19 deg and 1.30-7.35 deg, respectively. These alignment differences may have an influence on the rFHA measures that could change the overall results of the study (refer to Chapter 4). Future studies should ensure that a reference position trial is obtained in a controlled setting, ensuring consistent knee alignments.

7.5 Conclusions

The natural aging process may result in several musculoskeletal deficiencies, thus altering the kinematics of the knee. These altered kinematics have been speculated to assist in the onset or progression of tibiofemoral OA. Although these changes have been evident, the directionalities of these changes have been inconsistent between studies. For example, studies have reported both smaller knee RoM [178], [201] and larger knee RoM [94] in older groups when compared to younger groups. These directional inconsistencies may be partially attributed to errors within the methods used, specifically skin movement artifacts and crosstalk. To avoid these error sources, this study was the first to use the rFHA, in conjunction with HSBV, to compare knee kinematics of younger and older asymptomatic individuals. It was hypothesized that the older group would demonstrate greater magnitudes of rFHA path length, excursion, and orientation. The rFHA path length was significantly smaller (10.60 mm, effect size: 2.93, $p = 0.00$) in the older group than the younger group, refuting the study hypothesis. This finding suggests that older individuals develop a strategy to walk with a stiffer gait. This strategy then limits the amount of knee movement, with the purpose of maintaining a stable knee to reduce the risk of falling. The speculation of limited knee movement in the older participants was supported with smaller variability of the helical and

Cardan angles at PF (14.90-59.68% smaller IQR). These stiffer gait patterns are similar to previous findings of individuals with tibiofemoral OA. Therefore, the rFHA may provide promising measures that are sensitive to the kinematic changes associated with tibiofemoral OA. However, this cross-sectional study cannot identify this potential cause-effect relationship and longitudinal investigations are required to confirm these speculations.

Chapter Eight: Summary & Future Directions

8.1 Introduction

This thesis investigated the use of the rFHA as an alternative measure to quantify and characterize altered knee kinematics for individuals at high risk of tibiofemoral OA. The research is presented in seven chapters. The first chapter provided the motivation of the thesis, followed by an introduction to the biomechanical etiology of tibiofemoral OA and the methods used to record and quantify knee kinematics. Chapter 1 concluded with the current knowledge gaps relating to characterizing knee kinematics, followed by the objectives of the thesis, and the specific aims (SA) and hypotheses. A review of relevant literature on tibiofemoral OA kinematics using the CA and rFHA approaches, and the knowledge gaps associated with the rFHA were provided in the second chapter. The next three chapters (Chapters 3-5) provided a technical assessment of the rFHA as a biomechanical measure, specifically its response to different smoothing techniques within the HSBV, the influence of misaligned reference positions on the rFHA outcome measures, and the differences in rFHA measures between the HSBV and OMCS. Chapters 6 and 7 outlined the application of the rFHA to characterize differences in knee kinematics of participants who are at high risk of tibiofemoral OA relative to healthy participants. Chapter 6 investigated kinematic differences of ACLR knees in youths, while Chapter 7 investigated kinematic differences between younger and older participants with asymptomatic knees.

The objectives of this thesis were as follows:

1. To advance the applicability of the rFHA in describing clinically relevant knee joint kinematics by evaluating its accuracy within the HSBV and its sensitivity to errors. This will provide technical considerations when using the rFHA to characterize knee kinematics most accurately.

2. To determine if the rFHA is capable of distinguishing knee kinematics of individuals at higher risk for tibiofemoral OA, such as older or injured knees.

The first objective was achieved through the following SA:

SA 1. Determine the accuracy of the rFHA within the HSBV, and how different smoothing techniques applied to the ATM from the HSBV data may improve the accuracy (Chapter 3).

SA 2. Assess the mean differences and variabilities of the rFHA measures to reference position misalignments, thus establishing how sensitive the measures are to changes in the reference position (Chapter 4).

SA 3. Compare rFHA measure differences between the OMCS and HSBV to characterize potential skin movement artifact errors during movement tasks; and to identify rFHA measures that contain the least errors and therefore can be used with most confidence (Chapter 5).

The second objective was achieved through the final SA:

SA 4. Apply the rFHA to individuals at higher risk of tibiofemoral OA (specifically youths with a history of ACL injury and older, asymptomatic individuals) to characterize the knee kinematics during various movement tasks and compare them to healthy controls. (Chapters 6 and 7).

8.2 Key Findings and Contributions

SA 1. This was the first study to investigate the influence of different smoothing techniques for the ATM on the accuracy of the rFHA when using HSBV. It was speculated that applying the smoothing techniques to the ATM would increase the accuracy of the rFHA directionality and the rotational speed along the rFHA. A B-spline filter modified with an outlier removal process (SPOUT) provided the best performance when rated on rFHA

accuracy (RSD = 0.84-1.32 deg/s), followed by SLERP (RSD = 2.26-2.93 deg/s) and a moving average technique (RSD = 2.34-3.07 deg/s). These study findings inform HSBV data processing approaches as to what smoothing techniques are recommended to provide the most accurate knee kinematics.

SA 2. This was the first study to assess differences in the rFHA measures when presented with reference position misalignments. It was found that misalignments of the reference position had a substantial impact on the rFHA measures. Mean absolute differences of the translational and angular rFHA measures ranged from 1.17-19.53 mm and 0.77-5.45 deg, respectively. The variabilities of these differences were mostly associated with the F/E angle of the knee, with percent contributions ranging from 72.28-98.26%. These differences could potentially be minimized by using a 'correction function' and the use of a device to position the femur and tibia into appropriate and repeatable alignments.

SA 3. The difference in rFHA measures between the conventional OMCS and more accurate HSBV were determined for the first time in this study. It was hypothesized that the differences (HSBV – OMCS) between the two modalities would lie within the reported magnitudes of skin movement artifact errors (up to 4.4 deg and 13.0 mm). The rFHA location, path length, and excursion exceeded the expected errors due to skin movement artifacts (ranging from 18.67-101.84 mm), refuting the study hypothesis. The reason for this finding was speculated to originate from the measures being dependent on the rotations and translations of knee, thus being exposed to a compounded influence of both rotational and translational errors due to skin movement artifacts. The rFHA translation, orientation, and dispersion differences fell within the range of the expected errors (translation: 8.21-11.87 mm, orientation: 6.74 deg; dispersion: 1.49-4.13 deg), supporting

the study hypothesis. Consequently, the rFHA translation, orientation, and dispersion are recommended more strongly for use within the OMCS as they are not susceptible to compounded errors associated with skin movement artifacts.

SA 4. Characterizing knee kinematics with the rFHA measures has been reported previously in only one study investigating potential differences in knee kinematics of healthy and ACLD knees during a single leg squat and seated leg extension [40]. This thesis research applied the rFHA for the first time to characterize knee kinematics of two other populations who are at high risk of tibiofemoral OA: (a) individuals with an ACLR knee and (b) older, asymptomatic individuals. The purpose of these two studies was to identify potential differences in knee kinematics between high-risk tibiofemoral OA participants and healthy control participants. Insights derived from these studies are summarized as follows:

   a. Adolescents who sustained a sport related ACL injury, resulting in ACLR, had their knee kinematics compared to healthy matched controls during a VDJ using an OMCS. It was hypothesized that the rFHA would successfully detect kinematic differences in ACLR knees when compared to the matched controls. No statistically differences were found between the two groups to support the study hypothesis. However, the participants with ACLR tended to have greater magnitudes of rFHA dispersion (0.46 deg) throughout the first support phase of the VDJ, implying increased levels of knee instability. Additionally, lesser magnitudes of helical internal rotation (2.18 deg) at maximum knee flexion were observed for the ACLR group. This difference was not identified using the CA approach. Because smaller internal rotations of the knee have been found to reduce ACL strains, it was speculated that the lesser magnitudes of helical internal rotation

within the ACLR group was adopted as a safety mechanism to reduce ACL strains and prevent reinjury. However, this safety mechanism may result in abnormal contact locations within the knee, resulting in knee forces acting on unadapted cartilage and promoting tibiofemoral OA development. Lastly, the helical angles may provide an alternate approach to the CA for characterizing knee kinematics. The helical angles successfully detected kinematic differences where the CA could not. This may be due to the advantage of the helical angles being immune to crosstalk errors.

b. Using HSBV, the rFHA knee kinematics of younger and older participants with asymptomatic knees were compared during level treadmill walking from 0-25% gait cycle and 0-PF (or at PF). It was hypothesized that the older group would demonstrate greater magnitudes of rFHA path length, excursion, and orientation. No changes in the rFHA orientation were found, thus not supporting the study hypothesis. The rFHA path length was significantly smaller (10.60 mm, $p = 0.00$) in the older group from 0-25% gait cycle and contradicted the study hypothesis. Smaller path lengths suggest a 'stiffer' knee with minimal rotations and/or translations. This 'stiffer' gait may originate from increased muscular co-contractions to increase knee stability. However, increased muscular co-contractions may increase internal forces at the knee and promote tibiofemoral OA development. Additionally, smaller rFHA path lengths in the older group were substantiated with trends of smaller rFHA excursions (3.48-5.62 mm), translating to smaller knee RoM. Smaller knee RoM may result in knee loads acting within smaller surface areas of cartilage, thus exposing the cartilage to more frequent

loading and increasing the risk of cartilage degradation. These patterns are similar to individuals with tibiofemoral OA and may act as a biomechanical marker for tibiofemoral OA development. Longitudinal investigations are required to confirm these speculations.

8.3 Future Directions

8.3.1 Sample Size

Most of the studies in this thesis had a small sample size (n=1-10). The only study that was an exception was the pre-OA youth injury study (Chapter 6) that had a total of 96 participants, which is rare in biomechanical analyses and considered a strength of the study. Additionally, in studies involving the use of the HSBV having a sample size greater than 20-30 participants is uncommon. However, a larger sample size will provide greater statistical power and a stronger ability to generalize the results to the population of interest. There is also minimal literature available to conduct sample size calculations as the rFHA measures are relatively novel. This exploratory research is useful for generating data for power calculations and formulating research hypotheses for future rFHA studies. Finally, most of the participants within this thesis were male. A sample of female participants may provide insight to potential sex differences in knee kinematics for various age ranges, joint health status and across difference movement tasks.

8.3.2 Automation of SPOUT

The SPOUT was the top performing smoothing technique for smoothing kinematic data acquired with the HSBV. However, it is currently a subjective method that requires the user to manually select a smoothing factor to obtain the "ideal" kinematic curve. However, the selection of this smoothing factor can be determined automatically using Generalized Cross-Validation (GCV) [35]. Future studies are required to determine how the GCV would interact with the outlier removal

process and if the accuracy of the kinematics when using the original SPOUT are maintained or improved.

Furthermore, the use of SPOUT provides a series of polynomial functions that relate to the smoothed kinematic curves. Therefore, the derivatives of these functions would be much more accurate than the finite difference approximations. This is advantageous for the IHA, which depends on the accuracy of the calculated derivatives (refer to section 1.2.2.3.1). Therefore, it may be useful to incorporate the use of a GCV integrated SPOUT on HSBV data, allowing the accurate calculation of the IHA. This enables the comparison of the different HA methodologies (IHA, rFHA, and sFHA) and any relationships that may be present. This is especially important due to the fact that the absolute measures of the rFHA are not physically meaningful like the IHA or sFHA. Instead, the rFHA has relative measures with the purpose of comparing accurate kinematic patterns.

8.3.3 Reference Position Repeatability

Reference position misalignments and their influence on the rFHA measures were investigated using a controlled simulation (i.e., an original reference position was rotated to specific positions using rotation matrices; refer to Chapter 4). This approach is advantageous when determining the expected errors in the rFHA measures with specific reference position misalignments. However, the F/E and I/E rotation increments selected may not generalize to participant misalignments within the HSBV or OMCS. Therefore, future studies may consider determining the intra- and inter-session repeatability of the reference position in-vivo. This would provide a range of errors based on in-vivo experimental knee joint positioning that may occur when aligning participants to a reference position. Additionally, these further investigations would inform whether similar changes to the rFHA measures exist when compared to the simulated study.

Furthermore, it is likely that reference position misalignments will remain despite attempts to accurately position participants with visual inspection or alignment devices. However, it was seen that errors associated with reference position alignments are quantifiable with second order polynomials, referred to as a 'correction function'. Future studies focused on the development and implementation of these functions could potentially provide substantial improvements in the accuracy, repeatability, and reproducibility of the rFHA measures

8.3.4 Relating the rFHA to other Components of OA

The promise of the rFHA to quantify knee kinematics has been demonstrated in this research. However, based on the work of Andriacchi et al. (2015) altered knee rotations/translations are only one of several factors that contribute to the development of tibiofemoral OA [67]. The Systems Model of OA developed by Andriacchi suggests that OA development consists of integrated changes in mechanical, biological, and structural components. Therefore, relating the rFHA measures to other mechanical measures such as cartilage contact path and stiffness, muscle activation and co-contraction patterns, and kinetics (e.g., knee moments and joint reaction forces) may provide more detailed descriptions of tibiofemoral OA etiology. Additionally, the incorporation and integration of biological measures (e.g., MRI T2 relaxometry, which can provide information on cartilage health status, specifically free water content [202] and collagen fibril density [203]) and structural measures (e.g., skeletal alignment/structure, bone shape, and cartilage thickness and volume) may provide a composite joint profile to provide additional insights into the intricate pathogenesis of tibiofemoral OA.

8.3.5 Alternative Assessments of the rFHA Measures

The rFHA measures within this thesis were calculated as averaged or summed measures throughout a movement to perform statistical analyses, resulting in single quantity measures for statistical analyses. Similarly, the helical and Cardan angles were analyzed discretely by selecting

a specific time point in the movement of interest (e.g., at maximum knee flexion or at peak vertical ground reaction force). As a result, temporal patterns were only identified through visual inspections of rFHA unit vector or location tracings. The ability to analyze the rFHA measures temporally may provide further insights to the knee kinematic differences associated with tibiofemoral OA. This is possible with the use of statistical parametric mapping, an analysis approach designed for continuous, temporal data [204]. Future studies may consider the use of statistical parametric mapping with temporal rFHA measures, providing supplemental information about where the differences occur.

Additionally, only between-participant comparisons of the rFHA measures were performed. Further studies may include within-participant comparisons (e.g., injured versus contralateral knees or repeated measure studies) to further inform the development of tibiofemoral OA. Specifically, these studies will provide the rFHA measure magnitudes and variabilities that are associated with specific movement tasks and populations, assisting in the determination of clinically important differences in tibiofemoral OA.

8.3.6 Assessment of Different Movement Tasks

There is a need to better understand the main patterns within the rFHA measures that correspond to specific movements. Establishing the consistencies of these patterns in healthy individuals is important for future between-group comparisons based on age, sex, joint health status, or sport involvement/expertise. Assessing the rFHA measures of healthy individuals during different movement tasks would also enable developing a database of baseline kinematics that relate to various movement tasks. This baseline could be used to determine clinically important differences in the rFHA measures and enable the rFHA to be used for diagnostic and joint health monitoring purposes, as well as to assess the effect of joint treatments and intervention strategies. Ultimately,

in combination with CA, these could be developed into biomechanical measures that would identify individuals a high risk of developing early OA or progressing with OA.

8.3.7 Incorporation of the Helical Angles

The helical angles are a different approach to characterize knee kinematics within three rotational planes (F/E, Ab/Ad, and I/E rotation). The advantage of the helical angles is that they are not susceptible to the crosstalk errors present within the conventional CA approach. Additionally, the helical angles provide similar magnitudes and patterns of kinematics to the CA approach making them easy to comprehend. Because helical angles demonstrated a strong ability to characterize knee kinematics within high tibiofemoral OA risk populations, it may be a powerful and supplemental tool to quantify not only knee kinematics, but general joint kinematics.

8.4 Conclusion

The purpose of this thesis was to advance the applicability of the rFHA in characterizing knee kinematics during dynamic movement tasks. For the first time a technical assessment of the rFHA was performed regarding the determination of an optimal smoothing technique, the sensitivity of rFHA measures to reference position alignment, and the influence of skin movement artifacts on rFHA measures. The results of the technical studies indicated that 1) a B-spline filter with outlier removal process (SPOUT) was the best smoothing technique to use on ATM for subsequent rFHA calculations, 2) reference position misalignments have a substantial effect on the rFHA measures, and 3) differences in the rFHA measures exist between the OMCS and HSBV, with some exceeding CA skin movement artifact errors. Lastly, the rFHA was successfully applied for the first time to characterize knee joint kinematics in two high tibiofemoral OA risk populations: knees with ACLR and in older participants. The results of the application studies demonstrated the feasibility and promise of the rFHA measures as a biomechanical marker for tibiofemoral OA

Specifically, the rFHA dispersion, path length, excursion, and helical angles successfully detecting trends or statistical differences in knee kinematics of high-risk tibiofemoral OA populations.

References

[1] T. P. Andriacchi, A. Mündermann, R. L. Smith, E. J. Alexander, C. O. Dyrby, and S. Koo, "A framework for the in vivo pathomechanics of osteoarthritis at the knee," *Ann Biomed Eng*, vol. 32, no. 3, pp. 447–457, 2004.

[2] K. Mills, M. A. Hunt, and R. Ferber, "Biomechanical deviations during level walking associated with knee osteoarthritis: A systematic review and meta-analysis," *Arthritis Care Res.*, vol. 65, no. 10, pp. 1643–1665, 2013, doi: 10.1002/acr.22015.

[3] F. T. Sheehan, "The finite helical axis of the knee joint (a non-invasive in vivo study using fast-PC MRI)," *J. Biomech.*, vol. 40, no. 5, pp. 1038–1047, 2007, doi: 10.1016/j.jbiomech.2006.04.006.

[4] C. W. Spoor, "Explanation, verification and application of helical-axis error propagation formulas," *Hum. Mov. Sci.*, vol. 3, no. 1–2, pp. 95–117, 1984, doi: 10.1016/0167-9457(84)90007-1.

[5] E. L. Bishop, J. C. Küpper, I. R. Fjeld, G. Kuntze, and J. L. Ronsky, "Error reduction in the finite helical axis for knee kinematics," *Comput. Methods Biomech. Biomed. Engin.*, vol. 21, no. 2, pp. 186–193, 2018, doi: 10.1080/10255842.2018.1435780.

[6] E. L. Bishop, G. Kuntze, R. Frayne, C. Frank, and J. Ronsky, "Quantifying differences in passive knee laxity and finite helical axis measures between healthy and anterior cruciate ligament deficient individuals," *Osteoarthr. Cartil.*, vol. 22, pp. S120–S120, 2014.

[7] D. L. Benoit, D. K. Ramsey, M. Lamontagne, L. Xu, P. Wretenberg, and P. Renström, "Effect of skin movement artifact on knee kinematics during gait and cutting motions measured in vivo," *Gait Posture*, vol. 24, no. 2, pp. 152–164, 2006, doi: 10.1016/j.gaitpost.2005.04.012.

[8] G. A. Wood, "Data smoothing and differentiation procedures in biomechanics," *Exerc.*

Sport Sci. Rev., vol. 10, no. 1, pp. 308–362, 1982.

[9] T. P. Andriacchi and A. Mündermann, "The role of ambulatory mechanics in the initiation and progression of knee osteoarthritis," *Curr. Opin. Rheumatol.*, vol. 18, no. 5, pp. 514–518, 2006, doi: 10.1097/01.bor.0000240365.16842.4e.

[10] A. Chin, D. Lloyd, J. Alderson, B. Elliott, and P. Mills, "A marker-based mean finite helical axis model to determine elbow rotation axes and kinematics in vivo," *J. Appl. Biomech.*, vol. 26, no. 3, pp. 305–315, 2010, doi: 10.1123/jab.26.3.305.

[11] B. M. Nigg, V. Fisher, and J. L. Ronsky, "Gait characteristics as a function of age and gender," *Gait Posture*, vol. 2, no. 4, pp. 213–220, 1994, doi: https://doi.org/10.1016/0966-6362(94)90106-6.

[12] L. C. Schmitt and K. S. Rudolph, "Muscle stabilization strategies in people with medial knee osteoarthritis: The effect of instability," *J. Orthop. Res.*, vol. 26, no. 9, pp. 1180–1185, 2008, doi: 10.1002/jor.20619.

[13] F. Prince, H. Corriveau, R. Hebert, and D. Winter, "Gait in the elderly," *Gait Posture*, vol. 5, no. 2, pp. 128–135, 1997, doi: 10.1016/S0966-6362(97)01118-1.

[14] S. Farrokhi, S. Tashman, A. B. Gil, B. A. Klatt, and G. K. Fitzgerald, "Are the kinematics of the knee joint altered during the loading response phase of gait in individuals with concurrent knee osteoarthritis and complaints of joint instability? A dynamic stereo X-ray study," *Clin. Biomech.*, vol. 27, no. 4, pp. 384–389, 2012, doi: 10.1016/j.clinbiomech.2011.10.009.

[15] D. D. Lichti, G. B. Sharma, G. Kuntze, B. Mund, J. E. Beveridge, and J. L. Ronsky, "Rigorous geometric self-calibrating bundle adjustment for a dual fluoroscopic imaging system," *IEEE Trans. Med. Imaging*, vol. 34, no. 2, pp. 589–598, 2015, doi:

10.1109/TMI.2014.2362993.

[16] E. L. Brainerd *et al.*, “X-ray reconstruction of moving morphology (XROMM): precision, accuracy and applications in comparative biomechanics research,” *J. Exp. Zool. Part A Ecol. Genet. Physiol.*, vol. 9999A, no. May 2009, p. n/a-n/a, 2010, doi: 10.1002/jez.589.

[17] G. B. Sharma, G. Kuntze, D. Kukulski, and J. L. Ronsky, “Validating dual fluoroscopy system capabilities for determining in-vivo knee joint soft tissue deformation: A strategy for registration error management,” *J. Biomech.*, vol. 48, no. 10, pp. 2181–2185, 2015, doi: 10.1016/j.jbiomech.2015.04.045.

[18] E. Thorhauer and S. Tashman, “Validation of a method for combining biplanar radiography and magnetic resonance imaging to estimate knee cartilage contact,” *Med. Eng. Phys.*, vol. 37, no. 10, pp. 937–947, 2015, doi: 10.1016/j.medengphy.2015.07.002.

[19] D. L. Miranda, J. B. Schwartz, A. C. Loomis, E. L. Brainerd, B. C. Fleming, and J. J. Crisco, “Static and Dynamic Error of a Biplanar Videoradiography System Using Marker-Based and Markerless Tracking Techniques,” *J. Biomech. Eng.*, vol. 133, no. 12, p. 121002, 2011, doi: 10.1115/1.4005471.

[20] L. Meirovitch, “Motion Relative to Rotating Reference Frames,” in *Methods of Analytical Dynamics*, New York: McGraw-Hill, 1970, pp. 101–113.

[21] J. H. Challis, “A procedure for determining rigid body transformation parameters,” *J. Biomech.*, vol. 28, no. 6, pp. 733–737, 1995.

[22] CW Spoor and FE Veldpaus, “Rigid Body Motion Calculated From Spatial Co-Ordinates of Markers,” *J. Biomech.*, vol. 13, no. 4, pp. 391–393, 1980.

[23] J. Vince, *Quaternions for Computer Graphics*, 2nd ed. London: Springer London, 2021.

[24] E. S. Grood and W. J. Suntay, “A joint coordinate system for the clinical description of

three-dimensional motions: Application to the knee," *J. Biomech. Eng.*, vol. 105, no. 2, pp. 136–144, 1983, doi: 10.1115/1.3138397.

[25] A. Baudet *et al.*, "Cross-talk correction method for knee kinematics in gait analysis using Principal Component Analysis (PCA): A new proposal," *PLoS One*, vol. 9, no. 7, pp. 1–7, 2014, doi: 10.1371/journal.pone.0102098.

[26] A. Lees, G. Barton, and M. Robinson, "The influence of cardan rotation sequence on angular orientation data for the lower limb in the soccer kick," *J. Sports Sci.*, vol. 28, no. 4, pp. 445–450, 2010, doi: 10.1080/02640410903540352.

[27] G. K. Cole, B. M. Nigg, J. L. Ronsky, and M. R. Yeadon, "Application of the joint coordinate system to three-dimensional joint attitude and movement representation: A standardization proposal," *J. Biomech. Eng.*, vol. 115, no. 4, pp. 344–349, 1993, doi: 10.1115/1.2895496.

[28] J. H. Challis, "Quaternions as a solution to determining the angular kinematics of human movement," *BMC Biomed. Eng.*, vol. 2, no. 1, pp. 1–10, 2020, doi: 10.1186/s42490-020-00039-z.

[29] J. Sinclair, P. J. Taylor, C. J. Edmundson, D. Brooks, and S. J. Hobbs, "Influence of the helical and six available Cardan sequences on 3D ankle joint kinematic parameters," *Sport. Biomech.*, vol. 11, no. 3, pp. 430–437, 2012, doi: 10.1080/14763141.2012.656762.

[30] G. Wu *et al.*, "ISB recommendation on definitions of joint coordinate systems of various joints for the reporting of human joint motion - Part I: Ankle, hip, and spine," *J. Biomech.*, vol. 35, no. 4, pp. 543–548, 2002, doi: https://doi.org/10.1016/S0021-9290(01)00222-6.

[31] G. Wu *et al.*, "ISB recommendation on definitions of joint coordinate systems of various joints for the reporting of human joint motion - Part II: Shoulder, elbow, wrist and hand,"

J. Biomech., vol. 38, no. 5, pp. 981–992, 2005, doi: 10.1016/j.jbiomech.2004.05.042.

[32] V. Zatsiorsky, *Kinematics of human motion*. Champaign, IL, 1998.

[33] J. Woltring, "3-D attitude representation of human joints: A standardization proposal," *J. Biomech.*, vol. 27, no. 12, pp. 1399–1414, 1994.

[34] R. M. Ehrig and M. O. Heller, "On intrinsic equivalences of the finite helical axis, the instantaneous helical axis, and the SARA approach. A mathematical perspective," *J. Biomech.*, vol. 84, pp. 4–10, 2019, doi: 10.1016/j.jbiomech.2018.12.034.

[35] H. J. Woltring, A. de Lange, J. M. G. Kauer, and R. Huiskes, "Instantaneous Helical Axis Estimation Via Natural, Cross-Validated Splines," *Biomech. Basic Appl. Res.*, no. 1987, pp. 121–128, 1987, doi: 10.1007/978-94-009-3355-2_11.

[36] R. Chartrand, "Numerical Differentiation of Noisy, Nonsmooth Data," *ISRN Appl. Math.*, vol. 2011, pp. 1–11, 2011, doi: 10.5402/2011/164564.

[37] H. J. Woltring, R. Huiskes, A. de Lange, and F. E. Veldpaus, "Finite centroid and helical axis estimation from noisy landmark measurements in the study of human joint kinematics," *J. Biomech.*, vol. 18, no. 5, pp. 379–389, 1985, doi: 10.1016/0021-9290(85)90293-3.

[38] M. M. Panjabi, V. K. Goel, S. D. Walter, and S. Schick, "Errors in the center and angle of rotation of a joint: an experimental study," *J Biomech Eng*, vol. 104, no. 3, pp. 232–237, 1982, doi: 10.1115/1.3138354.

[39] A. Kettler *et al.*, "Finite helical axes of motion are a useful tool to describe the three-dimensional in vitro kinematics of the intact, injured and stabilised spine," *Eur. Spine J.*, vol. 13, no. 6, pp. 553–559, 2004, doi: 10.1007/s00586-004-0710-8.

[40] E. L. Bishop, "Quantifying temporal changes in knee joint laxity and dynamic knee stability for healthy and acute ACL injured individuals," University of Calgary, 2015.

[41] A. M. Bhosale and J. B. Richardson, “Articular cartilage: Structure, injuries and review of management,” *Br. Med. Bull.*, vol. 87, no. 1, pp. 77–95, 2008, doi: 10.1093/bmb/ldn025.

[42] A. J. Sophia Fox, A. Bedi, and S. A. Rodeo, “The basic science of articular cartilage: Structure, composition, and function,” *Sports Health*, vol. 1, no. 6, pp. 461–468, 2009, doi: 10.1177/1941738109350438.

[43] G. Li *et al.*, “Subchondral bone in osteoarthritis: Insight into risk factors and microstructural changes,” *Arthritis Res. Ther.*, vol. 15, no. 6, 2013, doi: 10.1186/ar4405.

[44] S. R. Goldring, “Role of Bone in Osteoarthritis Pathogenesis,” *Med. Clin. North Am.*, vol. 93, no. 1, pp. 25–35, 2009, doi: 10.1016/j.mcna.2008.09.006.

[45] R. Wong, A. Davis, E. Badley, R. Grewal, and M. Mohammed, “Prevalence of arthritis and rheumatic diseases around the world: A growing burden and implications for health care needs,” *Model. Care Arthritis, Bone Jt. Dis.*, no. April, pp. 1–110, 2010, doi: 10.1016/j.compind.2010.10.004.

[46] T. Neogi and Y. Zhang, “Epidemiology of Osteoarthritis,” *Rheum. Dis. Clin. North Am.*, vol. 39, no. 1, pp. 1–19, 2013, doi: 10.1016/j.rdc.2012.10.004.

[47] R. Bitton, “The Economic Burden of Osteoarthritis,” *Am. J. Manag. Care*, vol. 15, no. 8, pp. S230–S235, 2009, doi: 10.1002/art.1780290311.

[48] B. Sharif *et al.*, “Projecting the direct cost burden of osteoarthritis in Canada using a microsimulation model,” *Osteoarthr. Cartil.*, vol. 23, no. 10, pp. 1654–1663, 2015, doi: 10.1016/j.joca.2015.05.029.

[49] R. Birtwhistle *et al.*, “Prevalence and management of osteoarthritis in primary care: an epidemiologic cohort study from the Canadian Primary Care Sentinel Surveillance Network,” *C. Open*, vol. 3, no. 3, pp. E270–E275, 2015, doi: 10.9778/cmajo.20150018.

[50] M. Cross *et al.*, "The global burden of hip and knee osteoarthritis: Estimates from the Global Burden of Disease 2010 study," *Ann. Rheum. Dis.*, vol. 73, no. 7, pp. 1323–1330, 2014, doi: 10.1136/annrheumdis-2013-204763.

[51] S. Glyn-Jones *et al.*, "Osteoarthritis," *Lancet*, vol. 386, no. 9991, pp. 376–387, 2015, doi: 10.1016/S0140-6736(14)60802-3.

[52] K. S. Rudolph, L. C. Schmitt, and M. D. Lewek, "Age-Related Changes in Strength, Joint Laxity, and Walking Patterns: Are They Related to Knee Osteoarthritis?," *Phys. Ther.*, vol. 87, no. 11, pp. 1422–1432, 2007, doi: 10.2522/ptj.20060137.

[53] M. Lotz and R. F. Loeser, "Effects of aging on articular cartilage homeostasis," *Bone*, vol. 51, no. 2, pp. 241–248, 2012, doi: 10.1016/j.bone.2012.03.023.

[54] R. A. Bank *et al.*, "A simplified measurement of degraded collagen in tissues: Application in healthy, fibrillated and osteoarthritic cartilage," *Matrix Biol.*, vol. 16, no. 5, pp. 233–243, 1997, doi: 10.1016/S0945-053X(97)90012-3.

[55] K. Kimata and H. Y. Y. Watanabe, "Review Roles of Aggrecan , a Large Chondroitin in Cartilage Structure and Function Sulfate," *J. Biol. Chem.*, vol. 124, no. 4, pp. 687–693, 1998.

[56] H. Mitsuyama, R. M. Healey, R. A. Terkeltaub, R. D. Coutts, and D. Amiel, "Calcification of human articular knee cartilage is primarily an effect of aging rather than osteoarthritis," *Osteoarthr. Cartil.*, vol. 15, no. 5, pp. 559–565, 2007, doi: 10.1016/j.joca.2006.10.017.

[57] S. Hashimoto *et al.*, "Chondrocyte-derived apoptotic bodies and calcification of articular cartilage.," *Proc. Natl. Acad. Sci. U. S. A.*, vol. 95, no. 6, pp. 3094–3099, 1998, doi: 10.1073/pnas.95.6.3094.

[58] M. B. Schaffler, K. Choi, and C. Milgrom, "Aging and matrix microdamage accumulation

in human compact bone," *Bone*, vol. 17, no. 6, pp. 521–525, 1995, doi: 10.1016/8756-3282(95)00370-3.

[59] D. B. Burr and E. L. Radin, "Microfractures and microcracks in subchondral bone: Are they relevant to osteoarthrosis?," *Rheum. Dis. Clin. North Am.*, vol. 29, no. 4, pp. 675–685, 2003, doi: 10.1016/S0889-857X(03)00061-9.

[60] C. Buckland-Wright, "Subchondral bone changes in hand and knee osteoarthritis detected by radiography," *Osteoarthr. Cartil.*, vol. 12, no. SUPLL., pp. 10–19, 2004, doi: 10.1016/j.joca.2003.09.007.

[61] R. Strocchi, V. De Pasquale, A. Facchini, M. Raspanti, S. Zaffagnini, and M. Marcacci, "Age-related changes in human anterior cruciate ligament (ACL) collagen fibrils," *Ital. J. Anat. Embryol.*, vol. 101, no. 4, pp. 213–220, 1996.

[62] A. Hasegawa *et al.*, "Anterior cruciate ligament changes in the human knee joint in aging and osteoarthritis," *Arthritis Rheum.*, vol. 64, no. 3, pp. 696–704, 2012, doi: 10.1002/art.33417.

[63] S. R. Goldring and M. B. Goldring, "Changes in the osteochondral unit during osteoarthritis: Structure, function and cartilage bone crosstalk," *Nat. Rev. Rheumatol.*, vol. 12, no. 11, pp. 632–644, 2016, doi: 10.1038/nrrheum.2016.148.

[64] T. P. Andriacchi, S. Koo, and S. F. Scanlan, "Gait mechanics influence healthy cartilage morphology and osteoarthritis of the knee," *J. Bone Jt. Surg. - Ser. A*, vol. 91, no. SUPPL. 1, pp. 95–101, 2009, doi: 10.2106/JBJS.H.01408.

[65] J. B. Morrison, "The mechanics of the knee joint in relation to normal walking," *J. Biomech.*, vol. 3, no. 1, pp. 51–61, 1970, doi: 10.1016/0021-9290(70)90050-3.

[66] S. Koo, J. H. Rylander, and T. P. Andriacchi, "Knee joint kinematics during walking

influences the spatial cartilage thickness distribution in the knee," *J. Biomech.*, vol. 44, no. 7, pp. 1405–1409, 2011, doi: 10.1016/j.jbiomech.2010.11.020.

[67] T. P. Andriacchi, J. Favre, J. C. Erhart-Hledik, and C. R. Chu, "A Systems View of Risk Factors for Knee Osteoarthritis Reveals Insights into the Pathogenesis of the Disease," *Ann. Biomed. Eng.*, vol. 43, no. 2, pp. 376–387, 2015, doi: 10.1007/s10439-014-1117-2.

[68] Y. Hoshino and S. Tashman, "Internal tibial rotation during in vivo, dynamic activity induces greater sliding of tibio-femoral joint contact on the medial compartment," *Knee Surgery, Sport. Traumatol. Arthrosc.*, vol. 20, no. 7, pp. 1268–1275, 2012, doi: 10.1007/s00167-011-1731-6.

[69] T. P. Andriacchi, P. L. Briant, S. L. Bevill, and S. Koo, "Rotational changes at the knee after ACL injury cause cartilage thinning," *Clin. Orthop. Relat. Res.*, no. 442, pp. 39–44, 2006, doi: 10.1097/01.blo.0000197079.26600.09.

[70] A. Mündermann, C. O. Dyrby, and T. P. Andriacchi, "Secondary gait changes in patients with medial compartment knee osteoarthritis: Increased load at the ankle, knee, and hip during walking," *Arthritis Rheum.*, vol. 52, no. 9, pp. 2835–2844, 2005, doi: 10.1002/art.21262.

[71] D. E. Hurwitz, A. R. Ryals, J. A. Block, L. Sharma, T. J. Schnitzer, and T. P. Andriacchi, "Knee pain and joint loading in subjects with osteoarthritis of the knee," *J. Orthop. Res.*, vol. 24, no. 1, pp. 15–26, 2010, doi: 10.1016/j.berh.2009.08.006.

[72] B. D. Jackson, A. E. Wluka, A. J. Teichtahl, M. E. Morris, and F. M. Cicuttini, "Reviewing knee osteoarthritis - A biomechanical perspective," *J. Sci. Med. Sport*, vol. 7, no. 3, pp. 347–357, 2004, doi: 10.1016/S1440-2440(04)80030-6.

[73] Y. I. C. C. Pai, W. Z. Rymer, R. W. Chang, and L. Sharma, "Effect of age and osteoarthritis

on knee proprioception," *Arthritis Rheum.*, vol. 40, no. 12, pp. 2260–2265, 1997, doi: 10.1002/art.1780401223.

[74] D. A. Dennis, M. R. Mahfouz, R. D. Komistek, and W. Hoff, "In vivo determination of normal and anterior cruciate ligament-deficient knee kinematics," *J. Biomech.*, vol. 38, no. 2, pp. 241–253, 2005, doi: 10.1016/j.jbiomech.2004.02.042.

[75] L. Blankevoort, R. Huiskes, and A. de Lange, "Helical axes of passive knee joint motions," *J. Biomech.*, vol. 23, no. 12, pp. 1219–1229, 1990, doi: 10.1016/0021-9290(90)90379-H.

[76] F. Temporiti *et al.*, "Dispersion of knee helical axes during walking in young and elderly healthy subjects," *J. Biomech.*, vol. 109, p. 109944, 2020, doi: 10.1016/j.jbiomech.2020.109944.

[77] H. Grip, E. Tengman, and C. K. Häger, "Dynamic knee stability estimated by finite helical axis methods during functional performance approximately twenty years after anterior cruciate ligament injury," *J. Biomech.*, vol. 48, no. 10, pp. 1906–1914, 2015, doi: 10.1016/j.jbiomech.2015.04.016.

[78] J. L. Markström, H. Grip, L. Schelin, and C. K. Häger, "Individuals With an Anterior Cruciate Ligament–Reconstructed Knee Display Atypical Whole Body Movement Strategies but Normal Knee Robustness During Side-Hop Landings: A Finite Helical Axis Analysis," *Am. J. Sports Med.*, vol. 48, no. 5, pp. 1117–1126, 2020, doi: 10.1177/0363546520910428.

[79] I. M. Lee and D. M. Buchner, "The importance of walking to public health," *Med. Sci. Sports Exerc.*, vol. 40, no. 7 SUPPL.1, pp. 512–518, 2008, doi: 10.1249/MSS.0b013e31817c65d0.

[80] L. D. Duffell, S. J. Jordan, J. P. Cobb, and A. H. McGregor, "Gait adaptations with aging

in healthy participants and people with knee-joint osteoarthritis," *Gait Posture*, vol. 57, no. December 2015, pp. 246–251, 2017, doi: 10.1016/j.gaitpost.2017.06.015.

[81] N. M. Fisher, S. C. White, H. J. Yack, R. J. Smolinski, and D. R. Pendergast, "Muscle function and gait in patients with knee osteoarthritis before and after muscle rehabilitation," *Disabil. Rehabil.*, vol. 19, no. 2, pp. 47–55, 1997, doi: 10.3109/09638289709166827.

[82] J. D. Childs, P. J. Sparto, G. K. Fitzgerald, M. Bizzini, and J. J. Irrgang, "Alterations in lower extremity movement and muscle activation patterns in individuals with knee osteoarthritis," *Clin. Biomech.*, vol. 19, no. 1, pp. 44–49, 2004, doi: 10.1016/j.clinbiomech.2003.08.007.

[83] I. A. C. Baert, I. Jonkers, F. Staes, F. P. Luyten, S. Truijen, and S. M. P. Verschueren, "Gait characteristics and lower limb muscle strength in women with early and established knee osteoarthritis," *Clin. Biomech.*, vol. 28, no. 1, pp. 40–47, 2013, doi: 10.1016/j.clinbiomech.2012.10.007.

[84] D. Bytyqi, B. Shabani, S. Lustig, L. Cheze, N. Karahoda Gjurgjeala, and P. Neyret, "Gait knee kinematic alterations in medial osteoarthritis: Three dimensional assessment," *Int. Orthop.*, vol. 38, no. 6, pp. 1191–1198, 2014, doi: 10.1007/s00264-014-2312-3.

[85] J. L. Astephen, K. J. Deluzio, G. E. Caldwell, M. J. Dunbar, and C. L. Hubley-Kozey, "Gait and neuromuscular pattern changes are associated with differences in knee osteoarthritis severity levels," *J. Biomech.*, vol. 41, no. 4, pp. 868–876, 2008, doi: 10.1016/j.jbiomech.2007.10.016.

[86] T. L. Heiden, D. G. Lloyd, and T. R. Ackland, "Knee joint kinematics, kinetics and muscle co-contraction in knee osteoarthritis patient gait," *Clin. Biomech.*, vol. 24, no. 10, pp. 833–841, 2009, doi: 10.1016/j.clinbiomech.2009.08.005.

[87] Y. Nagano *et al.*, "Association between in vivo knee kinematics during gait and the severity of knee osteoarthritis," *Knee*, vol. 19, no. 5, pp. 628–632, 2012, doi: 10.1016/j.knee.2011.11.002.

[88] L. C. Schmitt and K. S. Rudolph, "Influences on knee movement strategies during walking in persons with medial knee osteoarthritis," *Arthritis Care Res.*, vol. 57, no. 6, pp. 1018–1026, 2007, doi: 10.1002/art.22889.

[89] J. Favre, J. C. Erhart-Hledik, and T. P. Andriacchi, "Age-related differences in sagittal-plane knee function at heel-strike of walking are increased in osteoarthritic patients," *Osteoarthr. Cartil.*, vol. 22, no. 3, pp. 464–471, 2014, doi: 10.1016/j.joca.2013.12.014.

[90] J. Favre, J. C. Erhart-Hledik, E. F. Chehab, and T. P. Andriacchi, "Baseline ambulatory knee kinematics are associated with changes in cartilage thickness in osteoarthritic patients over 5 years," *J. Biomech.*, vol. 49, no. 9, pp. 1859–1864, 2016, doi: 10.1016/j.jbiomech.2016.04.029.

[91] J. Weidow, R. Tranberg, T. Saari, and J. Karrholm, "Hip and knee joint rotations differ between patients with medial and lateral knee osteoartrhtitis: Gait analysis of 30 patients and 15 controls," *J. Orthop. Res.*, vol. 65, no. 12, pp. 354–359, 2016, doi: 10.1002/jor.

[92] G. M. Brouwer *et al.*, "Association between valgus and varus alignment and the development and progression of radiographic osteoarthritis of the knee," *Arthritis Rheum.*, vol. 56, no. 4, pp. 1204–1211, 2007, doi: 10.1002/art.22515.

[93] W. G. Hopkins, S. W. Marshall, A. M. Batterham, and J. Hanin, "Progressive statistics for studies in sports medicine and exercise science," *Med. Sci. Sports Exerc.*, vol. 41, no. 1, pp. 3–12, 2009, doi: 10.1249/MSS.0b013e31818cb278.

[94] K. A. Boyer, R. T. Johnson, J. J. Banks, C. Jewell, and J. F. Hafer, "Systematic review and

meta-analysis of gait mechanics in young and older adults," *Exp. Gerontol.*, vol. 95, pp. 63–70, 2017, doi: 10.1016/j.exger.2017.05.005.

[95] D. L. Benoit, D. K. Ramsey, M. Lamontagne, L. Xu, P. Wretenberg, and P. Renström, "In vivo knee kinematics during gait reveals new rotation profiles and smaller translations," *Clin. Orthop. Relat. Res.*, no. 454, pp. 81–88, 2007, doi: 10.1097/BLO.0b013e31802dc4d0.

[96] S. J. Piazza and P. R. Cavanagh, "Measurement of the screw-home motion of the knee is sensitive to errors in axis alignment," *J. Biomech.*, vol. 33, no. 8, pp. 1029–1034, 2000, doi: 10.1016/S0021-9290(00)00056-7.

[97] S. R. Augustsson, R. Tranberg, R. Zügner, and J. Augustsson, "Vertical drop jump landing depth influences knee kinematics in female recreational athletes," *Phys. Ther. Sport*, vol. 33, pp. 133–138, 2018, doi: 10.1016/j.ptsp.2018.08.002.

[98] M. J. Decker, M. R. Torry, T. J. Noonan, A. Riviere, and W. I. Sterett, "Landing adaptations after ACL reconstruction," *Med. Sci. Sports Exerc.*, vol. 34, no. 9, pp. 1408–1413, 2002, doi: 10.1097/00005768-200209000-00002.

[99] E. Delahunt *et al.*, "Lower limb kinematic alterations during drop vertical jumps in female athletes who have undergone anterior cruciate ligament reconstruction," *J. Orthop. Res.*, vol. 30, no. 1, pp. 72–78, 2012, doi: 10.1002/jor.21504.

[100] S. B. Clarke, I. C. Kenny, and A. J. Harrison, "Dynamic knee joint mechanics after anterior cruciate ligament reconstruction," *Med. Sci. Sports Exerc.*, vol. 47, no. 1, pp. 120–127, 2015, doi: 10.1249/MSS.0000000000000389.

[101] H. J. Woltring, "Representation and calculation of 3-D joint movement," *Hum. Mov. Sci.*, vol. 10, no. 5, pp. 603–616, 1991, doi: 10.1016/0167-9457(91)90048-3.

[102] A. J. van den Bogert, C. Reinschmidt, and A. Lundberg, "Helical axes of skeletal knee joint

motion during running," *J. Biomech.*, vol. 41, no. 8, pp. 1632–1638, 2008, doi: 10.1016/j.jbiomech.2008.03.018.

[103] C. Cescon, A. Tettamanti, M. Barbero, and R. Gatti, "Finite helical axis for the analysis of joint kinematics: comparison of an electromagnetic and an optical motion capture system," *Arch. Physiother.*, vol. 5, no. 1, p. 8, 2015, doi: 10.1186/s40945-015-0008-7.

[104] T. Gale and W. Anderst, "Tibiofemoral helical axis of motion during the full gait cycle measured using biplane radiography," *Med. Eng. Phys.*, vol. 86, pp. 65–70, 2020, doi: 10.1016/j.medengphy.2020.10.014.

[105] J. L. Markström, L. Schelin, and C. K. Häger, "A novel standardised side hop test reliably evaluates landing mechanics for anterior cruciate ligament reconstructed persons and controls," *Sport. Biomech.*, vol. 20, no. 2, pp. 213–229, 2021, doi: 10.1080/14763141.2018.1538385.

[106] M. Hofbauer, E. D. Thorhauer, E. Abebe, M. Bey, and S. Tashman, "Altered tibiofemoral kinematics in the affected knee and compensatory changes in the contralateral knee after anterior cruciate ligament reconstruction," *Am. J. Sports Med.*, vol. 42, no. 11, pp. 2715–2721, 2014, doi: 10.1177/0363546514549444.

[107] H. Jonsson and J. Karrholm, "Three-dimensional knee joint movements during a step-up: Evaluation after anterior cruciate ligament rupture," *J. Orthop. Res.*, vol. 12, no. 6, pp. 769–779, 1994, doi: 10.1002/jor.1100120604.

[108] T. F. Besier, D. L. Sturnieks, J. A. Alderson, and D. G. Lloyd, "Repeatability of gait data using a functional hip joint centre and a mean helical knee axis," *J. Biomech.*, vol. 36, no. 8, pp. 1159–1168, 2003, doi: 10.1016/S0021-9290(03)00087-3.

[109] N. M. Lenz, "The Effects of Femoral Fixed Body Coordinate System Definition on Knee

Kinematic Description," *J. Biomech. Eng.*, vol. 130, no. 2, p. 021014, 2008, doi: 10.1115/1.2898713.

[110] J. Yao and R. Taylor, "Assessing accuracy factors in deformable 2D/3D medical image registration using a statistical pelvis model," *Proc. IEEE Int. Conf. Comput. Vis.*, vol. 2, pp. 1329–1334, 2003, doi: 10.1109/iccv.2003.1238644.

[111] L. Zöllei, E. Grimson, A. Norbash, and W. Wells, "2D-3D rigid registration of X-ray fluoroscopy and CT images using mutual information and sparsely sampled histogram estimators," *Proc. IEEE Comput. Soc. Conf. Comput. Vis. Pattern Recognit.*, vol. 2, pp. 696–703, 2001, doi: 10.1109/cvpr.2001.991032.

[112] B. Postolka *et al.*, "Tibio-femoral kinematics of the healthy knee joint throughout complete cycles of gait activities," *J. Biomech.*, vol. 110, p. 109915, 2020, doi: 10.1016/j.jbiomech.2020.109915.

[113] B. Postolka, R. List, B. Thelen, P. Schütz, W. R. Taylor, and G. Zheng, "Evaluation of an intensity-based algorithm for 2D/3D registration of natural knee videofluoroscopy data," *Med. Eng. Phys.*, vol. 77, pp. 107–113, 2020, doi: 10.1016/j.medengphy.2020.01.002.

[114] M. P. Wachowiak, G. S. Rash, P. M. Quesada, and A. H. Desoky, "Wavelet-based noise removal for biomechanical signals: A comparative study," *IEEE Trans. Biomed. Eng.*, vol. 47, no. 3, pp. 360–368, 2000, doi: 10.1109/10.827298.

[115] C. C. Hsieh, "B-spline wavelet-based motion smoothing," *Comput. Ind. Eng.*, vol. 41, no. 1, pp. 59–76, 2001, doi: 10.1016/S0360-8352(01)00042-0.

[116] C. C. Hsieh *et al.*, "Noise smoothing for VR equipment in quaternions," *IIE Trans. (Institute Ind. Eng.*, vol. 30, no. 7, pp. 581–587, 1998, doi: 10.1080/07408179808966503.

[117] J. Lee and S. Y. Shin, "General construction of time-domain filters for orientation data,"

IEEE Trans. Vis. Comput. Graph., vol. 8, no. 2, pp. 119–128, 2002, doi: 10.1109/2945.998665.

[118] K. Shoemake, "Animating Rotation with Quaternion Curves," *SIGGRAPH '85 Proc. 12th Annu. Conf. Comput. Graph. Interact. Tech.*, vol. 19, no. 3, pp. 245–254, 1985, doi: 10.1109/3DV.2015.43.

[119] MathWorks, "Lowpass Filter Orientation Using Quaternion SLERP," 2020. [Online]. Available: https://www.mathworks.com/help/fusion/ug/lowpass-filter-orientation-using-quaternion-slerp.html;jsessionid=eae9261d416b07cd04f40ae5c1f5.

[120] M. Neubauer and A. Muller, "Smooth orientation path planning with quaternions using B-splines," *IEEE Int. Conf. Intell. Robot. Syst.*, vol. 2015-Decem, no. 1, pp. 2087–2092, 2015, doi: 10.1109/IROS.2015.7353654.

[121] H. J. Motulsky and R. E. Brown, "Detecting outliers when fitting data with nonlinear regression - A new method based on robust nonlinear regression and the false discovery rate," *BMC Bioinformatics*, vol. 7, pp. 1–20, 2006, doi: 10.1186/1471-2105-7-123.

[122] D. A. Winter, H. G. Sidwall, and D. A. Hobson, "Measurement and reduction of noise in kinematics of locomotion," *J. Biomech.*, vol. 7, no. 2, pp. 157–159, 1974, doi: 10.1016/0021-9290(74)90056-6.

[123] A. R. Ismail and S. S. Asfour, "Discrete wavelet transform: A tool in smoothing kinematic data," *J. Biomech.*, vol. 32, no. 3, pp. 317–321, 1999, doi: 10.1016/S0021-9290(98)00171-7.

[124] P. Dierckx, "An algorithm for smoothing, differentiation and integration of experimental data using spline functions," *J. Comput. Appl. Math.*, vol. 1, no. 3, pp. 165–184, 1975, doi: 10.1016/0771-050X(75)90034-0.

[125] A. De Lange, R. Huiskes, and J. M. G. Kauer, “Effects of data smoothing on the reconstruction of helical axis parameters in human joint kinematics,” *J. Biomech. Eng.*, vol. 112, no. 2, pp. 107–113, 1990, doi: 10.1115/1.2891160.

[126] L. Blankevoort, R. Huiskes, and A. de Lange, “The envelope of passive knee joint motion,” *J. Biomech.*, vol. 21, no. 9, pp. 705–720, 1988, doi: 10.1016/0021-9290(88)90280-1.

[127] P. Craven and G. Wahba, “Smoothing noisy data with spline functions - Estimating the correct degree of smoothing by the method of generalized cross-validation,” *Numer. Math.*, vol. 31, no. 4, pp. 377–403, 1978, doi: 10.1007/BF01404567.

[128] G. Giakas and V. Baltzopoulos, “A comparison of automatic filtering techniques applied to biomechanical walking data,” *J. Biomech.*, vol. 30, no. 8, pp. 847–850, 1997, doi: 10.1016/S0021-9290(97)00042-0.

[129] L. A. Figueroa, “Quantifying in vivo cervical spine kinematics: Validation of a novel data collection and processing pipeline,” 2020.

[130] S. Zhang, “Personal communication.” 2021.

[131] G. Kuntze, G. B. Sharma, D. Kukulski, J. Shank, and J. L. Ronsky, “Inter-rater accuracy and precision of markerless quantification of 3D tibiofemoral displacement using dual fluoroscopy,” in *Osteoarthritis and Cartilage*, 2014, vol. 22, no. 2014, p. S106, doi: 10.1016/j.joca.2014.02.199.

[132] N. Menvielle, Y. Goussard, D. Orban, and G. Soulez, “Reduction of beam-hardening artifacts in X-ray CT,” in *2005 IEEE Engineering in Medicine and Biology 27th Annual Conference*, 2005, pp. 1865–1868, doi: 10.1109/IEMBS.2005.1616814.

[133] R. A. Brooks and G. Di Chiro, “Beam hardening in X-ray reconstructive tomography,” *Phys. Med. Biol.*, vol. 21, no. 3, pp. 390–398, 1976, doi: 10.1088/0031-9155/21/3/004.

[134] M. A. Lafortune, P. R. Cavanagh, H. J. Sommer, and A. Kalenak, “Three-dimensional kinematics of the human knee during walking,” *J. Biomech.*, vol. 25, no. 4, pp. 347–357, 1992, doi: 10.1016/j.ceramint.2013.02.059.

[135] A. Kharb, V. Saini, Y. Jain, and S. Dhiman, “A review of gait cycle and its parameters,” *IJCEM Int J Comput Eng Manag*, vol. 13, no. July, pp. 78–83, 2011.

[136] E. Szczerbik and M. Kalinowska, “The influence of knee marker placement error on evaluation of gait kinematic parameters,” *Acta Bioeng. Biomech.*, vol. 13, no. 3, pp. 43–46, 2011.

[137] H. K. Ramakrishnan and M. P. Kadaba, “On the estimation of joint kinematics during gait,” *J. Biomech.*, vol. 24, no. 10, pp. 969–977, 1991, doi: 10.1016/0021-9290(91)90175-M.

[138] D. L. Miranda, M. J. Rainbow, E. L. Leventhal, J. J. Crisco, and B. C. Fleming, “Automatic determination of anatomical coordinate systems for three- dimensional bone models of the isolated human knee,” *J. Biomchanics*, vol. 43, no. 8, pp. 1623–1626, 2010, doi: 10.1016/j.jbiomech.2010.01.036.

[139] H. A. Gray, S. Guan, L. T. Thomeer, A. G. Schache, R. de Steiger, and M. G. Pandy, “Three-dimensional motion of the knee-joint complex during normal walking revealed by mobile biplane x-ray imaging,” *J. Orthop. Res.*, vol. 37, no. 3, pp. 615–630, 2019, doi: 10.1002/jor.24226.

[140] A. McPherson, J. Kärrholm, V. Pinskerova, A. Sosna, and S. Martelli, “Imaging knee position using MRI, RSA/CT and 3D digitisation,” *J. Biomech.*, vol. 38, no. 2, pp. 263–268, 2005, doi: 10.1016/j.jbiomech.2004.02.007.

[141] B. Gilles, R. Perrin, N. Magnenat-Thalmann, and J. P. Vallee, “Bone motion analysis from dynamic MRI: Acquisition and tracking,” *Acad. Radiol.*, vol. 12, no. 10, pp. 1285–1292,

2005, doi: 10.1016/j.acra.2005.08.006.

[142] N. Ying and W. Kim, “Use of dual Euler angles to quantify the three-dimensional joint motion and its application to the ankle joint complex,” *J. Biomech.*, vol. 35, no. 12, pp. 1647–1657, 2002, doi: 10.1016/S0021-9290(02)00241-5.

[143] P. A. G. Teixeira *et al.*, “Quantitative analysis of subtalar joint motion with 4D CT: Proof of concept with cadaveric and healthy subject evaluation,” *Am. J. Roentgenol.*, vol. 208, no. 1, pp. 150–158, 2017, doi: 10.2214/AJR.16.16434.

[144] L. Lucchetti, A. Cappozzo, A. Cappello, and U. Della Croce, “Skin movement artefact assessment and compensation in the estimation of knee-joint kinematics,” *J. Biomech.*, vol. 31, no. 11, pp. 977–984, 1998, doi: 10.1016/S0021-9290(98)00083-9.

[145] A. Cappozzo, F. Catani, A. Leardini, M. G. Benedetti, and U. Della Croce, “Position and orientation in space of bones during movement: Experimental artefacts,” *Clin. Biomech.*, vol. 11, no. 2, pp. 90–100, 1996, doi: 10.1016/0268-0033(95)00046-1.

[146] D. L. Miranda, M. J. Rainbow, J. J. Crisco, and B. C. Fleming, “Kinematic differences between optical motion capture and biplanar videoradiography during a jump-cut maneuver,” *J. Biomech.*, vol. 46, no. 3, pp. 567–573, 2013, doi: 10.1016/j.jbiomech.2012.09.023.

[147] C. A. Emery, W. H. Meeuwisse, and J. R. Mcallister, “Survey of Sport Participation and Sport Injury in Calgary and Area High Schools,” *Clin. J. Sport. Med.*, vol. 16, no. 1, pp. 20–26, 2006.

[148] Q. A. Louw, J. Manilall, and K. A. Grimmer, “Epidemiology of knee injuries among adolescents : a systematic review,” *Br. J. Sports Med.*, vol. 42, pp. 2–10, 2008, doi: 10.1136/bjsm.2007.035360.

[149] M. Englund, “The role of biomechanics in the initiation and progression of OA of the knee,” *Best Pract. Res. Clin. Rheumatol.*, vol. 24, no. 1, pp. 39–46, 2010, doi: 10.1016/j.berh.2009.08.008.

[150] F. Guilak, “Biomechanical factors in osteoarthritis,” *Best Pract. Res. Clin. Rheumatol.*, vol. 25, no. 6, pp. 815–823, 2011, doi: 10.1016/j.berh.2011.11.013.

[151] S. A. Richmond, R. K. Fukuchi, A. Ezzat, K. Schneider, G. Schneider, and C. A. Emery, “Are Joint Injury, Sport Activity, Physical Activity, Obesity, or Occupational Activities Predictors for Osteoarthritis? A Systematic Review,” *J. Orthop. Sport. Phys. Ther.*, vol. 43, no. 8, pp. 515-B19, 2013, doi: 10.2519/jospt.2013.4796.

[152] B. Snoeker *et al.*, “Risk of knee osteoarthritis after different types of knee injuries in young adults: A population-based cohort study,” *Br. J. Sports Med.*, vol. 54, no. 12, pp. 725–730, 2020, doi: 10.1136/bjsports-2019-100959.

[153] E. Poulsen, G. H. Goncalves, A. Bricca, E. M. Roos, J. B. Thorlund, and C. B. Juhl, “Knee osteoarthritis risk is increased 4-6 fold after knee injury-a systematic review and meta-analysis,” *Br. J. Sports Med.*, vol. 53, no. 23, pp. 1454–1463, 2019, doi: 10.1136/bjsports-2018-100022.

[154] H. F. Hart *et al.*, “Knee kinematics and joint moments during gait following anterior cruciate ligament reconstruction: A systematic review and meta-analysis,” *Br. J. Sports Med.*, vol. 50, no. 10, pp. 597–612, 2016, doi: 10.1136/bjsports-2015-094797.

[155] B. Akpinar, E. Thorhauer, J. J. Irrgang, S. Tashman, F. H. Fu, and W. J. Anderst, “Alteration of Knee Kinematics After Anatomic Anterior Cruciate Ligament Reconstruction Is Dependent on Associated Meniscal Injury,” *Am. J. Sports Med.*, vol. 46, no. 5, pp. 1158–1165, 2018, doi: 10.1177/0363546517753386.

[156] J. L. Whittaker *et al.*, “Health-related Outcomes after a Youth Sport-related Knee Injury,” *Med. Sci. Sports Exerc.*, vol. 51, no. 2, pp. 255–263, 2019, doi: 10.1249/MSS.0000000000001787.

[157] J. L. Whittaker, L. J. Woodhouse, A. Nettel-Aguirre, and C. A. Emery, “Outcomes associated with early post-traumatic osteoarthritis and other negative health consequences 3-10 years following knee joint injury in youth sport,” *Osteoarthr. Cartil.*, vol. 23, no. 7, pp. 1122–1129, 2015, doi: 10.1016/j.joca.2015.02.021.

[158] B. B. Rosner, “A Generalization of the Paired t-Test,” *J. R. Stat. Soc. Ser. C (Applied Stat.*, vol. 31, no. 1, pp. 9–13, 1982, doi: https://doi.org/10.2307/2347069.

[159] Y. Benjamini and Y. Hochberg, “Controlling the False Discovery Rate : A Practical and Powerful Approach to Multiple Testing,” *J. R. Stat. Soc. Ser. B*, vol. 57, no. 1, pp. 289–300, 1995.

[160] J. Cohen, *Statistical Power Analysis for the Behavioral Sciences*, 2nd ed. New York, 1988.

[161] R. Ferber, L. R. Osternig, M. H. Woollacott, N. J. Wasielewski, and J. H. Lee, “Gait mechanics in chronic ACL deficiency and subsequent repair,” *Clin. Biomech.*, vol. 17, no. 4, pp. 274–285, 2002, doi: 10.1016/S0268-0033(02)00016-5.

[162] A. Smeets, S. Verschueren, F. Staes, H. Vandenneucker, S. Claes, and J. Vanrenterghem, “Athletes with an ACL reconstruction show a different neuromuscular response to environmental challenges compared to uninjured athletes,” *Gait Posture*, vol. 83, no. October 2020, pp. 44–51, 2021, doi: 10.1016/j.gaitpost.2020.09.032.

[163] W. I. Drechsler, M. C. Cramp, and O. M. Scott, “Changes in muscle strength and EMG median frequency after anterior cruciate ligament reconstruction,” *Eur. J. Appl. Physiol.*, vol. 98, no. 6, pp. 613–623, 2006, doi: 10.1007/s00421-006-0311-9.

[164] R. M. Palmieri-Smith, A. C. Thomas, and E. M. Wojtys, “Maximizing Quadriceps Strength After ACL Reconstruction,” *Clin. Sports Med.*, vol. 27, no. 3, pp. 405–424, 2008, doi: 10.1016/j.csm.2008.02.001.

[165] E. G. Meyer and R. C. Haut, “Anterior cruciate ligament injury induced by internal tibial torsion or tibiofemoral compression,” *J. Biomech.*, vol. 41, no. 16, pp. 3377–3383, 2008, doi: 10.1016/j.jbiomech.2008.09.023.

[166] B. P. Boden, F. T. Sheehan, J. S. Torg, and T. E. Hewett, “Non-contact ACL Injuries: Mechanisms and Risk Factors,” *Am. Acad. Orthop. Surg.*, vol. 18, no. 9, pp. 520–527, 2010.

[167] S. Tashman, D. Collon, K. Anderson, P. Kolowich, and W. Anderst, “Abnormal rotational knee motion during running after anterior cruciate ligament reconstruction,” *Am. J. Sports Med.*, vol. 32, no. 4, pp. 975–983, 2004, doi: 10.1177/0363546503261709.

[168] A. Kroker, J. L. Bhatla, C. A. Emery, S. L. Manske, and S. K. Boyd, “Subchondral bone microarchitecture in ACL reconstructed knees of young women: A comparison with contralateral and uninjured control knees,” *Bone*, vol. 111, pp. 1–8, 2018, doi: 10.1016/j.bone.2018.03.006.

[169] G. Kuntze *et al.*, “Vertical drop jump biomechanics of participants with a 3-10 year history of youth sport-related anterior cruciate ligament reconstruction (under review),” *Orthop. J. Sport. Med.*, pp. 1–33, 2021.

[170] A. C. Looker, N. Sarafrazi Isfahani, B. Fan, and J. A. Shepherd, “Trends in osteoporosis and low bone mass in older US adults, 2005–2006 through 2013–2014,” *Osteoporos. Int.*, vol. 28, no. 6, pp. 1979–1988, 2017, doi: 10.1007/s00198-017-3996-1.

[171] A. E. M. Jørgensen, M. Kjær, and K. M. Heinemeier, “The effect of aging and mechanical loading on the metabolism of articular cartilage,” *J. Rheumatol.*, vol. 44, no. 4, pp. 410–

417, 2017, doi: 10.3899/jrheum.160226.

[172] B. C. Clark, "Neuromuscular Changes with Aging and Sarcopenia," *J. frailty aging*, vol. 8, no. 1, pp. 7–9, 2019, doi: 10.14283/jfa.2018.35.

[173] H. Yamada *et al.*, "Effects of aging on EMG variables during fatiguing isometric contractions," *J. Hum. Ergol. (Tokyo).*, vol. 29, no. 1, pp. 7–14, 2000, doi: https://doi.org/10.11183/jhe1972.29.7.

[174] J. Lexell, C. C. Taylor, and M. Sjöström, "What is the cause of the ageing atrophy?. Total number, size and proportion of different fiber types studied in whole vastus lateralis muscle from 15- to 83-year-old men," *J. Neurol. Sci.*, vol. 84, no. 2–3, pp. 275–294, 1988, doi: 10.1016/0022-510X(88)90132-3.

[175] W. R. Frontera, V. A. Hughes, R. A. Fielding, M. A. Fiatarone, W. J. Evans, and R. Roubenoff, "Aging of skeletal muscle: A 12-yr longitudinal study," *J. Appl. Physiol.*, vol. 88, no. 4, pp. 1321–1326, 2000, doi: 10.1152/jappl.2000.88.4.1321.

[176] M. R. Deschenes, "Effects of aging on muscle fibre type and size," *Sport. Med.*, vol. 34, no. 12, pp. 809–824, 2004, doi: 10.2165/00007256-200434120-00002.

[177] R. . Kirkwood, H. A. Gomes, R. F. Sampaio, E. Culham, and P. Costigan, "Biomechanical Analysis of Hip and Knee Joints," *Acta Ortop Bras*, vol. 15, pp. 267–271, 2007.

[178] J. O. Judge, S. Ounpuu, and R. B. Davis III, "Effects of age on the biomechanics and physiology of gait," *Clin. Geriatr. Med.*, vol. 12, no. 4, pp. 659–678, 1996, doi: https://doi.org/10.1016/S0749-0690(18)30194-0.

[179] V. Kefala *et al.*, "Assessment of Knee Kinematics in Older Adults Using High-Speed Stereo Radiography," *Med. Sci. Sports Exerc.*, vol. 49, no. 11, pp. 2260–2267, 2017, doi: 10.1249/MSS.0000000000001350.

[180] B. Ritchie, “Effect of aging on tibiofemoral cartilage and meniscal stiffness,” 2017.

[181] E. M. Roos, H. P. Roos, S. Lohmander, C. Ekdahl, and B. Beynnon, “Knee Injury and Osteoarthritis Outcome Score (KOOS)-Development of a Self-Administered Outcome Measure,” *J. Orthop. Sport. Phys. Ther.*, vol. 28, no. 2, pp. 88–96, 1998, doi: 10.2519/jospt.1998.28.2.88.

[182] J. R. Watt, J. R. Franz, K. Jackson, J. Dicharry, P. O. Riley, and D. C. Kerrigan, “A three-dimensional kinematic and kinetic comparison of overground and treadmill walking in healthy elderly subjects,” *Clin. Biomech.*, vol. 25, no. 5, pp. 444–449, 2010, doi: 10.1016/j.clinbiomech.2009.09.002.

[183] A. G. Culvenor, B. E. Øiestad, H. F. Hart, J. J. Stefanik, A. Guermazi, and K. M. Crossley, “Prevalence of knee osteoarthritis features on magnetic resonance imaging in asymptomatic uninjured adults: a systematic review and meta-analysis,” *Br. J. Sports Med.*, vol. 53, no. 20, pp. 1268–1278, 2019, doi: 10.1136/bjsports-2018-099257.

[184] D. J. Hunter *et al.*, “Evolution of semi-quantitative whole joint assessment of knee OA : MOAKS (MRI Osteoarthritis Knee Score),” *Osteoarthr. Cartil.*, vol. 19, no. 8, pp. 990–1002, 2011, doi: 10.1016/j.joca.2011.05.004.

[185] G. B. Sharma *et al.*, “Radiological method for measuring patellofemoral tracking and tibiofemoral kinematics before and after total knee replacement,” *Bone Joint Res.*, vol. 1, no. 10, pp. 263–271, 2012, doi: 10.1302/2046-3758.110.2000117.

[186] J. Kupper, “Dynamic In-Vivo Knee Cartilage Contact With Aging [Unpublished doctoral dissertation],” University of Calgary, 2020.

[187] A. Ferlinc, E. Fabiani, T. Velnar, and L. Gradisnik, “The Importance and Role of Proprioception in the Elderly: a Short Review,” *Mater. Socio Medica*, vol. 31, no. 3, p. 219,

2019, doi: 10.5455/msm.2019.31.219-221.

[188] F. Ribeiro and J. Oliveira, “Aging effects on joint proprioception: The role of physical activity in proprioception preservation,” *Eur. Rev. Aging Phys. Act.*, vol. 4, no. 2, pp. 71–76, 2007, doi: 10.1007/s11556-007-0026-x.

[189] K. Nagai, M. Yamada, K. Uemura, Y. Yamada, N. Ichihashi, and T. Tsuboyama, “Differences in muscle coactivation during postural control between healthy older and young adults,” *Arch. Gerontol. Geriatr.*, vol. 53, no. 3, pp. 338–343, 2011, doi: 10.1016/j.archger.2011.01.003.

[190] T. Hortobágyi and P. Devita, “Muscle pre- and coactivity during downward stepping are associated with leg stiffness in aging,” *J. Electromyogr. Kinesiol.*, vol. 10, no. 2, pp. 117–126, 2000, doi: 10.1016/S1050-6411(99)00026-7.

[191] M. D. Lewek, D. K. Ramsey, L. Snyder-Mackler, and K. S. Rudolph, “Knee stabilization in patients with medial compartment knee osteoarthritis,” *Arthritis Rheum.*, vol. 52, no. 9, pp. 2845–2853, 2005, doi: 10.1002/art.21237.

[192] C. Hubley-Kozey, K. Deluzio, and M. Dunbar, “Muscle co-activation patterns during walking in those with severe knee osteoarthritis,” *Clin. Biomech.*, vol. 23, no. 1, pp. 71–80, 2008, doi: 10.1016/j.clinbiomech.2007.08.019.

[193] L. Sharma, “Proprioceptive impairment in knee osteoarthritis,” *Rheum. Dis. Clin. North Am.*, vol. 25, no. 2, pp. 299–314, 1999, doi: 10.1016/S0889-857X(05)70069-7.

[194] G. Stoquart, C. Detrembleur, and T. Lejeune, “Effect of speed on kinematic, kinetic, electromyographic and energetic reference values during treadmill walking,” *Neurophysiol. Clin.*, vol. 38, no. 2, pp. 105–116, 2008, doi: 10.1016/j.neucli.2008.02.002.

[195] C. A. Fukuchi, R. K. Fukuchi, and M. Duarte, “Effects of walking speed on gait

biomechanics in healthy participants: A systematic review and meta-analysis," *Syst. Rev.*, vol. 8, no. 1, pp. 1–11, 2019, doi: 10.1186/s13643-019-1063-z.

[196] D. R. Wilson, J. D. Feikes, A. B. Zavatsky, and J. J. O'Connor, "The components of passive knee movement are coupled to flexion angle," *J. Biomech.*, vol. 33, no. 4, pp. 465–473, 2000, doi: 10.1016/S0021-9290(99)00206-7.

[197] O. Beauchet, G. Allali, G. Berrut, and V. Dubost, "Is low lower-limb kinematic variability always an index of stability?," *Gait Posture*, vol. 26, no. 2, pp. 327–328, 2007, doi: 10.1016/j.gaitpost.2007.02.001.

[198] B. C. Heiderscheit, "Movement variability as a clinical measure for locomotion," *J. Appl. Biomech.*, vol. 16, no. 4, pp. 419–427, 2000, doi: 10.1123/jab.16.4.419.

[199] Y. I. C. Pai, W. Z. Rymer, R. W. Chang, and L. Sharma, "Effect of age and osteoarthritis on knee proprioception," *Arthritis Rheum.*, vol. 40, no. 12, pp. 2260–2265, 1997, doi: 10.1002/art.1780401223.

[200] R. M. Kiss, "Effect of severity of knee osteoarthritis on the variability of gait parameters," *J. Electromyogr. Kinesiol.*, vol. 21, no. 5, pp. 695–703, 2011, doi: 10.1016/j.jelekin.2011.07.011.

[201] T. B. L. Kirkwood, "Understanding the odd science of aging," *Cell*, vol. 120, no. 4, pp. 437–447, 2005, doi: 10.1016/j.cell.2005.01.027.

[202] J. M. Mansour, *Biomechanics of cartilage*, vol. 2nd ed. Lippincott Williams & Wilkins, 2013.

[203] M. T. Nieminen *et al.*, "T2 relaxation reveals spatial collagen architecture in articular cartilage: A comparative quantitative MRI and polarized light microscopic study," *Magn. Reson. Med.*, vol. 46, no. 3, pp. 487–493, 2001, doi: 10.1002/mrm.1218.

[204] T. C. Pataky, “Generalized n-dimensional biomechanical field analysis using statistical parametric mapping.,” *J. Biomech.*, vol. 43, no. 10, pp. 1976–82, 2010, doi: 10.1016/j.jbiomech.2010.03.008.

[205] A. L. Bell, D. R. Pedersen, and R. A. Brand, “A comparison of the accuracy of several hip center location prediction methods,” *J. Biomech.*, vol. 23, no. 6, pp. 617–621, 1990, doi: https://doi.org/10.1016/0021-9290(90)90054-7.

APPENDIX A: Marker Locations

Marker #	Location
1	5th metatarsal joint, lateral, right
2	Superior navicular, right
3	Lateral calcaneus, right
4	Malleolus, medial, right
5	Malleolus, lateral, right
6	Distal tibia, lateral, right
7	Proximal tibia, anterior, right
8	Fibula head, right
9	Condyle, medial, right
10	Condyle, lateral, right
11	Distal thigh, right
12	Medial thigh, right
13	Proximal thigh, right
14	Greater trochanter, right
15	5th metatarsal joint, lateral, left
16	Superior navicular, left
17	Lateral calcaneus, left
18	Malleolus, medial, left
19	Malleolus, lateral, left
20	Distal tibia, lateral, left
21	Proximal tibia, anterior, left
22	Fibula head, left
23	Condyle, medial, left
24	Condyle, lateral, left
25	Distal thigh, left
26	Medial thigh, left
27	Proximal thigh, left
28	Greater trochanter, left
29	Anterior superior iliac spine, right
30	Anterior superior iliac spine, left
31	Posterior superior iliac spine, right
32	Posterior superior iliac spine, left
33	Sternum, half distance between manubrium/xiphoid process
34	Manubrium
35	C7
36	Acromion, right
37	Acromion, left
38	Helper marker - iliac crest, right

APPENDIX B: Anatomical Coordinate System Definitions

Segment	ACS	Definition
Thigh	Origin	Hip joint centre: Calculated using methods of Bell et al.[a] Briefly, the hip centre was defined as a percentage of the distance between the left and right anterior superior iliac spines: 14% medially, 19% posteriorly, and 30% inferiorly.
	Initial medio-lateral axis	Line that connects the medial and lateral femoral condyles, pointing laterally.
	Supero-inferior axis	Line that connects the knee joint centre (refer to definition of the shank origin) to the hip joint centre, pointing superiorly.
	Antero-posterior axis	Cross product between the supero-inferior axis and initial medio-lateral axis, pointing anteriorly.
	Medio-lateral axis	Cross product between the antero-posterior axis and supero-inferior axis, pointing laterally.
Shank	Origin	Knee joint centre: Defined as the midpoint of the line that connects the medial and lateral femoral condyles.
	Initial medio-lateral axis	Line that connects the medial and lateral femoral condyles, pointing laterally.
	Supero-inferior axis	Line that connects the ankle joint centre (defined as the midpoint of the line that connects the medial and lateral malleoli) and knee joint centre, pointing superiorly.
	Antero-posterior axis	Cross product between the supero-inferior axis and initial medio-lateral axis, pointing anteriorly.
	Medio-lateral axis	Cross product between the antero-posterior axis and supero-inferior axis, pointing laterally.

[a] Bell et al. [205]

APPENDIX C: Within-participant SD of the ACLR group and matched controls

Matched Pair	ACLR		Healthy	
	Orientation (deg)	Dispersion (deg)	Orientation (deg)	Dispersion (deg)
1	0.66	0.51	1.08	0.56
2	0.63	0.57	1.35	1.69
3	0.46	0.43	0.94	0.52
4	0.41	0.48	0.61	0.36
5	0.59	0.47	0.45	0.29
6	0.99	0.84	0.60	0.38
7	0.81	0.64	0.37	0.36
8	0.45	0.50	0.41	0.59
9	1.65	1.73	1.22	0.37
10	1.39	1.91	1.59	0.61
11	1.20	0.96	0.66	0.40
12	1.53	1.84	0.49	0.14
13	0.86	0.47	1.02	0.76
14	1.00	0.72	0.84	0.54
15	0.87	0.51	0.39	0.10
16	0.56	0.54	0.57	0.58
17	0.72	0.38	0.66	0.89
18	0.93	0.32	1.22	0.52
19	0.58	0.59	0.96	0.68
20	1.05	0.68	0.58	0.43
21	1.96	1.06	1.30	0.79
22	0.79	0.51	0.73	0.34
23	1.89	0.96	1.28	0.29
24	0.76	0.61	0.81	0.66
25	1.08	0.83	1.02	0.66
26	2.07	1.38	1.13	0.50
27	1.05	0.66	0.71	0.37
28	0.89	0.96	0.96	0.54
29	1.15	0.61	1.42	0.38
30	0.48	0.45	0.68	0.71
31	0.79	0.48	0.64	0.89
32	0.71	0.55	1.99	0.51
33	1.13	0.66	0.32	0.43
34	0.62	0.58	0.73	0.40
35	1.36	1.12	1.01	0.56
36	1.21	1.29	1.13	0.49
37	0.80	0.76	0.70	0.38
38	0.82	0.51	2.77	1.70
39	1.87	1.85	1.22	0.91
40	2.28	1.47	0.64	0.60
41	0.99	0.61	0.86	0.75
42	1.03	1.01	0.81	0.87
43	0.75	0.64	0.44	0.57
44	1.33	0.67	0.95	0.44
45	0.82	0.70	1.22	0.85
46	1.29	1.47	1.06	0.66
47	0.61	0.34	0.88	0.60
48	0.63	0.41	0.57	0.36
Average	1.01	0.80	0.92	0.58

APPENDIX D: Individual rFHA tracings

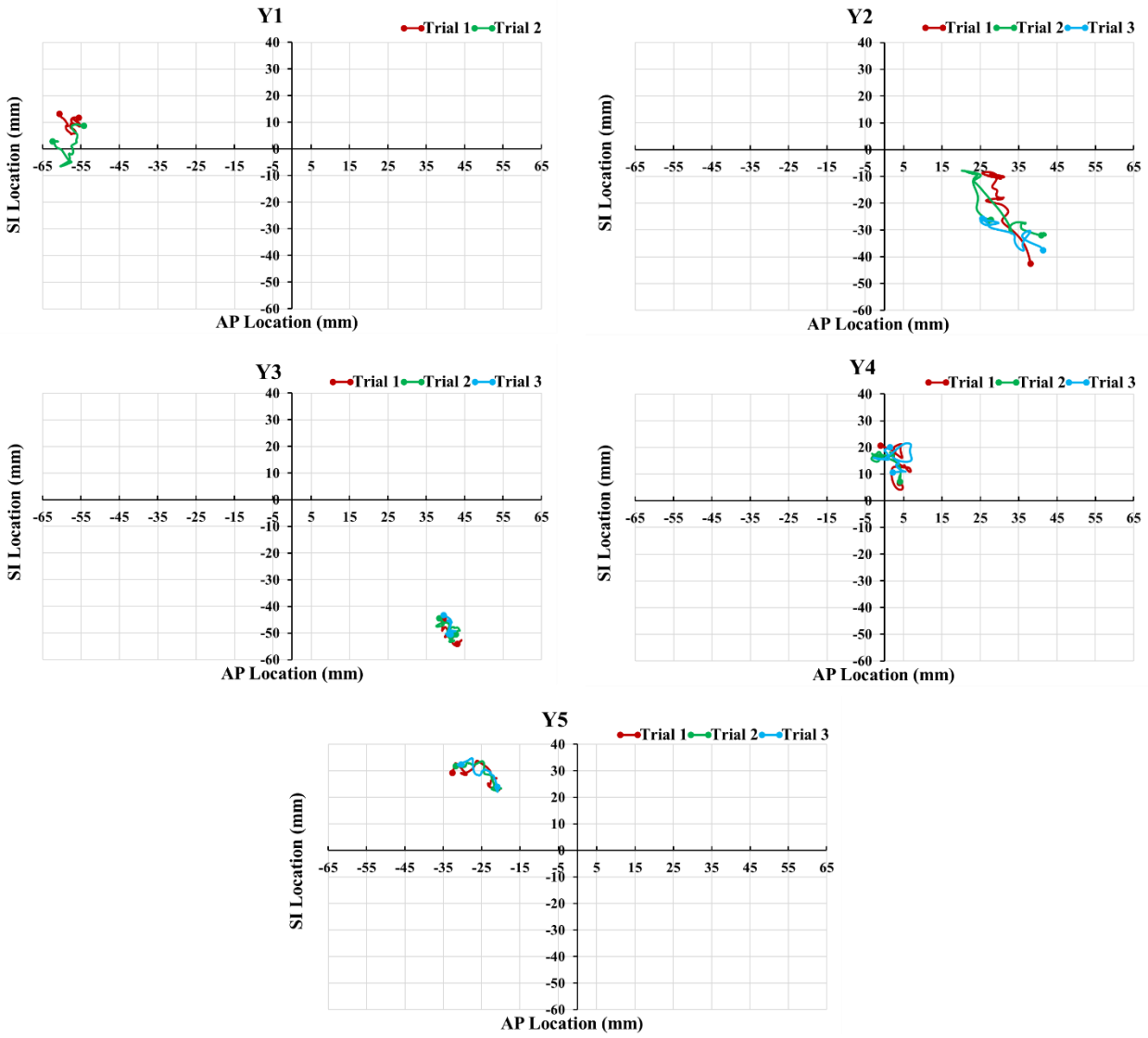

Figure D-1 – The individual rFHA tracings of the younger (Y1-5) and older (O 1-5) participants. All trials for each participant are provided to illustrate the within-participant variability (figure continued on next page).

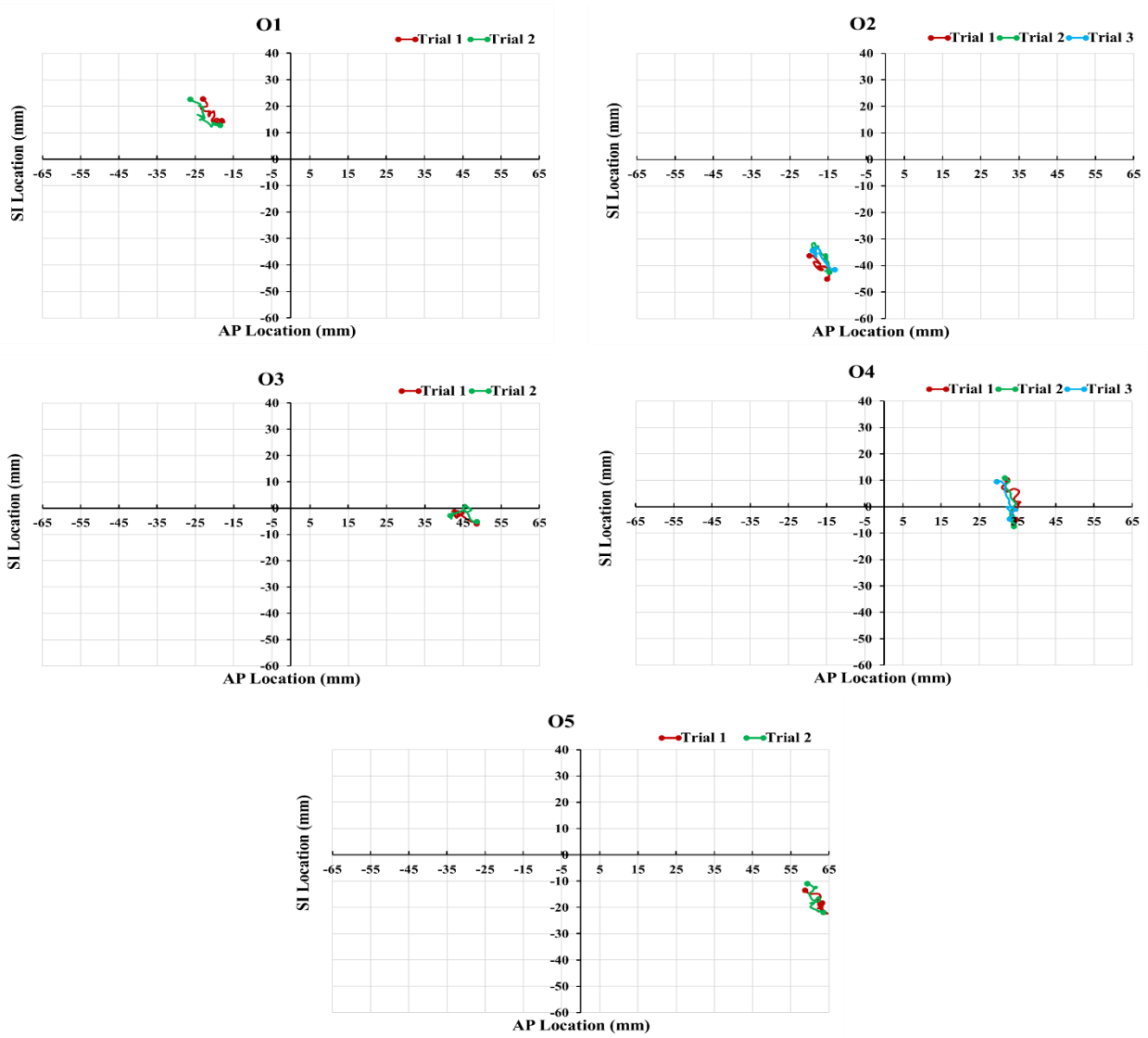

Figure D-1 – The individual rFHA tracings of the younger (Y1-5) and older (O 1-5) participants. All trials for each participant are provided to illustrate the within-participant variability.

APPENDIX E: Supplementary temporal graphs of the Cardan and helical angles

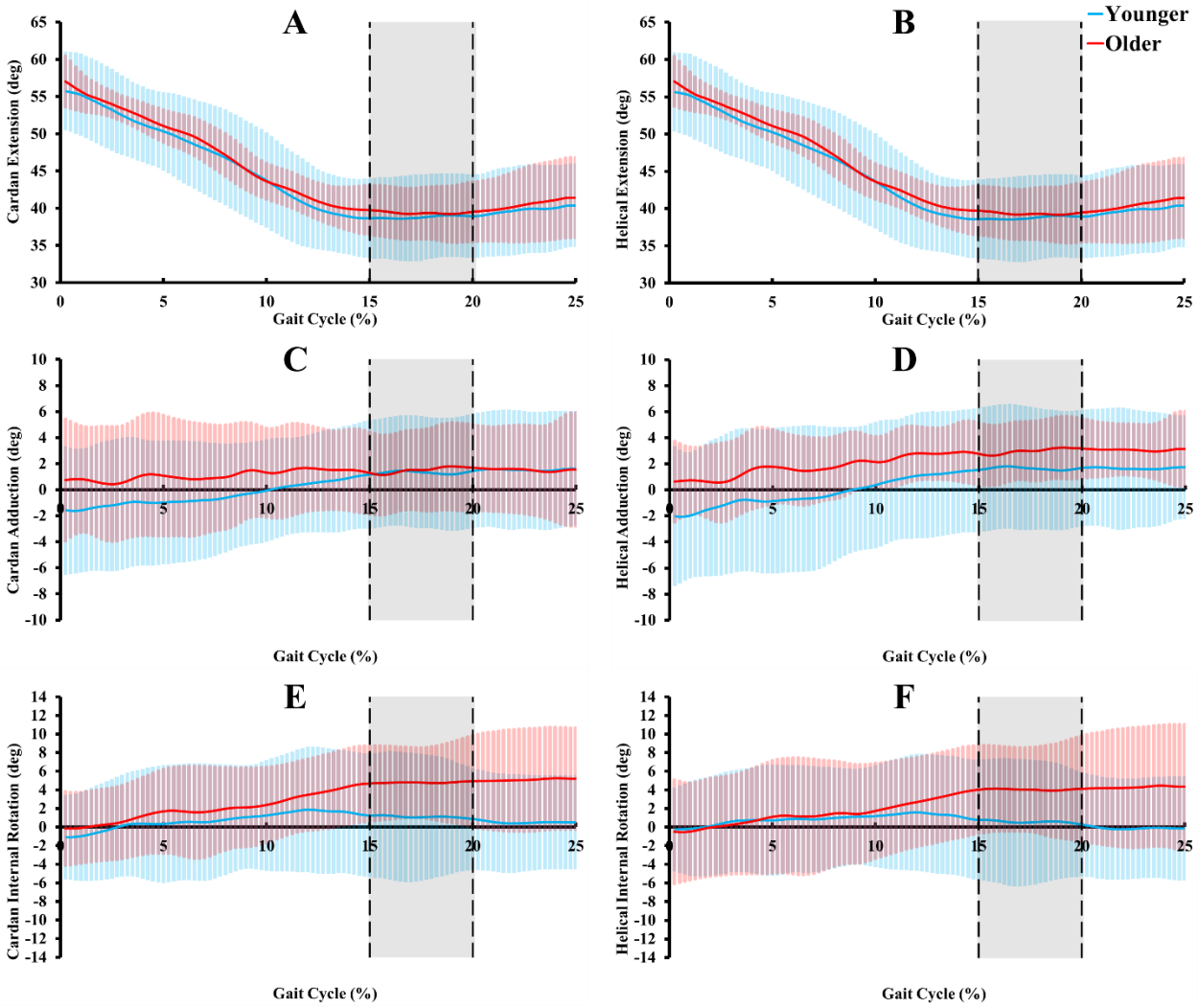

Figure E-1 – The CA (graphs A, C, and E) and helical angles (graphs B, D, and F) of the younger (blue) and older (red) groups from 0-25% gait cycle. The grey box indicates the time range of when PF occurred for a participant (between 15-20%).